

SCHOOL OF CHEMISTRY

CARDIFF UNIVERSITY



**Novel Polymers and Dendrimers of
Intrinsic Microporosity derived from
Triptycene and other Monomers of
High Internal Free Volume**

Thesis submitted for the degree of Doctor of Philosophy by:

Jonathan Keith Earl Walker

Supervisor: Neil B. McKeown

2010

UMI Number: U585530

All rights reserved

INFORMATION TO ALL USERS

The quality of this reproduction is dependent upon the quality of the copy submitted.

In the unlikely event that the author did not send a complete manuscript and there are missing pages, these will be noted. Also, if material had to be removed, a note will indicate the deletion.



UMI U585530

Published by ProQuest LLC 2013. Copyright in the Dissertation held by the Author.
Microform Edition © ProQuest LLC.

All rights reserved. This work is protected against
unauthorized copying under Title 17, United States Code.



ProQuest LLC
789 East Eisenhower Parkway
P.O. Box 1346
Ann Arbor, MI 48106-1346

To my family and friends

Acknowledgements

First of all I would like to thank my supervisor Professor Neil McKeown for his guidance, support and extreme patience throughout the course of my PhD.

I'd like to give a special thanks to Dr. Caterina Gavina Grazia Bezzu, for her encouragement and support during the most difficult times.

I'd also like to thank everyone in our group, particularly Rhys, Lino, Kadhum, Mo, and Egg for making the lab such a pleasant and friendly place to work.

Special thanks go to Dr. James Paine and Dr. Bader S. Ghanem for their guidance during the early stages of my PhD.

Thanks go to the team at The Hydrogen Laboratory, Birmingham University (Dr David Book, Dr. Allan Walton and Mr Steven Tedds) for aiding in the analysis of some specified samples.

Huge thanks to Dr. Rob Jenkins, Dr Benson Kariuki and the School's technical team for all their analytical expertise!

Last of all I'd like to thank all my friends in Cardiff for the good times and the memories over the past few years, and my family for their unconditional support and patience, without whom I would not be able to have achieved so greatly.

Abstract

The research described in this thesis is largely focused on monomers derived from the triptycene moiety, and their potential to form polymers of intrinsic microporosity (PIMs), organic molecules of intrinsic microporosity (OMIMs) and dendrimers of intrinsic microporosity (DIMs). Triptycene is of particular interest here due to its high internal molecular free volume (IMFV) and previously reported success in the formation of microporous materials – triptycene is in fact the basis of the most microporous PIM reported to date, and the basis of the only reported example of an amorphous molecular microporous material. The work later extends to incorporate other presumed high IMFV moieties based on spirobifluorene and propellane.

The research begins by focusing on the synthesis of potentially soluble polymers. They are of interest due to their processability, which when coupled with microporosity, can potentially yield permeable membranes suitable for selective gas separation. There has been much research into PIMs and their corresponding membranes, with particular interest surrounding **PIM-1**, a polymer formed between a spirobisindane based monomer, and 2,3,5,6-tetrafluoroterephthalonitrile.¹ The same nucleophilic aromatic substitution reaction (S_NAr) as is used to make **PIM-1** is employed throughout this thesis for the formation of final products.

The second section of this project focused on the synthesis of network polymers based around triptycene, introducing bitriptycenes, triptycene side groups, and unsymmetrical triptycenes with new functional groups, the main focus on increased surface area. Although highly microporous materials were prepared, no enhancement over previously obtained triptycene polymers was obtained.

The third section of the thesis focuses on the synthesis of novel microporous materials termed Organic Molecules of Intrinsic Microporosity (OMIMs) and Dendrimers of Intrinsic Microporosity (DIMs). These are discrete molecules lacking any long range order that cannot pack space efficiently due to their rigid structures, composed of monomer subunits with high IMFV. All materials were analysed for their apparent BET surface areas (N_2 adsorption at 77 K), which were in the range 0-700 $m^2 g^{-1}$.

Abbreviations

Molecule numbering

Non-commercial compounds synthesised and used in this project are denoted a single figure in bold, e.g. – **1**

The ladder and network polymers synthesised in this project are denoted the prefix P followed by a number, in bold, e.g. – **P1**

Dendrimers of intrinsic microporosity are denoted the prefix DIM followed by a number, in bold, e.g. – **DIM-1**

Organic molecules of intrinsic microporosity are denoted the prefix OMIM followed by a number, in bold, e.g. – **OMIM-1**

Dendrons and non microporous dendrimers are denoted the prefix D followed by a number, in bold, e.g. – **D1**

A table of compound structures is provided in **Appendix A**, and a table for polymers, DIMs, and OMIMs in **Appendix B**.

3D	3-Dimensional
Å	Angstrom
APCI	Atmospheric pressure chemical ionisation
aq	aqueous
Ar	Unspecified aryl substituent
atm	Standard atmospheric pressure
BET	Brunauer, Emmett, and Teller
br	Broad
calc.	Calculated
CMP	Conjugated Microporous Polymers
COF	Covalent-Organic-Frameworks
CTC	Cyclotricatechylene
DCE	Dichloroethane

DCM	Dichloromethane
DIM	Dendrimer of Intrinsic Microporosity
DME	Dimethyl ether
DMF	<i>N,N</i> -Dimethylformamide
DMSO	Dimethyl sulphoxide
DSC	Differential scanning calorimetry
EA	Ethyl acetate
EI ⁺	Electron Impact
eq.	Equivalent
ES	Electrospray
Et	Ethyl
EtOH	Ethanol
<i>f</i>	monomer functionality
F ₆ -HATN	2,3,8,9,14,15-hexafluoro-5,6,11,12,17,18-hexaazatrinaphthylene
g	Grams
GPC	Gel Permeation Chromatography
HATN/Cl ₆ -HATN	2,3,8,9,14,15-hexachloro-5,6,11,12,17,18-hexaazatrinaphthylene
HCP	Hyper-cross linked Polymer
hr(s)	Hour(s)
HRMS	High Resolution Mass Spectrometry
Hz	Hertz
IFV	Internal Free Volume
IM	Intrinsic Microporosity
IMFV	Internal Molecular Free Volume
IR	Infra Red
IUPAC	International Union of Pure and Applied Chemistry
<i>J</i>	Coupling constant (in Hz)
K	Kelvin
L	Litre
lit.	Literature
LRMS	Low Resolution Mass Spectrometry
m	Multiplet
m ²	Square Metre
mbar	millibar
Me	Methyl
MeOH	Methanol
min	Minute(s)
ml	Millilitre(s)
mmol	Millimole(s)
<i>M_n</i>	Number-average molecular weight
MOF	Metal Organic Framework
Mp	Melting point
<i>M_w</i>	Mass-average molecular weight
nm	nanometers
NMR	Nuclear Magnetic Resonance
OMIM	Organic Molecule of Intrinsic Microporosity

P/P ₀	Partial Pressure
Ph	Phenyl
PIM	Polymers of Intrinsic Microporosity
q	quartet
R	undefined group
r.t.	room temperature
RF	Retention Factor
s	singlet
S _N Ar	Nucleophilic Aromatic Substitution
Spirobifluorene	9,9'-spirobifluorene
STP	Standard Temperature and Pressure
t	triplet
<i>t</i> -Butyl	tert butyl
TF	2,3,5,6-tetrafluoroterephthalonitrile
TFA	TrifluoroAcetic acid
TGA	Thermo-Gravimetric Analysis
THF	Tetrahydrofuran
TLC	Thin Layer Chromatography
TMS	Trimethylsilyl
Trip	Triptycene
Triptycene	9,10-Dihydro-9,10-o-benzanthracene
V	Volume
vs.	versus
wt. %	weight percent
σ	Area occupied by molecular N ₂

Table of contents

Declaration	i
Acknowledgements.....	iii
Abstract	iv
Abbreviations	v
Table of contents	viii
1 Introduction.....	2
1.1 Porous materials	2
1.2 Quantifying microporosity	2
1.3 Microporous materials	6
1.4 Crystalline and framework-based microporous materials	6
1.4.1 Metal Organic Frameworks (MOFs)	6
1.4.2 Covalent Organic Frameworks (COFs)	8
1.4.3 Molecular Crystals	9
1.5 Amorphous microporous materials	11
1.5.1 Activated Carbon	11
1.5.2 Hypercrosslinked and network dependant microporous polymers.....	12
1.5.3 Amorphous Molecular Microporosity	14
1.6 Polymers of Intrinsic Microporosity (PIMs)	15
1.6.1 Internal Molecular Free Volume (IMFV)	15
1.6.2 Phthalocyanine Network-PIMs ⁶⁹	16
1.6.3 Porphyrin-based network-PIMs ⁷³	17
1.6.4 HATN network-PIM ⁷⁵	18

1.6.5	CTC derived Network-PIM ¹⁵	19
1.6.6	Non-network PIMs.....	21
1.6.7	Triptycene derived PIMs.....	22
1.7	Dendrimers	25
1.7.1	Origins.....	25
1.7.2	Divergent dendrimer growth	27
1.7.3	Convergent dendrimer growth ⁹⁴	27
1.7.4	Functions and advantages of dendritic macromolecules.....	28
1.8	Objectives.....	28
2	Ladder polymers	32
2.1	Monomers for triptycene ladder polymers.....	33
2.1.1	Synthesis of symmetrical anthracenes	34
2.1.2	Unsymmetrical anthracenes	35
2.2	Unsymmetrical polymer from tetrahydroxytriptycene 5.....	36
2.2.1	Synthesis of tetrahydroxytriptycene 5.....	36
2.2.2	General procedure for preparation and purification of polymers	40
2.2.3	Synthesis of ladder polymer P1	41
2.3	Ladder polymer with increased alkyl chain	42
2.3.1	Synthesis of tetrahydroxytriptycene 7.....	43
2.3.2	Synthesis of ladder polymer P2	44
2.4	Bitriptycene ladder polymer P3	44
2.4.1	Synthesis of monomer 10.....	45
2.4.2	Synthesis of ladder polymer P3	48
3	Network Polymers	51
3.1	General procedure for network polymers	51
3.2	Bi-triptycene network polymer P4.....	51
3.2.1	Synthesis of monomer 13	53
3.2.2	Synthesis of network polymer P4	54
3.3	Network Polymer with Triptycene side group P5	56
3.3.1	Synthesis of monomer 16.....	56
3.3.2	Proton NMR dynamic study of triptycene 17.....	60

3.3.3	Synthesis of Network Polymer P5	63
3.4	Network Polymer P6	64
3.4.1	Synthesis of Monomer 20	65
3.4.2	Synthesis of Network Polymer P6	66
3.5	Network Polymer P7 from monomer 20 and 21	67
3.5.1	Synthesis of Monomer 21	67
3.5.2	Synthesis of Network Polymer P7	68
3.5.3	Summary of network polymers	68
4	Organic Molecules and Dendrimers of Intrinsic Microporosity (OMIMs/DIMs)	73
4.1	Divergent triptycene dendrimer	73
4.1.1	Synthesis of branch unit 22	74
4.1.2	Synthesis of triptycene core 30	77
4.1.3	Synthesis of dendrimer D1	79
4.1.4	Synthesis of dendrimer D3	81
4.2	Triptycene tetramer, OMIM-1	83
4.2.1	Synthesis of OMIM-1	84
4.3	Triptycene dimer, D4	85
4.3.1	Synthesis of D4	86
4.4	Dendrimer with a triptycene core, DIM-1	87
4.4.1	Synthesis of triptycene based functional dendron D5	88
4.4.2	Synthesis of dendrimer DIM-1	89
4.5	Dendrimer with CTC core, DIM-2	94
4.5.1	Synthesis of DIM-2	95
4.6	Dendrimer with spiro-centre core, DIM-3	96
4.6.1	Synthesis of dendrimer DIM-3	97
4.7	Tetramer from dihydroxy-spirobifluorene 34, D6	97
4.7.1	Synthesis of 2,3-dihydroxy-9,9'-spirobifluorene 34	98
4.7.2	Synthesis of tetramer D6	98
4.8	Dendrimer from D7 and 30, D8	99
4.8.1	Synthesis of functional dendron D7	100
4.8.2	Synthesis of dendrimer D8	101

4.9	Propellane containing tetramer OMIM-2	102
4.9.1	Synthesis of pinacolone 37.....	103
4.9.2	Synthesis of dihydroxy-propellane 35	104
4.9.3	Synthesis of propellane tetramer OMIM-2	106
4.10	Propellane containing dendrimer DIM-4	107
4.10.1	Synthesis of tripropellane dendron OMIM-3	108
4.10.2	Synthesis of propellane dendrimer DIM-4.....	108
4.11	Dendrimer with bitriptycene core DIM-5.....	109
4.11.1	Synthesising bitriptycene core for dendrimer DIM-5	110
4.11.2	Synthesising dendrimer DIM-5	111
4.11.3	HATN based triptycene dendrimer	113
4.11.4	Summary of dendrimers and OMIMs	117
5	Conclusion	120
6	Future work.....	122
7	Experimental	125
7.1	Experimental techniques.....	125
7.2	Experimental Procedures.....	127
	Bibliography	180
	Appendix A.....	187
	Appendix B.....	195

Chapter 1: Introduction

1 Introduction

1.1 Porous materials

A pore in physical science is a term widely used to describe a void or cavity within a given structure. They can have many different shapes, be it well defined spherical, cylindrical, prisms etc, or undefined randomly shaped volumes of spatial confinement. They also have massively varying sizes, from sub-nanometre to over a centimetre and beyond. They can be inaccessible closed pores, or open-pores where interconnected channels exist that are easily accessible by a probe.²

Two important properties of porous materials with open-pores is their ability to act as adsorbents and as size exclusion filters. Very simplified examples of these properties is the action of a bath sponge adsorbing water or air, and an air filter removing large particles from a gas stream. As the pore size gets smaller, even more interesting extensions of these properties begin to come into play. For example, when a gas molecule is contained within a small enough pore, the extensive multi-walled interactions between the gas molecule and pore walls can cause the equilibrium vapour pressure to favour the condensed state of the gas molecule at higher temperatures and lower pressure than would be possible in a less restricted space, allowing even gases with low enthalpy of adsorption, such as hydrogen, to become adsorbed within the pores. This effect is most notable for micropores, which are defined as being pores with a width (measured as the smallest dimension in an irregular pore) of less than 2 nm.²

1.2 Quantifying microporosity

Microporous materials are said to be those which contain a large fraction of micropores of less than 2 nm in diameter that are accessible by a probe. A common measure for quantification of a material's microporosity is to probe the sample with N₂ (at 77K), and record its apparent surface area by analysis of the resulting

adsorption isotherm. The nitrogen gas interacts weakly with the surface of the material, in a reversible physisorption process (typical $\Delta H = 2 - 20$ KJ/mol), as opposed to chemisorption where a strong interaction is involved between the adsorbent and internal surface such as the formation of a covalent bond (typical $\Delta H = 20+$ KJ/mol). The process of adsorption is an equilibrium process in which the accessible surface is filled layer by layer. Measuring the volume of nitrogen required to saturate the first layer (monolayer) corresponds to the accessible surface area of the material. The surface area can then be calculated once the quantity of nitrogen required to fill the monolayer has been recorded. Each N_2 molecule adsorbed on the inner surface occupies a known surface area, σ (16.2 \AA^2). To calculate the volume of N_2 required to fill the monolayer, and hence the surface area, the method devised by Brunauer, Emmett, and Teller (BET)³ is commonly used, although other methodologies are employed.

The BET theory is a multilayer extension of the Langmuir theory. Some required assumptions are that gas molecules physically adsorb onto a solid in infinite layers, there is no interaction between each adsorption layer, and the Langmuir theory applies to each layer individually. The equation for multilayer adsorption is then taken to be:

$$\frac{P}{n(P-P_0)} = \frac{1}{cn_m} + \frac{c-1}{cn_m} \frac{P}{P_0}$$

In which P , P_0 , c , n , n_m are adsorption pressure, saturation vapour pressure, BET constant, amount adsorbed (moles per gram of adsorbent), and monolayer capacity (number of moles of adsorbent required to fill the monolayer per gram of adsorbent), respectively. Plots of $P/[n(P_0-P)]$ against (P/P_0) are found experimentally to be close to linear through the range $0.05 < P/P_0 < 0.35$. The slope (A) and intercept (I) can then be used to calculate n_m :

$$n_m = \frac{1}{A + I}$$

Then using the value of σ for the probe adsorbent (N_2), the specific surface area, S , can be calculate (where N_A is Avogadro's number):

$$S = N_A n_m \sigma$$

The data is obtained by adsorbing N_2 at low pressure and temperature (77K). A known quantity of N_2 is added, the system then waits for equilibrium (following adsorption) before recording the resulting pressure in the sample vessel. The data is then presented in a graph as a function of volume of nitrogen adsorbed against P/P_0 (an example of an experimental isotherm for Trip(Me)-PIM is given in Figure 1.2 chemical structure Scheme 1.10). In addition to the surface area, a visual assessment of the adsorption/desorption isotherm can provide indication as to what kind of pores are present in the adsorbate. The IUPAC classification of adsorption isotherms⁴ is illustrated in Figure 1.1, where characteristic curves indicate the type of adsorbate associated with each pattern.

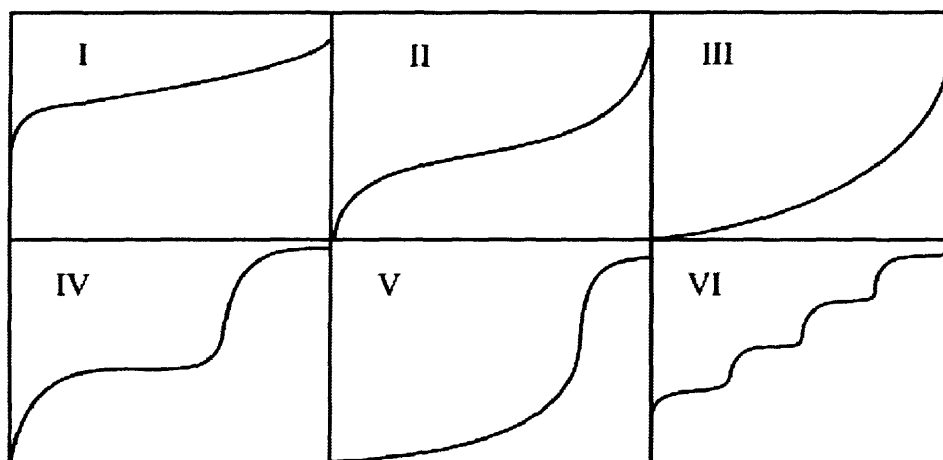


Figure 1.1 Type I: microporous. Type II, III, VI: non-porous. Type IV, V: mesoporous.⁴

The isotherm for Trip(Me)-PIM (Figure 1.2)⁵ is characteristic for the microporous polymers described herein. It shows a steep increase of N_2 adsorption at very low pressure, indicative of a type I isotherm (microporous material). There is also a slow and steady continued uptake of N_2 not generally associated with microporous materials, at increased pressure. The continued uptake is believed to be the result of swelling of the material⁵ creating further accessible pores as the pressure increases.

This adsorption process appears related to an unusually large degree of hysteresis between the adsorption and desorption curves.

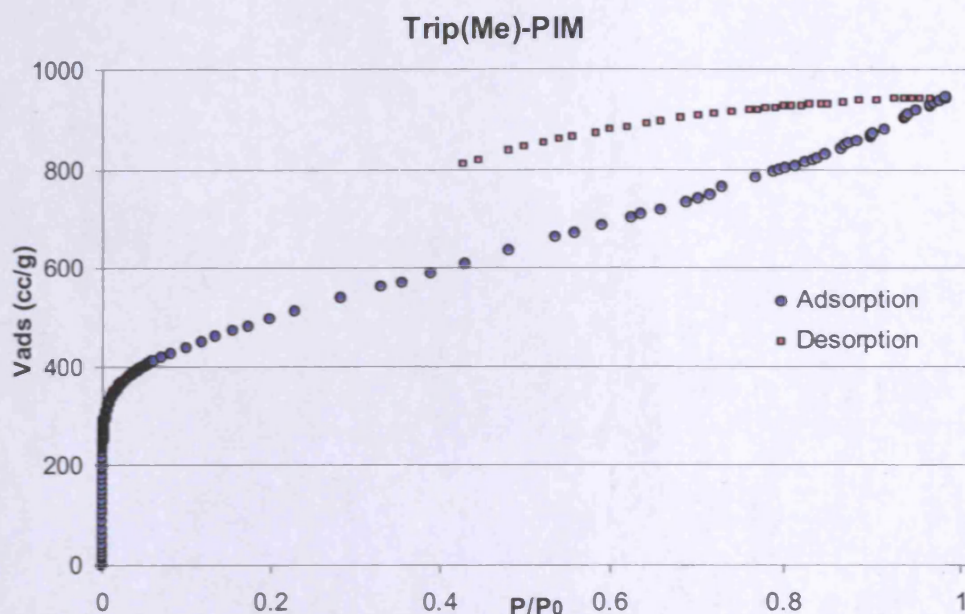


Figure 1.2 Adsorption/Desorption isotherm, N_2 77K, for trip(Me)-PIM⁵

To complement the BET analysis from N_2 adsorption, many of the samples prepared in the course of this project were also probed with H_2 using a gravimetric system. The weight of the sample is accurately recorded as H_2 is introduced to the system, and by plotting the percentage weight gained against the pressure of the system, a type I isotherm is again observed. It is noteworthy that the apparent surface areas recorded are subject to the ability of the probe to access the material and penetrate the pore network, for this reason the true surface area of a material may never be accurately known and many other complementary techniques are used to characterise porous materials. However, the BET method is a well established⁶ and standardised analytical tool allowing accurate comparison of a global network of results and is the one which is used throughout this thesis.

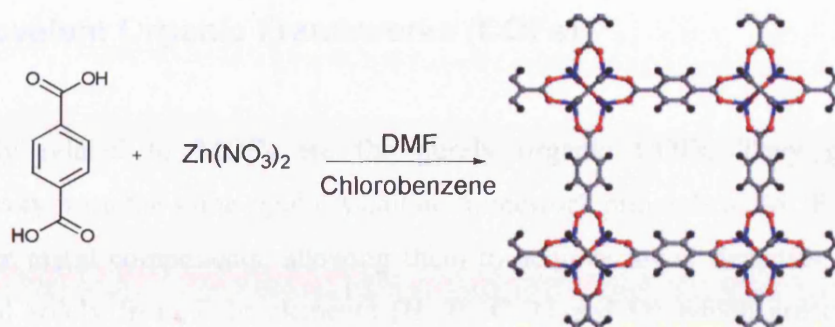
1.3 Microporous materials

Microporous materials have been investigated for many applications including membranes for selective gas separation⁷⁻¹⁰, gas storage¹¹⁻¹⁷, heterogeneous catalysis¹⁸, dielectrics¹⁹, and even as organic vapour sensors²⁰. Over the past decade, research into the synthesis of new microporous materials and their possible applications has been rapidly increasing. As a result of this high level of interest, current forms of microporous materials are more diverse than ever, with a range of microporous crystalline solids such as metal-organic-frameworks (MOFs), covalent-organic-frameworks (COFs) and new additions to the well-established family of zeolites. There are also amorphous network structures based on silica or activated carbon, and most recently, wholly organic polymers and amorphous molecules that display high levels of microporosity. Each category of microporous material has its own synthetic challenges and offer different advantages and disadvantages inherent to them.

1.4 Crystalline and framework-based microporous materials

1.4.1 Metal Organic Frameworks (MOFs)

Crystalline materials by their very nature offer the most ordered, and well defined pore sizes and pore size distribution. Some of the most microporous materials currently known belong to this category, with recent MOFs demonstrating apparent BET surface areas in excess of 5000 m² g⁻¹.²¹ The archetypal MOF, Yaghi's MOF-5^{22,23} (Scheme 1.1), was the first to demonstrate excellent potential for gas adsorption (e.g. methane = 240 cm³(STP)/g at 298 K, 36 atm²⁴). There is also good potential for MOFs in hydrogen storage (e.g. MOF-5 = 5.1 wt.% at saturation, 77 K²³ and MOF-177 = 7.5 wt.% at 80 bar, 77 K)²⁵ and for heterogeneous catalysis.²⁶



Scheme 1.1 Synthesis of MOF-5

The compounds used to synthesise MOF-5 have no internal free volume (see section 1.6.1), and the microporosity of the final MOF structure is a result of the framework holding the pores open. From single-crystal X-ray diffraction data the open pore structure, and regular, defined nature of this class of materials is clearly visible (Figure 1.3).

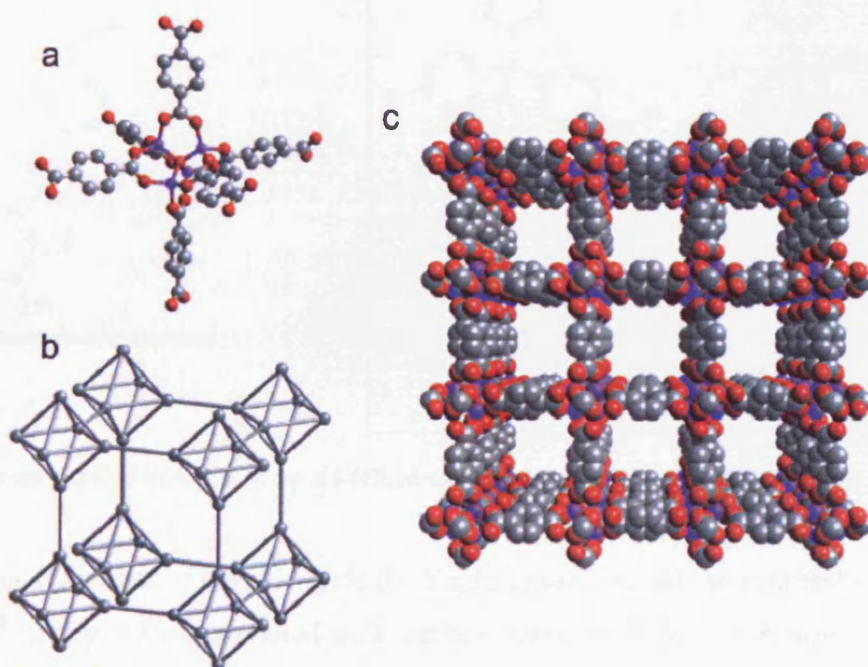


Figure 1.3 (a) Building unit present in crystals of $\text{Zn}_4\text{O}(\text{BDC})_3(\text{DMF})_8(\text{C}_6\text{H}_5\text{Cl})$ (MOF-5), where the carboxylate carbon atoms are in an octahedral geometry decorating (b) a primitive cubic lattice, and form (c) highly porous crystals; structures were drawn using single-crystal X-ray diffraction data.²²

that the crystal framework is mesoporous (i.e. with pore diameter > 2 nm), and the crystal density is one of the lowest known at 0.17 g cm^{-3} .²⁷

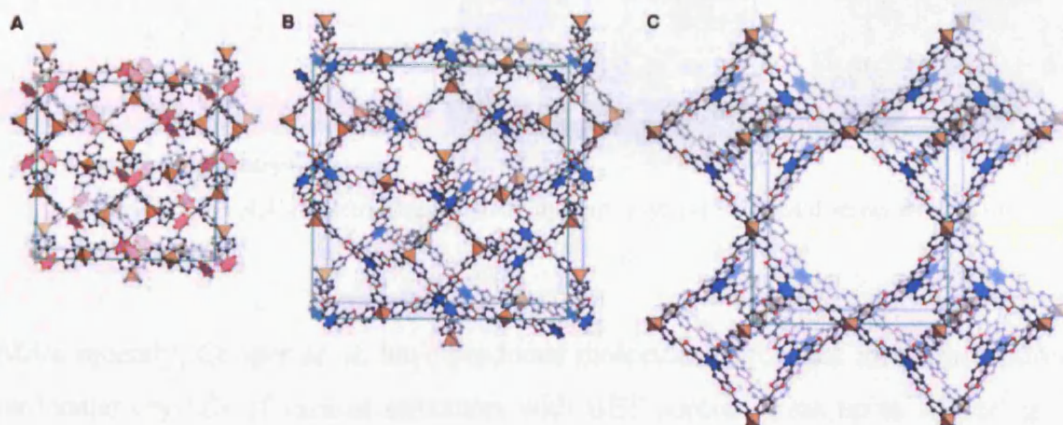
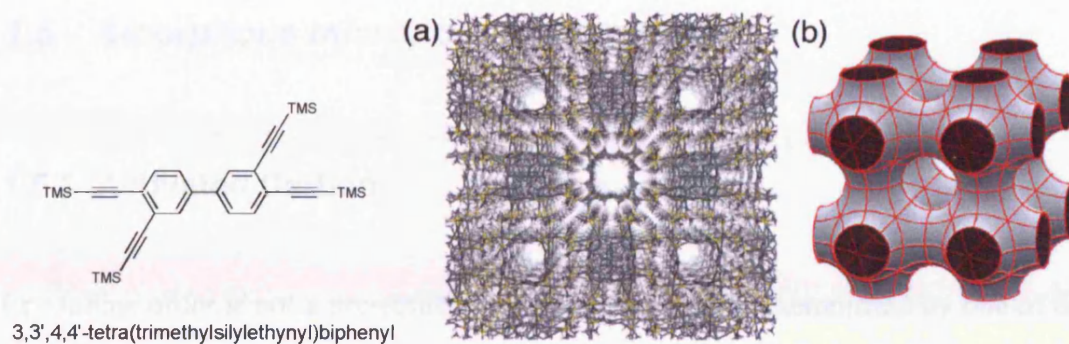


Figure 1.4 Atomic connectivity and structure of crystalline products of COF-102 (A), COF-105 (B), and COF-108 (C), based on PXRD and modelling. Hydrogen atoms are omitted for clarity. Carbon, boron, and oxygen atoms are represented as gray, orange, and red spheres, respectively.²⁷

1.4.3 Molecular Crystals

Recently there have been examples of molecular, non-covalent crystals which, like MOFs and COFs, maintain their structure and porosity even after removal of all the solvent included within their pore structure during formation.^{29,30} One example from The McKeown group is the molecular crystal of 3,3',4,4'-*tetra*(trimethylsilylethynyl)biphenyl (Figure 1.5), which has been reported to possess a BET surface area of $278 \text{ m}^2 \text{ g}^{-1}$, with a typical type I microporous isotherm.³¹



3,3',4,4'-tetra(trimethylsilylethynyl)biphenyl

Figure 1.5 3,3',4,4'-tetra(trimethylsilylethynyl)biphenyl (a) its crystal structure and (b) pore structure.³¹

More recently, Cooper *et al.* have produced molecular cages that form microporous molecular crystals of various structures with BET surface areas up to $650 \text{ m}^2 \text{ g}^{-1}$.³⁰ Also the McKeown group have stabilised a phthalocyanine based clathrate using molecular 'wall-ties' (bidentate ligands which coordinate to two phthalocyanine metal sites) to produce a molecular crystal with permanent microporosity and BET surface areas in the range $850\text{--}1000 \text{ m}^2 \text{ g}^{-1}$.²⁹

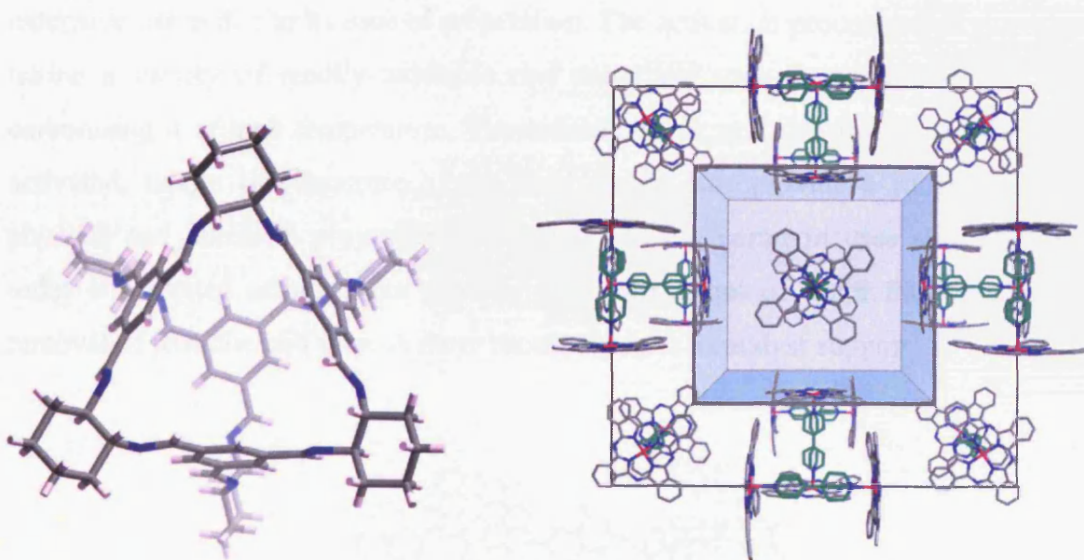


Figure 1.6 Left: Cooper's molecular cages³⁰. Right: Phthalocyanine nanoporous molecular crystals.²⁹

1.5 Amorphous microporous materials

1.5.1 Activated Carbon

Crystalline order is not a prerequisite for microporosity, as exemplified by one of the most widely used commercial microporous materials, activated carbon, which has been used throughout history as an adsorbent for the purification of water. Activated carbon is described as “a wide range of amorphous carbon-based materials prepared to exhibit a high degree of porosity and an extended interparticulate surface area” by Bansal, in his book titled “Activated Carbon”³². These remarkable materials are highly adsorbent and have a wide range of applications³³⁻³⁵. Their ability to act as adsorbents is primarily due to their extensive porosity and very large surface areas, reported to be in the range of 400-2500 m² g⁻¹ (some special cases >4000 m² g⁻¹).³⁶ High surface area and porosity make activated carbons useful for many applications including filtration³⁷, purification³⁸, deodorization³⁹, decolourisation⁴⁰, and separation³². Its extensive use is due to its ease of preparation. The activation process usually involves taking a variety of readily available raw materials, such as wood and coal, and carbonising it at high temperature. The source chosen, and the degree to which it is activated, tailors the structure of the final material to provide a range of useful physical and chemical properties⁴¹. One of the most common uses still employed today is activated carbon in its granular form as a means of water filtration, for the removal of particles and ions. A more recent use is as a catalyst support⁴².

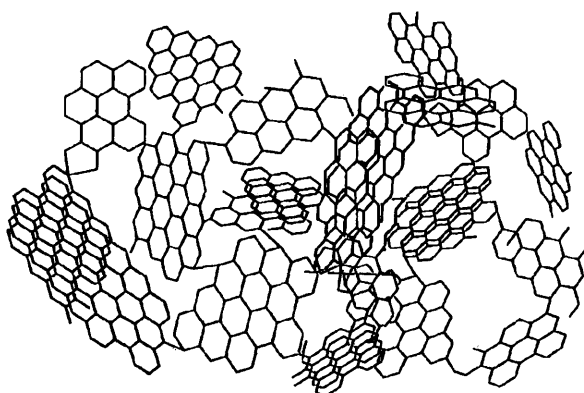
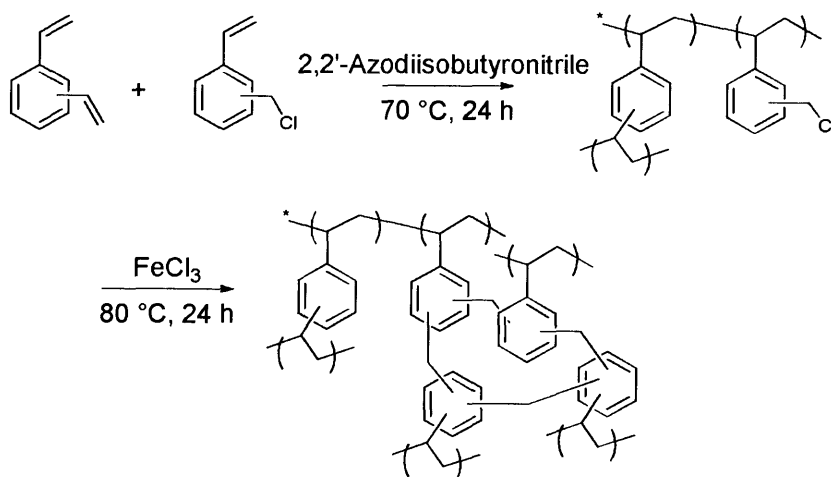


Figure 1.7 Illustration of activated carbon graphene porous-network

The structure of activated carbon is not fully understood, but generally believed to consist of randomly arranged hexagonal graphene sheets that are cross-linked by non-graphitised aliphatic units, to create a polymer network that cannot fill space efficiently (Figure 1.7). This results in a rigid nanoporous structure that is intrinsically microporous⁴³. Due to the harsh nature of the activation process, most activated carbons consist of a range of pore sizes, from ultramicropores ($< 0.7 \text{ nm}$)⁴⁴, micropores ($< 2 \text{ nm}$), mesopores ($2\text{-}50 \text{ nm}$) to macropores ($> 50 \text{ nm}$). This range of pore sizes, and the variety of residual oxygen and nitrogen containing functional groups present on the surface^{45,46} is likely a large contributing factor to activated carbons ability to adsorb a wide range of organic compounds and metal ions.

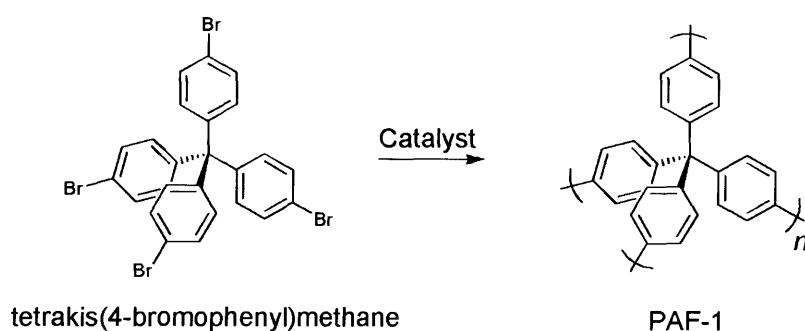
1.5.2 Hypercrosslinked and network dependant microporous polymers

Microporous network-polymers have previously been reported^{11,12,47-51}, with some polystyrene based cross-linked polymers achieving apparent BET surface areas in excess of $2000 \text{ m}^2 \text{ g}^{-1}$,^{11,52,53} and another hypercrosslinked polymer (HCP) resin achieving an impressive $3.04 \text{ wt } \%$ hydrogen uptake (at 77 K , 15 bar)⁵⁴. One well-established example of the synthesis of a HCP is that by Davankov, in which a swollen chloromethylated polystyrene is cross-linked *via* a Friedel-Crafts alkylation (Scheme 1.3).^{55,56}



Scheme 1.3 Hypercrosslinked polystyrene synthesis using Friedel-Crafts alkylation.

The cross-linking process yields the material initially as a solvent-swollen gel^{53,56}, which on removal of the solvent, displays permanent porosity. The microporosity within these HCPs originates from the template effect of the solvent molecules trapped within the polymer network as it forms, whereas the larger pores are due to phase separation of the growing polymer network from the solvent. The mechanism of micropore formation within HCPs appears closely related to that which occurs to give molecularly imprinted polymers (MIPs), in which a highly cross-linked polymer network is prepared around template molecules of interest, so that when the template is removed a receptor site of the correct size, shape, and binding functionality is obtained.⁵⁷ Therefore, the microporosity in MIPs and HCPs has been described as “extrinsic” with the relatively soft polymer matrix being moulded around a rigid template.⁵⁸



Scheme 1.4 PAF-1 synthesis.

A recent network polymer derived from tetrakis(4-bromophenyl)methane (PAF-1, Scheme 1.4) *via* an aryl-aryl coupling reaction is a semi-ordered 3D network polymer, whose structure has a tendency towards that of the diamond topology. Due to the non-reversible catalytic polymerisation the structure is not formed in an ordered crystalline state. The polymer does, however, have a reported apparent BET surface area of $5600 \text{ m}^2 \text{ g}^{-1}$, which makes it one of the highest reported for any material.⁵⁹

Another recent example of organic microporous network polymers are the conjugated microporous polymers (CMPs) introduced by Cooper.⁶⁰ In a similar fashion to the crystalline microporous MOFs and COFs, these CMPs have been demonstrated to have tuneable micropore size distribution and surface area by varying the length of the rigid organic linkers, but unlike MOFs and COFs, they have good thermal

stability, and also chemical stability towards weak acids (HCl) and bases (NaOH)⁶¹. The currently highest apparent BET surface area reported for this class of polymers was for CMP-0 (Figure 1.8),⁶² with an impressive $1018 \text{ m}^2 \text{ g}^{-1}$. Perhaps more importantly though is the structures inherent alkyne group, residual functionality from the Sonogashira-Hagihara coupling,⁶³ which opens the possibility for the introduction of further functionality, such as halides, to enhance gas storage properties⁶². Cooper *et al.* have also more recently published network polymers based on the same Sonogashira-Hagihara coupling incorporating various tetrahedral carbon- and silicon-centred monomers resulting in apparent BET surface areas ranging 488 to $1213 \text{ m}^2 \text{ g}^{-1}$ for E1 (Figure 1.8),⁶⁴ again demonstrating the potential for tuneable microporous polymers.

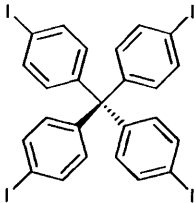

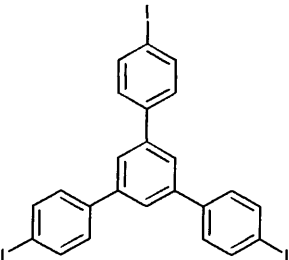
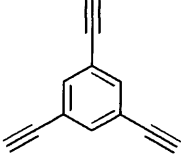
	Halogen monomer	Ethynyl monomer	BET surface area m^2/g
E1			1213
CMP-0			1018

Figure 1.8 Monomers for Sonogashira-Hagihara coupling polymerisation. E1⁶⁴, CMP-0⁶².

1.5.3 Amorphous Molecular Microporosity

In a similar fashion to the microporous dendrimers and organic molecules reported here, further evidence for this new area of microporous materials was offered by MacLachlan *et al.*⁶⁵ These amorphous (or near-amorphous) molecular microporous materials owe their microporosity to the free volume generated by the space blocking groups around the triptycene centre. A series of triptycene based metal-salphenes were

reported, with one example (Figure 1.9) exhibiting an apparent BET surface area of $499 \text{ m}^2 \text{ g}^{-1}$.

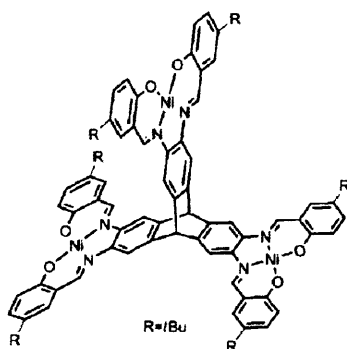


Figure 1.9 A triptycene-based microporous molecule, lacking both crystalline or polymeric long range order with an apparent BET surface area of $499 \text{ m}^2 \text{ g}^{-1}$ (N_2 , 77 K).⁶⁵

1.6 Polymers of Intrinsic Microporosity (PIMs)

The class of polymers dubbed Polymers of Intrinsic Microporosity (PIMs) have potential for a number of useful technologies. Unlike hypercrosslinked polymers, these polymers contain a monomer with “internal molecular free volume” (IMFV),⁶⁶ that when placed in a rigid polymer system results in intrinsic microporosity (IM). The latter has been defined as “a continuous network of interconnected intermolecular voids, which forms as a direct consequence of the shape and rigidity of the component macromolecules.”^{67,68}

1.6.1 Internal Molecular Free Volume (IMFV)

The term IMFV was devised by Swager⁶⁶, and describes the free volume of a rigid three-dimensional molecular structure. The initial example was for triptycene, whose rigid aromatic faces sweep out an area of guarded space defined as its internal free volume. Swager proposed an estimate of this IMFV by measuring geometrically the minimum volume obtained by the intercepts of straight lines resting on the rigid aromatic leading edges (hydrogens) of the triptycene unit (Figure 1.10).

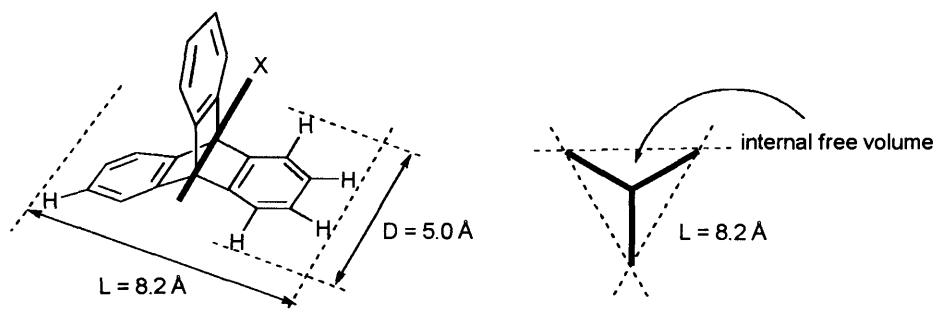
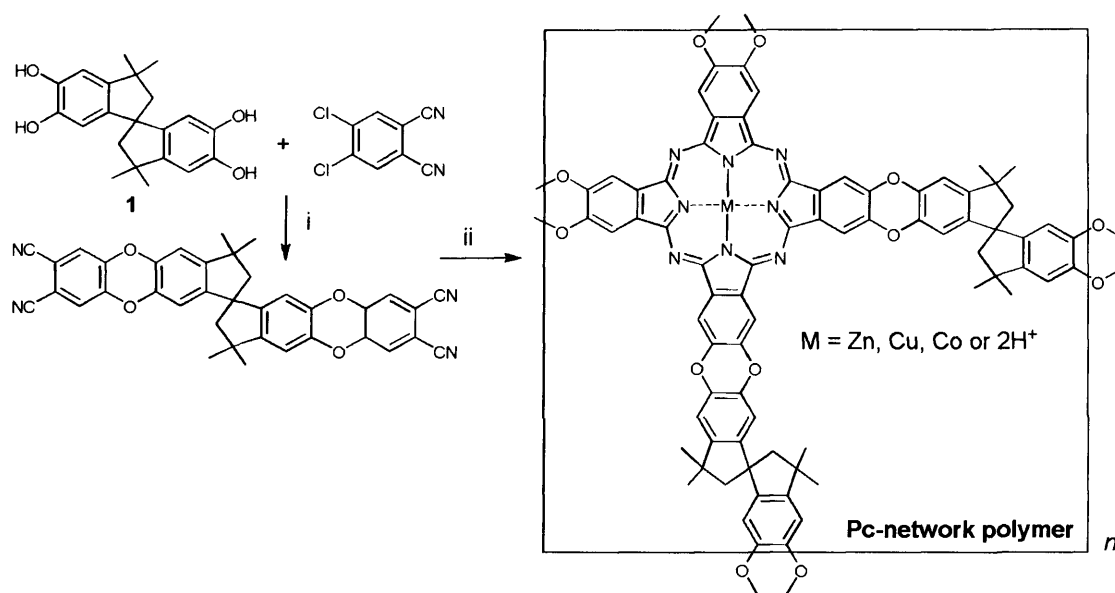


Figure 1.10 Swagers proposed internal molecular free volume of triptycene.⁶⁶

Perspective view (*left*), top down view (*right*).

1.6.2 Phthalocyanine Network-PIMs⁶⁹

Many examples of phthalocyanine network polymers had previously been synthesised from the cyclotetramerisation of bis-phthalonitriles,⁷⁰ but all resulted in non-porous materials.⁷¹ A likely explanation for this is the strong non-covalent interactions (primarily π - π interactions) between the aromatic, planar macrocycles. This causes them to aggregate into tightly packed columnar stacks, maximising these inter-macrocycle interactions. By addressing the challenge of designing a network system that restricted the phthalocyanine's ability to stack in columns or flat planes, the McKeown group came up with the novel idea of interlinking the macrocycles *via* rigid, fused ring spacers that contained a site of contortion. A perfect precursor for achieving this feat is 5,5',6,6'-tetrahydroxy-3,3,3',3'-tetramethyl-1,1'-spirobisindane **1** that possesses two sets of *ortho*-hydroxyl groups capable of forming the dioxane fused ring linkage on reaction with 4,5-dichlorophthalonitrile to give a bis-phthalonitrile. Also crucial is its central spiro-carbon (i.e. a single atom shared by two rings), which causes the equivalent aromatic rings, including the resulting phthalocyanine units of the polymer, on either side of the spiro-centre to have a dihedral angle of near 90°. The fused rings prevent rotational freedom along the resulting polymer backbone. As a result of these structural features the phthalocyanine network polymers (Scheme 1.5) demonstrate apparent BET surface areas in the range 535-895 m² g⁻¹ (N₂ adsorption, 77 K).⁶⁹

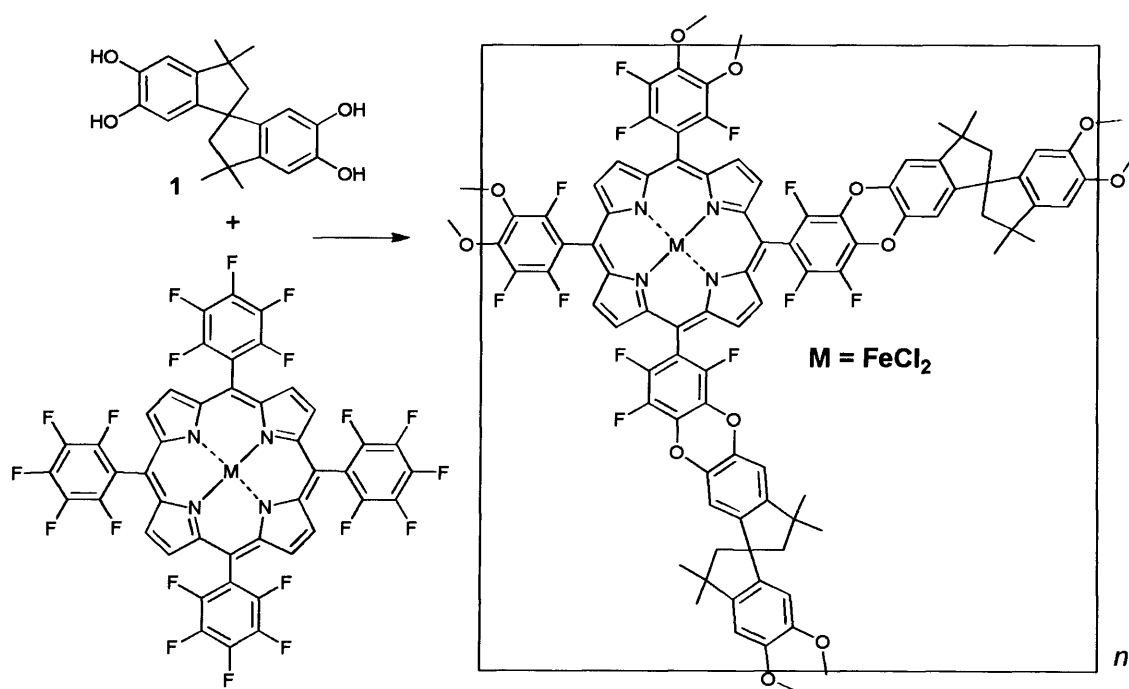


The phthalocyanine network polymer showed a far lower proportion of mesopores (>2 nm) than other amorphous materials with similar surface areas such as activated carbon. The lack of mesopores in the Pc-network polymer showed experimentally, a higher selectivity than activated carbon for the uptake of organic molecules, by excluding larger compounds (i.e. naphthalene-based dyes of diameter > 1 nm) whereas smaller molecules such as phenols are readily adsorbed.⁷² Similar phthalocyanine-based networks were found to act as heterogeneous catalysts.¹⁸

1.6.3 Porphyrin-based network-PIMs⁷³

Following on from the success of the phthalocyanine network-PIMs, a similar methodology was employed for another aromatic macrocycle, porphyrin. Porphyrins facilitate some of nature's most important chemical processes including photosynthesis, oxygen transport and catalytic oxidations.^{73,74} The possibility of useful heterogeneous catalysis makes porphyrins desirable components of microporous materials. For this reason, and to provide further conclusive proof that this methodology of synthesising rigid-contorted network polymers can provide intrinsic microporosity to an otherwise non-porous system, a porphyrin-based network PIM was synthesised by the direct benzodioxane-forming reaction between

meso-tetrakis-(2,3,4,5-pentafluorophenyl)porphyrin and monomer **1** (Scheme 1.6). The resulting polymer is not completely composed of fused rings as was the case with the phthalocyanine network polymers, as there is a single covalent bond between the porphyrin macrocycle and the aryl ring at the *meso*-position of the porphyrin which forms part of the linking group between macrocycles. Rotational freedom around this single carbon-carbon bond is however fairly restricted, and the resulting network is unable to relax into a non-porous configuration, as demonstrated by the reported apparent BET surface area of almost $1000 \text{ m}^2 \text{ g}^{-1}$.⁷³ Introduction of iron-cations into the central cavity of the porphyrin gave the resulting network-PIMs catalytic activity.¹⁸

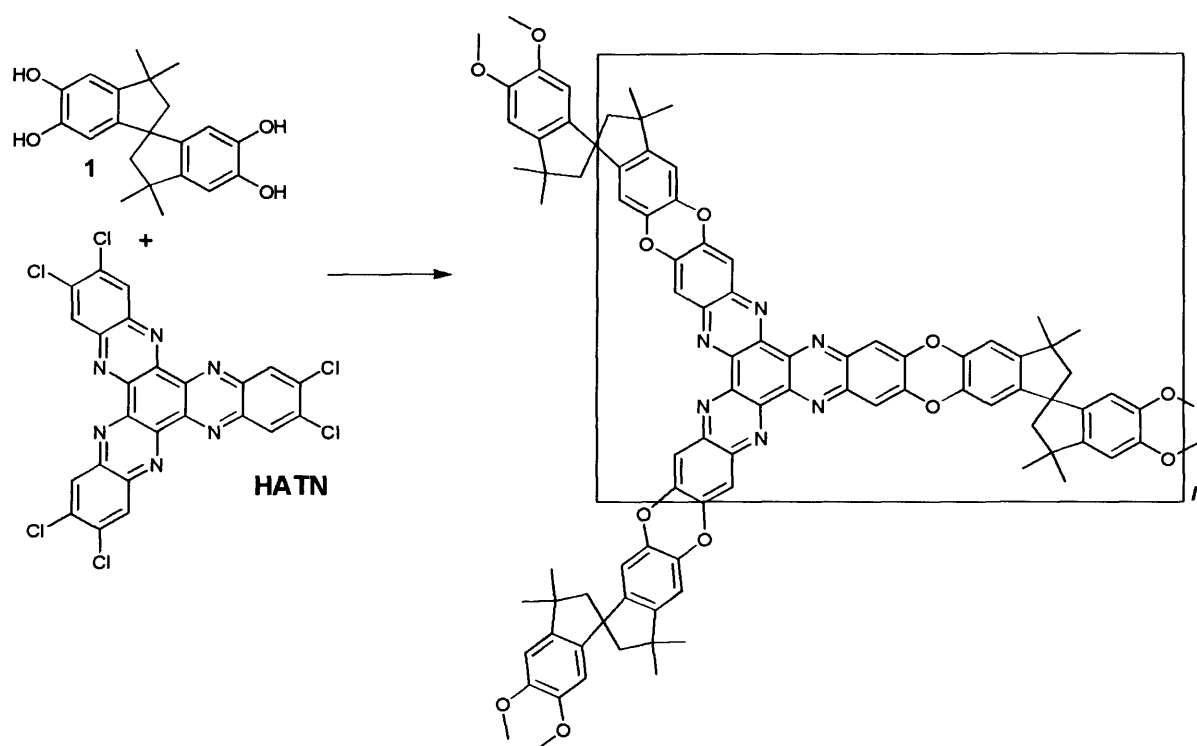


Scheme 1.6 Porphyrin-based Network-PIM formation.

Reagents and conditions: i K₂CO₃, DMF, 120 °C.

1.6.4 HATN network-PIM⁷⁵

By condensing hexaketonecyclohexane and 4,5-dichlorophenylene-1,2-diamine, the planar 2,3,8,9,14,15-hexachloro-5,6,11,12,17,18-hexaazatrinaphthylene (**HATN**) monomer can be obtained.⁷⁶⁻⁷⁸ It readily reacts with monomer **1**, to form a **HATN** based network-PIM (Scheme 1.7).⁷⁵



Scheme 1.7 Synthesis of **HATN**- network-PIM.

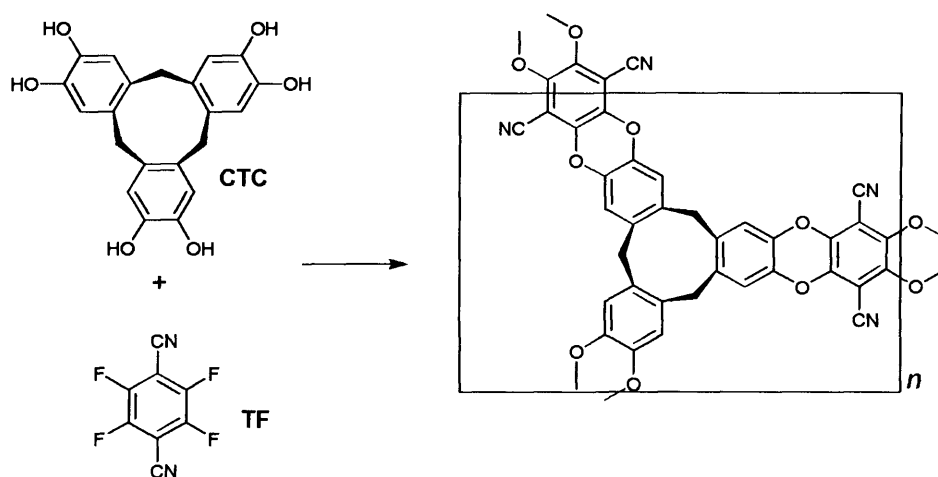
Reagents and conditions: K_2CO_3 , DMF, 120 °C.

The apparent BET surface area for the **HATN** derived polymer was reported to be in the range $750\text{--}850\text{ m}^2\text{ g}^{-1}$, with a characteristic adsorption isotherm consistent with microporosity. The **HATN** unit was shown to have the ability to bind to palladium(II)dichloride, and still remain microporous (albeit with a reduced BET surface area of $347\text{ m}^2\text{ g}^{-1}$), illustrating its potential for heterogeneous catalytic studies. It also displayed the ability to adsorb phenol from water, in solutions with concentrations of 0.2 mol/L , it was able to adsorb $\sim 5\text{ mmol/g}$ comparable to the best activated carbons.⁷⁵

1.6.5 CTC derived Network-PIM¹⁵

In the context of hydrogen adsorption PIMs may offer an attractive combination of properties including low intrinsic density (they are composed of only light elements- C, H, N, O- a real advantage over MOF materials), chemical homogeneity (an advantage over carbons), thermal and chemical stability, and synthetic

reproducibility. Of particular interest is the potential to tailor the micropore structure by choice of monomer precursors, for example, by the use of monomers that contain pre-formed cavities to provide sites of an appropriately small size for hydrogen adsorption. To investigate this possibility, the bowl-shaped receptor monomer, cyclotricatechylene (CTC)⁷⁹, was incorporated within a network-PIM by again using 2,3,5,6-tetrafluoroterephthalonitrile (TF) in the S_NAr benzodioxane fused ring forming reaction (Scheme 1.8).¹⁵



Scheme 1.8 CTC derived network polymer formation.

Reagents and conditions: K_2CO_3 , DMF, 65 °C.

The N_2 -adsorption properties of the resulting material, designated **CTC**-network-PIM were comparable to those of **HATN**-network-PIM (Table 1.1) but, notably, the **CTC**-derived PIM has an increased ability to successfully adsorb hydrogen (nearly 9% increase of H_2 uptake at 10 bar, 77 K). This indicates that not only the overall packing and surface area of the polymer is important for enhanced H_2 uptake, but also the shape and magnitude of the internal free volume (IFV) of the incorporated monomers.

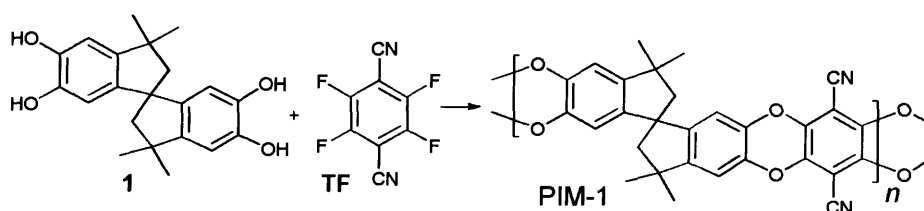
PIM	BET Area ($m^2 g^{-1}$)	% mass H_2 (1 bar, 77K)	% mass H_2 (10 bar, 77 K)	H_2 per fused ring
HATN	820	1.37	1.56	0.43
CTC	830	1.43	1.70	0.56

Table 1.1 Gas adsorption data for **CTC** and **HATN** based PIMs.

1.6.6 Non-network PIMs

The microporous materials discussed so far consist of insoluble polymer networks, crystalline MOFs and COFs (the dissolution of which would disassemble the material), insoluble activated carbons, and silicates. All of these materials have good microporosity, and adsorbent capabilities, but due to their inability to be dissolved, processability and full characterisation by solution-based methods is impossible.

Using the same concepts and synthetic methodology as used successfully for network-PIMs (rigid and contorted structures, incorporating monomers of high IFV), a set of soluble polymers has been synthesised and studied⁸⁰, the most studied of which is **PIM-1** (Scheme 1.9).^{1,81}



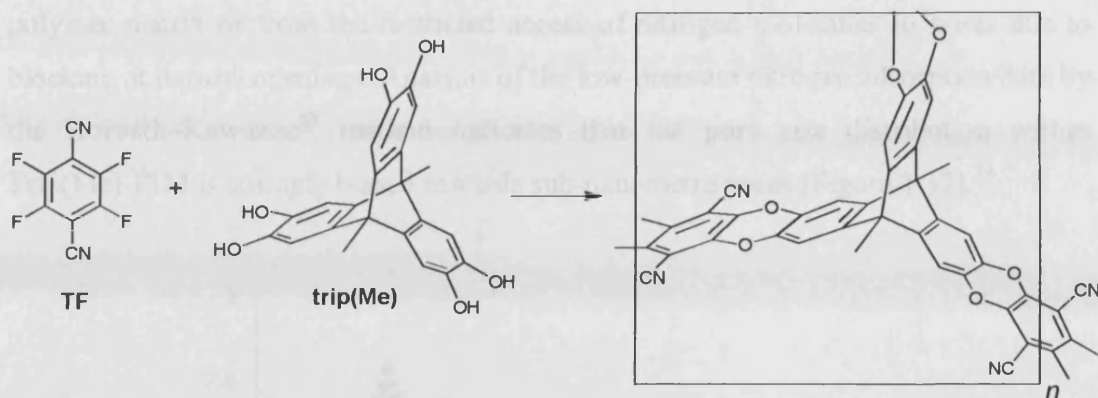
Scheme 1.9 Synthesis of **PIM-1**. Reagents and conditions: K_2CO_3 , DMF, 65 °C.

Generally non-network polymers pack space efficiently, as their mobile chains can bend and twist to arrange themselves in close contact to maximise molecular interactions, generating amorphous non-porous materials. The combination of the “site of contortion” (i.e. spiro-centre), IFV, and the rigidity of the dibenzodioxane ring formed during the polymerisation, produces a non-network polymer that cannot re-orientate itself to pack space efficiently in the solid state.⁸⁰ This lack of mobility retains the free volume between polymer strands, keeping an open structure in which the IFV around the spiro-centre is accessible, resulting in a microporous material (BET surface area of $780 \text{ m}^2 \text{ g}^{-1}$, N_2 , 77 K⁸⁰) which is soluble in common organic solvents (e.g. THF, chloroform). The solubility means that unlike network-PIMs which can only be characterised by IR spectroscopy, thermal gravimetric analysis (TGA), BET and elemental analysis, these PIMs can also be further studied by solution NMR and gel permeation chromatography (GPC). Much research has been conducted around **PIM-1**, including synthesis optimisations,⁸²⁻⁸⁴ and its ability to cast

a free-standing film. The resulting flexible free-standing films are suitable for study as microporous membranes for selective gas-permeability, with excellent results.^{1,8-10,85,86} Due to the potential of this new class of microporous polymers, research has been carried out to modify the monomers used for synthesis, for example, extensive work was carried out to replace the methyl groups of the spirobisindane used in **PIM-1** with bulky rigid fluorene groups to enhance the IFV of the monomer, resulting in a slightly higher BET surface area of $895 \text{ m}^2 \text{ g}^{-1}$, but losing the film-forming capability.⁸⁷

1.6.7 Triptycene derived PIMs

The most microporous amorphous network reported to date using the concept of intrinsic microporosity (IM) is that derived from 9,10-dimethyl-2,3,6,7,12,13-hexahydroxytriptycene, **Trip(Me)-PIM** (Scheme 1.10), which demonstrates an apparent BET surface area of $1730 \text{ m}^2 \text{ g}^{-1}$.¹⁴ Consideration of a molecular model of an ideal fragment of Trip(Et)-PIM (Figure 1.11) reveals that the triptycene component clearly provides the necessary nonlinearity required for microporosity, a role performed by the spiro-centre in **PIM-1** (Scheme 1.9) and the **HATN-PIM** (Scheme 1.7), or the bowl-shaped subunit in the **CTC-network** (Scheme 1.8). Furthermore, the shape of the triptycene monomer also constrains the growth of the polymer within the same plane to provide a rigid macromolecular structure with large concavities. The faces of the ribbon-like “struts” between the triptycenes are oriented perpendicular to the plane of the macromolecular growth. It is possible that this arrangement blocks face-to-face association between these planar struts, leading to greater IM. For this network there is also likely to be a significant contribution to the IM from macrocycles.



Scheme 1.10 Synthesis of trip(Me)-PIM. *Reagents and Conditions:* K_2CO_3 , DMF, 65 °C.

A series of triptycene based PIMs was synthesised and showed a successive decrease in surface area with increased alkyl chain length at the bridge head carbon (Table 1.2).⁵

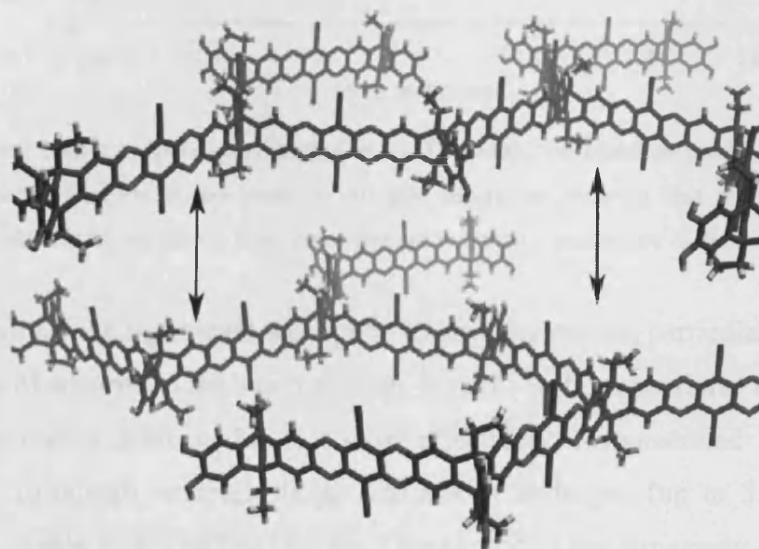


Figure 1.11 Representation of two ideal fragments of the network of Trip(Et)-PIM showing how the shape of each macromolecule, as dictated by the architecture of the triptycene units, prevents close intermolecular interactions between the planar "struts". The loose network which arises from the ideal layered structure may account for the tendency of the materials to swell in organic solvents or during nitrogen adsorption, as indicated by the arrows.⁵

The adsorption isotherm displays a remarkably distinct hysteresis extending to low partial pressures between the adsorption and desorption cycles (Figure 1.2). This indicates that there is activated adsorption arising either from a swelling of the

polymer matrix or from the restricted access of nitrogen molecules to pores due to blocking at narrow openings. Analysis of the low-pressure nitrogen adsorption data by the Horvath–Kawazoe⁸⁸ method indicates that the pore size distribution within Trip(Me)-PIM is strongly biased towards sub-nanometre pores (Figure 1.12).¹⁴

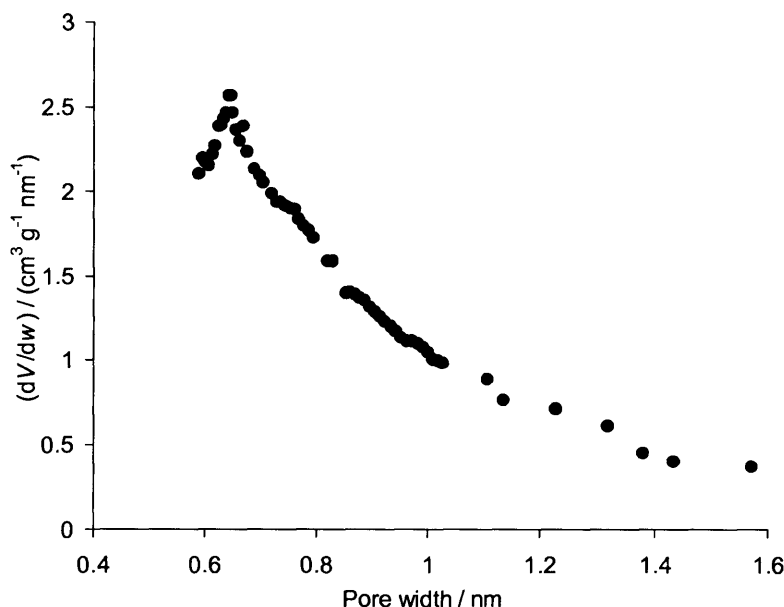


Figure 1.12 Micropore size distribution for Trip(Me)-PIM based on the Horvath-Kawazoe analysis of low-pressure nitrogen adsorption showing that the major contribution to porosity is from pores that are less than a nanometre in diameter.¹⁴

A requirement for the significant adsorption of gaseous probes, particularly those with low enthalpy of adsorption such as hydrogen, is multi-wall interactions. For hydrogen, smaller pore widths achieve this feat most effectively, demonstrated by Trip(Me)-PIMs ability to adsorb relatively large amounts of hydrogen (up to 3.2 % mass at 10 bar, 77 K, Table 1.2). The fact that the Trip(Me)-PIM has a majority of its pores in the sub-nanometer range means that these micropores are suitable for the adsorption of hydrogen at relatively low pressure – potentially one use of which could be in hydrogen storage applications,^{5,58} an area of research that is receiving much interest due to its crucial role in the inception of a ‘hydrogen economy’. However, it is worth noting that the performance of triptycene-based PIMs are far from that demanded by the target set by the United States Department of Energy (DOE) of 9 weight % by 2015.⁸⁹

Side chain	BET area (m ² g ⁻¹)	N ₂ uptake (mmol g ⁻¹)	Density (ml g ⁻¹)	H ₂ uptake, 77 K, mmol/g (%mass)	
				1 bar	10 bar
Me	1760	42.2	1.67	8.90 (1.79)	15.6 (3.2)
Et	1416	39.5	1.40	8.33 (1.68)	13.7 (2.8)
Pr	1343	32.1	1.40	7.69 (1.55)	12.2 (2.5)
Bu	978	23.8	1.48	6.55 (1.32)	10.3 (2.1)
Pent	947	17.9	1.48	5.61 (1.13)	8.8 (1.8)
Oct	618	11.6	1.27	3.67 (0.74)	6.0 (1.2)

Table 1.2 Gas Adsorption Data for the Trip(R)-PIM series.⁵

1.7 Dendrimers

1.7.1 Origins

In 1952 Flory hypothesised about designing a system of highly branched, but well defined polymers suitable for investigations to determine the influence that non-linearity has on the physical properties of macromolecules.⁹⁰ Flory concluded that by using a monomer with a single functional group A of one type, and two or more of another type B, it would be possible to grow a polymer that started from a single point and became progressively more branched (Figure 1.13). Such a monomer was termed AB₂.

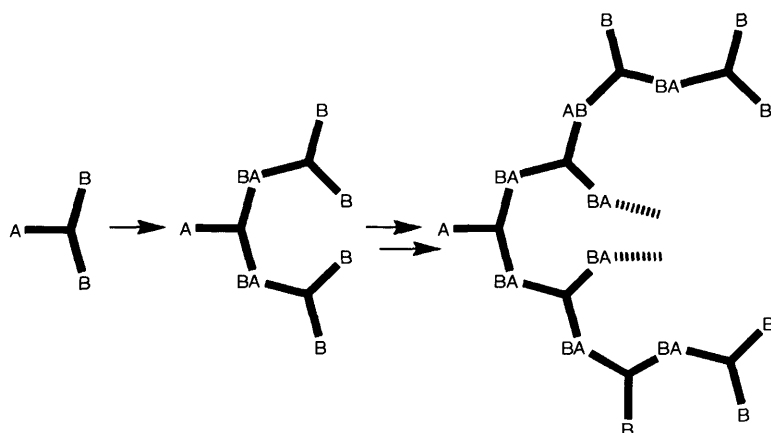


Figure 1.13 Illustration of Flory's⁹⁰ hypothesis for highly branched polymer growth using an AB_2 monomer. Some segments omitted for clarity.

As the idea progressed, these types of macromolecules converging on a single functional point became known as dendrons, and their more symmetrical cousins as 'starburst polymers'⁹¹. The term 'dendrimer' is now more commonly used to describe highly branched, monodisperse macromolecular compounds, owing to the Greek word *dendra* for tree.⁹² The principle behind the first dendrimers was a simple extension of that of the AB_2 type polymer formation, in which two or more of these branches grew from a central point, known as the dendrimer core, to give a radial arrangement. As the layers are added the molecule becomes increasingly more spherical and monodisperse.

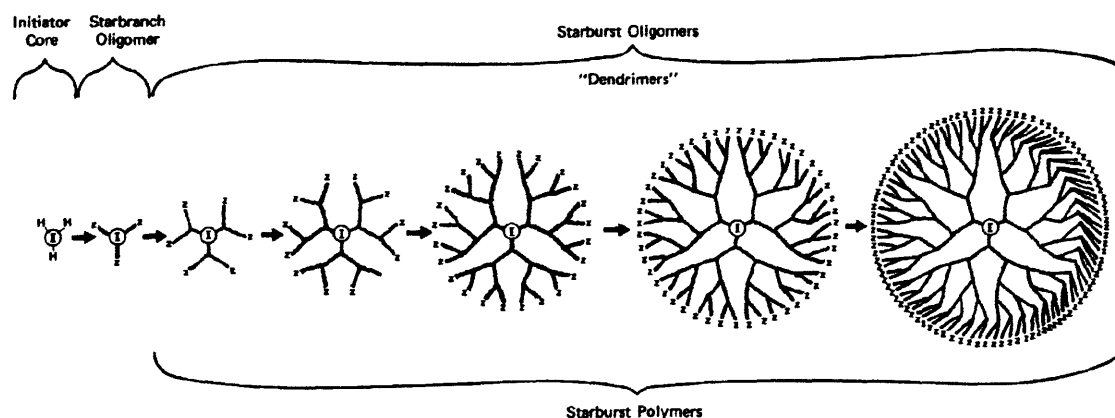


Figure 1.14 Illustration of a growing dendrimer.⁹¹

1.7.2 Divergent dendrimer growth

This original approach using AB_x monomers is known as *divergent* dendrimer growth, starting from the core and working outward, successive branch units are attached to the outer shell. Although very large dendrimers have been prepared in this way, incomplete growth steps and side-reactions lead to slightly imperfect samples.⁹² These divergently grown dendrimers are virtually impossible to purify as they have only minor structural differences to their by-products.

Each time a branch unit is attached to the core the dendrimer is assigned a generation number 'n' where the core and one level of branching is $n = 0$ (note: $n = 1$ was the system proposed by Tomalia and is still used for his PAMAM dendrimers but it is now conventional to use the number of branch units between core and terminal group to define generation, as is done throughout this thesis).⁹² The generation number is a measure of the size and extent of branching, and helps to quickly describe a dendrimer. As the generation number increases, the number of monomers in the dendrimers outer shell increases exponentially. This growth can continue up until the steric limit which describes the highest possible generation number attainable for a given dendrimer. This limit owes to the fact that the exponentially increasing monomers in the outer shell only have an increase in available space that is related to the cube of the generation number, eventually arriving at the point where no more space is available for dendrimer growth.⁹³

1.7.3 Convergent dendrimer growth⁹⁴

The convergent method was developed some years after the divergent approach, in an attempt to overcome many of the weaknesses inherent with previous dendrimer synthesis.^{92,94-98} The convergent growth process begins with what will later become the terminal group at the surface of the completed dendrimer, and works inwards to a non-functional focal point which can later be activated to 'converge' on the chosen core in a final step. The main advantage of this method is the ability to more readily isolate and purify the extended dendrons, in preparation of completing the final dendrimer. The completed dendrons are usually three or more times smaller

(depending on the functionality of the core) than the final dendrimer, thus more easily distinguished and separated from their by-products. The convergent method does have its own problems however, with each successive step requiring purification and loss of mass (where as the divergent method increasingly gains mass). Both methods were exercised in this project and both suffer from the problems described above.

1.7.4 Functions and advantages of dendritic macromolecules

Attempts have been made to functionalise dendrimers of different designs towards all sorts of applications,^{99,100} including light sensing,^{101,102} organic light emitting diodes (OLEDs),^{103,104} liquid crystals,^{105,106} catalysis,¹⁰⁷ membrane flow catalysis,¹⁰⁸ molecular containers for guest molecules,¹⁰⁹⁻¹¹¹ and drug delivery¹¹²⁻¹¹⁶ to name but a few. Most of the applications are based around the shape of aggregating dendrimers, which is often in columnar stacks for low generation numbers, which can be tuned to spherical macrostructures by increasing the generation number.^{117,118} Within the surface of the dendrimer is a microenvironment which is often dependant on solvent to retain its shape. Herein we investigate the possibility of developing rigid dendritic structures that retain their shape even under vacuum (i.e. shape-persistent), in an attempt to generate microporous materials.

1.8 Objectives

Polymers of intrinsic microporosity (PIMs) have shown significant adsorption and membrane separation selectivity. Of all these previously reported PIMs, the network Trip-PIM series offers the highest level of accessible micropores (as illustrated by the BET surface area). In an attempt to build on this success the main focus of this project was to synthesise a range of triptycene based monomers.

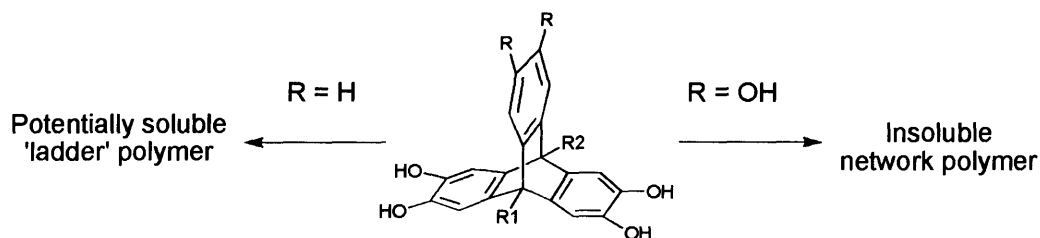


Figure 1.15 Triptycene with functionality $f = 2$ ($\text{R} = \text{H}$), and $f = 3$ ($\text{R} = \text{OH}$).

Triptycene of the type used in the Trip-PIM series contains 6 hydroxy groups, and a pair of alkyl chains on the bridgehead carbons ($\text{R} = \text{OH}$, $\text{R1} = \text{R2} = \text{alkyl chain}$; Figure 1.15). As illustrated by the study of the affect of alkyl chain length on the microporosity of a network Trip-PIM, it is clear that the alkyl chain does not enhance microporosity. The presence of longer alkyl chains instead adds unnecessary weight, coupled with the pore blocking effect of having a flexible mass residing in the area surrounding the triptycene. For these reasons it was decided that the first objective would be to introduce other less flexible components on the bridgehead carbons, with the hope of inducing more IFV, and introduce new functional groups for further processing, such as attaching a catalyst to the polymer. The previously reported triptycene based polymers have all been symmetrical with respect to the alkyl chains present on the bridgehead carbons (ranging from methyl to pentyl), so it was our aim to develop a system where two different groups could be introduced to allow more flexibility in the functionality of the triptycene monomers (i.e. $\text{R1} \neq \text{R2}$; Figure 1.15)

Previously reported triptycene polymers were also all based on the triptycene monomer with functionality $f = 3$ (i.e. 3 pairs, 6 total hydroxy groups), forming insoluble networks. In order to form a membrane for gas separation techniques a ladder polymer must be synthesised from monomers with $f = 2$ (i.e. $\text{R} = \text{H}$; Figure 1.15). Unfortunately there had been little success in the past of forming soluble triptycene polymers, so this area was decided to be a good place to begin the study.

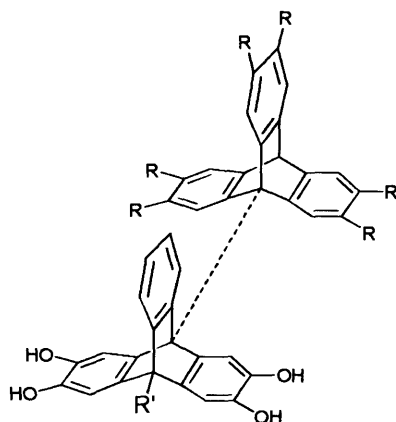


Figure 1.16 Target bitriptycene system, where the secondary triptycene can act as a bulky side group ($R = H$), or to increase the functionality of the monomer ($R = OH$).

Since the Trip-PIM was the basis for the highest performing PIM to date (with respect to apparent BET surface area), it was decided that network monomers would also be targeted with varying levels of functionality and side chain substituent's that may enhance porosity in the final polymer. By increasing the functionality f of the monomers above the previously used $f = 3$ it was hoped there might be scope for restricting flexibility and freedom of the final network system leading to decreased packing efficiency (and greater accessible porosity). It was also hoped that by introducing an aryl or triptycene unit (at the bridge head carbon, $R1/R2$; Figure 1.15, example of proposed bitriptycene: Figure 1.16) stacked above the triptycene that forms the polymer backbone we would be able to reduce the ability of polymer fragments to stack on top of each other.

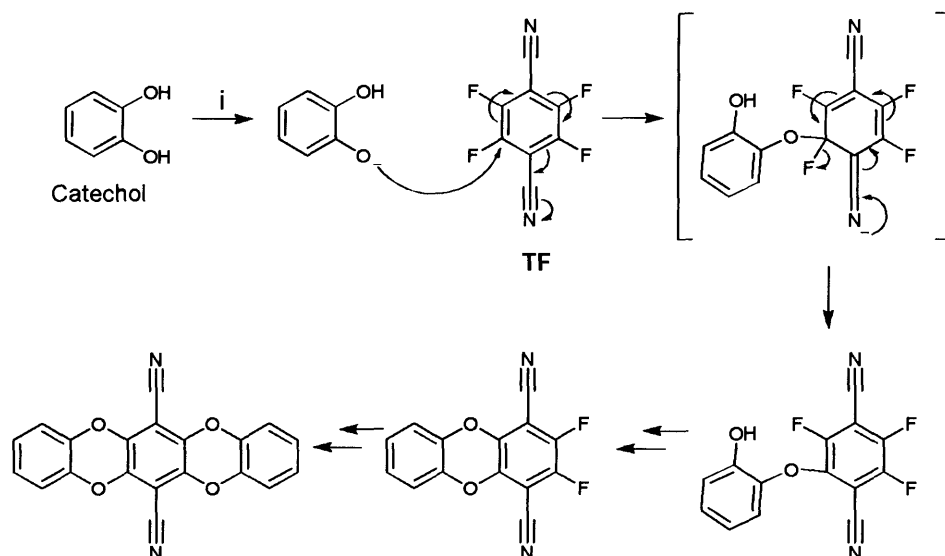
The final area for interest at the outset of the project was to investigate the possibility of taking the success of triptycene based network polymers and incorporate them into dendrimers and large organic molecules. We also set out to try and evaluate what features of triptycene make it so successful in generating high levels of free volume, and investigate related high IFV moieties that have potential to build on this success.

Chapter 2: Ladder Polymers

2 Ladder polymers

The polymers described in this chapter are derived from reaction mixtures containing two or more monomers with an overall average functionality (f) of two, comprised either of a monomer with two catechol units (i.e. *ortho*-1,2-dihydroxybenzene) or two *ortho*-dihalogenated aromatic rings. The method of polymerization is step-growth, with the bond-forming reaction being a double nucleophilic aromatic substitution reaction (S_NAr) to provide a fused-ring dioxane group, which suggests the 'ladder' nomenclature for the resulting polymer. The average functionality (f) of two means that these polymers have the possibility of being soluble in common organic solvents as they cannot form intractable network polymers.

In order for the reaction to proceed readily under mild conditions, the aromatic ring(s) of the halogen-containing monomer must carry electron-withdrawing groups (in this case nitrile) in order to activate the S_NAr mechanism. For all of the reactions used in the present study the leaving group is the highly electronegative fluorine atom chosen for its ability to act as an efficient leaving group in S_NAr reactions. This behaviour is ascribed to its electronegativity, which draws electron density from the adjacent aromatic carbon helping to direct the nucleophilic attack at this position. To illustrate this reaction, catechol was reacted with 2,3,5,6-tetrafluoroterephthalonitrile in the presence of K_2CO_3 as base (Scheme 2.1).



Scheme 2.1 Mechanism for double S_NAr in dioxane fused-ring formation.

Reagents and conditions: i K_2CO_3 , DMF, 65 °C.

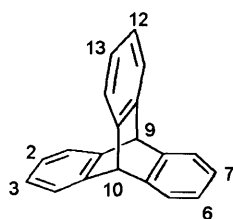
The fast and efficient reaction rates experienced for polymer synthesis using 2,3,5,6-tetrafluoroterephthalonitrile (TF) can best be shown by the optimization experiments conducted by Guiver *et al.* which showed that **PIM-1** of a number average molecular mass (M_n) of 102,000 can be achieved in a reaction time of only 8 min.⁸³

2.1 Monomers for triptycene ladder polymers

The major focus for this project was to prepare and analyse a range of triptycene monomers for microporous materials with varying substituents and functionality. Triptycene derivatives are most commonly synthesised *via* a Diels-Alder cycloaddition reaction between an anthracene (diene) and a benzyne (dienophile), so we set out to modify these precursors to provide us with a range of substituted triptycenes.

For the target monomers, the required substituents attached to the 2,3,6,7,12 and 13 carbons of triptycene (as numbered by the conventional nomenclature system – Scheme 2.2) are *o*-hydroxy groups, which can be prepared directly from methoxy group by demethylation. The ability to introduce one, two, or three pairs of *o*-methoxy groups on triptycene means that it can act as a precursor to a terminal group, ladder

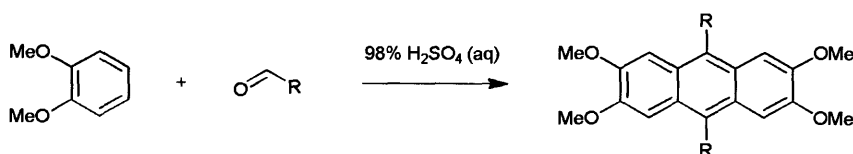
polymer, or network polymer (or core for a dendrimer), respectively. The desired substituents at the 9 and 10 bridgehead positions are alkyl chains (or phenyl rings), which can be the same (symmetrical) or different (unsymmetrical).



Scheme 2.2 Triptycene numbering system

2.1.1 Synthesis of symmetrical anthracenes

The previously reported anthracene **2** (Scheme 2.3, R = ethyl) had been used in the construction of trip(Et)-PIM.⁵ The anthracene was produced by an acid catalysed condensation between propionaldehyde and veratrol. The methoxy groups of the veratrol provide both an electron-rich aromatic ring (essential to drive the condensation forward), and the source of the hydroxyl groups in the final monomers. For these reasons veratrol cannot be replaced and only the aldehyde can be varied. By altering the aldehyde a number of symmetrical 9,10-dialkyl-2,3,6,7-tetramethoxyanthracenes can be produced (Scheme 2.3).

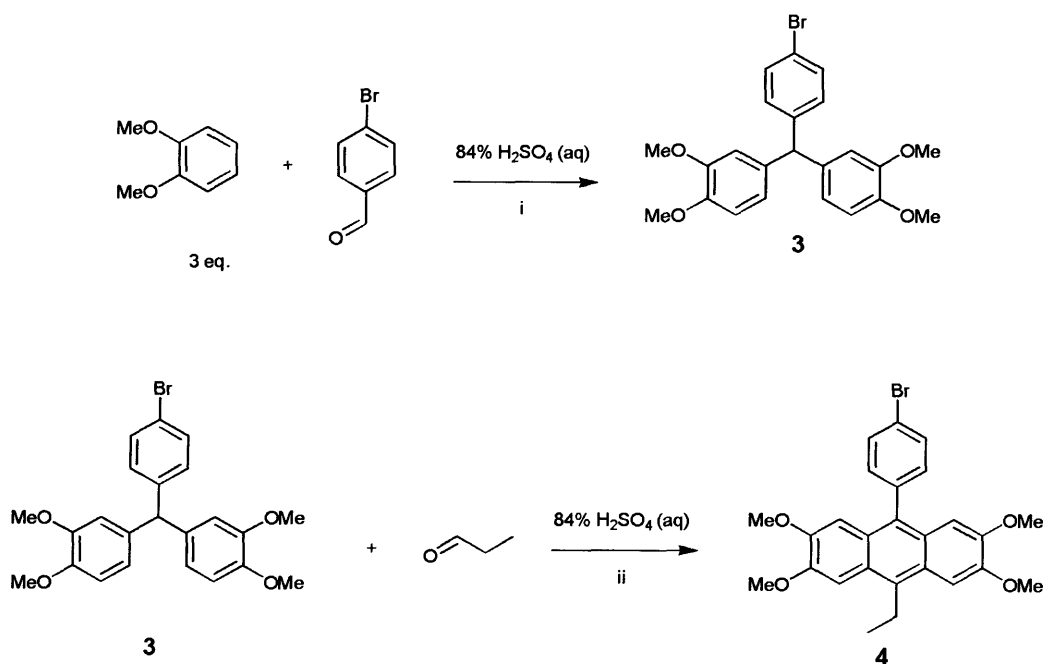


Scheme 2.3 General procedure for anthracene synthesis. (R = ethyl, 20% yield)

For example, 9,10-diethyl-2,3,6,7-tetramethoxyanthracene **2** (where R = ethyl) was readily obtained with modest yield (22%) following the procedure by Shklyayev.¹¹⁹

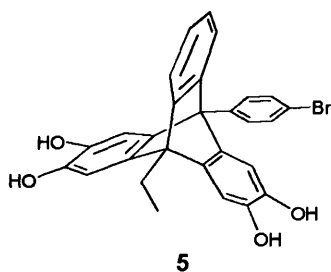
2.1.2 Unsymmetrical anthracenes

In order to obtain a wider variety of useful triptycenes, unsymmetrical anthracenes were synthesised to allow independent variation of the bridgehead substituents. The first step was to produce the anthracene precursor 4-bromo-3,3',4,4'-tetramethoxytriphenylmethane **3** following a procedure by Goossens¹²⁰ where an aldehyde (4-bromobenzaldehyde) is reacted with an excess of veratrole (1,2-dimethoxybenzene) (3/1). The procedure was efficient (72%) and the sparingly soluble product was easily isolated (Scheme 2.4).



Scheme 2.4 Synthesis of unsymmetrical anthracene **4**. Reaction times: i 1 hr (72%); ii 4 hrs (59%).

2.2 Unsymmetrical polymer from tetrahydroxytriptycene 5



Scheme 2.5 Monomer for ladder polymer,
9-(4'-bromophenyl)-10-ethyl-2,3,6,7-tetrahydroxytriptycene **5**.

The first target monomer was the unsymmetrical triptycene derivative, 9-(4'-bromophenyl)-10-ethyl-2,3,6,7-tetrahydroxytriptycene **5**, with functionality $f = 2$ (note that each 'catechol' residue acts as a single functional group with regards to polymer formation). It was anticipated that a soluble ladder polymer (and potentially a self-standing film suitable for the determination of membrane properties) could be obtained and the presence of an aryl bromide could lead to further enhancements (e.g. *via* Suzuki coupling reactions). For example, if a membrane could be cast, the aryl bromide in the presence of a catalyst might allow cross-linking of the polymer chains, resulting in an insoluble, more durable, membrane structure. Alternatively, it could allow for a catalyst to be covalently attached to the membrane, for use in a catalytic flow system.

2.2.1 Synthesis of tetrahydroxytriptycene 5

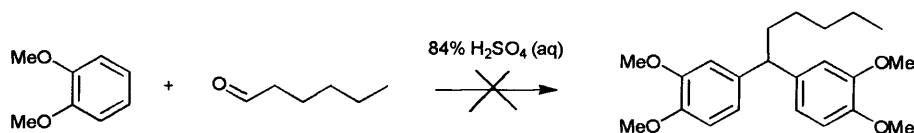
The anthracene precursor **3** was treated with propionaldehyde to give 9-(4'-bromophenyl)-10-ethyl-2,3,6,7-tetramethoxyanthracene **4**. Using the standard molar equivalence of aldehyde to reactant (1/1) gave a poor yield (12%).^{119,121} It was clear that a multi-gram quantity of the anthracene **4** would be required so time was taken to optimise the yield of this reaction. From systematic experimentation (Table 2.1), it was found that 2.5 equivalents of aldehyde with a reaction time of 4 hrs was optimum (59%). Further reaction times offered reduced yield most likely due to the decomposition of **3**, releasing veratrole back into the reaction mixture. As a result of

this decomposition the 16 hrs experiment afforded a second anthracene that was isolated and found to be the symmetrical 9,10-diethyl-2,3,6,7-tetramethoxyanthracene **2**.

Equivalence of aldehyde	Time (hr)	Yield (%)
1	1	12
1.5	1	17
	4	28
2	1	27
	4	45
2.5	1	30
	4	59
	8	54
	16	32
3	4	58

Table 2.1 Optimising the reaction between **3** and propionaldehyde.

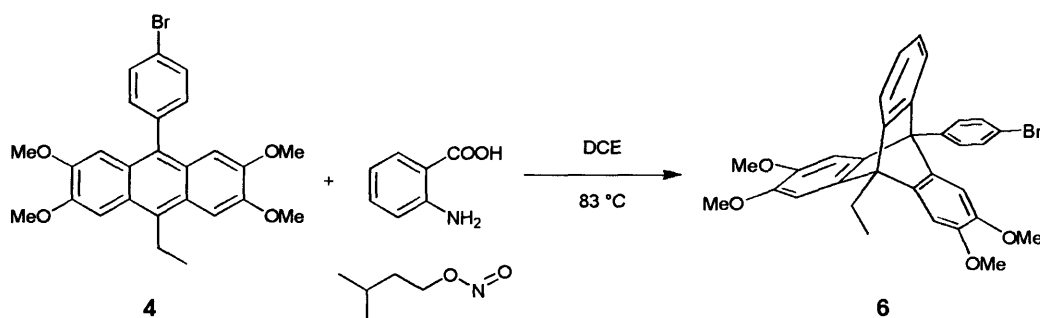
An attempt to investigate an alternative route to anthracene precursors going *via* the alternative intermediate (Scheme 2.6) was conducted, but proved to be far inferior to the original route (Scheme 2.4) with a yield of less than 1%. Due to the stoichiometric requirements for this reaction (3/1 excess of veratrole, aldehyde cannot be used in excess) and limited reaction time (to prevent decomposition of products) little can be done to optimise the yield of this product.



Scheme 2.6 Anthracene precursor starting with an alkyl aldehyde.

Using the optimised route, a large quantity of anthracene **4** was prepared. The next step was to react **4** with benzyne in a well-established Diels-Alder reaction in order to form 9-(4'-bromophenyl)-10-ethyl-2,3,6,7-tetramethoxytryptcene **6** (Scheme 2.7).

The highly reactive and unstable benzyne cannot be isolated but fortunately is readily formed *in-situ* from the thermal decomposition of benzenediazonium-2-carboxylate chloride. The diazonium salt itself is also formed *in-situ* from the reaction of anthranilic acid with a nitrosonium ion (from isoamyl nitrite).

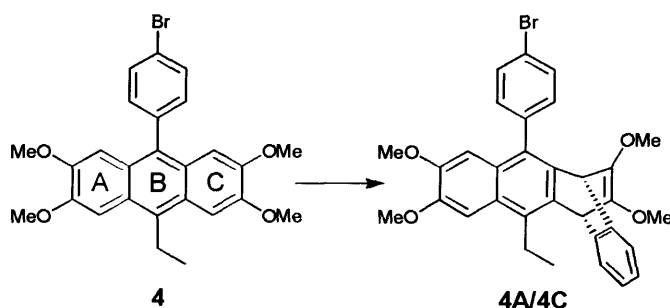


Scheme 2.7 Diels-Alder reaction to form triptycene **6** (14% yield).

Almost immediately after anthranilic acid and isoamyl nitrite are introduced to refluxing 1,2-dichloroethane (DCE), effervescence is observed, owing to nitrogen and carbon dioxide gas being released in the formation of benzyne. Although the reaction proceeds easily, the high reactivity of benzyne leads to a large number of side products and an extremely tedious workup. Effort was made to make the addition of the benzyne precursors to a hot solution containing anthracene **4** as slow as possible in order to maximise the excess of anthracene to benzyne at all times. Unfortunately, the yield from this reaction is not reliable. Exposing the anthracene to a larger excess of benzyne also did not improve the yield, and regardless of stoichiometry and reaction time, the yield remained in the range 0-14%. In order to effectively separate pure triptycene **6** from anthracene **4**, column chromatography was the only solution. To first reduce some of the crude mass (which was greater than 17 g), a plug of silica was used to remove the highly polar impurities and reduce the mass of crude residue to a more manageable quantity.

Possible reasons for a low yield in the case of anthracene **4** with benzyne compared to other anthracenes previously reported^{122,123} could be the presence of the aryl ring at the 9 position. Bulky groups in this position offer significant steric hindrance, blocking the approaching benzyne and preventing the Diels-Alder mechanism from taking place. The slower reaction rate encourages benzyne-benzyne couplings, and

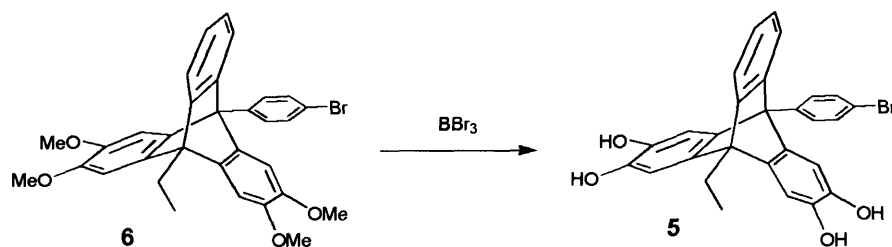
also likely directs a more significant portion of the benzyne to the competing off-centre diene positions (A and C, Scheme 2.8).



Scheme 2.8 Illustration of benzyne Diels-Alder competing positions.

It was reported by Klanderman and Criswell¹²⁴ that for 9,10-dimethylantracene reacting with benzyne the ratio of the B/A ring products was ca. 200. For 9-phenylantracene that ratio dropped to 35. They also noted that the relative reactivity towards benzyne for 9,10-dimethylantracene and 9-phenylantracene was 19.2:1.0. This lower reactivity towards benzyne and decreased selectivity offers a good explanation as to why it was so difficult for us to obtain a reasonable amount of triptycene from this reaction, where a phenyl ring is present on the B ring (9 position). It can also be noted that benzyne addition to 9,10-diphenylantracene occurs exclusively at the non-central rings.¹²⁵

Once the product **6** had been obtained in sufficient quantity, it was treated with boron tribromide under an inert atmosphere to give the monomer **5** (Scheme 2.9). This strong Lewis acid readily demethylated all four methoxy groups with near quantitative yield in less than 1 hr. However, care had to be taken in purification as the pale pink product was readily degraded in air to a dark purple powder. It was found beneficial to dry the product thoroughly but at ambient temperature under vacuum to prevent this colour change, likely a result of oxidation and oxidative coupling of the electron-rich aromatic groups.



Scheme 2.9 Reagents and conditions: DCM, addition of BBr_3 0 °C, RT 1 hr, N_2 atm. (91% yield)

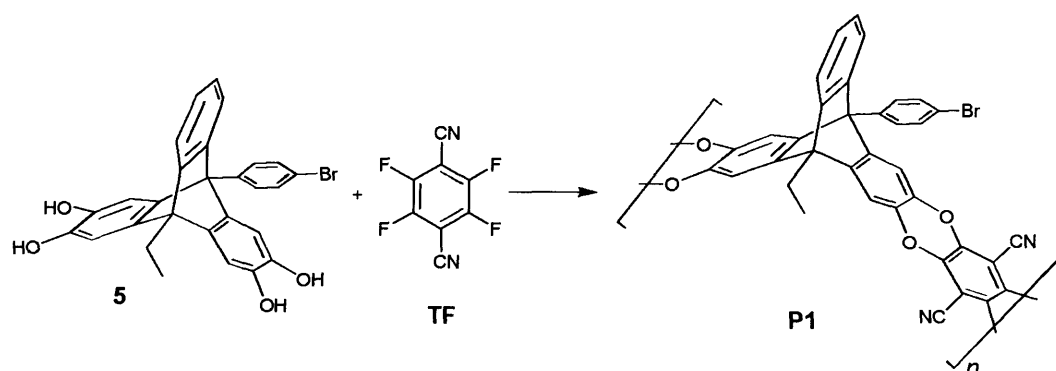
2.2.2 General procedure for preparation and purification of polymers

The general procedure used to form polymers between catechol-containing and activated aryl fluoride-containing monomers (most often 2,3,5,6-tetrafluoroterephthalonitrile) is based on that optimised for **PIM-1**.¹ Step-growth polymers of this type are exceptionally sensitive to stoichiometry, degree of conversion and impurities, so rigorous reaction conditions were required together with high monomer purity. To maximise the polymer chain length, anhydrous dimethylformamide (DMF) was used under an inert nitrogen atmosphere, with as pure as possible starting materials of mass carefully measured to three decimal places. This helped to ensure that the reaction was efficient and that the reactants were present in equimolar quantities. The monomers were then added to DMF at 65 °C, and only once they were completely dissolved was the K_2CO_3 base added to initiate the aromatic nucleophilic substitution polymerisation. Almost immediately after the reaction starts a bright yellow or orange colour was observed as oligomers and short chains were formed rapidly. The reaction was kept stirring and allowed to proceed for 72 to 96 hrs after which time higher mass polymer chains were formed. The purification was achieved by dissolving the polymer in a suitable solvent (usually THF or chloroform) and then adding the solution drop-wise to a vigorously stirred non-solvent (usually methanol, acetone or hexane). This procedure helps remove the more readily soluble oligomers from the product, which lower the average molecular mass of the polymer and degrade its ability to cast a free-standing film suitable for membrane studies. Before attempting to cast the film the polymers were also dissolved and passed through a fine filter to remove any particles.

For the polymers that were insoluble the purification was achieved by washing the crude powder with acetone, and then refluxing in multiple solvents (acetone, chloroform, THF and methanol). This procedure helped remove the more readily soluble oligomers, by-products and impurities which can occupy the micropores, reducing the apparent BET surface area. Methanol was always used as the final solvent for washing due to its proven ability to remove less volatile residual solvent.⁹ Once washed, the polymers were ground with pestle and mortar into a fine powder and dried in a vacuum oven at high temperature (usually 120 °C).

2.2.3 Synthesis of ladder polymer P1

The tetrahydroxytritycene **5** was reacted with 2,3,5,6-tetrafluoroterephthalonitrile (**TF**) as shown in Scheme 2.10.



Scheme 2.10 Triptycene ladder polymer **P1**. *Reagent and conditions:* K_2CO_3 , DMF, 70 °C, N_2 atm. (69% yield).

Unfortunately the new polymer showed little solubility in any solvent. This excluded the possibility of using solution-based NMR or GPC in the analysis of the product. The resulting solid was instead ground into a fine powder and refluxed in a range of organic solvents (acetone, chloroform, then methanol) and dried under vacuum at high temperature (120 °C) to give a powder with an apparent BET surface area of $300 \text{ m}^2 \text{ g}^{-1}$. The adsorption/desorption of N_2 shows a distinct hysteresis, likely due to swelling of the polymer in the presence of the guest probe molecule, which later

becomes trapped as the desorption takes place and the polymer returns to a more relaxed state (Figure 2.1).

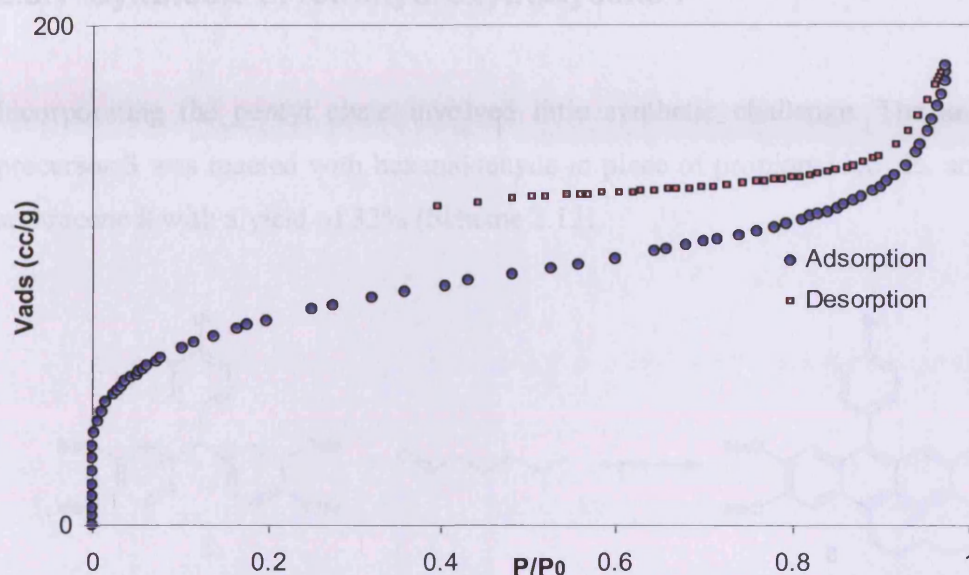
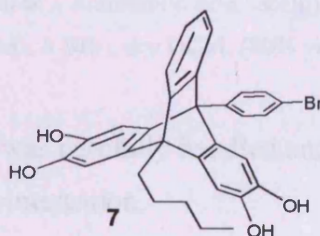


Figure 2.1 Adsorption/Desorption isotherm, N₂ 77K, for trip-PIM-P1.

2.3 Ladder polymer with increased alkyl chain

The insolubility of polymer **P1** in common solvents meant that characterisation proved problematic and films could not be cast from solution for further study. In an attempt to create a polymer with essentially the same functionality (i.e. tetrahydroxytritycene, $f=2$, and an aryl bromide side group) but increased solubility, the ethyl chain was replaced by pentyl (Scheme 2.11). The longer alkyl chain has greater rotational freedom and it was anticipated that it would act to decrease strong intramolecular interactions in the solid (e.g. dipole-dipole interaction of the nitrile groups) and increase the solvent-polymer interactions.

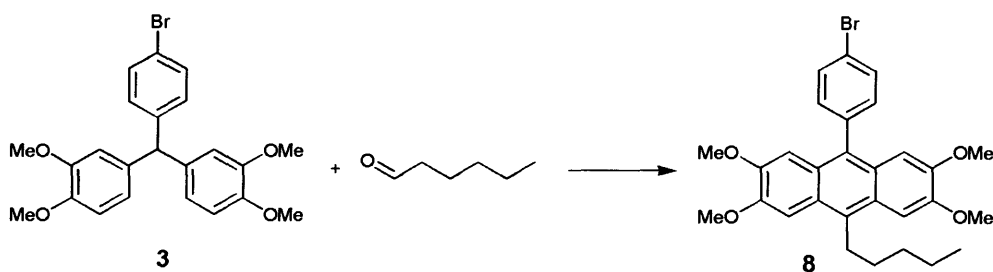


Scheme 2.11 Triptycene with increased alkyl chain length,

9-(4'-bromophenyl)-10-pentyl-2,3,6,7-tetrahydroxytryptycene **7**.

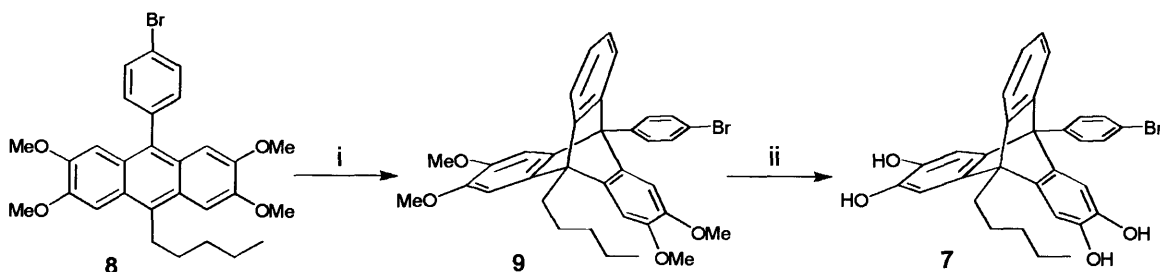
2.3.1 Synthesis of tetrahydroxytryptycene **7**

Incorporating the pentyl chain involved little synthetic challenge. The anthracene precursor **3** was reacted with hexanaldehyde in place of propionaldehyde, arriving at anthracene **8** with a yield of 32% (Scheme 2.12).



Scheme 2.12 Synthesis of anthracene **8**. *Reagent and conditions:* H₂SO₄, 0-5 °C. (32% yield).

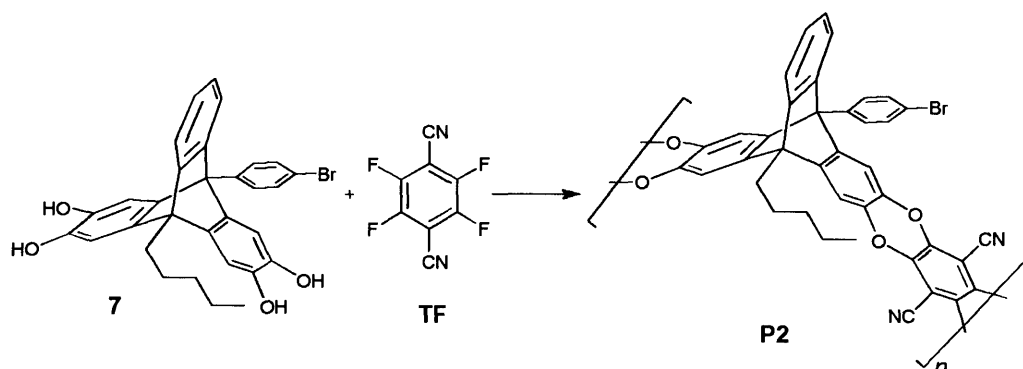
The anthracene was then reacted with anthranilic acid and isoamyl nitrite (Scheme 2.13) to give **9** (15%) in a similar poor yield as seen with **6** (14%). This was presumably again due to the steric hindrance resulting from the presence of the aryl ring at the 9- position. Tryptycene **9** was readily demethylated with BBr₃ to give **7**, which showed high sensitivity to oxidation evident from its rapid colour change in hot solvents or even in the solid state over time.



Scheme 2.13 *Reagents and conditions:* i Anthranilic acid, isoamyl nitrite, DME, N₂ atm., 83 °C (15% yield); ii BBr₃, dry DCM. (80% yield).

The tetrahydroxytryptycene **7** was carefully handled and dried under vacuum at 40 °C to limit oxidation prior to polymerisation.

2.3.2 Synthesis of ladder polymer P2

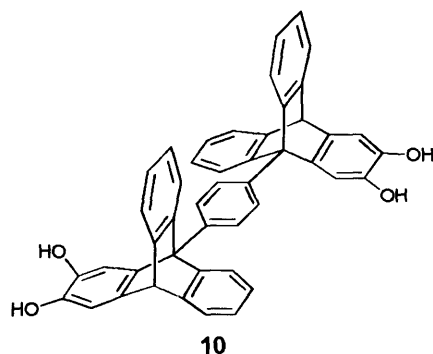


Scheme 2.14 Reagents and conditions: K_2CO_3 , dry DMF, 65 °C, 72 hrs. (30% yield).

The dry monomer **7** was reacted with 2,3,5,6-tetrafluoroterephthalonitrile in the standard way previously described, in dry DMF at 65 °C for 72 hrs. On quenching, the resulting crude product was again found to be insoluble in common organic solvents so a membrane could not be cast. The resulting dark green solid was ground into a fine powder and heated in various solvents to remove impurities. The dry powder had an apparent BET surface area of $190 \text{ m}^2 \text{ g}^{-1}$. The reduction in surface area can most likely be attributed to the non-rigid alkyl chain occupying some of the IFV generated by the triptycene units. Increasing the length of the alkyl chain yet further might make the polymer soluble but the lower surface area (and microporosity) would likely render the resulting membranes permeability below a useful level.

2.4 Bitriptycene ladder polymer P3

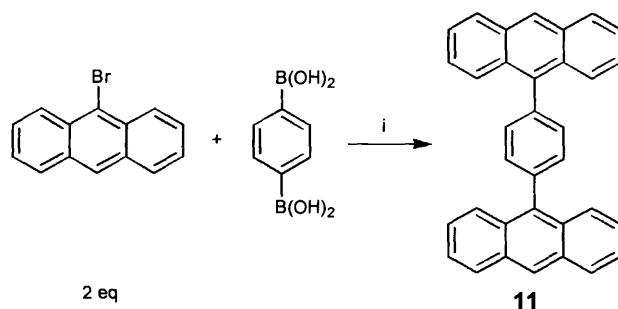
The next system we explored was a ladder polymer incorporating the bitriptycene monomer **10** (Scheme 2.15). This new system was the first devised for a polymer of this type where triptycene units are not only in the plane of the polymer, but also staggered above and below providing an extra rigid directional change along the polymer backbone. The two single bonds (although restricted in rotation) should introduce good flexibility to the polymer chain, increasing the possibility of solubility and a flexible membrane to be cast.



Scheme 2.15 Bitriptycene 10.

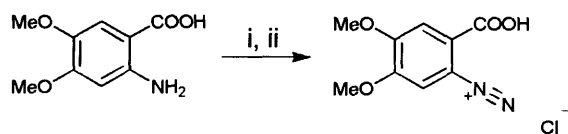
2.4.1 Synthesis of monomer 10

The synthesis started from the commercially available 9-bromoanthracene. It was successfully reacted with benzene-1,4-diboronic acid under palladium-mediated Suzuki coupling conditions, to give 1,4-di(anthracene-9'-yl)-benzene **11** (Scheme 2.16). The reaction proceeded to give a good yield (86%) following a procedure described by Myoung-Seon Gong.¹²⁶

Scheme 2.16 Reagents and conditions: i) K_2CO_3 , $\text{Pd}(\text{PPh}_3)_4$, DME, H_2O , N_2 atm, 80°C . (86% yield).

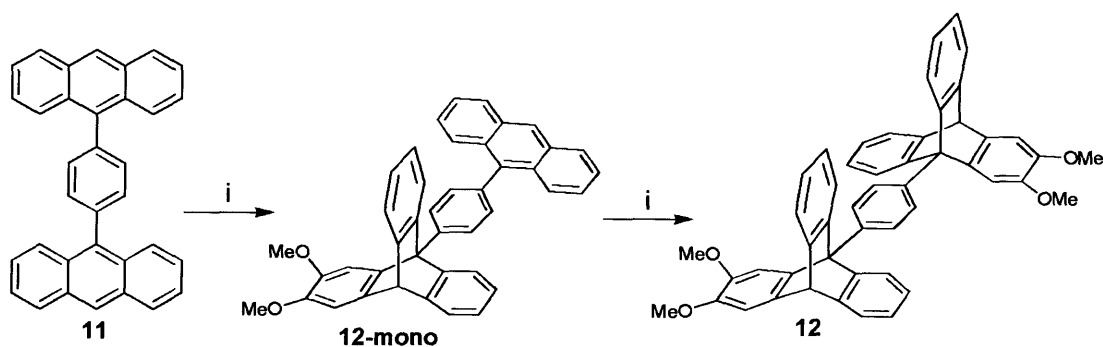
To introduce the methoxy groups into the final bitriptycene we used 1,2-dimethoxybenzyne. Synthesis of the benzyne was first attempted *in-situ*, as described previously (Scheme 2.7), using 2-amino-4,5-dimethoxybenzoic acid instead of anthranilic acid. The yield was even lower than that obtained for **6**, so a new synthetic method was used. Instead of the *in-situ* preparation of the relatively stable diazonium salt, it was first isolated, using the modified method of Chuan-Feng Chen¹²³ of Klandermans work on benzyne.¹²⁴ The reaction between isoamyl nitrite and 2-amino-4,5-dimethoxybenzoic acid proceeded readily to give

4,5-dimethoxybenzenediazonium-2-carboxylate chloride (Scheme 2.17) in almost quantitative yield.



Scheme 2.17 Reagents and conditions: i $\text{HCl}_{(\text{aq})}$, EtOH , $0\text{ }^{\circ}\text{C}$; ii isoamyl nitrite.

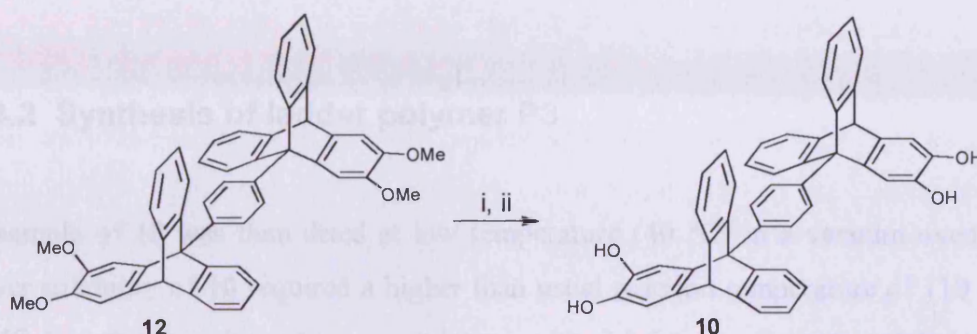
The diazonium salt was then added as a solid in small batches to a refluxing solution of **11** in DCE and propylene oxide. With time the solution became a very dark colour, indicating that a reaction was occurring. On work-up it was found that only a very small amount of the bitriptycene **12** had been formed, along with a slightly higher quantity of the mono Diels-Alder cyclo-adduct **12-mono** (Scheme 2.18). The only way to push the reaction further to completion and obtain a reasonable amount of **12** was to use flash chromatography to remove the by-products from the decomposition of the diazonium salt. A clean sample of **11** and **12-mono** was then re-entered into the reaction with the diazonium salt, each time yielding slightly more **12-mono** and **12**. This laborious process was repeated until a sufficient quantity of **12** had been obtained for further study.



Scheme 2.18 Reagents and conditions: i 4,5-dimethoxybenzenediazonium-2-carboxylate chloride, DCE, propylene oxide, reflux. (12% yield).

Unfortunately an impurity was visible in the TLC for the sample of **12**, with the same RF and with such similar solubility that no combination of crystallisation from common organic solvents or chromatography was able to remove the impurity effectively. It was decided to proceed to the demethylation using BBr_3 with the

impurity still present. The reaction produced a very dark coloured solution immediately after addition of BBr_3 which was not common during demethylation of the other triptycenes synthesised in this project.



Scheme 2.19 Reagents and conditions: i) BBr_3 , dry DCM; ii) H_2O . (37% yield).

On work up a very deep purple solid was obtained, it was decided that further purification would be required as the product **10** is unlikely to contain a strong chromophore to impart colour. The crude sample was dissolved in ethyl acetate and precipitated with slow addition of hexane. Once a dark precipitate was formed it was removed by filtration and more hexane added to the filtrate, this process was repeated until the precipitate became a light beige colour. The usual near quantitative yield was far lower this time with only 37% recovery of 1,4-di(2',3'-dihydroxytriptycene-9'-yl)benzene **10**.

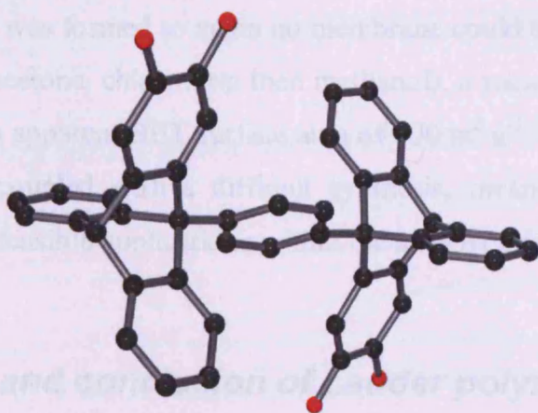


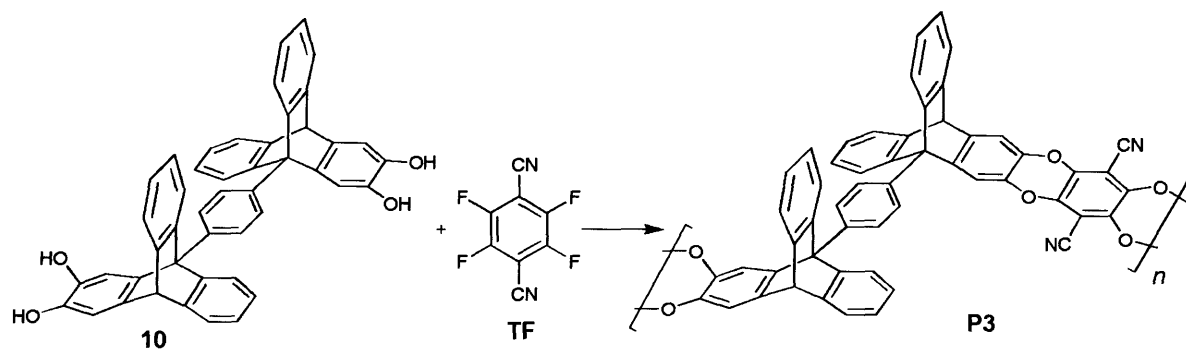
Figure 2.2 Crystal structure of bitriptycene **10**.

Crystals were grown for the tetrahydroxy-bitriptycene **10** from slow diffusion of non-solvent (hexane) into a solution of the bitriptycene **10** in diethyl ether. The crystal

structure is triclinic belonging to space group $P\bar{1}$, with cell lengths a 10.4970(2), b 12.5010(2), c 19.2740(5) Å, and cell angles α 95.3020(10), β 91.5820(10), γ 110.7890(10). The cell volume is 2349.45 Å³ with 2 molecules of **10**, and 5 molecules of diethyl ether present.

2.4.2 Synthesis of ladder polymer P3

A sample of **10** was then dried at low temperature (40 °C) in a vacuum oven. The lower solubility of **10** required a higher than usual reaction temperature of 110 °C in DMF to achieve a homogeneous solution with 2,3,5,6-tetrafluoroterephthalonitrile before the reaction was initiated with K₂CO₃. The reaction was stirred for a further 72 hrs at 110 °C before quenching in water.



Scheme 2.20 Reagents and conditions: K₂CO₃, dry DMF, 110 °C, 72 hrs. (86% yield).

An insoluble powder was formed so again no membrane could be cast. After refluxing in various solvents (acetone, chloroform then methanol), a vacuum oven dried sample was found to have an apparent BET surface area of 100 m² g⁻¹. Lack of solubility and low microporosity, coupled with a difficult synthesis, means that polymer **P3** is unlikely to have any feasible applications within the aims of this project.

2.5 Summary and conclusion of Ladder polymers

The goal of this chapter was to design a strategy for synthesising a soluble triptycene based polymer. None of the polymers synthesised were soluble in any common organic solvents, they did however all display some degree of microporosity.

Although unsuccessful in yielding a soluble polymer, targeting the monomers required for polymers **P1** and **P2** has led to the synthesis and optimisation of some interesting unsymmetrical tetramethoxy-anthracenes and triptycenes. Increasing the alkyl chain length on the triptycene from **P1** to **P2** led to a decrease in observable microporosity (from $300 \text{ m}^2 \text{ g}^{-1}$ in **P1** to $190 \text{ m}^2 \text{ g}^{-1}$ in **P2**), and no observable increase in solubility. From this observation it is reasonable to assume that no viable triptycene based monomer undergoing the dioxane ring polycondensation of the type used here will yield a soluble product. This is likely due to the rigidity of the triptycene units and polymer backbone as a whole becoming entangled with nearby growing chains, maximising the interactions between triptycene faces, reducing solvent-polymer interactions. Such tight packing would also serve to explain the relatively low surface areas observed compared to network polymers based around triptycene (e.g.: **Trip(Me)-PIM** $1730 \text{ m}^2 \text{ g}^{-1}$).

The bitriptycene monomer **10** was selected due to its vertical triptycene stacking topology, and the inherent flexibility and rotational freedom offered by the 2 single bonds. Although this flexibility appears to have allowed the porous structure to collapse (evident from the low surface area of $100 \text{ m}^2 \text{ g}^{-1}$) it still was not enough to allow sufficient solvent-polymer interaction.

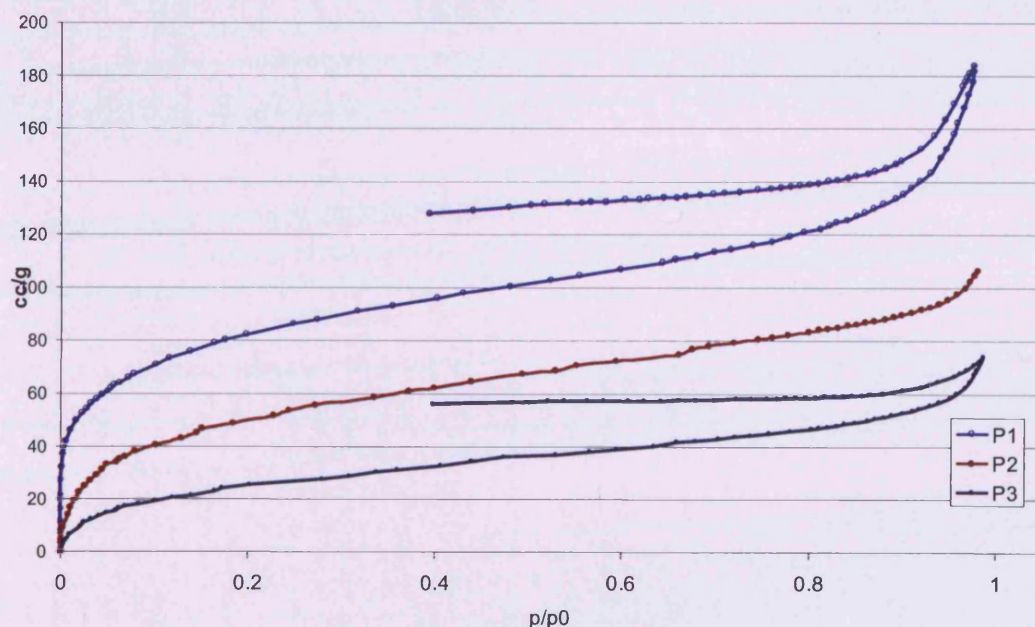


Figure 2.3 Adsorption/desorption isotherms for Ladder PIMs (N_2 77K).

Chapter 3: Network Polymers

3 Network Polymers

The network polymers described below were synthesised in a similar manner to the previous ladder polymers, but contain at least one monomer with average functionality (f) greater than 2.

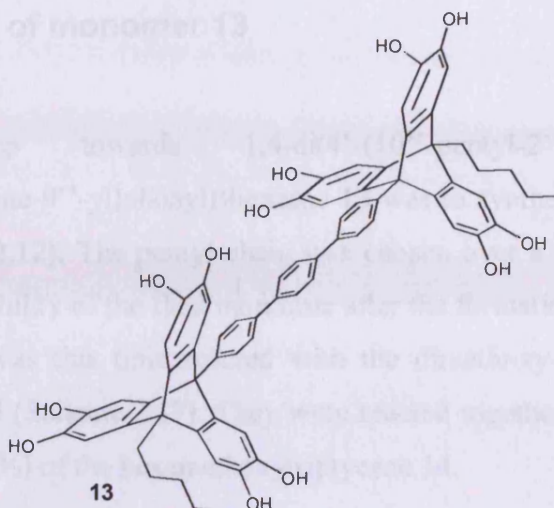
3.1 General procedure for network polymers

The general procedure used to form network polymers was synthetically equivalent to that for ladder polymers discussed earlier. The monomers are heated in dry DMF under a N₂ atmosphere until they were fully dissolved. Once the monomers were completely dissolved K₂CO₃ base was added to initiate the polymerisation. Almost immediately after the reaction starts a bright yellow or orange precipitate was observed. The reaction was kept stirring and allowed to proceed for 72-96 hrs to allow the polymerisation to approach completion. The reaction mixture was then poured into water, filtered and washed with water to remove the DMF. The residue was then left on a suction filter until the water was removed and a dry powder was obtained. The purification of network polymers was the same as that described for insoluble ladder polymers (Section 2.2.2).

3.2 Bi-triptycene network polymer P4

The first target monomer was **13** (Scheme 3.1), an analogue of the original high performing trip-PIMs⁵ but with two triptycenes joined perpendicularly to the network plane *via* three aryl rings.

3.2.1 Synthesis of monomer 13



Scheme 3.1 Network polymer target monomer.

The aim was to create a less planar triptycene network polymer, and create a system that is less able to stack plane on plane. The introduced connection between triptycenes was anticipated to further restrict packing in the final polymer and generate a more porous material (Figure 3.1).

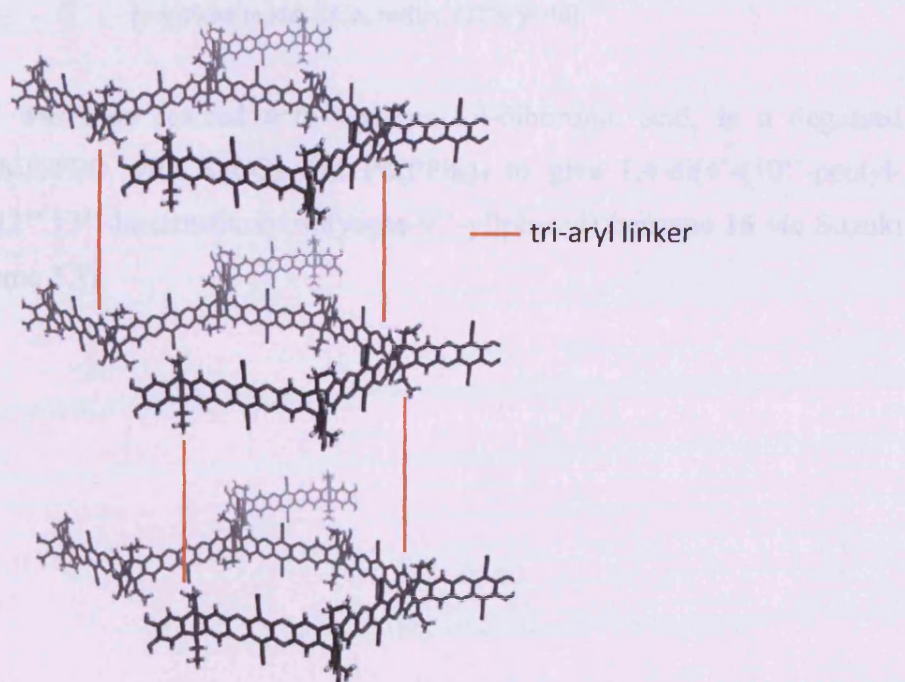
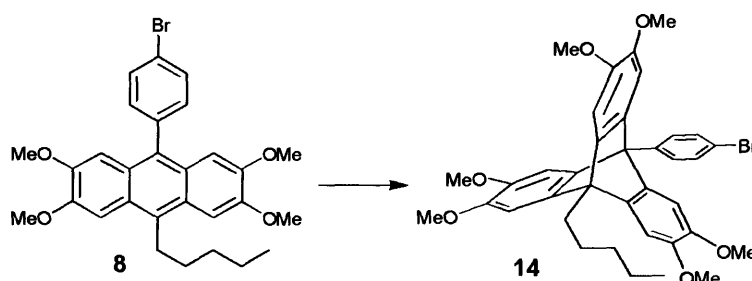


Figure 3.1 Illustration of tri-aryl links between layered polymer fragments limiting mobility.

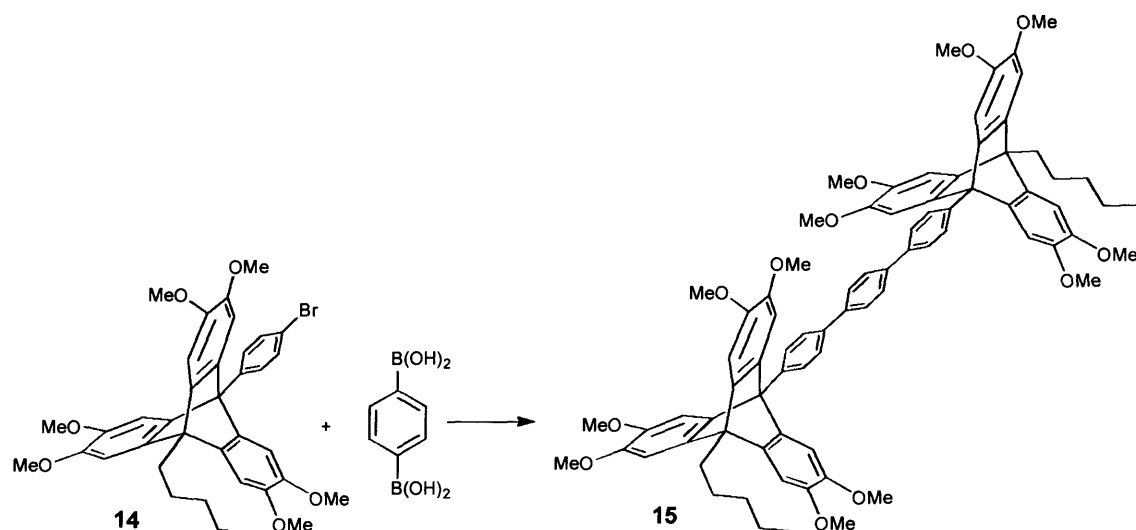
3.2.1 Synthesis of monomer 13

The first step towards 1,4-di(4'-(10''-pentyl-2'',3'',6'',7'',12'',13''-hexahydroxytriptycene-9''-yl)phenyl))benzene **13** was to synthesise the anthracene **8** as before (Scheme 2.12). The pentyl chain was chosen over a shorter substituent to help ensure full solubility of the final monomer after the formation of the bitriptycene. The anthracene **8** was this time reacted with the dimethoxy-diazonium salt, also previously discussed (Scheme 2.17). They were reacted together in DCE, and gave a reasonable yield (27%) of the hexamethoxytriptycene **14**.



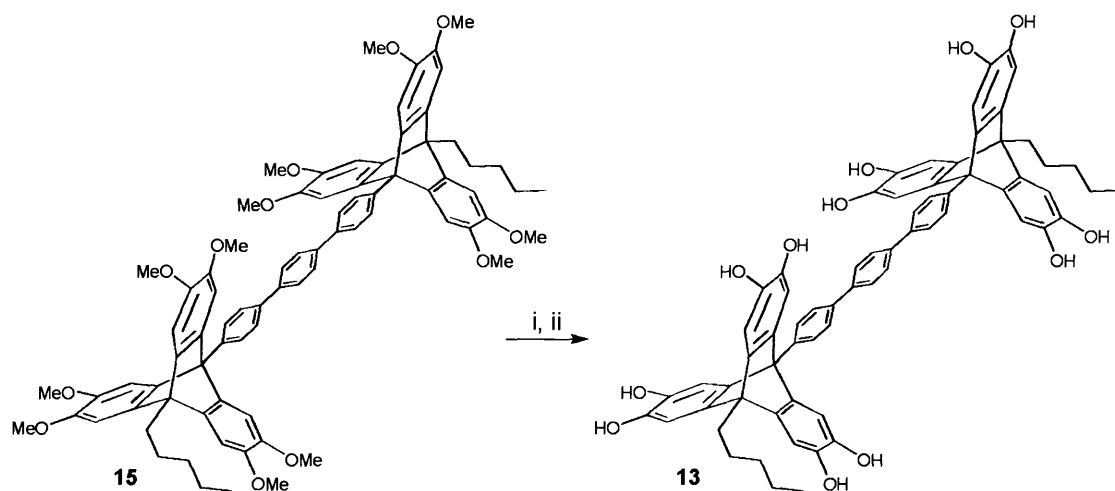
Scheme 3.2 Reagents and conditions: 4,5-dimethoxybenzenediazonium-2-carboxylate chloride, propylene oxide, DCE, reflux. (27% yield).

Triptycene **14** was then reacted with benzene-1,4-diboronic acid, in a degassed solution of DME/H₂O with K₂CO₃ and Pd(PPh₃)₄ to give 1,4-di(4'-(10''-pentyl-2'',3'',6'',7'',12'',13''-hexamethoxytriptycene-9''-yl)phenyl))benzene **15** via Suzuki coupling (Scheme 3.3).



Scheme 3.3 Reagents and conditions: K_2CO_3 , $Pd(PPh_3)_4$, DME, H_2O , N_2 atm, $80\text{ }^\circ\text{C}$. (87% yield).

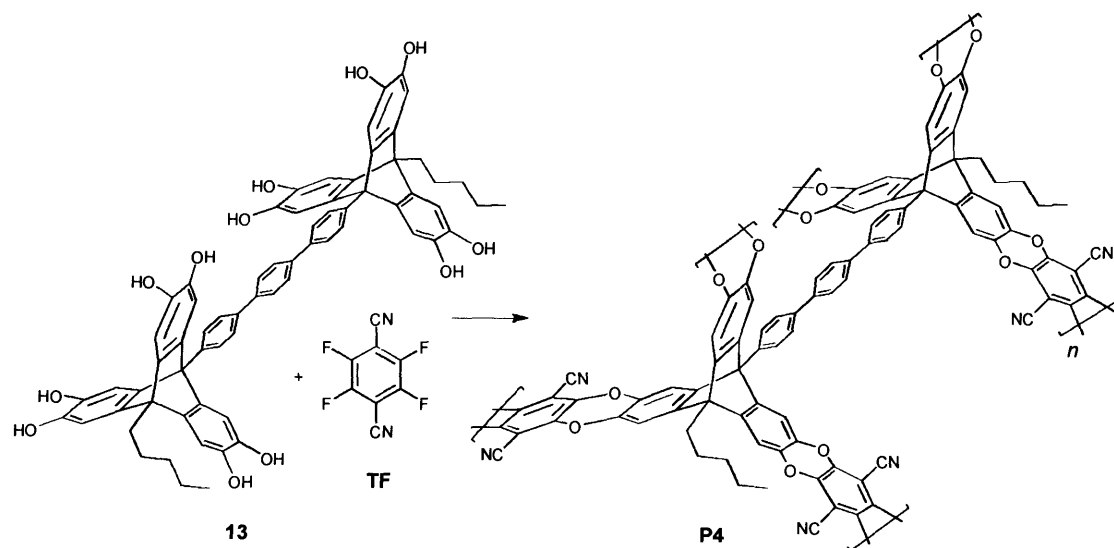
The Suzuki coupling reaction proceeded in good yield (87%) and a pure sample of **15** was easily obtained using flash chromatography. The triptycene was then dried and demethylated with BBr_3 to give **13** (Scheme 3.4). The product was obtained in good yield (92%) but showed severe susceptibility to oxidation, made visible by the rapid colour degradation from light pink to deep purple.



Scheme 3.4 Reagents and conditions: i BBr_3 , dry DCM; ii H_2O . (92% yield).

3.2.2 Synthesis of network polymer P4

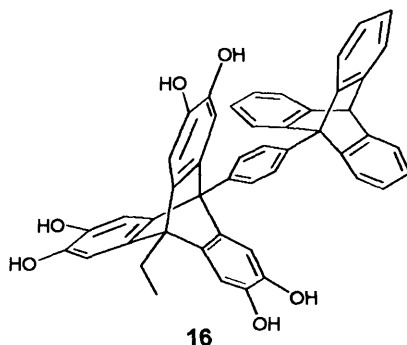
The monomer **13** was readily soluble in DMF at 65 °C, and so the reaction was carried out using the standard procedure for 72 hrs. On quenching in water, the resulting insoluble material was washed and refluxed in acetone, then chloroform, THF and finally methanol (20 hrs each). The solid was collected by vacuum filtration and dried in a vacuum oven at 110 °C for 24 hrs to give the product **P4** (78%) with an apparent BET surface area of 880 m² g⁻¹.



Scheme 3.5 Reagents and conditions: K₂CO₃, dry DMF, 65 °C, 72 hrs. (78% yield).

Although the polymer shows significant microporosity, it offers no improvement over the current best triptycene-based PIM (Trip(Me)-PIM, surface area = 1760 m² g⁻¹)⁵. It is expected that part of the intrinsic microporosity provided by the rigid polymer framework will be occupied by the more flexible pentyl chains. Even taking this into account by comparing the apparent surface area with the previously prepared Trip(Pe)-PIM, (surface area = 947 m² g⁻¹)⁵ which contains a pentyl group attached to the two bridgehead positions of the triptycene unit, there is no enhancement of porosity. The elemental analysis returned fairly erroneous results due to the entrapment of organic molecules in the microporous material, but a value of 4.2 % wt/wt of fluorine suggests that the polymer network was fairly incomplete, likely a result of restricted growth due to some functional sites becoming inaccessible. Alternatively, the fluorine content could be due to insoluble particles of KF, a by-product of reaction, being trapped inside the network.

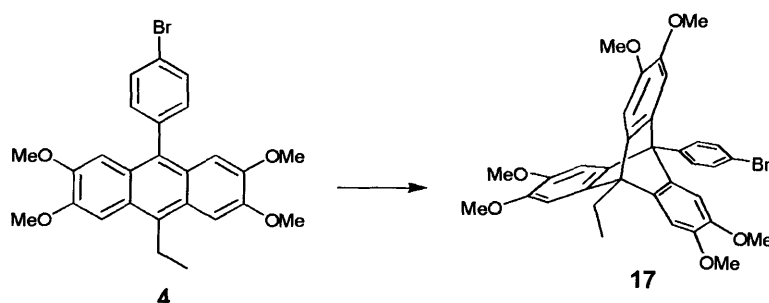
3.3 Network Polymer with Triptycene side group P5



Scheme 3.6 Target monomer **16**.

The next target monomer for a network polymer was **16**. This monomer only has $f = 3$ (in contrast to **P4** where $f = 6$), and effectively has the same polymer backbone structure as the trip-PIM series⁵. It differs at the 9 position, where one of the alkyl chains has been replaced with a bulky triptycene group. The lower average functionality should allow the polymer to grow in a more efficient manner, hopefully preventing functional sites from becoming enclosed and inaccessible in the macrostructure of the network polymer particles. The inclusion of the bulky group perpendicular to the plane was hoped to act to reduce the efficiency of packing within the polymer, while the added triptycene should also introduce more IFV if rigid enough.

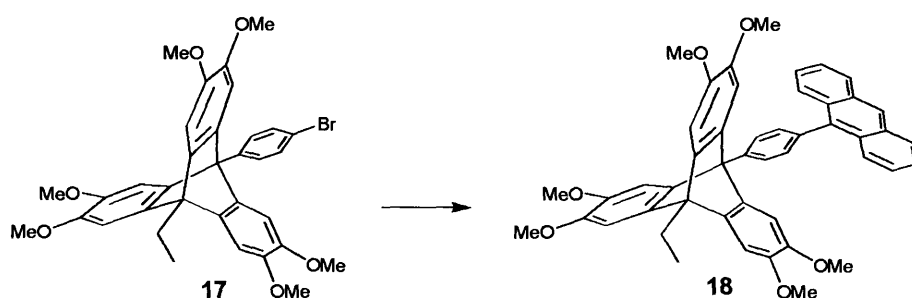
3.3.1 Synthesis of monomer **16**



Scheme 3.7 Reagents and conditions: 4,5-dimethoxybenzenediazonium-2-carboxylate chloride, propylene oxide, DCE, reflux. (22% yield).

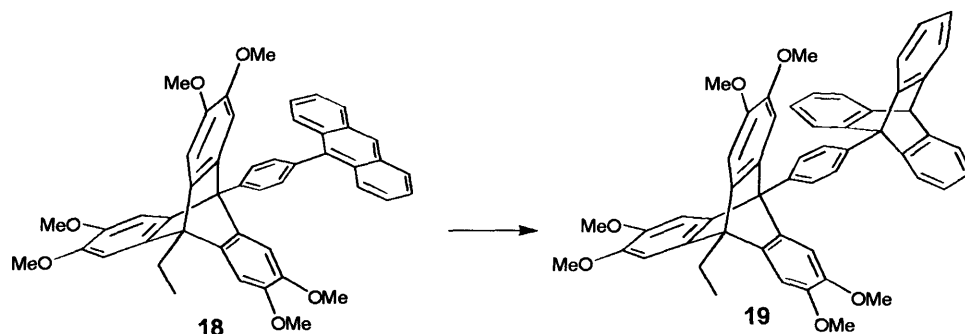
The anthracene **4** was synthesised as previously described (Scheme 2.4). The triptycene **17** was then synthesised in the same way described for **12** (Scheme 2.17) using 4,5-dimethoxybenzenediazonium-2-carboxylate chloride as the benzyne precursor. It was recovered with a low, but acceptable yield (22%) for this type of reaction.

The next step was to replace the aryl bromide with anthracene to arrive at the triptycene **18** (Scheme 3.8). It was achieved *via* a Suzuki coupling of 9-anthraceneboronic acid using $\text{Pd}(\text{PPh}_3)_4$ as the catalyst using an adaptation of the procedure used by Gong¹²⁶.



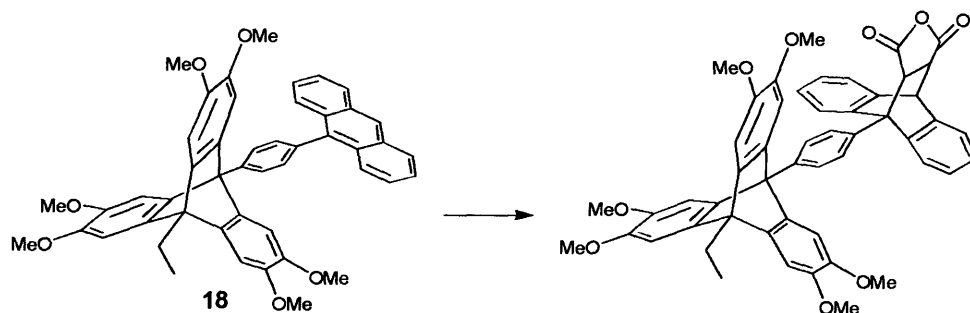
Scheme 3.8 Suzuki coupling reaction, *Reagents and conditions*: 9-Anthraceneboronic acid, K_2CO_3 , $\text{Pd}(\text{PPh}_3)_4$, THF, H_2O , N_2 atm. (70% yield).

The Suzuki coupling reaction used expensive reagents, but provided an efficient and effective way of arriving at the target molecule. Care was taken to ensure the reaction was as free of oxygen as possible, with solvents degassed over a few hours prior to the expensive catalyst being introduced. By taking care to minimize the level of oxygen in this way a satisfactory yield (70%) was achieved. When drying a sample of 9-anthraceneboronic acid it was found that it decomposes at temperatures above 100 °C. This susceptibility to thermal decomposition of the boronic acid is likely the main factor in the yield not being higher for this reaction. Visible oxidation of the palladium catalyst was not observed until the workup, suggesting that catalytic turn over was not the limiting factor in the overall yield. Small amounts of the catalyst and 9-anthraceneboronic acid were added to the reaction mixture after 48 hrs in an attempt to enhance the yield, but no significant increase in yield was observed.



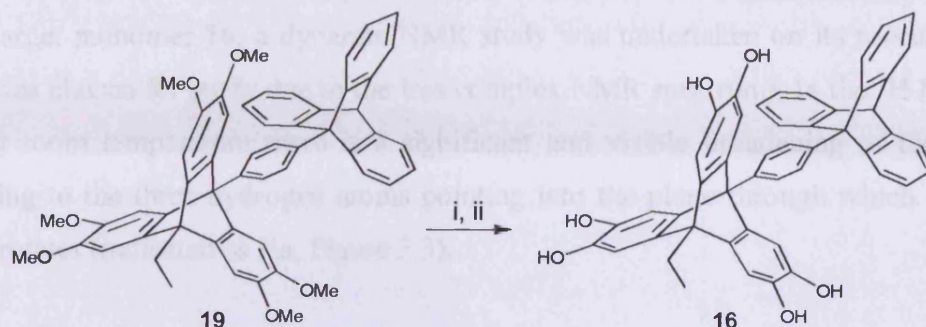
Scheme 3.9 Reagents and conditions: Anthranilic acid, isoamyl nitrite, DME, N_2 atm., 83 °C. (42% yield).

The anthracene group contained within triptycene **18** was then reacted with anthranilic acid in the same way as previously described (Scheme 2.7). The product **19** (Scheme 3.9) was difficult to obtain in good yield. After performing the reaction with anthranilic acid it was found that the polarities of **19** and **18** were too similar to allow effective separation by flash chromatography. Instead, we obtained a ‘clean’ mixture of **19** and **18** from a flash column to react with more anthranilic acid. This process of isolating **18** and **19** from the by-products and then reacting with fresh anthranilic acid was repeated 4 times until a significant amount of **18** had been consumed. The final mixture of clean **18** and **19** recovered from chromatography was analysed by 1H NMR. The NMR suggested that **19** was present in the mixture in a higher proportion than **18**, so it was decided that the remaining starting material **18** would be sacrificed to a Diels-Alder reaction with maleic anhydride (Scheme 3.10).¹²⁷ This process made it possible to obtain a pure sample of **19** (42%) from chromatography, which would have been impossible to separate without altering the polarity of **18**.



Scheme 3.10 Trapping of **18** using maleic anhydride,
Reagents and conditions: Maleic anhydride, toluene, reflux, 0.5 hr.

The final step to target monomer **16** was to demethylate **19** with boron tribromide. The reaction proceeded smoothly and was complete within 1 hr (Scheme 3.11).



Scheme 3.11 Reagents and conditions: i BBr_3 , dry DCM; ii H_2O . (96% yield).

The hexahydroxytriptycene **16** was obtained with excellent yield (96%). The only purification required was washing with a small amount of acetone, followed by a mixture of DCM/hexane (1/1). The triptycene showed better stability than **13** as severe colour change was not observed, likely due to the reduced number of hydroxyl groups present.

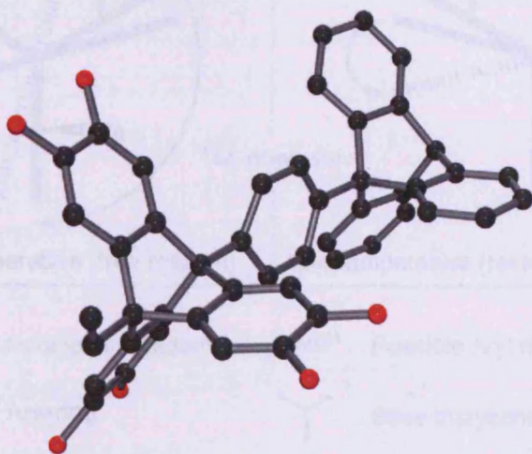


Figure 3.2 Crystal structure of bitriptycene **16**.

Due to the enhanced stability and low sensitivity towards methanol, the triptycene **16** was recrystallised from methanol by slow evaporation. The crystal was found to contain methanol in the crystal structure, and belonged to the orthorhombic space group $P 2_1 2_1 2_1$. The cell lengths were found to be a 16.8637(4), b 17.8527(7), c 17.9973(6) Å with cell angles $\alpha = \beta = \gamma = 90.00$. The cell volume is 5418.31 Å³ containing 4 molecules of **16**, 12 of methanol and 8 of water.

3.3.2 Proton NMR dynamic study of triptycene **17**

In order to gauge the rigidity and rotational freedom of the triptycene side group of the target monomer **16**, a dynamic NMR study was undertaken on its precursor, **17** (**17** was chosen for study due to the less complex NMR spectrum). In the ^1H NMR of **17** at room temperature there is a significant and visible broadening of the signal relating to the three hydrogen atoms pointing into the plane through which the aryl ring rotates (indicated as Ha, Figure 3.3).

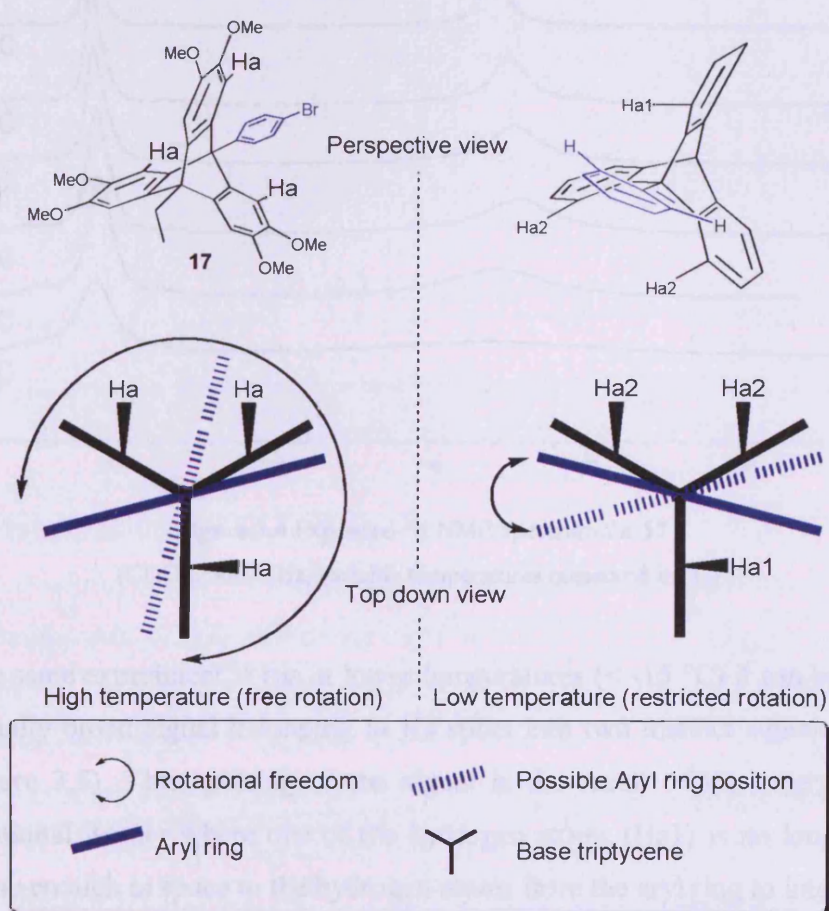


Figure 3.3 Illustration of the existence of unique proton environments, in an otherwise symmetrical molecule.

The broadening of the signal is due to interactions between the hydrogen atoms located on the aryl ring and the Ha hydrogen atoms on the triptycene. As the ring rotates around the single carbon-carbon bond adjoining it to the triptycene bridgehead carbon, the hydrogen atoms come within close proximity to each other at certain

points. As the temperature of the sample was raised (Figure 3.4) from 25 °C to 50 °C there is a clear sharpening of the peak relating to the signal from hydrogen atoms Ha. This effect is the result of overcoming the energy barrier associated with the steric hindrance experienced by the aryl ring as it rotates past the hydrogen atoms Ha. The sharper peak observed at higher temperatures (> 40 °C) is a result of rapid rotation around the carbon-carbon bond on the NMR timescale.

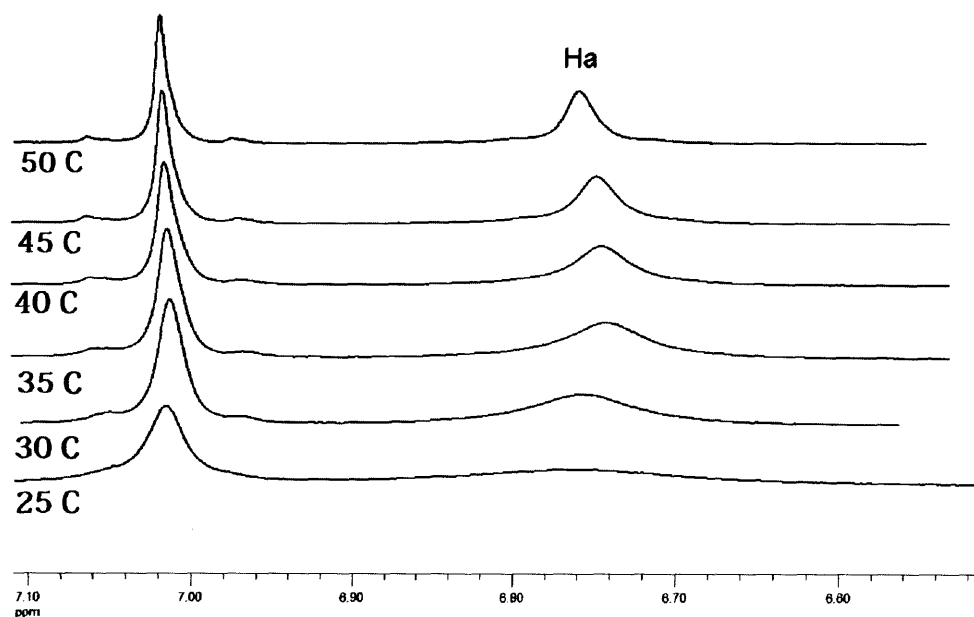


Figure 3.4 Expanded ¹H NMR spectrum for 17
(CDCl₃, 500 MHz, variable temperatures measured in °C).

When the same experiment is run at lower temperatures (< -15 °C) it can be seen that the originally broad signal belonging to Ha splits into two distinct signals (Ha1 and Ha2, Figure 3.5). This splitting of the signal is the result of the emergence of a conformational isomer where one of the hydrogen atoms (Ha1) is no longer able to come close enough in space to the hydrogen atoms from the aryl ring to interact.

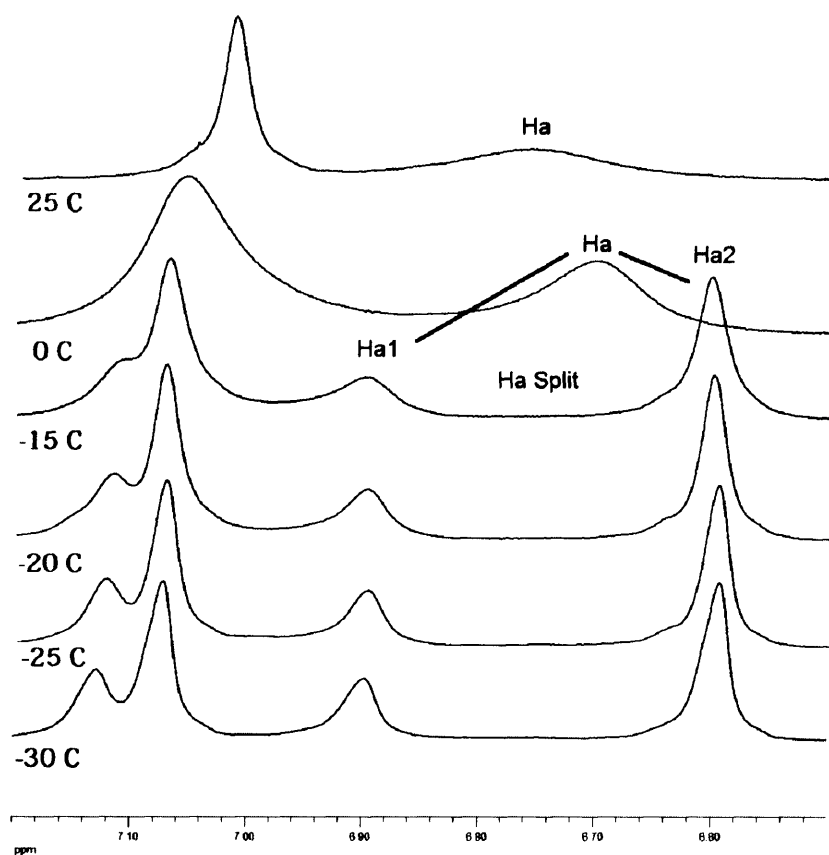
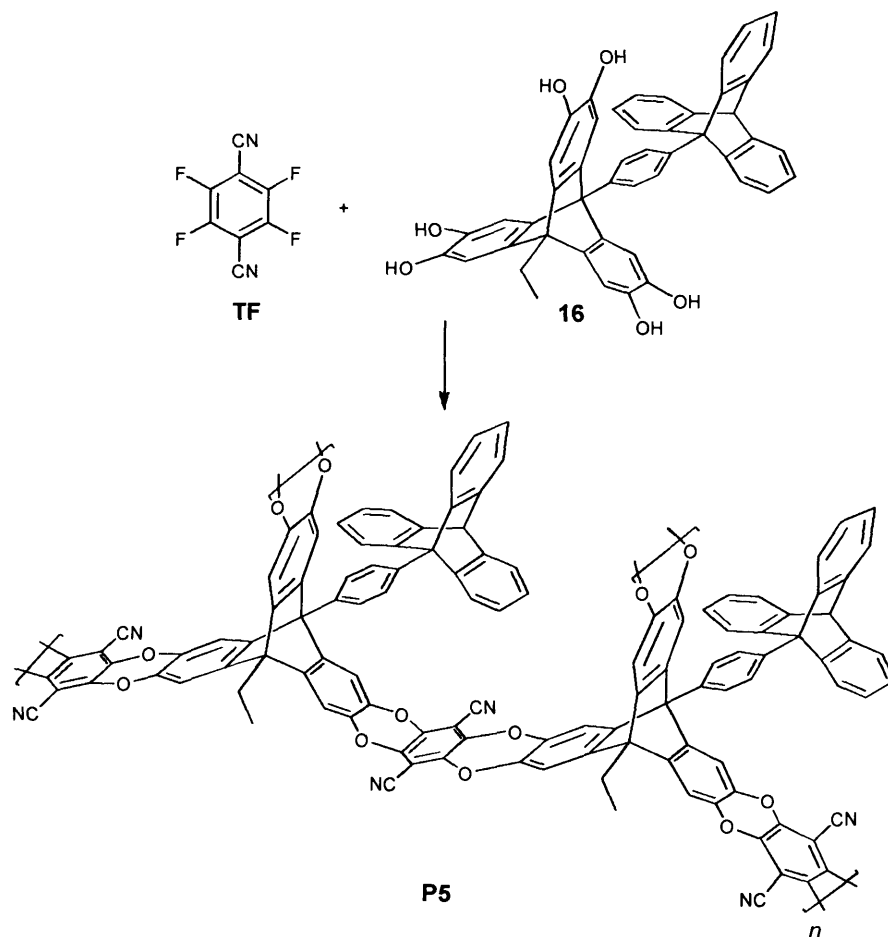


Figure 3.5 Expanded ^1H NMR spectrum for **17**
(CDCl_3 , 500 MHz, variable temperatures measured in $^\circ\text{C}$).

Between the temperature range $40\text{ }^\circ\text{C}$ and $-15\text{ }^\circ\text{C}$ the transformation from total rotational freedom on the NMR timescale to a locked system is observed. From this data it is reasonable to assume that the triptycene side group (in **16**) that replaces the bromine from **17** will suffer similar steric hindrance, and become sufficiently rigid at the temperatures required to perform the BET analysis (77 K). This rigidity should potentially enhance the intrinsic microporosity of the resulting polymer, as opposed to reducing it as is observed for increasing lengths of flexible alkyl chains.⁵

3.3.3 Synthesis of Network Polymer P5



Scheme 3.12 Reagents and conditions: K_2CO_3 , dry DMF, 65 °C, 72 hrs. (93% yield).

Despite this observation, a disappointing apparent BET surface area of $460 \text{ m}^2 \text{ g}^{-1}$ was obtained from nitrogen adsorption analysis of **P5**, which indicated that the triptycene side-groups diminish microporosity presumably by pore-blocking as is observed for the Trip-PIM networks with longer flexible alkyl chains. Interlocking of the triptycene substituents to enhance packing might contribute to this effect. Since the triptycene side-group appears not to contribute towards accessible micropores, the considerable mass added by its presence therefore only acts to decrease the pore density.

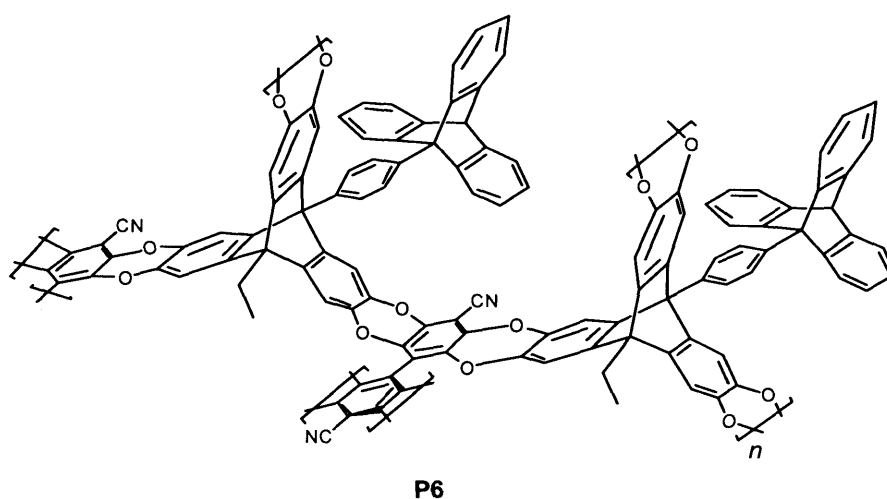
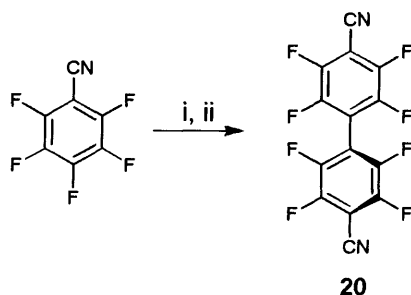


Figure 3.6 Network polymer with bulky triptycene side group, **P6**.

3.4.1 Synthesis of Monomer 20

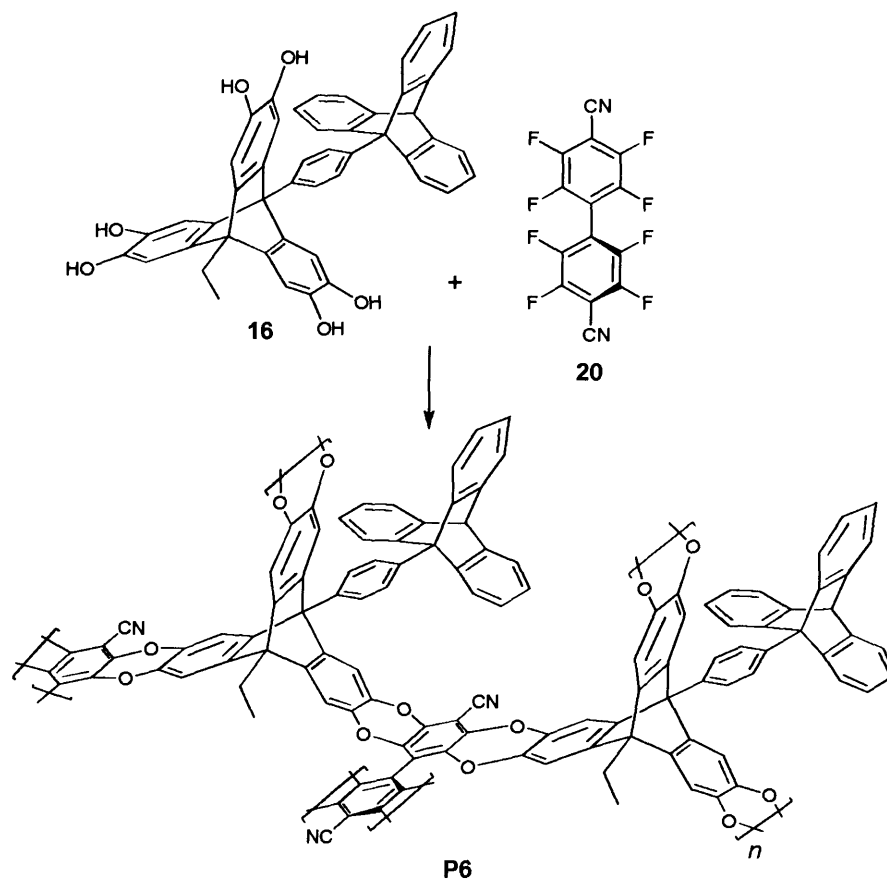
The target monomer **20** was synthesised in one step from commercially available starting materials. The synthetic procedure was deduced from information provided in a patent application.¹²⁸



Scheme 3.13 *Reagents and conditions:* i tris(diethylamino)phosphine, diethyl ether, N₂ atm.
ii 1M HCl. (46% yield).

Pentafluorobenzonitrile was reacted with tris(diethylamino)phosphine in diethyl ether with an ice bath for cooling due to the exothermic nature of the reaction. After 2 hrs the reaction was quenched with 1M HCl, and the product purified using flash chromatography to give 4,4'-dicyano-2,2',3,3',5,5',6,6'-octafluorobiphenyl **20** as a colourless solid with reasonable yield (46%, Scheme 3.13). The monomer was then oven dried at 60 °C and used without further purification.

3.4.2 Synthesis of Network Polymer P6



Scheme 3.14 Synthesis of network polymer **P6**. *Reagents and Conditions:* K_2CO_3 , DMF, 80 °C. (96% yield).

The apparent BET surface area of $940 \text{ m}^2 \text{ g}^{-1}$ demonstrated by nitrogen adsorption analysis is encouraging in that is twice the value obtained for the related polymer **P5**. However, it still falls short of the apparent BET surface area of the network polymer prepared from **20** and 9,10-dimethyl-2,3,6,7,12,13-hexahydroxytritycene by Dr. Kadhum Msayib, which is $1575 \text{ m}^2 \text{ g}^{-1}$.

3.5 Network Polymer P7 from monomer 20 and 21

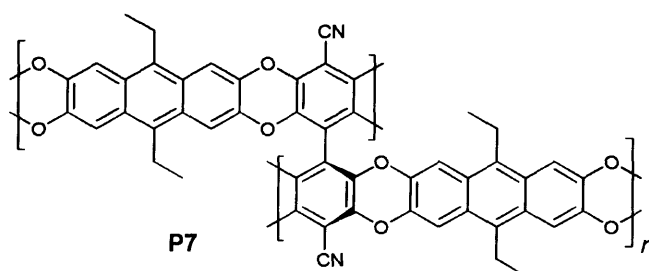
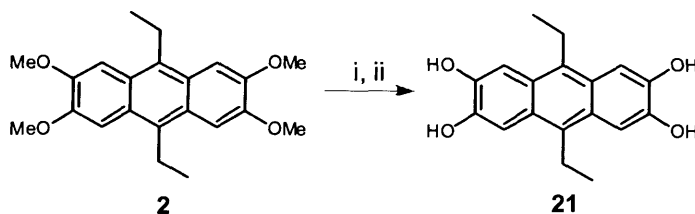


Figure 3.7 Network polymer P7.

This polymer was chosen as a target due to the fact that the catechol-containing monomer is, unusually, completely planar, and the only site of contortion is generated from the biphenyl monomer.

3.5.1 Synthesis of Monomer 21

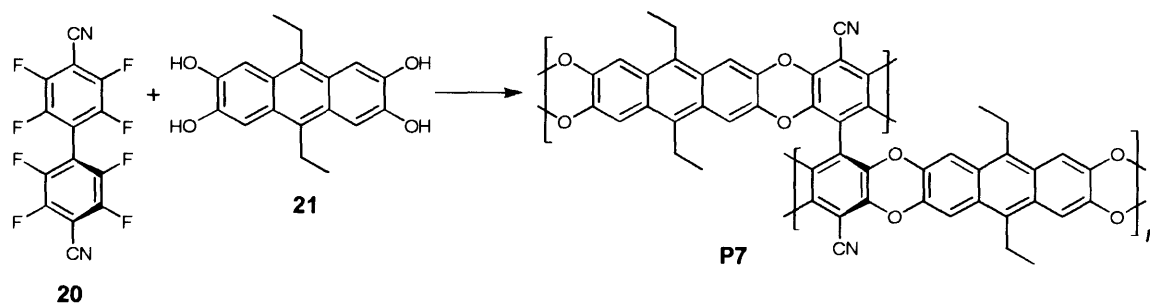
The monomer **21** was synthesised by demethylating the previously obtained anthracene **2** (Scheme 2.3).



Scheme 3.15 Reagents and Conditions: i BBr_3 , DCM, $0\text{ }^\circ\text{C}$; ii H_2O . (67% yield).

A sample of anthracene **2** was synthesised as previously described, and then recrystallised multiple times from ethanol until a high purity sample was obtained. The sample was then treated with BBr_3 in the usual way described in this project, to give **21** in good yield (67%). The sample was dried under vacuum in preparation to polymerisation.

3.5.2 Synthesis of Network Polymer P7



Scheme 3.16 Reagents and Conditions: K_2CO_3 , DMF, 65 °C. (82% yield).

The BET surface area of $626 \text{ m}^2 \text{ g}^{-1}$ obtained for **P7** is encouraging as the only ‘site of contortion’ is provided by the biphenyl unit. (Note added in Proof: the analogous polymer to **21** but containing methyl groups rather than ethyl groups at the 9,10 positions of the anthracene units was recently prepared by Mr. Mohammed Hassan and found to possess an apparent BET surface area of $912 \text{ m}^2 \text{ g}^{-1}$. This difference in surface area can be related to the enhanced pore blocking of the larger ethyl group and is very similar to that seen for the Trip(R)-PIM network polymers (Me = $1730 \text{ m}^2 \text{ g}^{-1}$; Et = $1415 \text{ m}^2 \text{ g}^{-1}$).¹

3.5.3 Summary of network polymers

The four network polymers synthesised in this chapter are insoluble, as predicted, indicating that polymerisation has occurred. They are all fairly stable (Degradation > 400-500 °C by TGA), and all exhibit good microporosity. Unfortunately, none of the polymers have surface areas above that of the reported standard trip(R)-PIM series.

Elemental analysis of the products (although inaccurate for chemical composition determination due to high levels of impurities inherent in microporous materials) indicated that considerable amounts of fluorine were present in the products. It is not simple to determine the exact reason for the presence of this fluorine, but it’s likely a result of KF trapped within the insoluble polymer particles, residual end groups resulting from a degree of condensation less than 100%, or a combination of both. Entrapped KF would only act to add weight, block pores and thus artificially decrease

the apparent surface area, a problem that could be rectified using mechanical grinding and washing. The problem of incomplete polycondensation would likely lead to an inherently less microporous material, an issue that can only be rectified by optimisation of the reactions and conditions, requiring considerable amounts of starting materials.

For the polymers **P5** and **P6** it appears as though the introduced triptycene side group did nothing to increase the microporosity and instead just added molecular weight, possibly coupled with a pore blocking effect. The rotational NMR data indicated that the triptycene side groups would be sufficiently rigid enough to maintain a constant open topology and limit compacting of the polymer chains, but the final surface area data suggests that these triptycene side groups have been largely detrimental to the porosity of the polymers. This may have arisen due to the fact that the triptycene side groups are free to interlock with other triptycene units (from the polymer backbone or other nearby side groups, Figure 3.8) resulting in strong π - π interactions between phenyl ring faces. This interaction results in close interlocking of polymer fragments resulting in an overall more dense compacted material with fewer micropores and increased mass. A solution to prevent triptycene faces from interlocking would be to introduce t-butyl groups along the leading edges, and should be considered for future work.

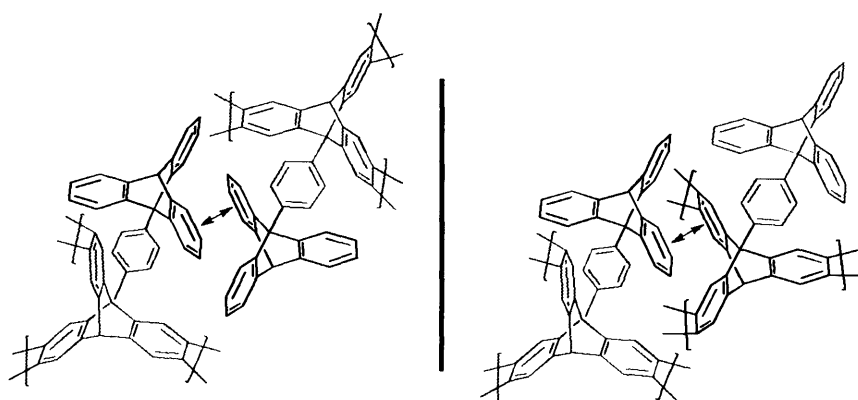


Figure 3.8 Phenyl ring π - π interaction (red arrow).

Left: Side group - side group; *Right:* Side group - polymer chain interaction.

Unless some unforeseen property can be found that warrants the difficult synthesis, these polymers offer no advantage over the previously published triptycene network PIMs.

Polymer	Monomer f		T_{onset} (°C)	BET (m ² g ⁻¹)
P4	6	2	447	880
P5	3	2	483	460
P6	3	4	482	940
P7	2	4	438	626

Table 3.1 Summary of network PIMs physical properties.

Below is a summary of the four network polymers N₂ adsorption/desorption isotherms, all exhibit classic Type I curves, confirming they possess pores in the micropore region.

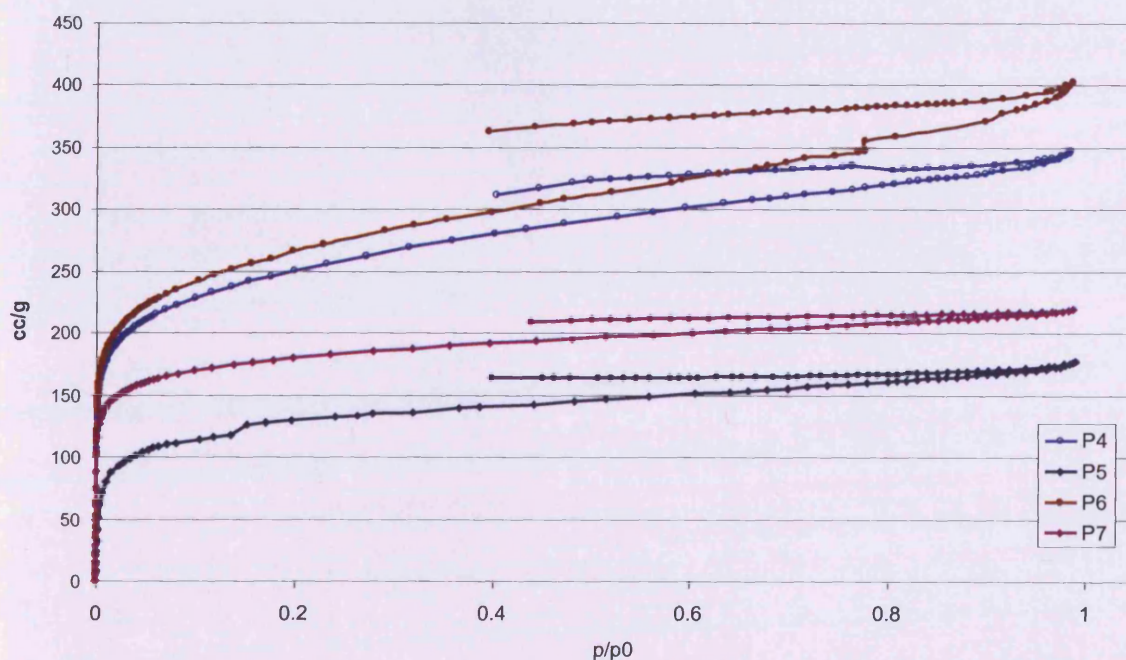


Figure 3.9 Adsorption/desorption isotherms for network PIMs (N₂ 77K).

Chapter 4: Organic Molecules and Dendrimers of Intrinsic Microporosity (OMIMs/DIMs)

4 Organic Molecules and Dendrimers of Intrinsic Microporosity (OMIMs/DIMs)

In this chapter we discuss a series of organic molecules of intrinsic microporosity (OMIMs), and dendrimers of intrinsic microporosity (DIMs). The OMIMs, DIMs, and precursor dendrons in this chapter afforded extremely broad and complex ^1H and ^{13}C NMRs, in cases where the NMR was sufficiently clear they are reported (as broad peaks/clusters). Carbon NMR proved to be particularly difficult as obtaining a sufficient concentration in the available deuterated solvents was not straight forward. In order to help gauge the purity, the samples that were sufficiently soluble in chloroform were analysed by GPC. The retention time for the GPC is calibrated for polystyrene and, due to the difference in hydrodynamic properties of the rigid, compact OMIMs and DIMs relative to the rigid-coil configuration of polystyrene in solution, the molecular masses reported do not represent the true values of the samples analysed. Instead the M_n/M_w distribution value is of more interest, as it is a strong indication of the purity of the sample. Crude samples analysed showed broad distributions, and often multiple peaks. Samples analysed displaying single peaks and $M_n/M_w < 1.05$ were considered of high purity.

4.1 Divergent triptycene dendrimer

To evaluate the possibility of constructing dendrimers of intrinsic microporosity it was decided to initially investigate a system where the dendrimers could be built up using a divergent synthesis to give the required generation number. The first synthetic challenge was devising an unsymmetrical triptycene system that had $f = 1$ that can be attached to the growing dendrimer, then subsequently have its outer edge activated in preparation for the addition of further branched units (Figure 4.1), effectively an AB_2 monomer. In the illustration (Figure 4.1) type A (green) reacts with type B (red) to form new bonds.

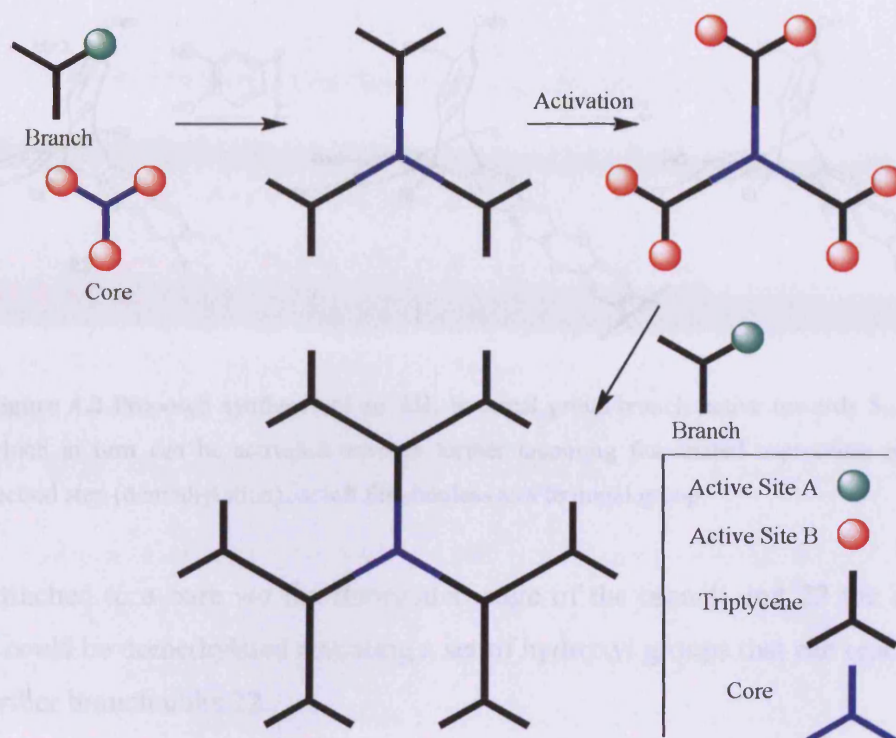


Figure 4.1 Illustration of dendrimer divergent growth, two active sites are required to form a new bond. Further growth requires the activation of the outer edge of the growing dendrimer, and introduction of new branch or terminal groups.

4.1.1 Synthesis of branch unit **22**

In order to achieve the required functionality, the molecule **22** was targeted where one aryl ring of the triptycene has fluorine groups active towards nucleophilic aromatic substitution due to the fused pyrazine ring, which is sufficiently electron withdrawing to activate the reaction.

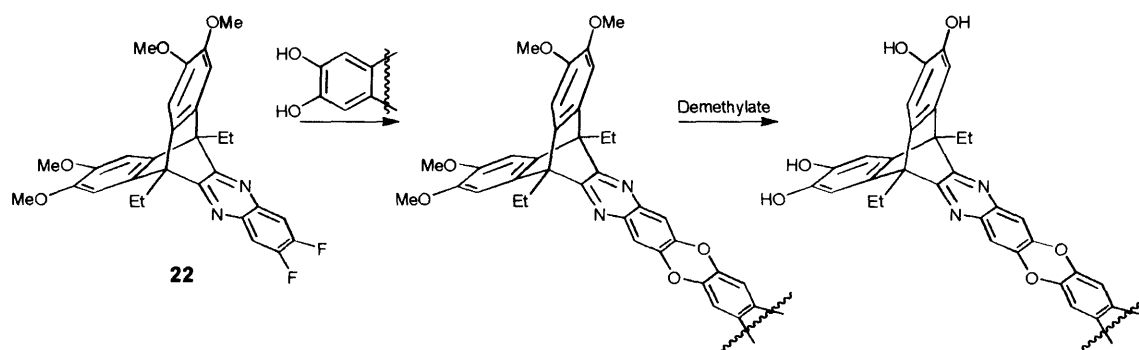


Figure 4.2 Proposed synthesis of an AB₂ terminal group/branch active towards S_NAr, which in turn can be activated towards further incoming fluorinated triptycenes in a second step (demethylation), or left functionless as a terminal group.

Once attached to a core *via* the fluorinated edge of the branch unit **22** the methoxy groups could be demethylated revealing a set of hydroxyl groups that can react readily with further branch units **22**.

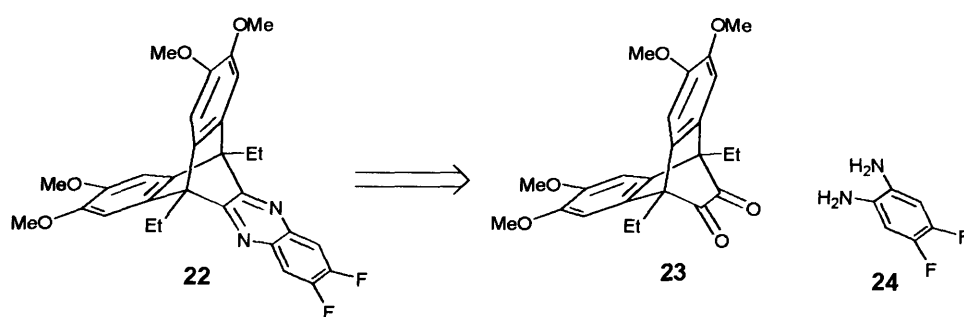
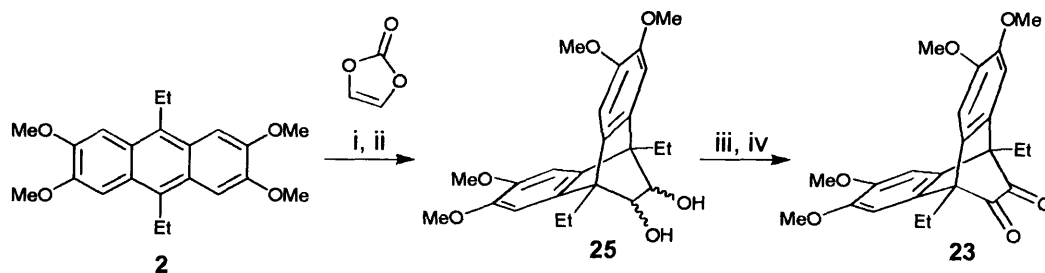


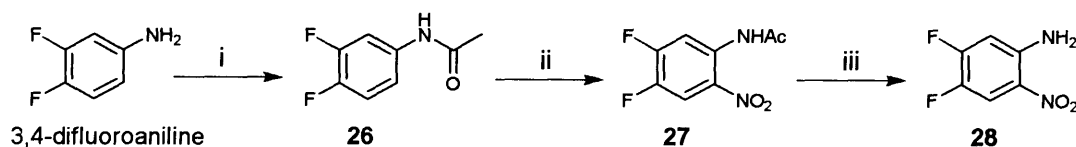
Figure 4.3 Retro synthetic analysis of target branch **22**.

From a retro synthetic analysis it was decided to target an anthracene with a diketone bridge **23** and 4,5-difluoro-1,2-phenylenediamine **24**. Hence, anthracene **2** was subjected to a microwave-mediated Diels-Alder reaction with vinylene carbonate. Microwave irradiation was used in favour of an autoclave due to the shorter reaction time (8 hrs microwave versus 72 hrs suggested for autoclave in literature¹²⁹) and higher yield of the Diels-Alder adduct. The carbonate was then hydrolysed to give the corresponding diol **25** (90%). A classical Swern oxidation of diol **25** gave the diketone **23** in good yield (89%).



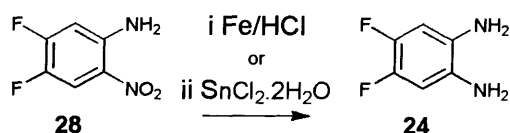
Scheme 4.1 *Reagents and Conditions:* i vinylene carbonate, toluene, microwave heating 8 hrs, 180 °C; ii sodium hydroxide solution reflux (40% aq) (90% yield); iii trifluoroacetic anhydride, DMSO, chloroform, -78 °C, triethylamine; iv HCl (2 M), 5 °C. (89% yield).

The next step was to synthesise the 4,5-difluoro-1,2-phenylenediamine **24**. Starting from the commercially available 3,4-difluoroaniline, the amine group was protected as an acetamide group to give **26**. This compound was nitrated to give **27**, deprotected by hydrolysis of the acetamide to give **28**, and finally the nitro group was reduced to give the required diamine **24**.



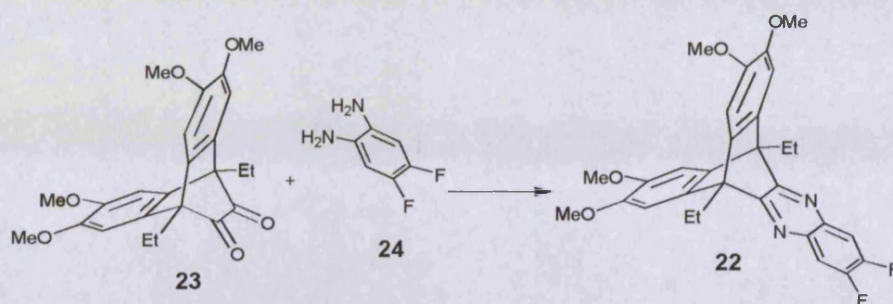
Scheme 4.2 *Reagents and Conditions:* i acetic anhydride, sodium acetate, HCl, H₂O (82% yield); ii HNO₃, H₂SO₄ (74% yield) iii Ethanol, HCl, H₂O (79% yield).

For this initially problematic reduction, two methods were tested using Fe/HCl (71% yield), and SnCl₂.2H₂O/HCl (62% yield). Although the iron reduction gave a higher yield, the large amounts of iron oxide generated from the reaction lead to a tedious workup, so the SnCl₂ method was preferred.



Scheme 4.3 *Reagents and Conditions:* i Iron powder, HCl (1 M), MeOH, NH₄OH (71% yield); ii SnCl₂.2H₂O (62% yield).

The amino groups from **24** and keto groups from **23** were condensed together under acid catalysed dehydrating conditions to give the final target branch unit **22** (66%).



Scheme 4.4 Reagents and Conditions: Acetic acid, reflux 15 hr (66% yield).

A single crystal x-ray diffraction study indicates that the molecule adopts the same desirable three-fold symmetry as a true triptycene with three concave faces of approximately 120° angles around the central axis. The crystal belongs to the monoclinic space group $C 2/c$, with cell lengths: a 30.8470(7), b 8.9960(2), c 8.5250(5) Å and cell angles α 90.00, β 102.5730(10), γ 90.00. The cell volume was 5017.4 Å³ with 8 molecules per unit cell, and no solvent.

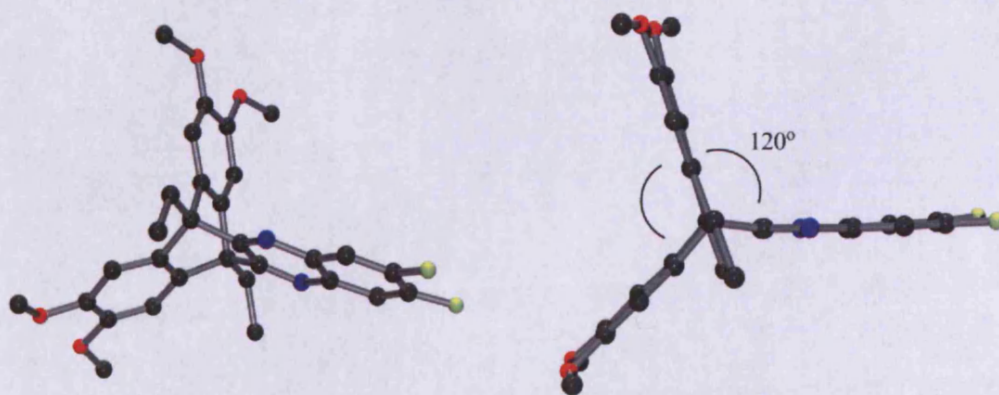
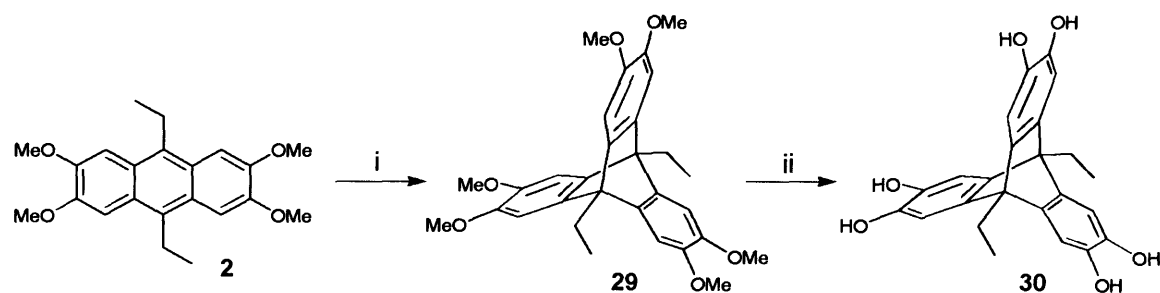


Figure 4.4 Structures drawn from crystal data for functional triptycene like branch **22**.

4.1.2 Synthesis of triptycene core **30**

The first target dendrimer core was the hexahydroxy-triptycene **30** with $f = 3$. It was chosen as it links 3 branch units together in a trigonal planar arrangement, has its own

IFV, and 3D molecular modelling suggested that steric hindrance should not prevent all 3 branch units surrounding the core.



Scheme 4.5 Reagents and conditions: i 4,5-dimethoxybenzenediazonium-2-carboxylate chloride, DCE, 83 °C (42% yield); ii BBr₃, DCE, 0 °C (79% yield).

The first step in the synthesis of the previously synthesised 9,10-diethyl-2,3,6,7,12,13-hexahydroxytriptycene **30**⁵ was to remake tetramethoxyanthracene **2** (Scheme 2.3) and then to react it with 4,5-dimethoxybenzenediazonium-2-carboxylate chloride in DCE under reflux (Scheme 4.5). The resulting crude product was purified by flash chromatography to give a good amount of hexamethoxytriptycene **29** (42%). A recrystallised sample of **29** (ethanol) was demethylated using BBr₃ with little problem (79%). The product obtained was found to be highly sensitive to colour degradation (from pink to purple), and so was handled with care as described previously for similar triptycene monomers.

4.1.3 Synthesis of dendrimer D1

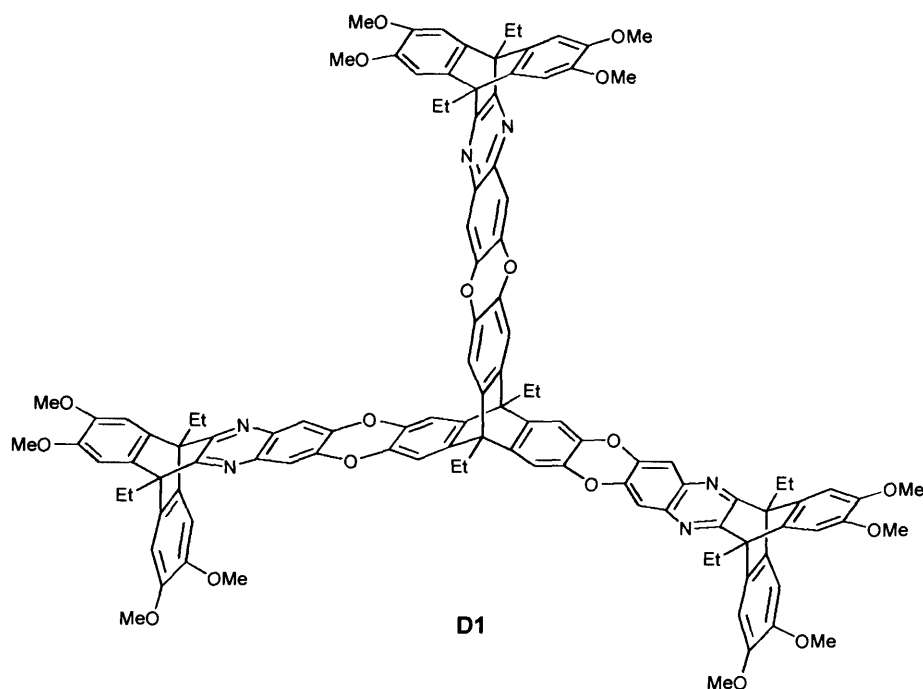


Figure 4.5 Chemical structure of zero-generation dendrimer **D1**.

The synthesis of the “zero-generation” divergent dendrimer **D1** began with a nucleophilic aromatic substitution reaction between branch unit **22** and the hexahydroxytritycene **30**. The fluorines of **22** showed slightly decreased reactivity towards nucleophilic aromatic substitution when compared to previous fluorinated compounds used in this project (i.e. compounds **20** and 2,3,5,6-tetrafluoroterephthalonitrile). This decrease in reactivity is almost certainly related to the less potent electron withdrawing pyrazine present in **22**, as compared to the nitrile groups of **20** and 2,3,5,6-tetrafluoroterephthalonitrile. To counteract the lower reactivity, the reaction temperature was elevated from the usual 60-80 °C to 120 °C as this was found to be sufficient for the reaction to proceed readily.

The product was isolated *via* flash chromatography in fair yield (54%) and found to have an apparent BET surface area of 10 m² g⁻¹. This low value corresponds to that of a fine powder. The lack of microporosity is likely due to the planar structure of the molecule, which although has plenty of IFV from its triptycene subunits, the IFV would seem to be inaccessible, preventing penetration of the probe molecules. The near-honeycomb structure of dendrimer **D1** is akin to that of a small fragment of the

trip-PIM series, but it would appear that the long-range polymer chain entanglement present in the trip-PIM polymers significantly reduces mobility and packing efficiency and as a result generates accessible surface area. In addition to the planarity of the structure, the flexibility of the methoxy substituents on the terminal triptycene units may contribute to the apparent lack of microporosity analogous to the significant reduction in surface area observed for the Trip-PIM containing ethyl groups at the triptycene bridgeheads ($1400 \text{ m}^2 \text{ g}^{-1}$) as compared to the Trip-PIM substituted with methyl groups ($1730 \text{ m}^2 \text{ g}^{-1}$). There is also the distance between triptycene bridgehead carbons to consider, for a regular Trip-PIM polymer there are a minimum of eight bonds between them, and for dendrimer **D1** the minimum bond count is ten. The extra distance (owing to the introduction of the pyrazine ring) might be sufficient to enable the high IFV triptycene subunits to pack more efficiently *via* interlocking of the dendritic arms.

4.1.4 Synthesis of dendrimer D3

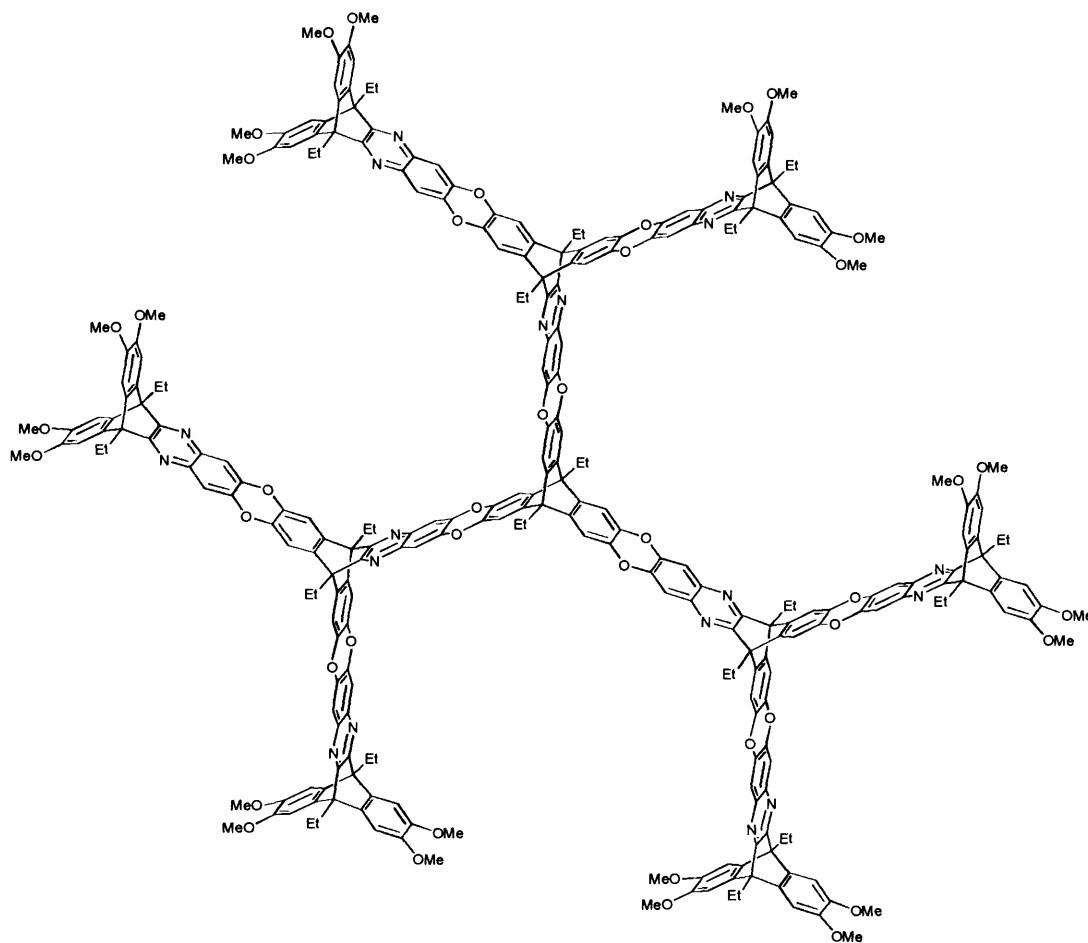
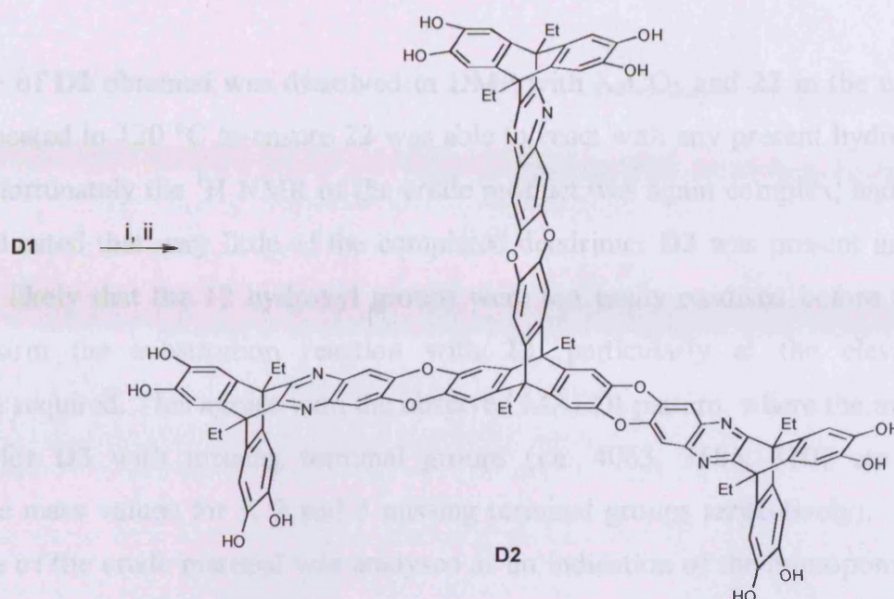


Figure 4.6 Chemical structure of first generation dendrimer **D3**.

Despite **D1** being non-microporous it was decided to continue on to the first-generation dendrimer **D3**. It was hoped that the increased dimensions of the molecule could cause reduced packing efficiency to generate accessible micropores. It also allowed us to evaluate the effectiveness of our system for a step-wise construction of a divergent PIM-like dendrimer.



Scheme 4.6 Reagents and Conditions: i BBr_3 , DCM, 0°C ; ii H_2O (86% yield).

The first stage in the synthesis of this dendrimer was demethylation of dendrimer **D1**. The demethylation was not without problems as the required amount of the demethylating agent (up to 24 equivalents, 12 equivalents for each methoxy group and a further 12 equivalents for remaining heteroatoms) BBr_3 appeared to cause degradation of the product. The product was only slightly soluble in $\text{DMSO}-d_6$, in which further visible colour degradation was quickly observed. The only analysis that returned a satisfactory results was the ^1H NMR, it appeared a good match for the expected spectra so the synthesis continued to the next step, toward **D3**, which would contain no unstable functional groups and be more readily characterised.

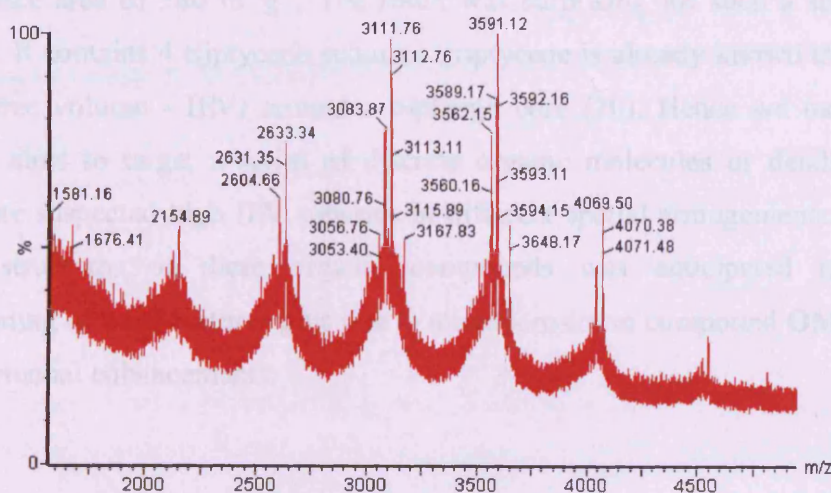


Figure 4.7 MALDI of **D3** crude sample. Pattern represents missing terminal groups.

The sample of **D2** obtained was dissolved in DMF with K_2CO_3 and **22** in the usual way, then heated to 120 °C to ensure **22** was able to react with any present hydroxyl groups. Unfortunately the 1H NMR of the crude product was again complex, and the MALDI indicated that very little of the completed dendrimer **D3** was present in the crude. It is likely that the 12 hydroxyl groups were too easily oxidised before they could perform the substitution reaction with **22**, particularly at the elevated temperature required. This agrees with the observed MALDI pattern, where the major peaks are for **D3** with missing terminal groups (i.e. 4063, 3585, 3107 etc are approximate mass values for 1, 2 and 3 missing terminal groups respectively). The surface area of the crude material was analysed as an indication of the microporosity of the dendrimer and was again found to be negligible. Although this novel approach to divergent dendrimer construction at first seemed promising, the synthetic practicalities rendered this route obsolete.

4.2 Triptycene tetramer, OMIM-1

Thus far in the field of organic microporous materials it was believed that microporosity was a result of the packing inefficiency resulting from long-range rigid non-linear polymer chain entanglement or crystalline order. We discovered that the triptycene tetramer compound **OMIM-1** (Figure 4.8), which was prepared in order to determine the reactivity of octafluorobiphenyl **20** towards catechols, had an apparent BET surface area of $580\text{ m}^2\text{ g}^{-1}$. The result was surprising for such a small simple molecule. It contains 4 triptycene subunits (triptycene is already known to have high internal free volume - IFV) around a biphenyl core (**20**). Hence we modified our synthetic aims to target a series of discrete organic molecules or dendrimers that incorporate suspected high IFV subunits in different spatial arrangements. The well-defined structures of these organic compounds was anticipated to enhance understanding of what features give rise to microporosity in compound **OMIM-1**, and lead to potential enhancements.

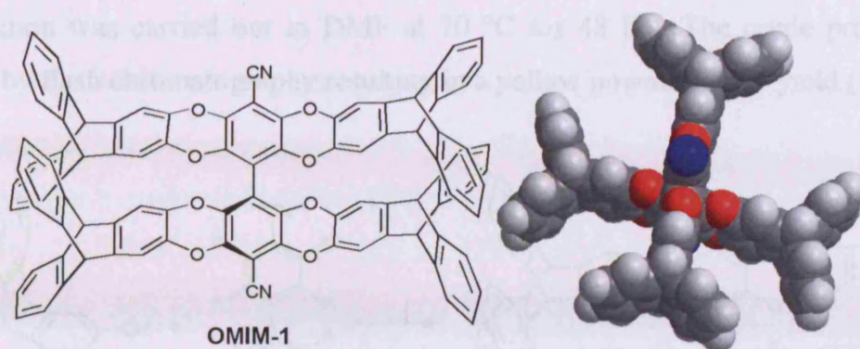
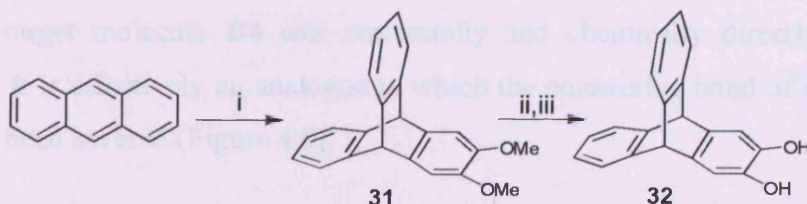


Figure 4.8 Chemical and space filling energy minimised structure of **OMIM-1**, which demonstrates an apparent BET surface area = $580 \text{ m}^2 \text{ g}^{-1}$ (N_2 , 77K).

We first considered how the lower molecular weight **OMIM-1** (fw = 1333.40 g/mol), which incorporates only 4 triptycene units demonstrates significant microporosity whereas the previously prepared zeroth-generation dendrimer **D1** (fw = 1842.02 g/mol) also with 4 triptycene units, has none. A potential difference between these two molecules is the planar nature of **D1** compared to the more compact 3-dimensional ‘globular’ structure of **OMIM-1**. This evidence suggests that when designing a potential microporous molecule/dendrimer the aspect ratio should be considered, with potential targets being as awkwardly shaped as possible in all 3-dimensions.

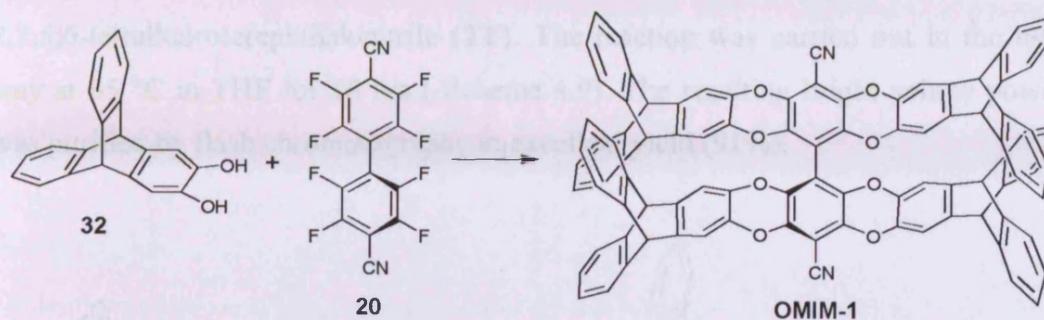
4.2.1 Synthesis of OMIM-1

The synthesis of **OMIM-1** was fairly straight-forward, requiring a nucleophilic aromatic substitution reaction between the previously synthesised 2,3-dihydroxytriptycene **32** (Scheme 4.8) and octafluorobiphenyl **20**.



Scheme 4.7 Synthesis of 2,3-dihydroxytriptycene **32**. *Reagents and Conditions:* i 4,5-dimethoxybenzenediazonium-2-carboxylate chloride, DCE, 83 °C (22% yield); ii BBr_3 , DCE, 0 °C; iii H_2O (79% yield).

The reaction was carried out in DMF at 70 °C for 48 hrs. The crude product was purified by flash chromatography resulting in a yellow powder in fair yield (68%).



Scheme 4.8 Synthesis of **OMIM-1**. Reagents and conditions: K_2CO_3 , DMF, 70 °C (68% yield).

The final product had an apparent BET surface area of $580 \text{ m}^2 \text{ g}^{-1}$, which was used as the reference point for subsequent products.

4.3 Triptycene dimer, D4

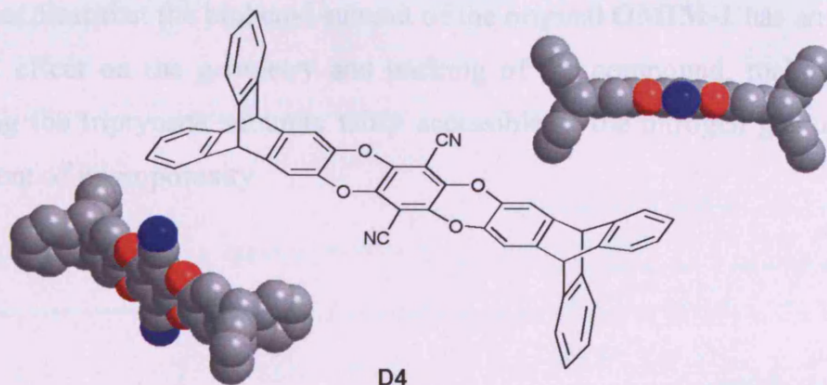
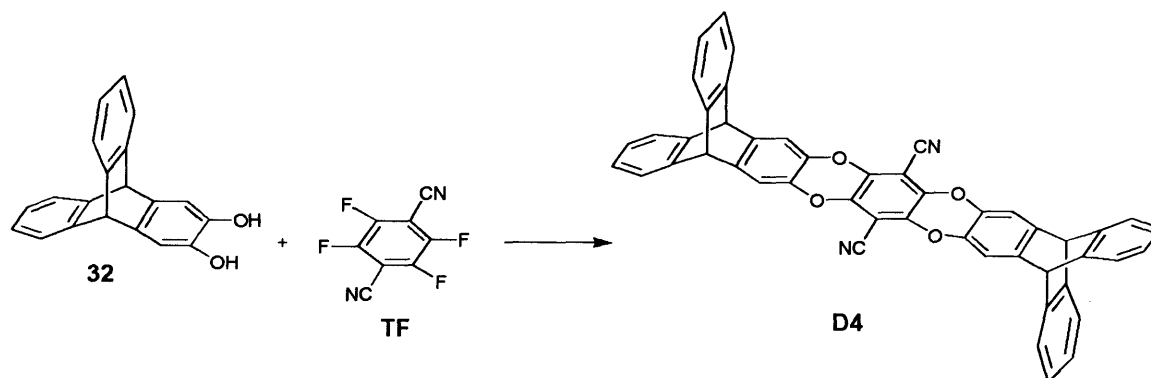


Figure 4.9 Chemical and space filling energy minimised structure of **D4**.

The first target molecule **D4** was structurally and chemically directly related to **OMIM-1**. It is effectively an analogue in which the connecting bond of the biphenyl centre has been severed (Figure 4.9).

4.3.1 Synthesis of D4

The synthesis of **D4** was similar to that for **OMIM-1**, reacting **32** this time with 2,3,5,6-tetrafluoroterephthalonitrile (**TF**). The reaction was carried out in the usual way at 65 °C in THF for 18 hrs (Scheme 4.9). The resulting bright yellow powder was purified by flash chromatography in excellent yield (91%).



Scheme 4.9 Reagents and conditions: K_2CO_3 , DMF, 70 °C (91% yield).

The isolated final product had an apparent BET surface area of 0 m² g⁻¹. From this result it was clear that the biphenyl subunit of the original **OMIM-1** has an extremely significant effect on the geometry and packing of the compound, making the IFV surrounding the triptycene subunits fairly accessible to the nitrogen gas used in the measurement of microporosity.

4.4 Dendrimer with a triptycene core, DIM-1

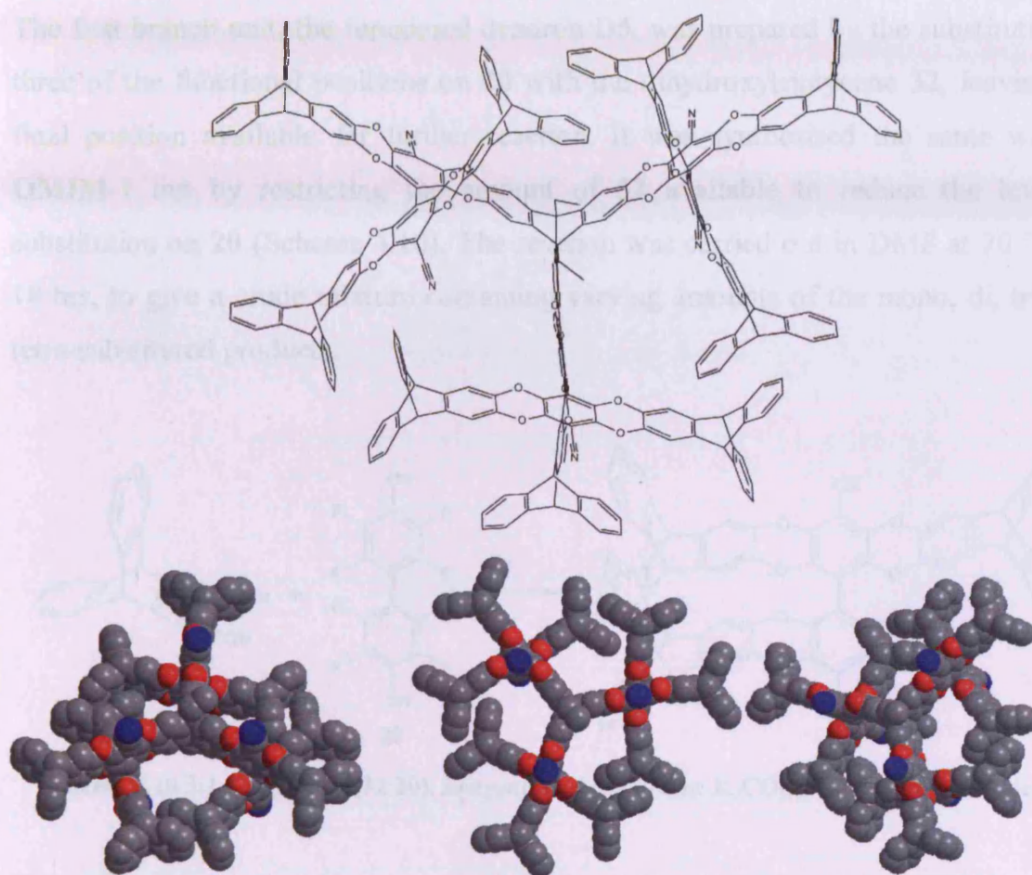
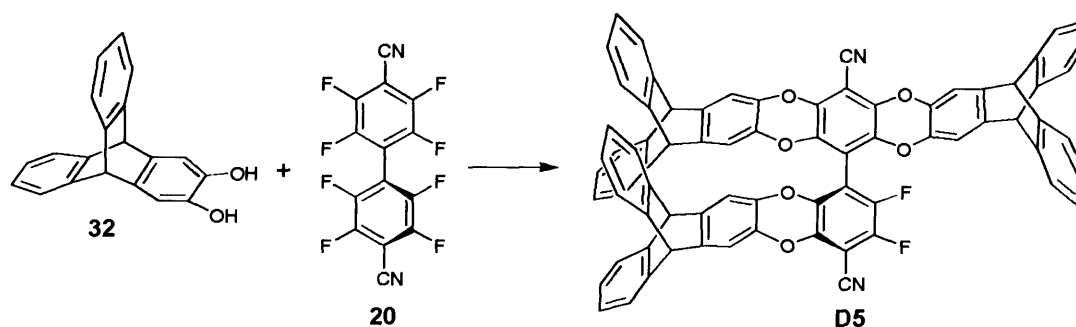


Figure 4.10 The chemical structure and three views of a molecular model of **DIM-1** from different directions.

As reducing the overall size of the molecule resulted in total loss of microporosity (as with **D4**), it was decided instead to increase the size of the next target molecule. We decided to generate a reactive unit with functionality $f = 1$ containing as much of the structural features of **OMIM-1** as possible, so that it could then be attached to a core to build up a larger dendritic molecule. This process of attaching branches to a core is commonly termed ‘a convergent strategy’ in the context of dendrimer synthesis. This convergent method allowed us to ensure that the branch used in the final step was pure and contains the exact features we want derived from **OMIM-1**. It also means we can vary the core readily so that the branches have different spatial arrangements to interpret what affect this has on the resulting microporosity.

4.4.1 Synthesis of triptycene based functional dendron D5

The first branch unit, the functional dendron **D5**, was prepared by the substitution of three of the functional positions on **20** with the dihydroxytriptycene **32**, leaving the final position available for further reaction. It was synthesised the same way as **OMIM-1** but by restricting the amount of **32** available to reduce the level of substitution on **20** (Scheme 4.10). The reaction was carried out in DMF at 70 °C for 18 hrs, to give a crude mixture containing varying amounts of the mono, di, tri, and tetra-substituted products.



Scheme 4.10 3:1 equivalents (**32:20**). *Reagents and conditions:* K₂CO₃, DMF, 70 °C (42% yield).

The required tri-substituted product **D5** was obtained with extreme difficulty from careful column chromatography to eliminate higher and lower substituted products that would have a detrimental effect on further reactions. The required functional dendron **D5** with $f=1$ was eventually obtained in fair yield (42%) after a considerable amount of effort. In order to check the purity of the sample ($f_w = 1087.08$), which could not easily be distinguished by ¹H NMR from the di- ($f_w = 840.77$) and tetra- ($f_w = 1333.40$) substituted products, MALDI-TOF was used.

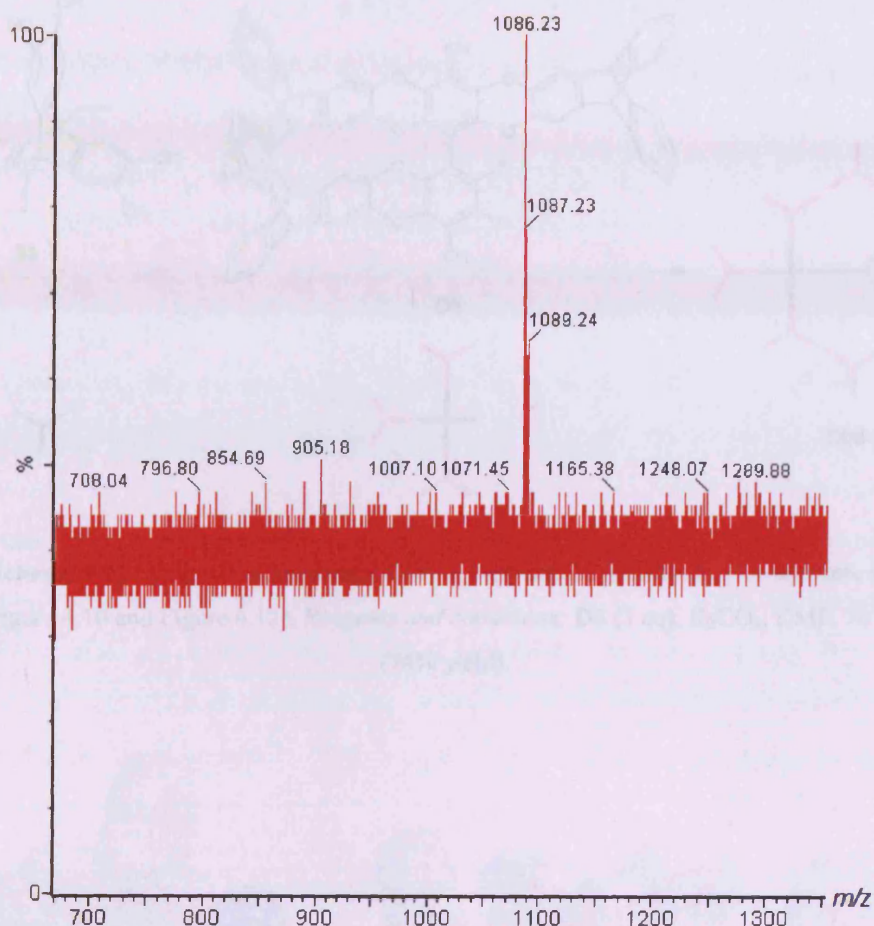
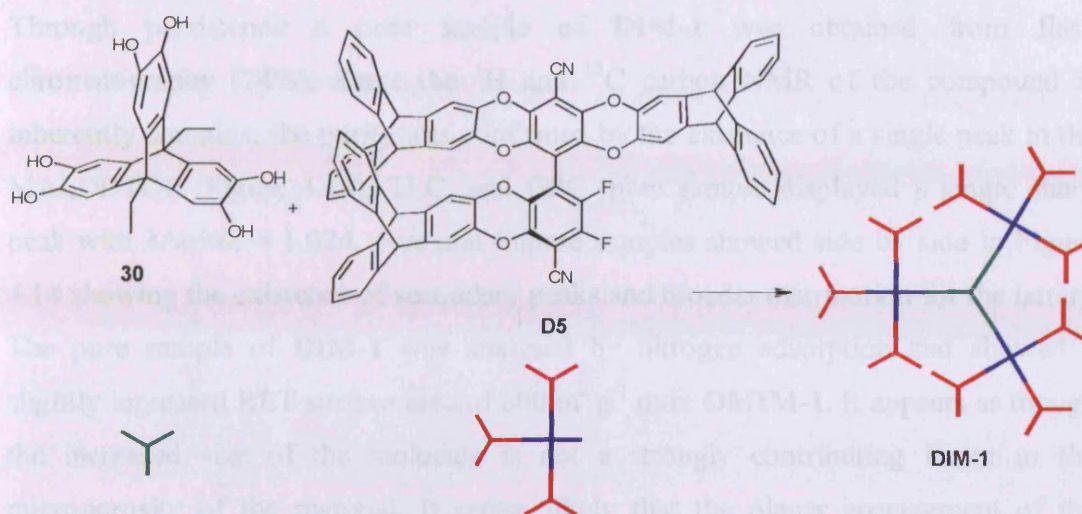


Figure 4.11 MS (MALDI-TOF) for functional dendron **D5**. Single peak corresponding to a likely pure sample (confirmed by TLC).

4.4.2 Synthesis of dendrimer DIM-1

A pure sample of **D5** was dissolved in DMF with the triptycene core **30** and K_2CO_3 at 70 °C for 18 hrs (Scheme 4.11). On quenching with water the yellow precipitate was purified by flash chromatography which proved to be an extremely difficult process. The sample appeared to aggregate on the silica, often becoming stationary. The addition of toluene acted to help increase the compounds ability to pass through the column but chromatography still remained an inefficient process. Unfortunately other methods of purification (including multiple precipitations from various solvent/non-solvent systems, and recrystallisation) proved even less effective.



Scheme 4.11 Synthesis of dendrimer **DIM-1**, represented graphically (for structure see Figure 4.10 and Figure 4.12). *Reagents and conditions:* **D5** (3 eq), K_2CO_3 , DMF, $70\text{ }^\circ\text{C}$ (74% yield).

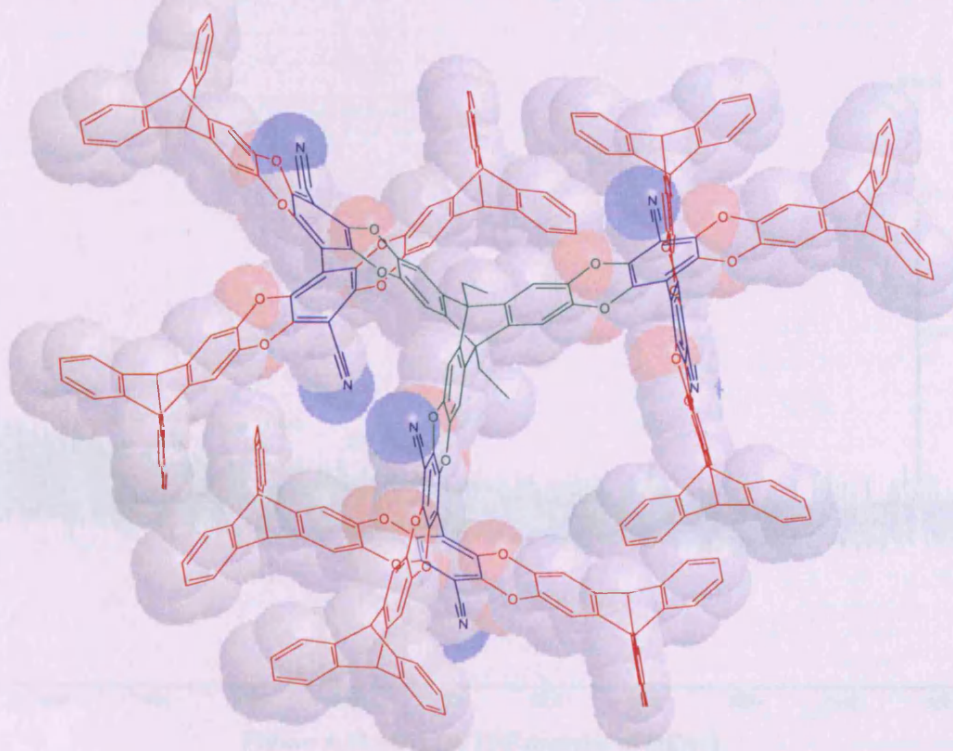


Figure 4.12 Chemical structure of **DIM-1**. Colours highlight origin of subunits (illustrated in Scheme 4.11). 3D space filling model in background.

Through persistence a pure sample of **DIM-1** was obtained from flash chromatography (74%). Since the ^1H and ^{13}C carbon NMR of the compound is inherently complex, the purity was confirmed by the existence of a single peak in the MALDI-TOF (Figure 4.13), TLC, and GPC (pure sample displayed a single sharp peak with $M_w/M_n = 1.024$, pure and impure samples showed side by side in Figure 4.14 showing the existence of secondary peaks and broader distribution for the latter). The pure sample of **DIM-1** was analysed by nitrogen adsorption and showed a slightly increased BET surface area of $600\text{ m}^2\text{ g}^{-1}$ over **OMIM-1**. It appears as though the increased size of the molecule is not a strongly contributing factor to the microporosity of the material. It seems likely that the planar arrangement of the branch units (**D5**) does little to increase microporosity, and instead the accessible surface remains around the biphenyl segments inherent from **OMIM-1**. This observation adds to a growing body of evidence which suggest that intrinsic microporosity within a polymer arises from the local structure around certain rigid units of a particular shape rather than the packing of the extended macromolecule.⁵⁸

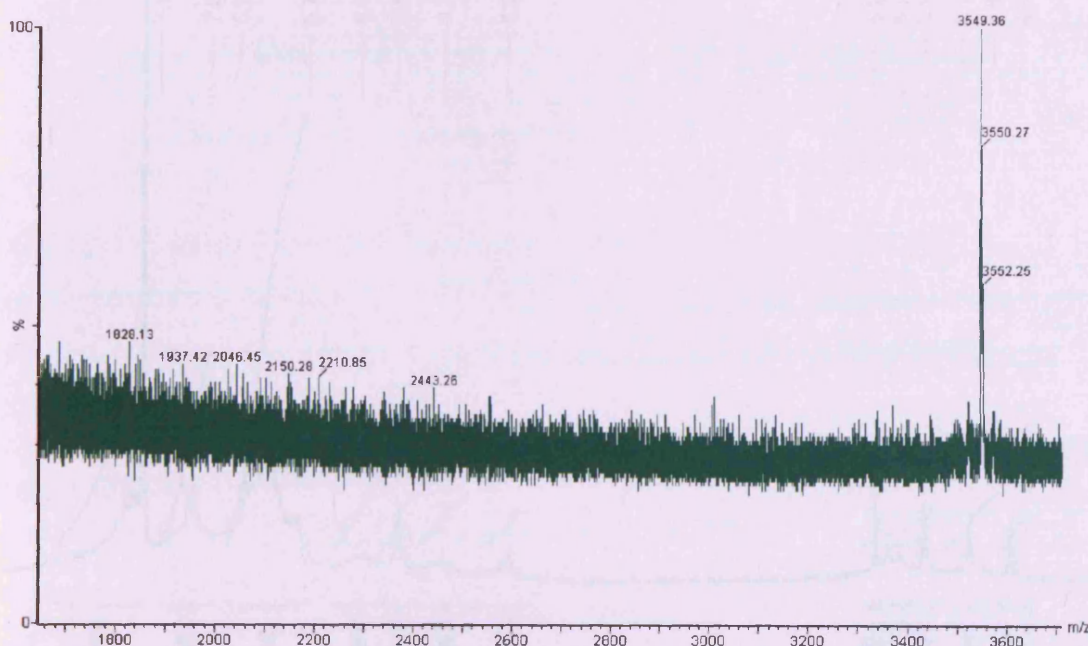


Figure 4.13 MALDI-TOF analysis of **DIM-1**.

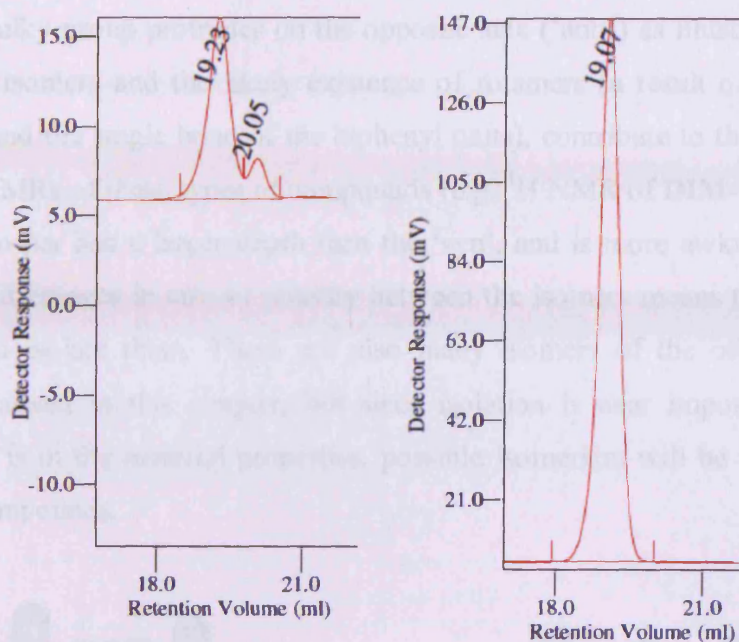


Figure 4.14 GPC run of an impure sample (*left*) displaying two distinct peaks, and the same sample purified (*right*) with only one single sharp peak.

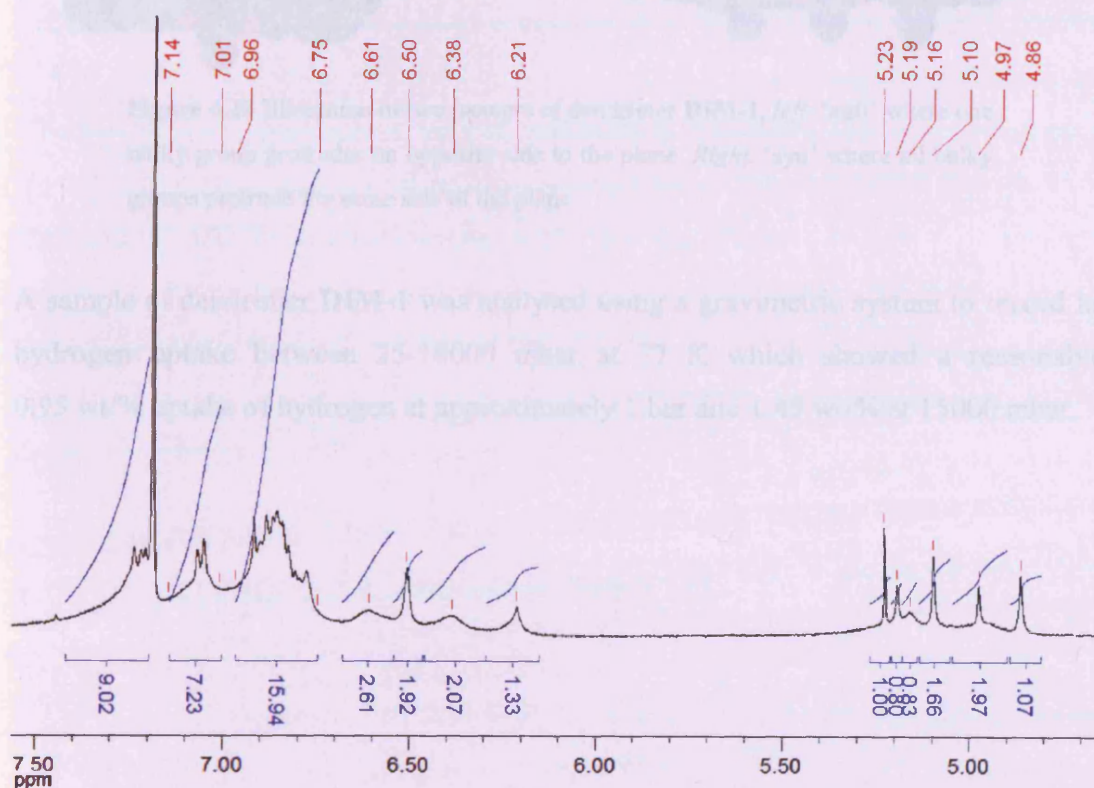


Figure 4.15 Expansion of DIM-1 ^1H NMR (400 MHz, CDCl_3) illustrating broad peaks.

It is also noteworthy that stereoisomers of dendrimer **DIM-1** exist, in which all three bulky groups protrude on the same side of the plane of the core (dubbed ‘syn’), or

where one bulky group protrudes on the opposite side ('anti') as illustrated in Figure 4.16. These isomers and the likely existence of rotamers (a result of the restricted rotation around the single bond of the biphenyl units), contribute to the complex and broadened NMRs of these types of compounds (e.g. ^1H NMR of **DIM-1** Figure 4.15). The 'anti' isomer has a larger depth than the 'syn', and is more awkwardly shaped. The minor differences in size or polarity between the isomers means that no attempt was made to isolate them. There are also many isomers of the other DIMs and OMIMs discussed in this chapter, but since isolation is near impossible, and the interest here is in the material properties, possible isomerism will be ignored for all but stated compounds.

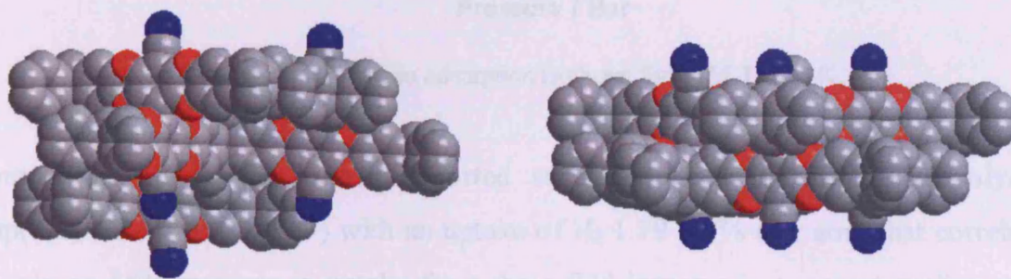


Figure 4.16 Illustration of two isomers of dendrimer **DIM-1**, *left*: 'anti' where one bulky group protrudes on opposite side to the plane. *Right*: 'syn' where all bulky groups protrude the same side of the plane.

A sample of dendrimer **DIM-1** was analysed using a gravimetric system to record its hydrogen uptake between 25-18000 mbar at 77 K which showed a reasonable 0.95 wt/% uptake of hydrogen at approximately 1 bar and 1.45 wt/% at 15000 mbar.

4.5 Dendrimer with CTC core, DIM-2

Attaching three BA branch units together in a point arrangement has little effect on microporosity, therefore a core structure is required with a different spatial arrangement. The cyclotriphosphazene (CTC) core, which has been previously used as porous PBA networks with reasonable surface area ($100 \text{ m}^2 \text{ g}^{-1}$)¹⁰ has the open functionality as the arylating core ($\gamma = 3$), but the three functional groups are directed pointing away from a

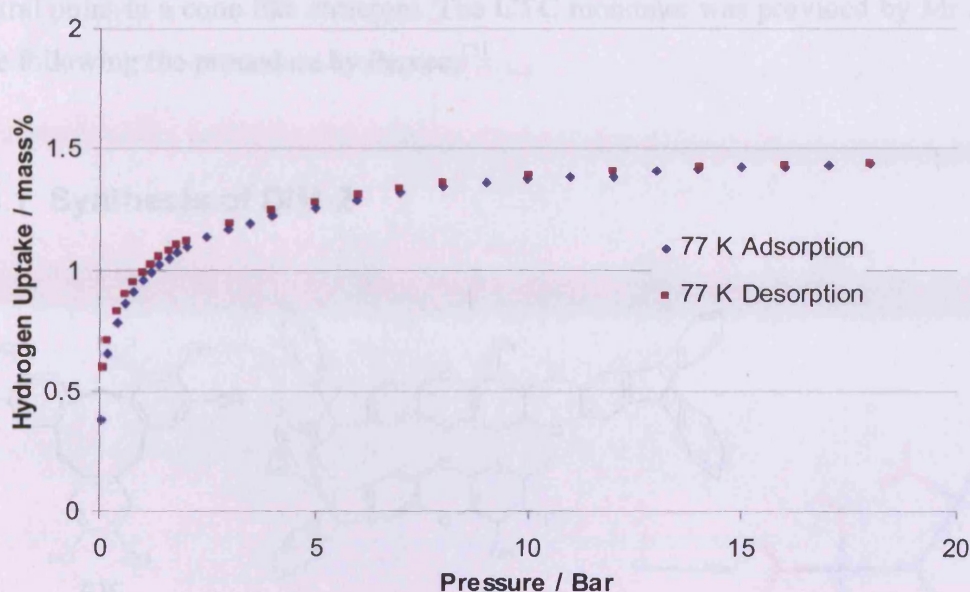


Figure 4.17 Hydrogen adsorption isotherm for **DIM-1** at 77 K.

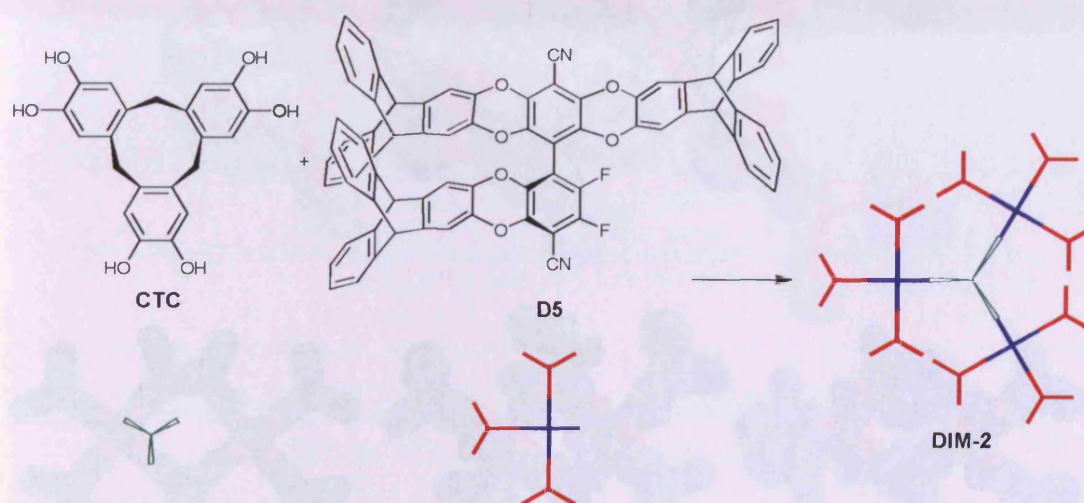
Comparing this to the highest reported surface area triptycene based polymer Trip(Me)-PIM ($1760 \text{ m}^2 \text{ g}^{-1}$) with an uptake of H_2 1.79 wt/% at 1 atm, that correlates to only an 88% increase in uptake for a three fold increase in apparent surface area. The chemical composition of the two materials is essentially the same, containing aromatic, dioxane, alkyl and nitrile functional groups so the enthalpy of adsorption of hydrogen should be comparable for both materials. Further studies (i.e. accurate analysis of pore size distribution) need to be conducted to help conclude a reason behind this observation. It is however plausible that the sample of **DIM-1** contains a larger percentage of ultramicropores ($< 0.7 \text{ nm}$) which energetically favours the uptake of hydrogen over larger micropores at low pressures.¹³⁰

4.5 Dendrimer with CTC core, DIM-2

Attaching three **D5** branch units together in a planar arrangement had little affect on microporosity, therefore, a new core was targeted with a different spatial arrangement. The cyclotricatecylenene (**CTC**) unit, which has been previously used to prepared PIM-networks with reasonable surface area ($830 \text{ m}^2 \text{ g}^{-1}$)¹⁵ has the same functionality as the triptycene core ($f=3$), but the three functional sites are arranged pointing away from a

central point in a cone like structure. The **CTC** monomer was provided by Mr James Vile following the procedure by Percec.¹³¹

4.5.1 Synthesis of DIM-2



Scheme 4.12 Reagents and conditions: K_2CO_3 , DMF, 70 °C. (62% yield).

The synthesis of **DIM-2** was similar to **DIM-1**. The functional dendron **D5** and **CTC** core was dissolved in DMF and heated with K_2CO_3 at 70 °C for 18 hrs before being quenched in water (Scheme 4.12). Again difficulties with purification were experienced, but a pure sample of **DIM-2** was obtained and found to have an apparent BET surface area of $535 \text{ m}^2 \text{ g}^{-1}$. The slight drop in microporosity from **OMIM-1** likely results from a combination of the slightly more flexible **CTC** core, and the potential for these cone shaped molecules to stack on top of each other.



4.6 Dendrimer with spiro-centre core, DIM-3

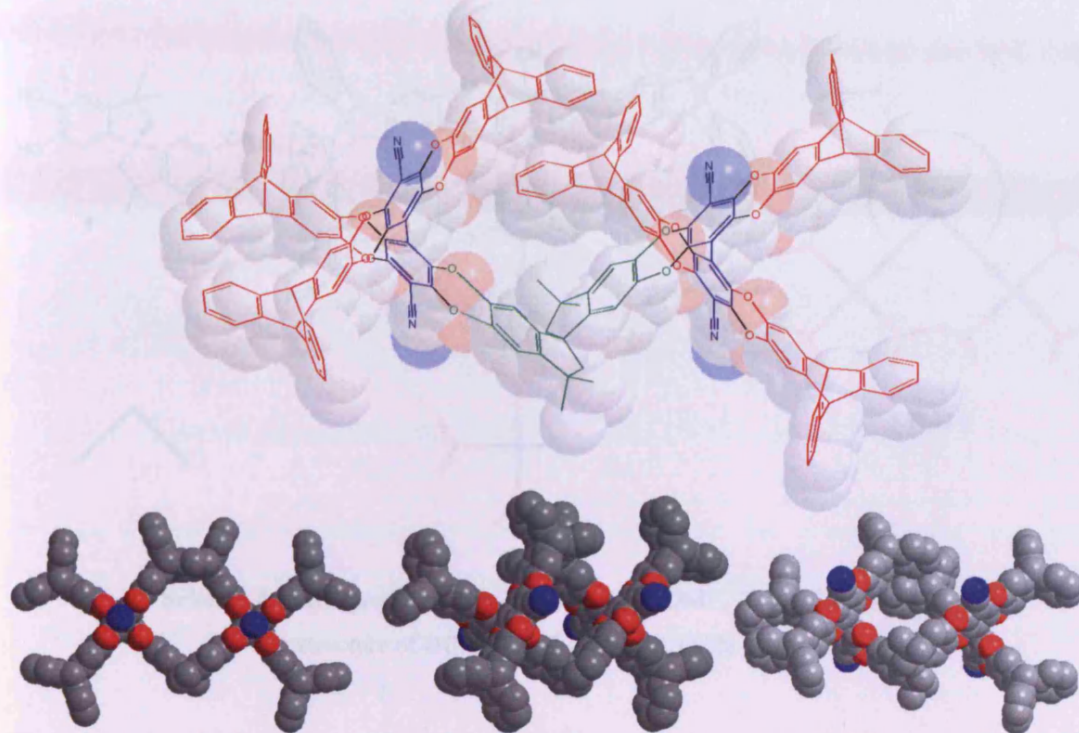
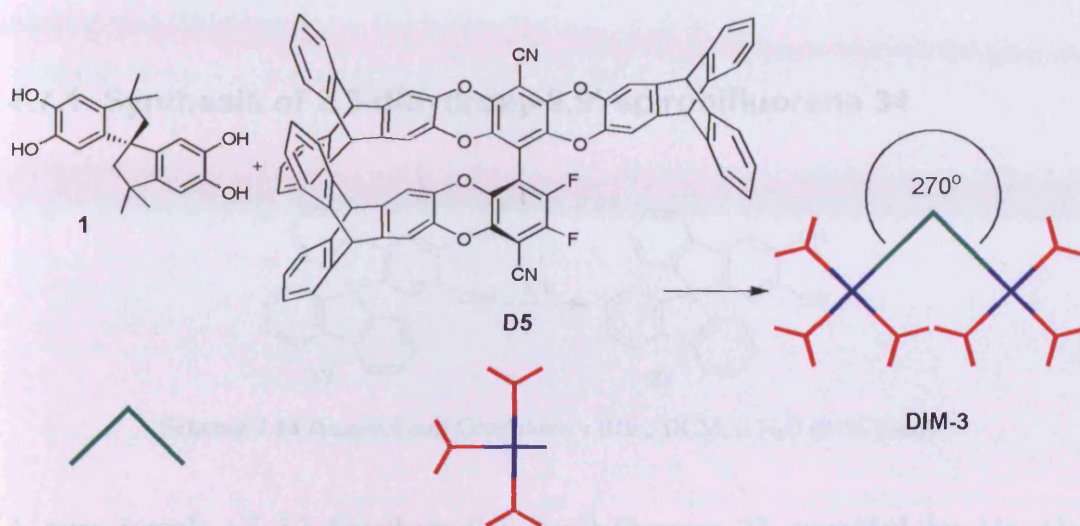


Figure 4.18 Illustrations of the energy minimised space filling structure of one isomer of DIM-3 from multiple angles.

The next logical step was to use 5,5',6,6'-tetrahydroxy-3,3,3',3'-tetramethyl-1,1'-spirobisindane which is commercially available and is a proven monomer for the synthesis of a number of PIMs^{1,73,75} as a core. It has a functionality $f=2$ and the spiro-centre will cause the two branch units to be held at an angle of 90° relative to each other.

4.6.1 Synthesis of dendrimer DIM-3



Scheme 4.13 Reagents and conditions: K_2CO_3 , DMF, 70 °C. For chemical structure of **DIM-3** see Figure 4.18. (51% yield).

The functional dendron **D5** and 5,5',6,6'-tetrahydroxy-3,3,3',3'-tetramethyl-1,1'-spirobisindane core were reacted in DMF with K_2CO_3 at 70 °C for 18 hrs. The isolated product was found to have an apparent BET surface area of $420 \text{ m}^2 \text{ g}^{-1}$. The drop in microporosity was an unexpected result, but likely due to the lack of guarded space around the exposed 270° angle of the core unit.

4.7 Tetramer from dihydroxy-spirobifluorene 34, D6

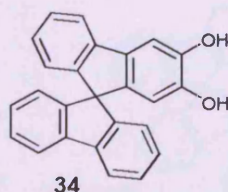
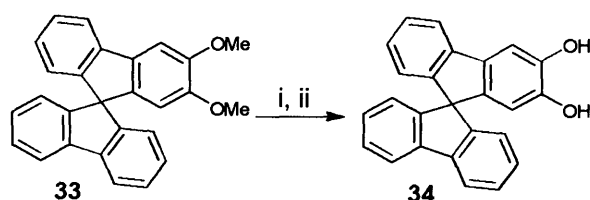


Figure 4.19 Terminal group 2,3-dihydroxy-9,9'-spirobifluorenone.

The next target was based around the spiro-centre that was so successful in **PIM-1**. This time though the spiro-centre was guarded in all four directions by phenyl rings to

give a solid tetrahedral structure, which was presumed to result in enhanced IFV around the spiro-centre.

4.7.1 Synthesis of 2,3-dihydroxy-9,9'-spirobifluorene **34**

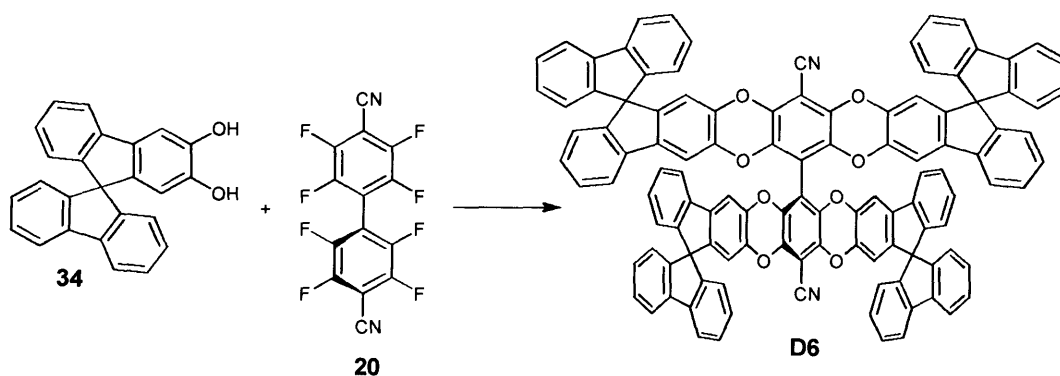


Scheme 4.14 Reagents and Conditions: i BBr_3 , DCM; ii H_2O (91% yield).

A pure sample of 2,3-dimethoxy-9,9'-spirobifluorene **33**, provided by Mr Alex Tonkins, was demethylated with BBr_3 to give 2,3-dihydroxy-9,9'-spirobifluorene **34** (Scheme 4.14) in excellent yield (91%). The product appeared stable with no obvious visual evidence of degradation.

4.7.2 Synthesis of tetramer D6

The tetramer was synthesised using 4 equivalents of the terminal group 2,3-dihydroxy-9,9'-spirobifluorene **34** (plus a slight excess) with **20** acting as a core connecting unit. The reaction was carried out under the same conditions as similar nucleophilic aromatic substitutions in this project, in DMF at 70 °C for 18 hrs.



Scheme 4.15 Reagents and conditions: K_2CO_3 , DMF, 70 °C (54% yield).

The reaction appeared to proceed without any complication, and the product was isolated by flash chromatography with only a little difficulty. Once purified the sample was found to have an apparent BET surface area of $0 \text{ m}^2 \text{ g}^{-1}$. This is an unexpected result, which at present defies a simple explanation.

4.8 Dendrimer from D7 and 30, D8

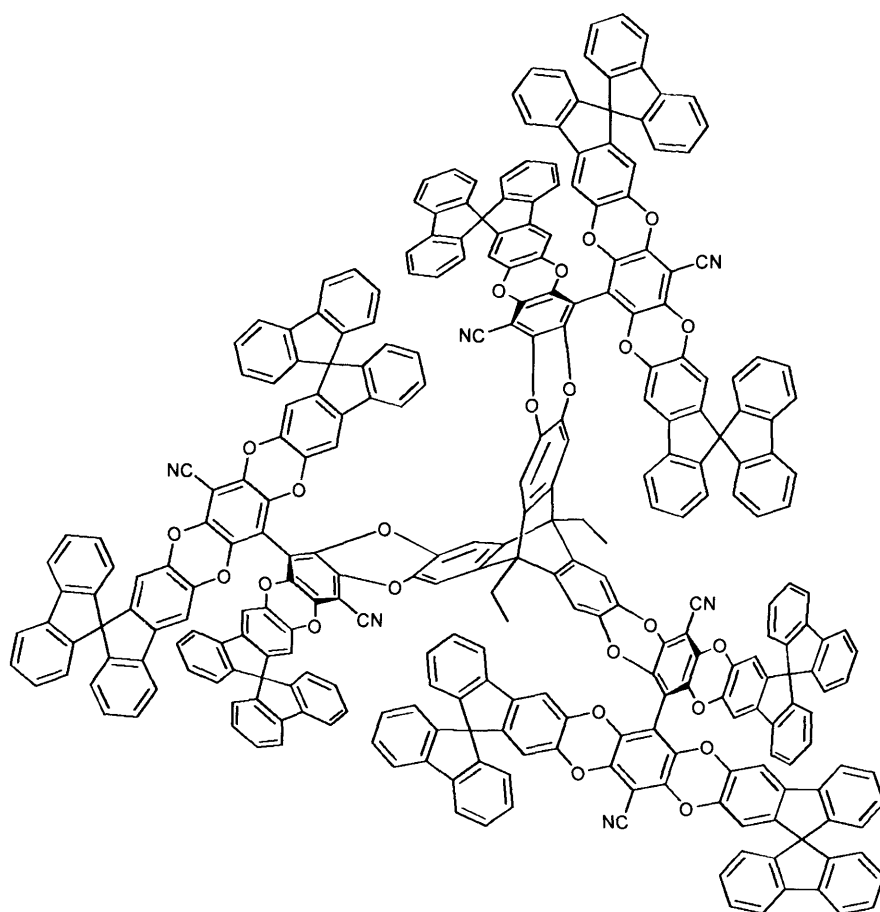


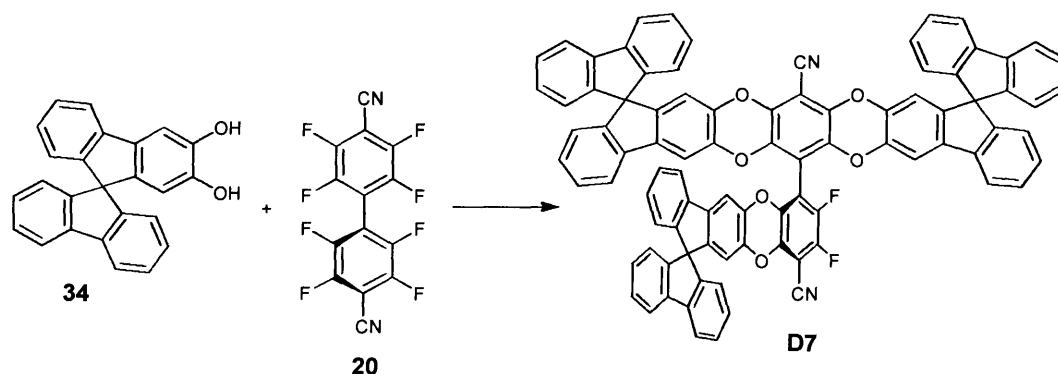
Figure 4.20 Structure of dendrimer **D8**. Some bonds distorted to enable some clarity.

Advancing on from the tetramer **D6**, which surprisingly offered no N_2 accessible surface area, it was decided to make the dendritic structure **D8**. Discovering whether a spirobifluorene-based dendrimer could achieve microporosity could offer further evidence about how accessible free volume arises. If the larger dendritic structure **D8** showed surface area above what was observed for the tetramer **D6**, then it could be deduced that the overall packing and restricted movement (result of longer range order) of the spiro-centres is the major component in micropore accessibility, and that

pores around the central heavily guarded triptycene contribute significantly. If the dendrimer **D8** also showed no evidence of significant nitrogen adsorption, then this favours a more localised origin of intrinsic microporosity (i.e. packing inefficiency resulting directly from the spiro-bifluorene terminal groups, with accessible free volume surrounding these spiro-centres and the biphenyl unit).

4.8.1 Synthesis of functional dendron **D7**

The first step towards the target dendrimer **D8** was obtaining the dendron **D7**. The terminal group **D7** with functionality $f = 1$ was synthesised in the same way as tetramer **D6**, but limiting the amount of 2,3-dihydroxy-9,9'-spirobifluorene **34** available to 3.3 equivalents.

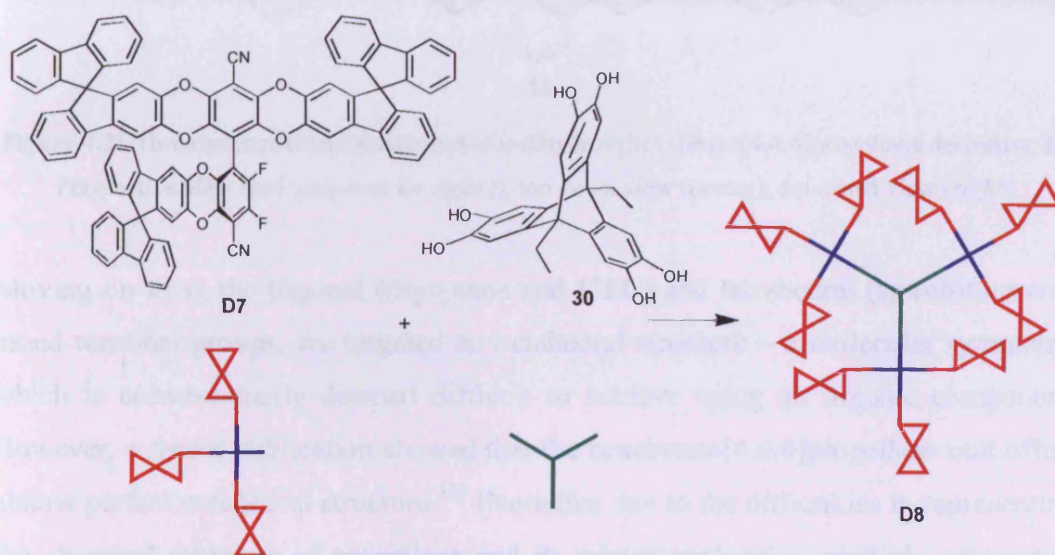


Scheme 4.16 Equivalents of **34/20**, 3.3/1 respectively. *Reagents and conditions:* K_2CO_3 , DMF, 70 °C (37% yield).

The reaction proceeded well and was purified using flash chromatography with much less frustration than some of the triptycene based dendrons synthesised in this project. A pure sample was obtained quite readily but in a low yield (37%) largely due to the fact that a large number of mono, di and tetra substituted by-products were present at the end of the reaction. A possibility for increasing the achievable yield might be to add the 2,3-dihydroxy-9,9'-spirobifluorene **34** to the reaction mixture over a period of time. Once oven-dried, the dendron **D7** was used without further purification.

4.8.2 Synthesis of dendrimer D8

Using the same method employed for **DIM-1**, the hexahydroxytyritycene core **30** and functional dendron **D7** were dissolved in DMF, and stirred with K_2CO_3 at 70 °C for 18 hrs.



Scheme 4.17 Reagents and Conditions: DMF, K_2CO_3 , 70 °C, 18 hrs (16% yield).

The crude obtained was again soluble, but did not easily pass through silica gel. The product was precipitated from solvent/non-solvent (chloroform/hexane) multiple times, and again checked by TOF-MALDI to confirm the existence of the desired dendrimer **D8**. The precipitations reduced the crude mass significantly, and by the time a minimum sample was obtained (65 mg, lower masses introduce significant difficulties in loading, and errors in measuring surface areas), the MALDI indicated that significant amounts of the di-substituted product remained. Without better means for separation the materials was taken as is, its surface area was analysed and found to be non-microporous ($17 \text{ m}^2 \text{ g}^{-1}$). This result is surprising, and no obvious explanation can be offered at this time without further investigation, especially as the presence of the di-substituted oligomer in the final material may reduce microporosity. However, this fact alone seems an unlikely explanation for the complete lack of microporosity as even the pure tetramer **D6** was found to be non-microporous.

4.9 Propellane containing tetramer OMIM-2

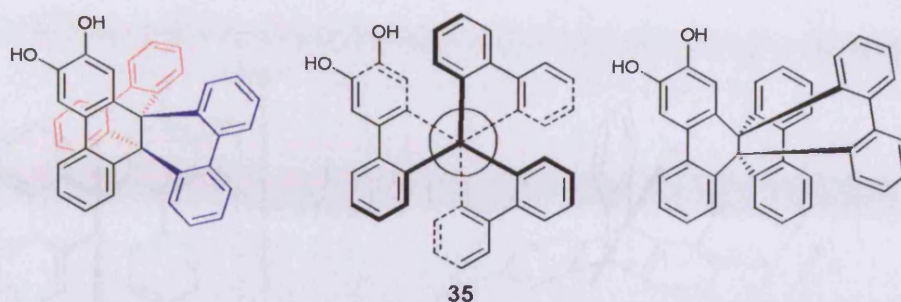


Figure 4.21 Three structural representations of *o*-dihydroxyhexabenzopropellane derivative **35**. Perspective view (*left*, coloured for clarity), top down view (*centre*), deformed view (*right*).

Moving on from the trigonal (tritycene and **CTC**) and tetrahedral (spirobifluorene) based terminal groups, we targeted an octahedral structure – a molecular symmetry, which is conventionally deemed difficult to achieve using an organic component. However, a recent publication showed that the hexabenzopropellane unit offers almost perfect octahedral structure.¹³² (Note that due to the difficulties in representing the chemical structure of propellane and its related molecules, multiple schematics and illustrations will be used to help clarify the 3-dimensional shape). The target propellane-based molecule **35** has functionality $f = 1$ and consists of three biphenyl units bound at the 2,2' carbon atoms by two central tertiary carbon atoms. The reported crystal structure¹³² illustrates the twisted helical nature of the molecule, with three guarded channels between each biphenyl unit located around the central axis (Figure 4.21, Figure 4.22). The three channels are analogous to the three concave faces around triptycene, with three segments comprising of 120° with similar dimensions, but in the case of propellane the depth of each face (D) is in the order of 7.4 \AA versus 5.0 \AA for triptycene (Figure 4.22). The increased depth was hoped to provide added IFV and lead to increased guarded space in the final tetramer **OMIM-2** in comparison to its triptycene based counterpart **OMIM-1**. Based upon energy minimised conformations it can be deduced that an approximation of the maximum potential volume of guarded space in the ideal structures for both triptycene and propellane is 146 \AA^3 and 237 \AA^3 , respectively (dimensions taken from crystal structure of propellane,¹³² and energy minimised structure of triptycene illustrated in

Figure 4.22, volume calculated as a prism where $V = ((L^2\sqrt{3})/4)D \text{ \AA}^3$, assuming area is of equilateral triangle with length of side L , and prism with depth D).

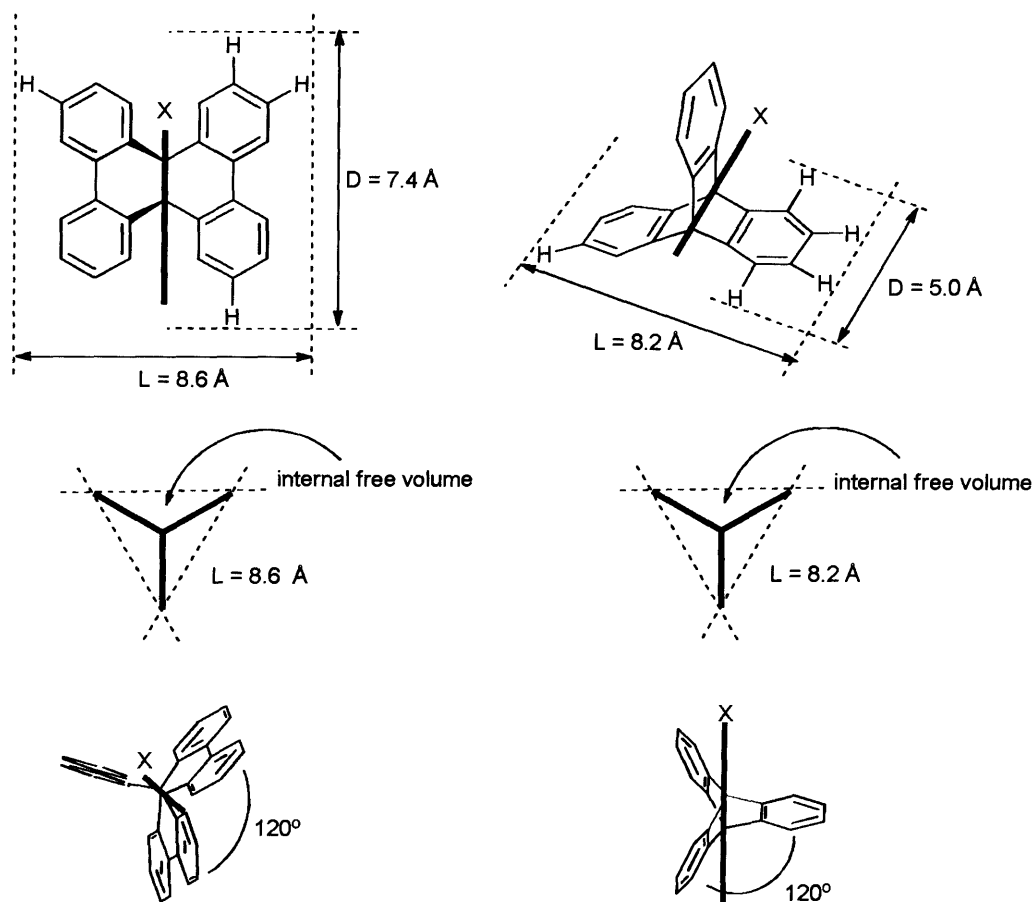
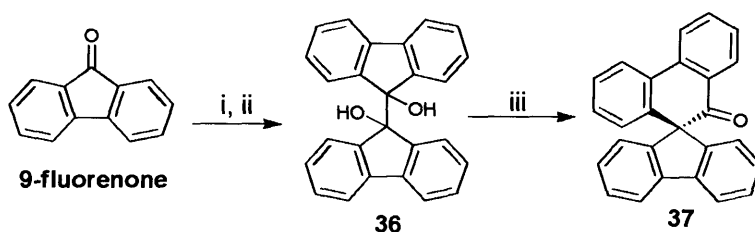


Figure 4.22 Comparison of the generalised dimensions of hexabenzo[4.4.4]propellane (*left*) and triptycene (*right*).

4.9.1 Synthesis of pinacolone 37

The first step towards synthesising dihydroxy-propellane **35** was preparation of 9,9'-bifluorene-9,9'-diol **36**, which is the precursor for pinacolone **37** (Scheme 4.18). Commercially available 9-fluorenone was coupled together using zinc and zinc chloride to give the diol **36** which immediately underwent a pinacol rearrangement under acidic conditions to give the pinacolone product **37**. It was carried out in glacial acetic acid with H_2SO_4 as catalyst. The conditions suggested in literature (reflux, 45 mins)¹³³ afforded an insoluble by-product and very little recoverable pinacolone **37**.

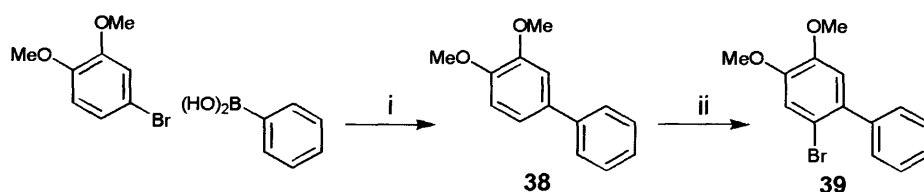


Scheme 4.18 Reagents and Conditions: i) ZnCl_2 , Zn (30 mesh), THF, H_2O ; ii) HCl (3 M) (79% yield); iii) glacial acetic acid, conc. H_2SO_4 (43% yield).

Instead, multiple attempts allowed the optimisation of the conditions and it was found that 45 mins at 90 °C, rather than reflux temperature was ample for full consumption of the diol **36** and gave higher yield of the product **37** (43%) from the pinacol rearrangement.

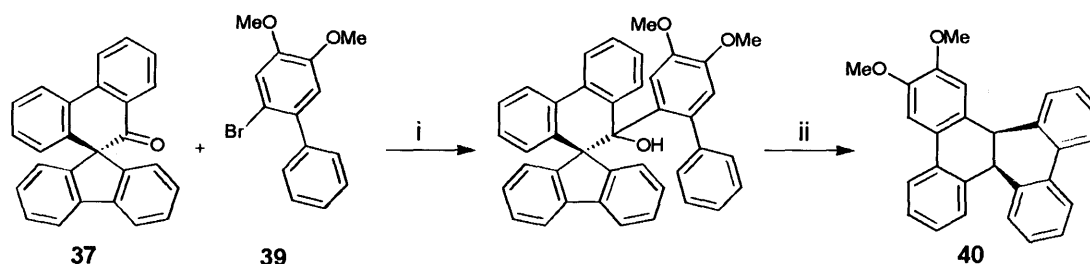
4.9.2 Synthesis of dihydroxy-propellane 35

Starting from 4-bromoveratrole and phenylboronic acid, a Suzuki coupling reaction yielded 4-phenylveratrole **38**. This was then readily brominated to give 4-phenyl-5-bromoveratrole **39**.



Scheme 4.19 Reagents and Conditions: i) $\text{Pd}(\text{PPh}_3)_4$, K_2CO_3 , DME, H_2O , 80 °C (82% yield); ii) Br_2 , chloroform (82% yield).

Following a procedure by Debroy¹³², the organolithium salt of 4-phenyl-5-bromoveratrole **39** was formed at low temperature (-78 °C) and the pinacolone **37** was introduced. The resulting crude mixture was treated with dehydrating acetic acid and H_2SO_4 at 95 °C for 2 hrs, resulting in the dimethoxy-propellane **40** (45%).



Scheme 4.20 *Reagents and Conditions:* i n-Butyllithium (2.5 M in hexane), anhydrous diethyl ether, -78 °C; ii glacial acetic acid, H₂SO₄ conc., 95 °C (45% yield).

A pure sample of dimethoxy-propellane was then treated with BBr₃ to give the dihydroxy-propellane monomer **35** (79%, Figure 4.21). A sample of dihydroxy-propellane **35** was crystallised and analysed by X-ray single crystal diffraction. The crystal structure contained no guest solvent molecules, and the oxygen atoms were found to be disordered over the 12 possible sites with occupancy ranging from 0.08 to 0.27, indicating the orientation of the molecule and the hydroxyl groups in the crystal packing has little effect on the bonding forces, so non-hydrogen interactions must dominate. The crystal is tetragonal with space group I4₁cd. The cell lengths were a 16.9375(6), b 16.9324(6), c 34.3414(10) Å with cell angles $\alpha = \beta = \gamma = 90.00$. The cell volume was 9848.86 Å³ with 16 molecules per unit cell, and no solvent.

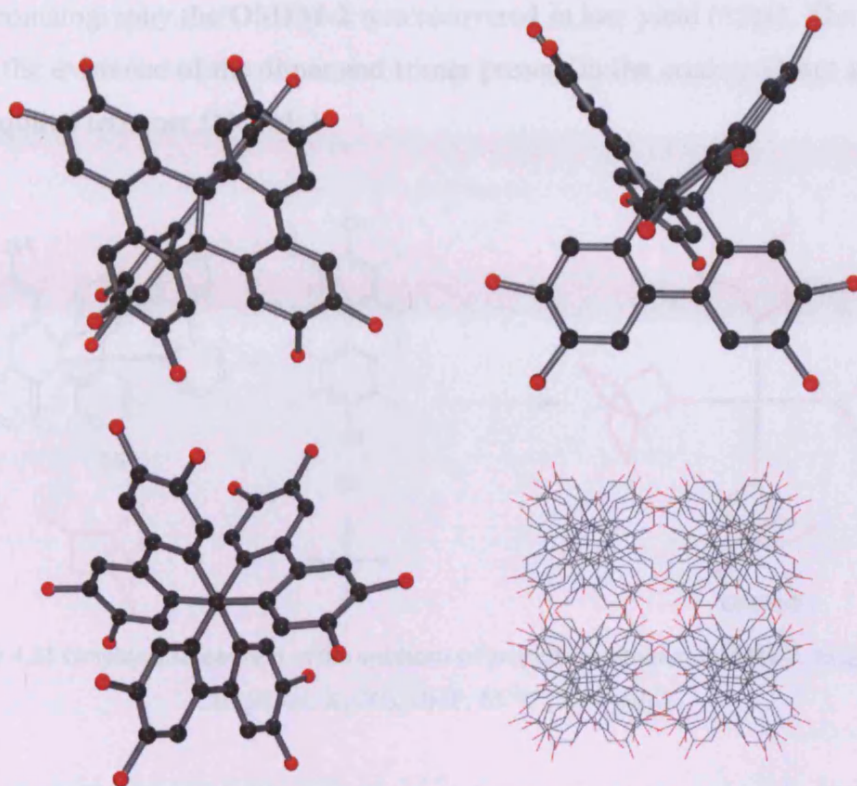


Figure 4.23 Structures drawn from crystal data for dihydroxy-propellane **35**.

4.9.3 Synthesis of propellane tetramer OMIM-2

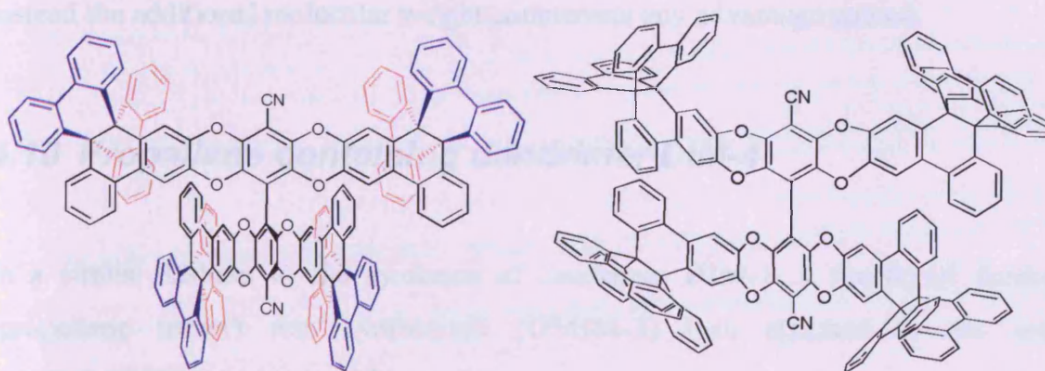
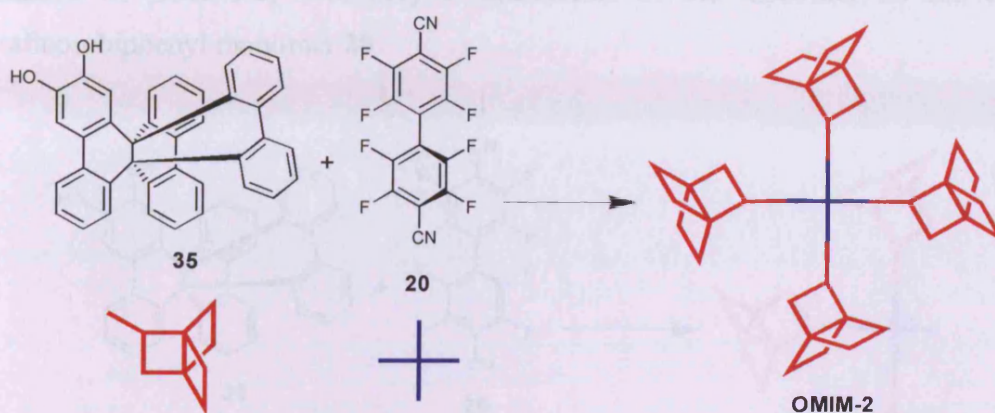


Figure 4.24 Two structural representations of **OMIM-2**.

The first target material to contain the propellane moiety was the tetramer formed between octafluorobiphenyl **20** and the dihydroxy-propellane **35**. They were reacted together under the usual conditions (K_2CO_3 , DMF, 65 °C), and after purification by

flash chromatography the **OMIM-2** was recovered in low yield (35%). The low yield owes to the existence of the dimer and trimer present in the crude product in addition to the required tetramer **OMIM-2**.



Scheme 4.21 Graphical illustration of the synthesis of propellane tetramer **OMIM-2**. *Reagents and Conditions:* K_2CO_3 , DMF, 65 °C (35% yield).

The tetramer **OMIM-2** was found to have an apparent BET surface area of $546 \text{ m}^2 \text{ g}^{-1}$ (N_2 , 77 K), and so can be successfully assigned to a growing category of organic molecules of intrinsic microporosity (OMIMs). The slight reduction in surface area when compared to its triptycene counterpart (**OMIM-1**) suggests that the higher internal free volume (IFV) propellane does little to increase microporosity, and instead the additional molecular weight counteracts any advantage gained.

4.10 Propellane containing dendrimer DIM-4

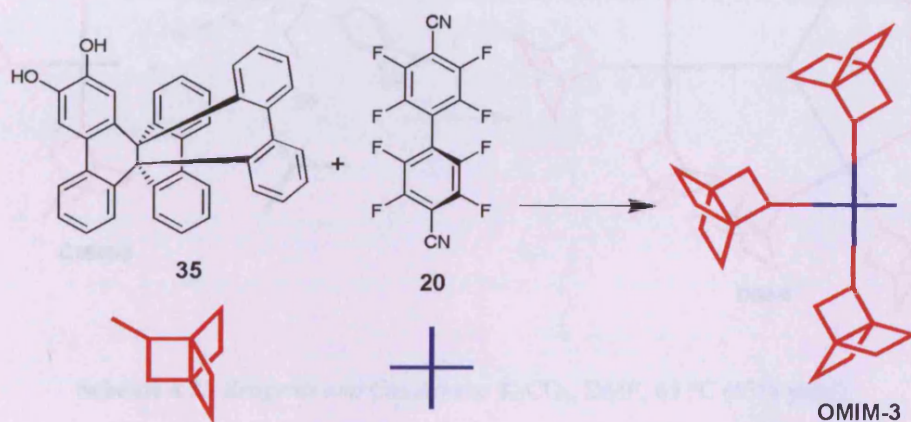
In a similar fashion to the synthesis of dendrimer **DIM-1**, a functional dendron (propellane trimer) was synthesised (**OMIM-3**) then attached to the same hexahydroxytriptycene core **30**.

4.10.2 Synthesis of propellane dendrimer DIM-4

Using the same strategy between hexahydroxytriptycene core **30** and functional propellane dendron **OMIM-3**, the dendrimer **DIM-4** was successfully synthesised (43%). After the usual problems inherent with purification, a sample was analysed

4.10.1 Synthesis of tripropellane dendron OMIM-3

The synthesis of the tripropellane dendron **OMIM-3** was again similar to the synthesis of **OMIM-2**, with only 3 equivalents of the monomer **35** for every octafluorobiphenyl monomer **20**.



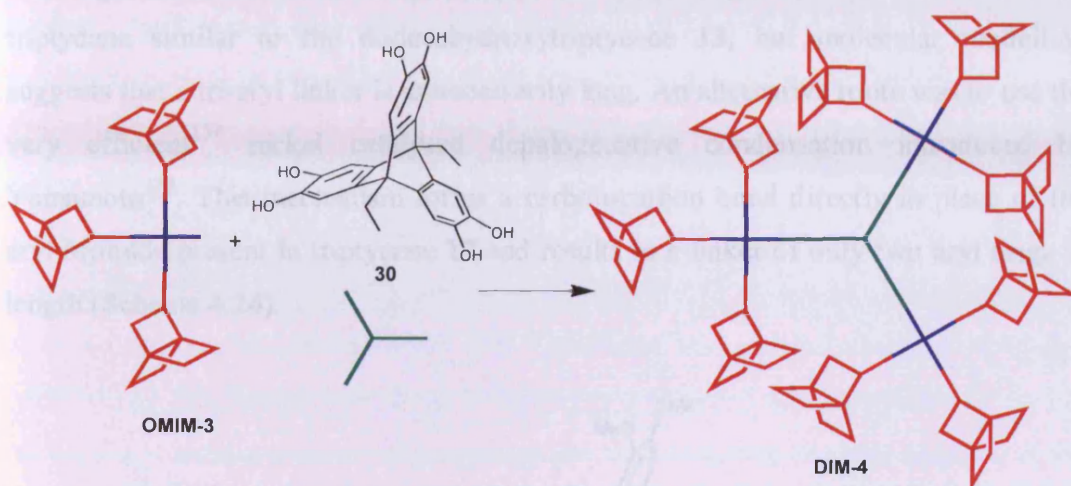
Scheme 4.22 Graphical illustration of the synthesis of functional dendron **OMIM-3**. *Reagents and Conditions:* K_2CO_3 , DMF, 65 °C (21% yield).

The crude product was found to be a mixture of the mono-, di-, tri- and tetra-substituted biphenyl, and attempts at stoichiometric control could not prevent the occurrence of these unwanted byproducts. As with all the larger molecules in this project there was difficulty eluting the compounds through a silica flash column, and also the difference in polarity of the oligomers was extremely low. In order to obtain reasonably pure samples, difficult flash chromatography had to be performed many times, but finally yielded the functional dendron **OMIM-3** in low yield (21%). Unlike the triptycene-based dendron **D5**, which had no measurable surface area, this propellane based analogue was found to have an apparent BET surface area of $505 \text{ m}^2 \text{ g}^{-1}$ (N_2 , 77 K).

4.10.2 Synthesis of propellane dendrimer DIM-4

Using the S_NAr reaction between hexahydroxytriptycene core **30** and functional tripropellane dendron **OMIM-3**, the dendrimer **DIM-4** was successfully synthesised (43%). After the usual problems inherent with purification, a sample was analysed

and found to have an apparent BET surface area of $642 \text{ m}^2 \text{ g}^{-1}$, the highest of any OMIM or dendrimer reported here.



Scheme 4.23 Reagents and Conditions: K_2CO_3 , DMF, 65°C (43% yield).

4.11 Dendrimer with bitriptycene core DIM-5

The next target for our convergent dendrimer design was to create a linker between the triptycene cores of two **DIM-1** dendrimers, and form the largest dendrimer in the project with a molecular weight of 7189.35 (For synthesis and structure of **DIM-1** see Scheme 4.11). A graphical illustration of linking two **DIM-1** dendrimers is shown in Figure 4.25.

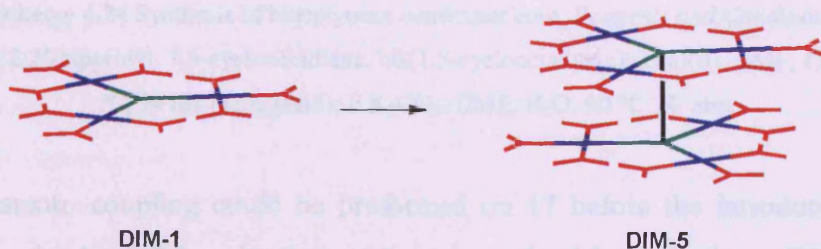
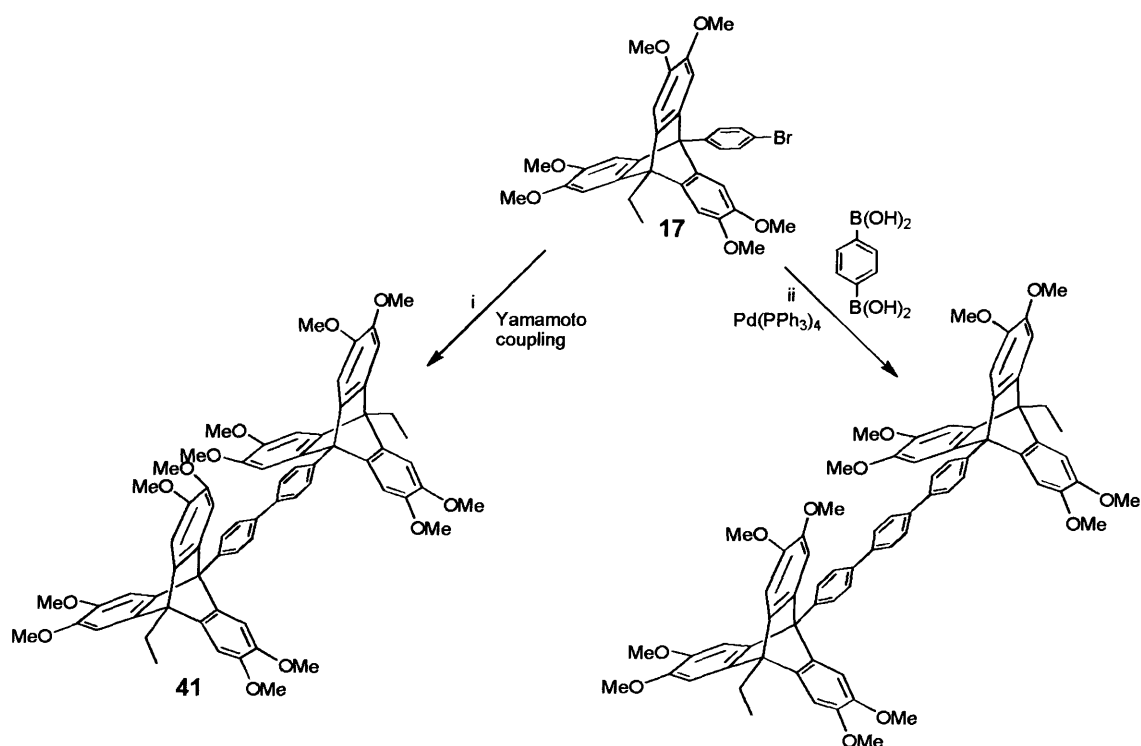


Figure 4.25 Dendrimer analogue of **DIM-1** with a covalently bound linker between two cores.

4.11.1 Synthesising bitriptycene core for dendrimer DIM-5

The target molecule **DIM-5** could be achieved by reacting 6 equivalents of **D5** with a triptycene similar to the dodecahydroxytriptycene **13**, but molecular modelling suggests that a tri-aryl linker is unnecessarily long. An alternative route was to use the very efficient¹³⁴ nickel catalysed dehalogenative condensation introduced by Yamamoto¹³⁵. This mechanism forms a carbon-carbon bond directly in place of the aryl bromide present in triptycene **17** and results in a linker of only two aryl rings in length (Scheme 4.24).



Scheme 4.24 Synthesis of bitriptycene dendrimer core. *Reagents and Conditions:*

i 2,2'-bipyridyl, 1,5-cyclooctadiene, bis(1,5-cyclooctadiene)nickel(0), DMF, 120 °C, 24 hrs (88% yield); ii K₂CO₃, DME, H₂O, 90 °C, N₂ atm.

The Yamamoto coupling could be preformed on **17** before the introduction of the terminating dendrons **D5**, or by first synthesising a dendrimer similar to **DIM-1** which could be coupled together in a final step. The decision was made to opt for a pre-coupled dodecahydroxytriptycene core (**42**, Scheme 4.25), based on the steric requirements. Unlike the case of dendrimer **DIM-1** where only two possible stereoisomers exist (dubbed 'syn' where the protruding segments of the biphenyl ring

are all on one side of the plane, and ‘anti’ where one or two biphenyl segments protrude on the opposite face to the normal, Figure 4.16), using an unsymmetrical triptycene as the starting core reduces the overall symmetry resulting in four possible isomers. Furthermore, once the link between two cores is made the number of isomers increases to sixteen. Growing the dendrimer from a pre-formed bitriptycene core maximises steric constraints and likely decreases the fraction of isomers where the bulky group resides in the gap between the triptycene cores (examples of both extremes, totally inward directed, and outward directed bulky groups is illustrated in the space filling models in Figure 4.26). In addition to preventing this build up of inward facing bulky groups in the final dendrimer, this method of precoupling two cores avoids the potential for the aryl bromides at the core becoming encased by the surrounding structure, potentially blocking the final coupling reaction pathway if the coupling was carried out after the introduction of the dendrons **D5**.

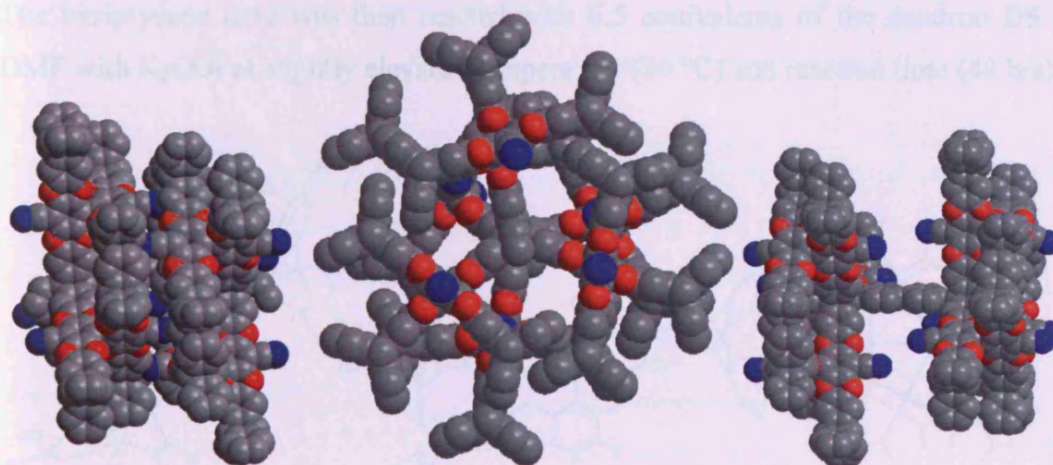
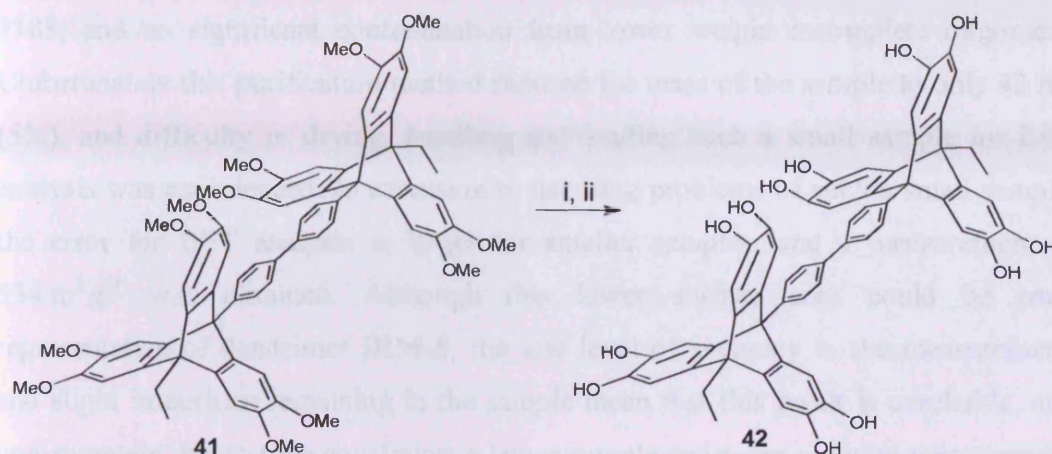


Figure 4.26 Space filling energy minimised illustrations of **DIM-5**. *Left:* All bulky groups reside in the central cavity; *Centre:* Top down view of both isomers which appears equivalent from above; *Right:* Isomer where all bulky groups are facing outward. Note: there are 14 more possible isomers only the two extremes are shown.

4.11.2 Synthesising dendrimer DIM-5

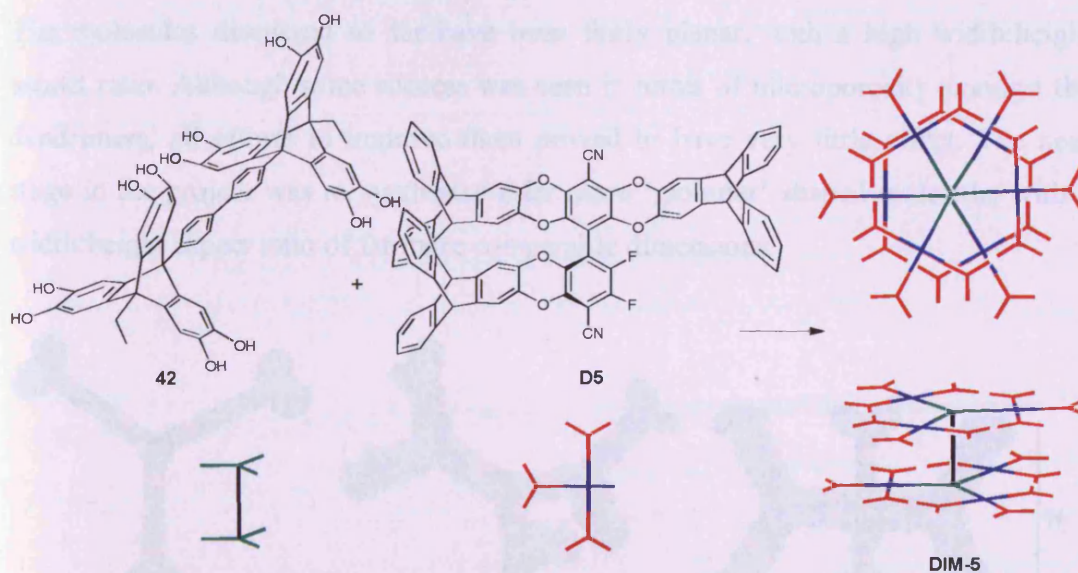
Starting from the previously synthesised triptycene **17**, the successfully coupled bitriptycene **41** was obtained in fair yield (88%, Scheme 4.24). It was then

demethylated in the usual way to give 4,4'-di(10''-ethyl-2'',3'',6'',7'',12'',13''-hexahydroxytriptycene-9''-yl)phenyl)biphenyl **42**.



Scheme 4.25 Reagents and Conditions: i BBr_3 , DCM, 0 °C; ii H_2O (63% yield).

The bitriptycene core was then reacted with 6.5 equivalents of the dendron **D5** in DMF with K_2CO_3 at slightly elevated temperature (80 °C) and reaction time (48 hrs).



Scheme 4.26 Reagents and Conditions: **D5** (6.5 eq), K_2CO_3 , DMF, 80 °C, 48 hrs (5% yield).

The more rigorous conditions were used to help alleviate any decreased reaction rate due to the added steric hindrance of such a large molecule. The final dendrimer obtained was extremely difficult to purify, although it was fairly soluble in common solvents (DCM and chloroform) it did not pass easily through a flash column, likely

due to its large size. Using the method of solvent/non-solvent reprecipitation (chloroform and hexane respectively) until a sample was obtained that when analysed using MALDI-TOF gave a significant signal for the complete dendrimer at mass 7188, and no significant contamination from lower weight incomplete oligomers. Unfortunately this purification method reduced the mass of the sample to only 42 mg (5%), and difficulty in drying, handling and loading such a small sample for BET analysis was experienced. In extension to handling problems of such a small sample, the error for BET analysis is larger for smaller samples, and a measurement of $534 \text{ m}^2 \text{ g}^{-1}$ was obtained. Although this lower surface area could be truly representative of dendrimer **DIM-5**, the low level of accuracy in the measurement, and slight impurities remaining in the sample mean that this result is unreliable, and unfortunately due to time constraints a larger sample and more accurate measurement could not be made.

4.11.3 HATN based triptycene dendrimer

The molecules discussed so far have been fairly planar, with a high width:height aspect ratio. Although some success was seen in terms of microporosity amongst the dendrimers, all efforts to improve them proved to have very little effect. The next stage in the project was to synthesise a far more 'globular' shaped molecule, with a width:height aspect ratio of far more comparable dimensions.

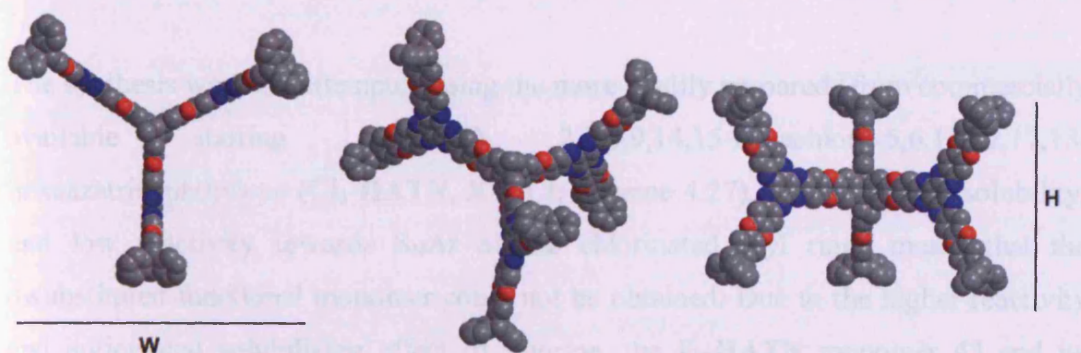
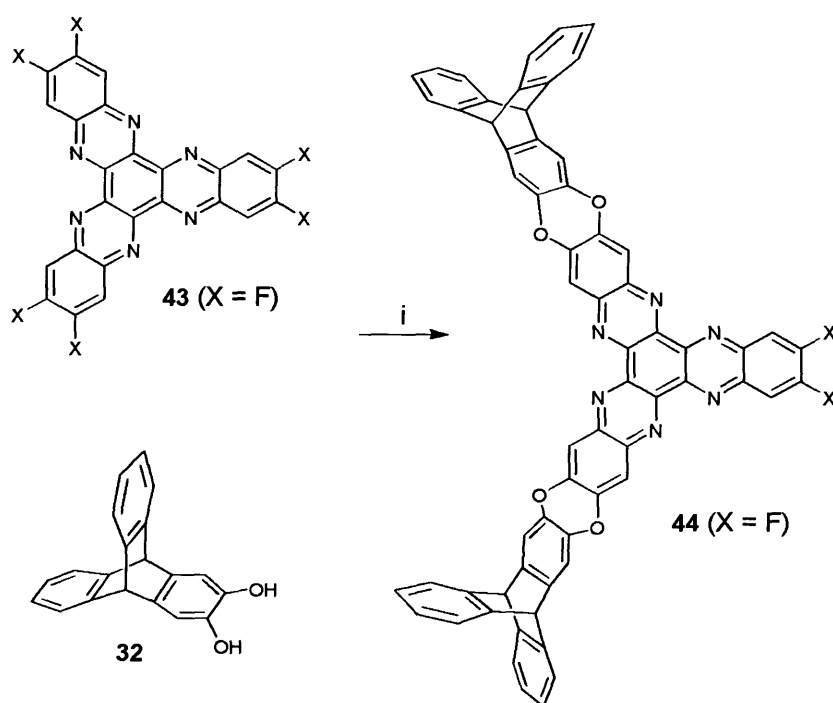


Figure 4.27 Geometry illustration of the energy minimised molecular model of a dendrimer incorporating the **HATN** unit. *Right*: top down; *Centre*: Perspective view; *Left*: side view. The models illustrate that the width (W) and height (H) are of similar magnitude.

The basis to obtaining the desired shape was the 2,3,8,9,14,15-hexafluoro-5,6,11,12,17,18-hexaazatrinaphthylene (**F₆-HATN**) monomer, which when attached to a triptycene core, extends out in three directions at 60° above, and three below the plane of the core. The target molecule consists of the hexahydroxytriptycene core (**30**) previously used, with three **F₆-HATN** monomers attached to it, terminated with six dihydroxytriptycene **32** monomers (Scheme 4.29).

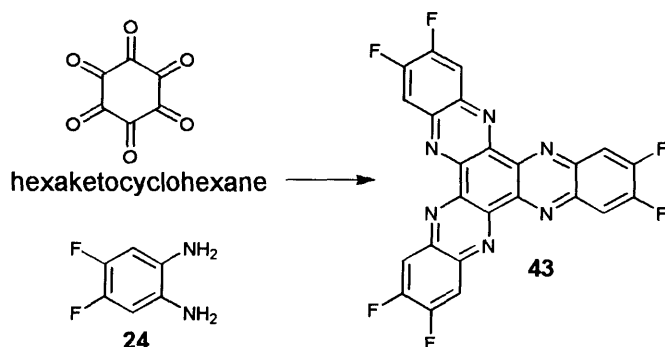


Scheme 4.27 Synthesis of functional **HATN** containing dendron.

Cl₆-HATN (X = Cl)/**F₆-HATN** (X = F). Reagents and conditions: i K_2CO_3 , DMF, 75 °C (30% yield).

The synthesis was first attempted using the more readily prepared (from commercially available starting materials) 2,3,8,9,14,15-hexachloro-5,6,11,12,17,18-hexaazatrinaphthylene (**Cl₆-HATN**, X = Cl; Scheme 4.27), but the lack of solubility, and low reactivity towards S_NAr of the chlorinated aryl rings meant that the disubstituted functional monomer could not be obtained. Due to the higher reactivity and anticipated solubilising effect of fluorine, the **F₆-HATN** monomer **43** and its more problematic synthesis was chosen. The **F₆-HATN** monomer **43** was obtained by reacting the previously synthesised 4,5-difluoro-1,2-phenylenediamine **24** with commercially available hexaketocyclohexane in glacial acetic acid (Scheme 4.28). From the reaction precipitated an insoluble product, which was filtered and washed

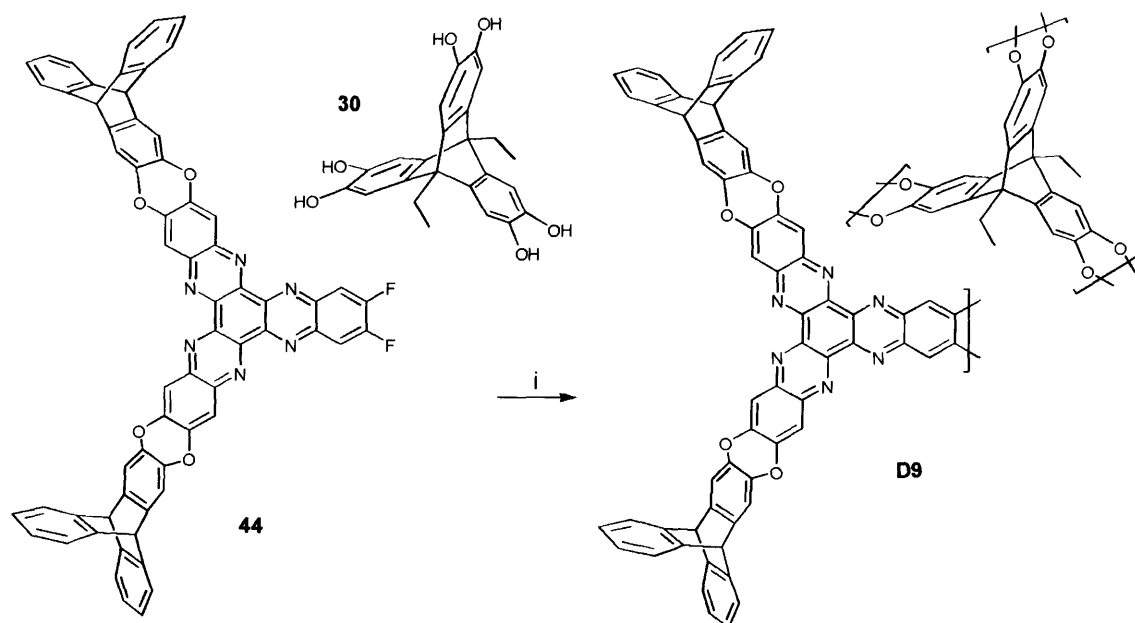
with copious amounts of hot acetic acid. Unfortunately the F₆-HATN monomer **43** was not readily soluble in any common organic solvents (as is the case for the Cl₆-HATN counterpart) and thus its presence could only be confirmed by MS MALDI-TOF. Elemental analysis was also preformed but varied slightly from the calculated result likely due to the presence of small amounts of solvents trapped within the insoluble material.



Scheme 4.28 Synthesis of F₆-HATN monomer **43**.

Reagents and Conditions: glacial acetic acid, reflux (79% yield).

The S_NAr reaction was carried out between the monomers **43** and **32** (1.5/1 equivalents, Scheme 4.29), but the opaque orange reaction mixture afforded very little of the required compound **44**. The product was fairly insoluble in common organic solvents, but flash chromatography was possible by first dissolving the compound in a hot chloroform/trifluoroacetic acid solution and finely dispersing it over silica (by evaporation of solvent). The flash column yielded the fairly insoluble target **44** in fair yield (30%). The presence and purity of the sample was confirmed by MS MALDI-TOF in preparation for reaction with hexahydroxy-triptycene **30**. Unfortunately the usual S_NAr reaction between the F₆-HATN monomer **43** and triptycene **30** did not appear to afford the target molecule. When loaded onto silica the crude product did not pass easily through a flash column, and multiple reprecipitation did not yield the target (crude analysed *via* MS MALDI-TOF). The crude sample was also found to have no apparent BET surface area (N₂, 77K; all other microporous materials tested in their crude state showed surface areas near to that of the final pure sample). Due to the limitations of solubility throughout the problematic synthesis, and lack of signs of microporosity the target product was not pursued further.



Scheme 4.29 Synthesis of HATN based dendrimer **D9**.

Reagents and Conditions: i K_2CO_3 , DMF.

When an energy minimised space filling model of the compound **D9** is compared to the known microporous **OMIM-1**, the difference in compactness is clear (Figure 4.28). The high IFV triptycene subunits are far closer in space in the **OMIM-1**, possibly providing a more effective system of guarding space around the centre of the molecule. Although the geometric arrangement of using a subunit like **F₆-HATN 43** provides a presumably more desired globular shape, it would seem structural compactness is something which also needs to be seriously considered.

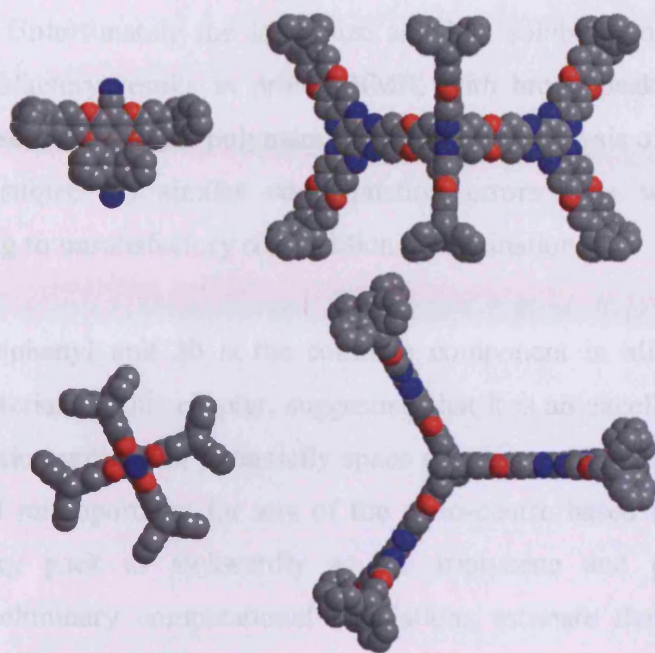


Figure 4.28 Energy minimised molecular models of **OMIM-1** and targeted dendrimer **D9**. Side view (*top*), plan view (*bottom*).

Top and bottom left: OMIM-1. Top and bottom right: Target dendrimer D9.

4.11.4 Summary of dendrimers and OMIMs

The goal of this chapter was to target and synthesis a range of dendritic and amorphous organic compounds that exhibit microporosity without any long range order or crystallinity, an area of chemistry in which less than a handful of examples are currently well publicised. As can be seen clearly in the summary (Table 4.1), 8 such compounds are reported here, with the highest performing dendrimer (and non-polymeric organic compound synthesised in this project) being the propellane based dendrimer **DIM-4**. With a surface area of $642 \text{ m}^2\text{g}^{-1}$, **DIM-4** has accessible micropores as high as some polymers. Propellane is also the base unit for the only microporous dendron measured here (**OMIM-3**, $505 \text{ m}^2\text{g}^{-1}$), and thus it can be concluded that it is an excellent candidate for further study, such as incorporation into polymers.

The X-ray powdered diffraction analysis showed no detectable diffraction patterns, indicative of no crystallinity in the compounds. The products obtained were all soluble in chloroform in some portions, allowing NMR, GPC, and MALDI-TOF data

to be obtained. Unfortunately the large size and low solubility of the compounds produced unsatisfactory results in proton NMR, with broad peaks being obtained similar to those seen for soluble polymers. The elemental analysis of the microporous materials was subject to similar contamination errors seen with microporous polymers, leading to unsatisfactory composition determination.

The octafluorobiphenyl unit **20** is the common component in all the successfully microporous materials in this chapter, suggesting that it is an excellent candidate for further investigation with other potentially space guarding monomers. Noteworthy is the total lack of microporosity for any of the spiro-centre based molecules, which should in theory pack as awkwardly as the triptycene and propellane based counterparts. Preliminary computational simulations estimate that the propellane, triptycene and spirocentre based tetramers (**OMIM-2**, **OMIM-1** and **D6**) would all pack space insufficiently, with the spirocentre based tetramer having the least but yet still considerable amount of microporosity. The only rational explanation as to why **D6** displayed no surface area in this study is likely a question of purity. The ascertained analytical data suggested the correct structure and high purity of the samples, but the total lack of nitrogen adsorption warrants further investigation.

Compound	Class	IFV moiety	BET
D1	Dendrimer (D)	Triptycene	0
D3	Dendrimer (D)	Triptycene	0
D6	Tetramer	Spirobifluorene	0
D8	Dendrimer (C)	Spirobifluorene	0
D4	Dimer	Triptycene	0
D5	Dendron	Triptycene	0
D7	Dendron	Spirobifluorene	0
DIM-3	Dendrimer (C)	Triptycene	420
OMIM-3	Dendron	Propellane	505
DIM-5	Dendrimer (C)	Triptycene	534
DIM-2	Dendrimer (C)	Triptycene	535
OMIM-2	OMIM	Propellane	546
OMIM-1	OMIM	Triptycene	580
DIM-1	Dendrimer (C)	Triptycene	600
DIM-4	Dendrimer (C)	Propellane	642

Table 4.1 Chapter 4 BET surface area summary. For dendrimers: (C) convergent, (D) divergent.

Adsorption/Desorption summary for OMIMs and DIMs

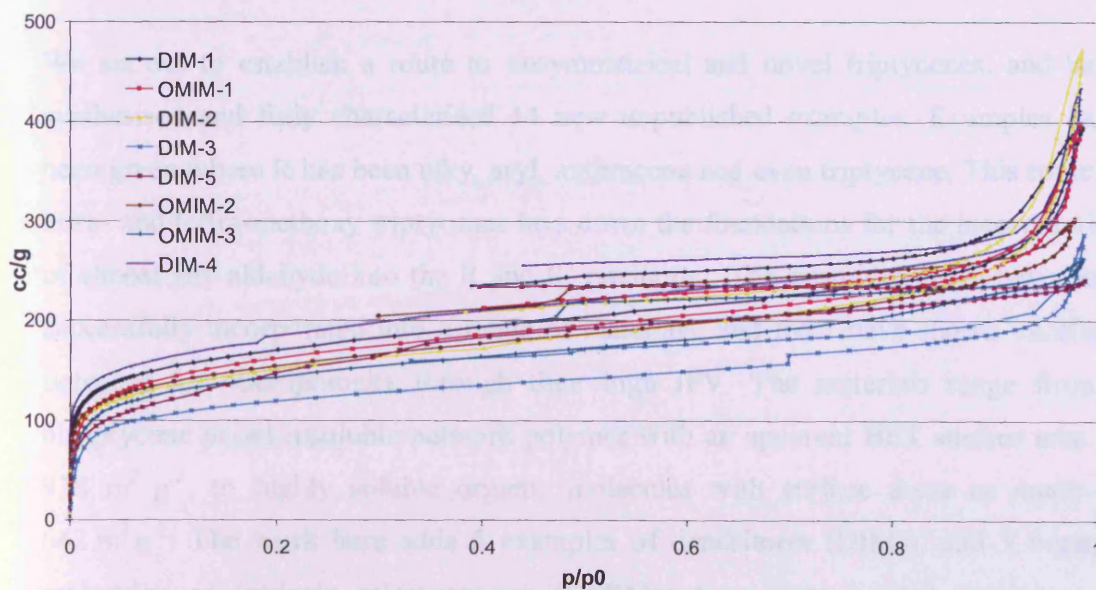
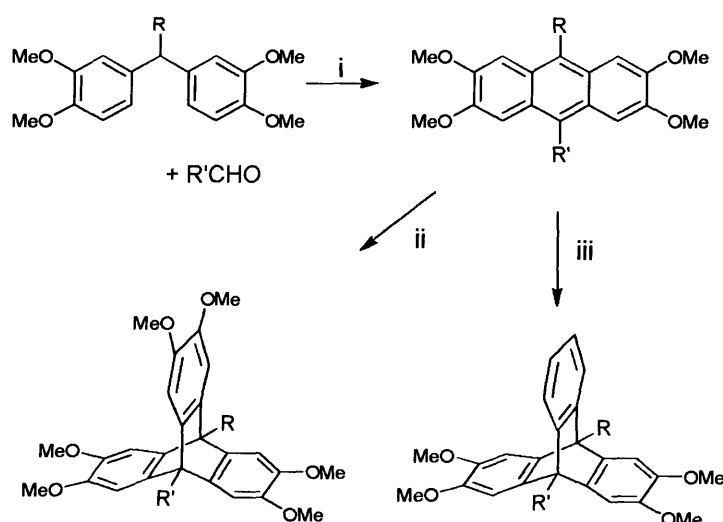


Figure 4.29 Adsorption isotherms for all DIMs/OMIMs each displaying characteristic type I microporous isotherms and apparent BET surface areas. (N_2 , 77 K).

5 Conclusion

The work in this thesis describes the successful synthesis of a family of microporous materials based mainly around triptycene, and includes some other high IFV moieties. The materials include ladder, and network polymers, and some of the first known dendrimers and organic molecules with intrinsic microporosity. All the materials produced have been analysed for their potential adsorbent capabilities through the method of nitrogen BET surface area analysis, and also had their thermal stabilities recorded.



Scheme 5.1 Newly established route to unsymmetrical tetra- and hexamethoxy-triptycenes.

We set out to establish a route to unsymmetrical and novel triptycenes, and have synthesised and fully characterised 14 new unpublished examples. Examples have been given where R has been alkyl, aryl, anthracene and even triptycene. This route to hexa- and tetra-methoxy triptycenes lays down the foundations for the incorporation of almost any aldehyde into the R and R' positions. The examples given have been successfully incorporated into a range of materials, and most have shown excellent potential for microporosity through their high IFV. The materials range from a bitriptycene based insoluble network polymer with an apparent BET surface area of $938 \text{ m}^2 \text{ g}^{-1}$, to highly soluble organic molecules with surface areas as much as $642 \text{ m}^2 \text{ g}^{-1}$. The work here adds 5 examples of dendrimers (DIMs), and 3 organic molecules of intrinsic microporosity (OMIMs) to a very limited catalogue of microporous materials of this type.

We had hoped to be able to produce a soluble processable triptycene ladder polymer, but have so far been unsuccessful. We attempted to introduce an aryl bromide, and increased length alkyl chains into the bridgehead R/R' positions, but still yielded insoluble products. An attempt was also made to introduce flexibility into the polymer backbone by passing through a bitriptycene monomer (**10**) containing two single bonds, unfortunately after a problematic synthesis this also failed to produce a soluble polymer.

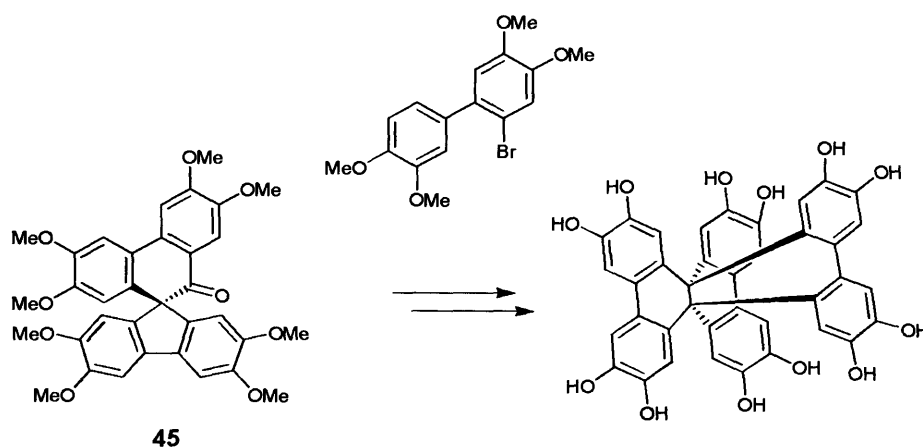
Compound	Solubility	Tonset (°C)	Weight loss (%)	BET (m ² g ⁻¹)
Ladder Polymers				
P1	Insoluble	496	35	300
P2	Insoluble	455	30	190
P3	Insoluble	515	18	100
Network Polymers				
P4	Insoluble	447	36	880
P5	Insoluble	483	24	460
P6	Insoluble	482	30	940
P7	Insoluble	438	30	626
Dendrimers and Organic Molecules				
DIM-3	DCM*	483	28	420
OMIM-3	DCM*	530	30	505
DIM-5	DCM*	538	31	534
DIM-2	DCM*	504	22	535
OMIM-2	DCM*	556	28	546
OMIM-1	DCM*	531	25	580
DIM-1	DCM*	580	24	600
DIM-4	DCM*	540	28	642

6 Future work

The future work of the ladder polymer section of this project will be focused on finding new novel ways of introducing more flexibility in the polymer backbone (e.g. more single bonds or a move away from the dioxane ring formation), in an effort to obtain a triptycene based polymer that is both soluble and microporous, with potential to form a permeable membrane.

The network polymers will be enhanced by introducing triptycene or other side groups that contain numerous t-butyl units. The t-butyl group has been shown to reduce packing efficiency in other microporous materials,⁶⁵ and might prevent the interlocking of any introduced triptycene side groups.

The future work of the DIM/OMIM section of this project will be based on enhancing and optimising the compact globular nature of the molecules. One such example would be to construct a dodecahydroxy-propellane core (Scheme 6.1) that would provide a near octahedral starting point from which to grow microporous materials.



Scheme 6.1 Proposed future synthesis of dodeca-hydroxy-propellane.

Work has already been carried out to synthesise the required pinacolone **45** and a ^1H NMR sample was obtained as proof of concept (Figure 6.1). It is presumable that by using the functional dendrons synthesised in this project (e.g. dendron **D5**) in the octahedral arrangement that a dodecahydroxy-propellane core would provide, could

achieve a far more compact and globular dendrimer than previously attained, potentially with increased microporosity.

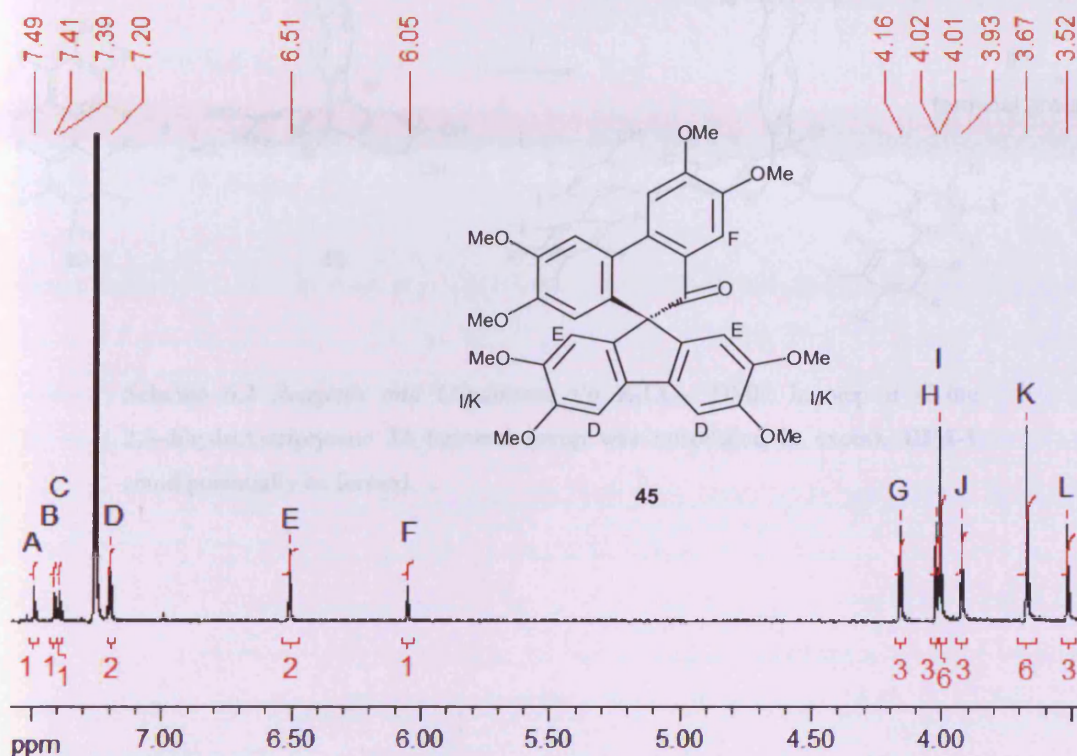
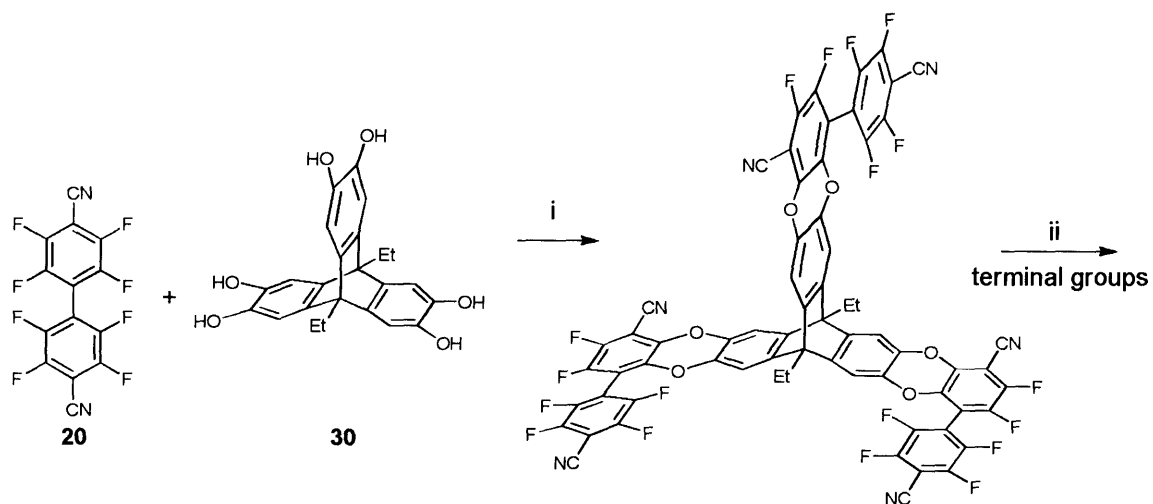


Figure 6.1 Pinacolone **45** ^1H NMR (400 MHz, CDCl_3).

The purification method of DIMs/OMIMs would also be investigated to make further work feasible, as the synthetic challenges are far outweighed by the problematic purification processes available. One such example would be to trial preparative-GPC methods capable of distinguishing *ca.* 1000 mw. An alternative synthetic route might be able to eliminate the purification step, if the octafluorobiphenyl **20** could be reacted with the desired core in large excess (to prevent oligomer formation) and then purified, in one final step a first generation dendrimer could be synthesised by introducing an excess of the relatively stable terminal groups (e.g. 2,3-dihydroxytritycene **32**, dihydroxy-propellane **35**). Since the growing core/dendrimer would have no hydroxyl groups it would not be susceptible to degradation before the reaction has been driven to completion, allowing the introduction of further terminal groups if needed and more vigorous reaction conditions.



Scheme 6.2 *Reagents and Conditions:* i/ii K_2CO_3 , DMF. In step ii if the 2,3-dihydroxytryptcene **32** terminal group was introduced in excess, **DIM-1** could potentially be formed.

7 Experimental

7.1 Experimental techniques

General remarks

Commercially available reagents were used without further purification. Anhydrous dichloromethane was obtained by distillation over calcium hydride under nitrogen atmosphere. Dry THF was obtained by drying over sodium in presence of sodium benzophenone as indicator. Anhydrous *N,N*-dimethylformamide was bought from Aldrich. All reactions using air/moisture sensitive reagents were performed in oven-dried or flame-dried apparatus, under a nitrogen atmosphere.

TLC analysis refers to analytical thin layer chromatography, using aluminum-backed plates coated with Merck Kieselgel 60 GF₂₅₄. Flash chromatography was performed on silica gel 60A (35-70 micron) chromatography grade (Fisher Scientific).

Under vacuum refers to evaporation at reduced pressure using a rotary evaporator and diaphragm pump, followed by the removal of trace volatiles using a vacuum oven.

Melting points were recorded using a Gallenkamp Melting Point Apparatus and are uncorrected.

Nuclear Magnetic Resonance (NMR)

¹H NMR spectra were recorded in CDCl₃ (unless otherwise stated) using an Avance Bruker DPX 400 instrument (400 MHz) or an Avance Bruker DPX 500 (500 MHz), with ¹³C NMR spectra recorded at 100 MHz or 125 MHz respectively. Chemical shifts (δ_{H} and δ_{C}) were recorded in parts per million (ppm) from tetramethylsilane (or chloroform) and are corrected to 0.00 (TMS) and 7.26 (chloroform) for ¹H NMR and 77.00 (chloroform), centre line, for ¹³C NMR. The abbreviations s, d, t, q, m and br.

denote singlet, doublet, triplet, quartet, multiplet and broadened resonances; all coupling constants were recorded in hertz (Hz).

InfraRed spectra (IR)

Infrared spectra were recorded in the range 4000-600 cm^{-1} using a Perkin-Elmer 1600 series FTIR instrument either as a thin film or as a nujol mull between sodium chloride plates. All absorptions are quoted in cm^{-1} .

Mass spectrometry

Low-resolution mass spectrometric data were determined using a Fisons VG Platform II quadrupole instrument using electrospray ionisation (ES) unless otherwise stated. High-resolution mass spectrometric data were obtained in electrospray (ES) or electron impact (EI) mode unless otherwise reported, on a Waters Q-TOF micromass spectrometer.

MALDI-TOF analyses were performed with a Waters MALDI Micro MX spectrometer.

Nitrogen adsorption/desorption

Low-temperature (77 K) N_2 adsorption/desorption measurements of materials were made using a Coulter SA3100. Samples were generally degassed for 800 min at 120 °C under high vacuum prior to analysis.

Thermo Gravimetric Analysis (TGA)

The TGA was performed using the device Thermal Analysis SDT Q600 at a heating rate of 10 °C/min from room temperature to 1000 °C.

X-Ray crystal structure determination

X-Ray measurements were made at Cardiff University using a Bruker-Nonius Kappa CCD area-detector diffractometer equipped with an Oxford Cryostream low temperature cooling device operating at 150(2) K ($\lambda = 0.71073 \text{ \AA}$).

Gel permeation chromatography

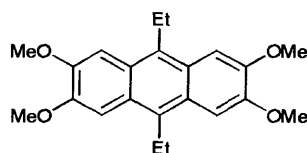
Gel permeation chromatography (GPC) analysis was carried out at Cardiff University using a GPC MAX variable loop equipped with two KF-805L SHODEX columns in THF, with a RI(VE3580) detector using a GPC MAX pump operating at flow rate of 1 ml/min. Calibration was achieved using a series of Viscotek polystyrene standards up to $M_w = 9.4 \times 10^5 \text{ g mol}^{-1}$.

Elemental analysis

Elemental analyses were obtained from Warwick Analytical Service, using the CE440 Elemental Analyser.

7.2 Experimental Procedures

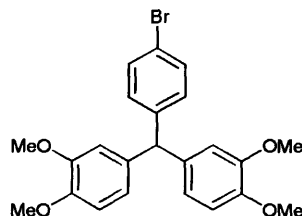
9,10-diethyl-2,3,6,7-tetramethoxyanthracene **2**^{121,136}



A solution of propionaldehyde (5.8 g, 100 mmol) in veratrole (13.8 g, 100 mmol) was added drop-wise to sulfuric acid (98%, 50 ml) at 0 – 5 °C over 20 mins. The reaction mixture was then stirred for 1 hr at room temperature before being quenched in ice water (500 ml) and neutralised with ammonia solution. The crude mixture was extracted with DCM (3 x 75 ml). The combined organic layers were washed with brine (2 x 100 ml) and the solvent evaporated under reduced pressure. The crude

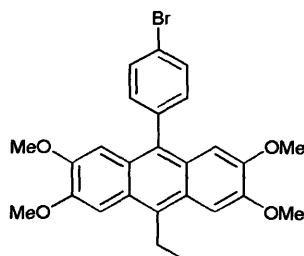
residue was boiled in ethanol to give 9,10-diethyl-2,3,6,7-tetramethoxyanthracene **2** (3.85 g, 10.86 mmol, 22%) as a yellow powder. Mp 238-249 °C, Lit¹³⁷: 236-247 °C; ¹H NMR (400 MHz; CDCl₃) δ 7.41 (4H, s, ArH), 4.07 (12H, s, OCH₃), 3.47 (4H, q, J = 7.6 Hz, CH₂), 1.44 (6H, t, J = 7.6 Hz, CH₃).

4-bromo-3,3',4,4'-tetramethoxytriphenylmethane **3**¹²⁰



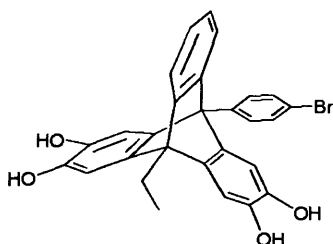
A solution of 4-bromobenzaldehyde (9.0 g, 48.6 mmol) in veratrole (20.1 g, 145.5 mmol) was added drop wise to sulfuric acid (84%, 50 ml) at 0 – 5 °C over 20 mins. The reaction mixture was then stirred for 1 hr at room temperature before being quenched in ice water (500 ml) and neutralised with ammonia solution. The crude mixture was extracted with DCM (3 x 75 ml). The combined organic layers were washed with brine (2 x 100 ml) and the solvent evaporated under reduced pressure. The crude residue was boiled in ethanol to give 4-bromo-3,3',4,4'-tetramethoxytriphenylmethane **3** (15.51 g, 35.0 mmol, 72%, Lit: 70%¹²⁰) as a white precipitate. Mp 150-152 °C, Lit¹²⁰: 136 °C; ¹H NMR (400 MHz; CDCl₃) δ 7.40 (2H, m, ArH), 6.98 (2H, m, ArH), 6.78 (2H, m, ArH), 6.64 (2H, m, ArH), 6.56 (2H, m, ArH), 5.39 (1H, s, CH), 3.86 (6H, s, OCH₃), 3.77 (6H, s, OCH₃); ¹³C NMR (125 MHz; CDCl₃) δ 148.6, 147.4, 143.3, 135.9, 131.2, 130.9, 121.1, 120.0, 112.3, 110.7, 55.7, 55.7, 55.2.

9-(4'-bromophenyl)-10-ethyl-2,3,6,7-tetramethoxyanthracene **4**



A suspension of 4-bromo-3,3',4,4'-tetramethoxytriphenylmethane **3** (3.0 g, 6.8 mmol) and propionaldehyde (2.5 eq, 1.0 g, 17.2 mmol) in DCM (5 ml) was added drop wise to sulfuric acid (84%, 30 ml) at 0 – 5 °C over 0.5 hr. The reaction mixture was then stirred for 4 hrs at room temperature before being quenched in ice water (300 ml) and neutralised with ammonia solution. The crude mixture was extracted with DCM (3 x 75 ml). The combined organic layers were washed with brine (2 x 100 ml) and the solvent evaporated under reduced pressure. The crude residue was recrystallised from ethanol to give 9-(4'-bromophenyl)-10-ethyl-2,3,6,7-tetramethoxyanthracene **4** (1.9 g, 4.0 mmol, 59%) as yellow needles. Mp 176-180 °C; IR (film)/cm⁻¹: 3100, 3056, 3000, 2960, 2942, 2909, 2872, 2828, 2057, 1635, 1531, 1463, 1434, 1241, 1203, 1148, 1069, 1040, 1011, 846, 836, 756, 735; ¹H NMR (400 MHz; CDCl₃) δ 7.71 (2H, m, ArH), 7.42 (2H, s, ArH), 7.30 (2H, m, ArH), 6.73 (2H, s, CH), 4.08 (6H, s, OCH₃), 3.75 (6H, s, OCH₃), 3.53 (2H, q, *J* = 7.6 Hz, CH₂), 1.49 (3H, t, *J* = 7.6 Hz, CH₃); ¹³C NMR (125 MHz; CDCl₃) δ 148.9, 148.5, 138.8, 132.7, 132.0, 131.6, 130.1, 125.7, 124.3, 121.2, 104.0, 101.3, 55.5, 55.3, 21.7, 14.2; HRMS Calc. for C₂₆H₂₅O₄⁷⁹Br 480.0936 (⁷⁹Br M⁺), found 480.0934 (⁷⁹Br M⁺), 482.1016 (⁸¹Br M⁺).

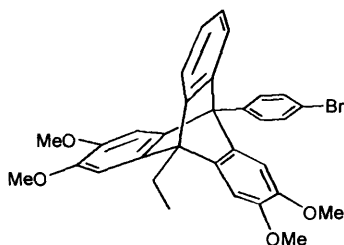
9-(4'-bromophenyl)-10-ethyl-2,3,6,7-tetrahydroxytriptycene **5**



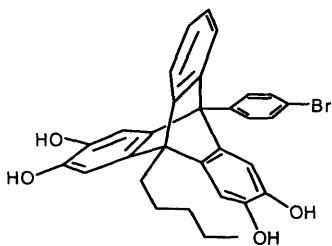
To a solution of 9-(4'-bromophenyl)-10-ethyl-2,3,6,7-tetramethoxytriptycene **6** (0.51 g, 0.9 mmol) in dry DCM (10 ml) at 0 °C under a N₂ atmosphere was added BBr₃ (1.40 g, 5.58 mmol). The reaction mixture was stirred for 1 hr at room temperature before being quenched in water (5 ml), filtered and washed with water (2 x 5 ml), then DCM/hexane (1/1, 2 x 5 ml). The off white powder was then dried under vacuum to give 9-(4'-bromophenyl)-10-ethyl-2,3,6,7-tetrahydroxytriptycene **5** (0.41 g, 0.82 mmol, 91%). Mp decomposes above 80 °C; IR (nujol)/cm⁻¹: 3379, 2924, 2853, 2727, 1616, 1463, 1377, 1287, 1209, 1156, 1082, 1027, 1009, 922, 797, 752; ¹H NMR (400

MHz; Acetone-D₆) δ 8.01 (2H, m, ArH), 7.84 (2H, m, ArH), 7.57-7.31 (1H, br m, ArH), 7.30-7.06 (2H, br s, ArH), 7.01 (1H, m, ArH), 6.96 (1H, m, ArH), 6.88 (1H, m, ArH), 6.82-6.46 (1H, br s, ArH), 6.41 (1H, m, ArH), 2.88 (2H, q, $J = 7.1$ Hz, CH₂), 1.66 (3H, t, $J = 7.1$ Hz, CH₃); ¹³C NMR (100 MHz; Acetone-D₆) δ 151.3, 150.9, 142.8, 142.8, 142.2, 138.6, 135.5, 133.1, 125.9, 122.3, 114.1, 59.9, 54.3, 21.7, 12.3, 5 carbons missing or obscured; HRMS Calc. for C₂₈H₂₁O₄⁷⁹Br 500.0623 (⁷⁹Br M⁺), found 500.0625 (⁷⁹Br M⁺), 502.0607 (⁸¹Br M⁺).

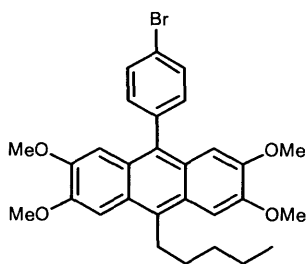
9-(4'-bromophenyl)-10-ethyl-2,3,6,7-tetramethoxytriptycene 6



To a solution of 9-(4'-bromophenyl)-10-ethyl-2,3,6,7-tetramethoxyanthracene **4** (9.9 g, 20.6 mmol) in DCE (180 ml) under N₂ atmosphere at 83 °C was added isoamyl nitrite (7.55 g, 64.42 mmol) portion wise ahead of anthranilic acid (8.78 g, 64.02 mmol, in THF 20 ml) over 1 hr. After 18 hrs the solution was cooled and the solvent evaporated under reduced pressure. The crude residue was purified by flash chromatography (ethyl acetate/hexane, 3/7) to give 9-(4'-bromophenyl)-10-ethyl-2,3,6,7-tetramethoxytriptycene **6** (1.55 g, 2.78 mmol, 14%) as a white solid. Mp 214-218 °C; IR (film)/cm⁻¹: 3060, 2993, 2934, 2845, 2828, 1582, 1492, 1463, 1436, 1275, 1241, 1201, 1180, 1148, 1131, 1089, 1058, 1011, 846, 749; ¹H NMR (400 MHz; CDCl₃) δ 8.03 (2H, m, ArH), 7.81 (2H, m, ArH), 7.58-7.32 (1H, br d, $J = 7.5$ Hz, ArH), 7.24-7.12 (1H, br m, ArH), 7.03 (2H, s, ArH), 7.02-6.89 (2H, br m, ArH), 6.89-6.65 (2H, br s, ArH), 3.85 (6H, s, OCH₃), 3.67 (6H, s, OCH₃), 3.01 (2H, q, $J = 7.1$ Hz, CH₂), 1.77 (3H, t, $J = 7.1$ Hz, CH₃); ¹³C NMR (125 MHz; CDCl₃) δ 148.5, 145.5, 144.9, 141.2, 136.0, 133.1, 131.4, 128.8, 128.0, 124.3, 123.8, 123.1, 121.6, 121.1, 109.4, 107.5, 58.6, 56.1, 56.0, 53.0, 19.9, 10.9; HRMS Calc. for C₃₂H₂₉O₄⁷⁹Br 556.1249 (⁷⁹Br M⁺), found 556.1246 (⁷⁹Br M⁺).

9-(4'-bromophenyl)-10-pentyl-2,3,6,7-tetrahydroxytriptycene 7

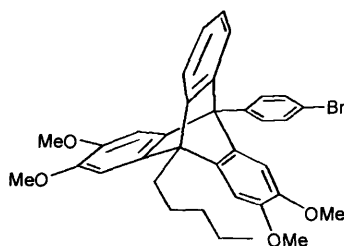
To a solution of 9-(4'-bromophenyl)-10-pentyl-2,3,6,7-tetramethoxytriptycene **9** (1.72 g, 2.9 mmol) in dry DCM (40 ml) at 0 °C under a N₂ atmosphere was added BBr₃ (3.6 g, 14.4 mmol). The reaction mixture was stirred for 1 hr at room temperature before being quenched in water (100 ml), filtered and washed with water (2 x 10 ml). The precipitate was then dissolved in diethyl ether (40 ml) and dried with magnesium sulfate. Hexane (50 ml) was added to the solution to precipitate 9-(4'-bromophenyl)-10-pentyl-2,3,6,7-tetrahydroxytriptycene **7** (1.26 g, 2.3 mmol, 80%) as a pink powder which was dried under high vacuum. Mp decomposes above 70 °C; ¹H NMR (400 MHz; Acetone-D₆) δ 7.95 (2H, d, *J* = 8.7 Hz, Ar*H*), 7.82 (2H, d, *J* = 8.7 Hz, Ar*H*), 7.55 (2H, s, ArOH), 7.53 (2H, s, ArOH), 7.34 (1H, s, Ar*H*), 7.2 (1H, m, Ar*H*), 6.96 (2H, m, Ar*H*), 6.93 (1H, m, Ar*H*), 6.84 (1H, m, Ar*H*), 6.56 (1H, s, Ar*H*), 2.74 (2H, t, *J* = 7.5 Hz, CH₂), 2.14 (2H, m, CH₂), 1.79 (2H, m, CH₂), 1.6 (2H, m, CH₂), 1.03 (3H, t, *J* = 7.3 Hz, CH₃).

9-(4'-bromophenyl)-10-pentyl-2,3,6,7-tetramethoxyanthracene 8

A suspension of 4-bromo-3,3',4,4'-tetramethoxytriphenylmethane **3** (5.6 g, 12.6 mmol) and hexanal (1.5 g, 15.0 mmol) in DCM (10 ml) was added drop wise to sulfuric acid (84%, 50 ml) at 0-5 °C over 0.5 hr. The reaction mixture was then stirred for 5 hrs at room temperature before being quenched in ice water (300 ml) and

neutralised with ammonia solution. The crude mixture was extracted with DCM (3 x 75 ml). The combined organic layers were washed with brine (2 x 100 ml) and the solvent evaporated under reduced pressure. The crude residue was then recrystallised from ethanol to give 9-(4'-bromophenyl)-10-pentyl-2,3,6,7-tetramethoxyanthracene **8** (2.1 g, 4.0 mmol, 32%) as yellow needles. Mp 210-212 °C; IR (film)/cm⁻¹: 2924, 2856, 2829, 1632, 1527, 1495, 1465, 1451, 1435, 1389, 1242, 1205, 1148, 1037, 1013, 847, 836, 754; ¹H NMR (400 MHz; CDCl₃) δ 7.71 (2H, m, ArH), 7.42 (2H, s, ArH), 7.31 (2H, m, ArH), 6.72 (2H, s, ArH), 4.07 (6H, s, OCH₃), 3.75 (6H, s, OCH₃), 3.48 (2H, m, CH₂), 1.89 (2H, m, CH₂), 1.61 (2H, m, CH₂), 1.51 (2H, m, CH₂), 0.98 (3H, t, *J* = 7.2 Hz, CH₃); ¹³C NMR (125 MHz; CDCl₃) δ 149.0, 148.7, 139.1, 132.9, 131.8, 131.2, 130.3, 125.9, 124.9, 121.4, 104.4, 101.8, 55.7, 55.5, 32.5, 29.8, 28.6, 22.5, 14.1; HRMS Calc. for C₂₉H₃₁⁷⁹BrO₄ 522.1406 (⁷⁹Br M⁺), found 522.1423 (⁷⁹Br M⁺), 524.1429 (⁸¹Br M⁺).

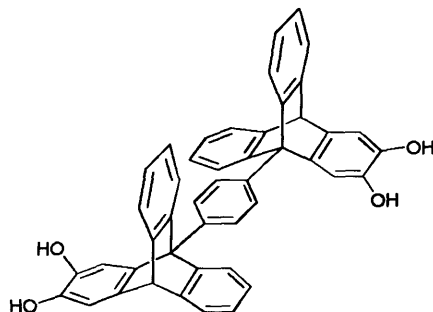
9-(4'-bromophenyl)-10-pentyl-2,3,6,7-tetramethoxytriptycene **9**



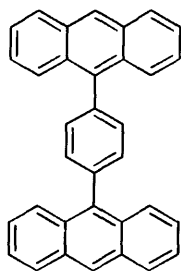
To a solution of 9-(4'-bromophenyl)-10-pentyl-2,3,6,7-tetramethoxyanthracene **8** (6.3 g, 12.0 mmol) in DME (60 ml) under N₂ atmosphere at 83 °C was added isoamyl nitrite (3.45 ml, 25.9 mmol) portion wise ahead of anthranilic acid (3.51 g, 25.6 mmol, in DME 25 ml) over 1 hr. After 18 hr the solution was cooled and the solvent evaporated under reduced pressure. The crude residue was purified by flash chromatography (DCM) to give 9-(4'-bromophenyl)-10-ethyl-2,3,6,7-tetramethoxytriptycene **9** (1.08 g, 1.8 mmol, 15%) as a white solid. Mp 170–172 °C; IR (film)/cm⁻¹: 2952, 2849, 1582, 1488, 1463, 1438, 1400, 1275, 1199, 1179, 1130, 1074, 1054, 1011, 747; ¹H NMR (400 MHz; CDCl₃) δ 7.84 (2H, d, *J* = 8.7 Hz, ArH), 7.62 (2H, d, *J* = 8.7 Hz, ArH), 7.10 (1H, s, ArH), 7.00 (4H, s, ArH), 6.89 (1H, m, ArH), 6.77 (2H, s, ArH), 3.87 (6H, s, OCH₃), 3.67 (6H, s, OCH₃), 2.88 (2H, t, *J* = 6.8 Hz, CH₂), 2.22 (2H, m, CH₂), 1.85 (2H, m, CH₂), 1.58 (2H, m, CH₂), 1.07 (3H, t, *J* =

7.3 Hz, CH_3); ^{13}C NMR (100 MHz; CDCl_3) δ 148.7, 145.6, 145.0, 141.3, 136.2, 133.4, 131.6, 124.6, 121.4, 109.5, 58.8, 56.2, 52.8, 34.3, 28.7, 25.5, 23.0, 14.2, 7 carbons missing or obscured; HRMS Calc. for $\text{C}_{35}\text{H}_{35}\text{O}_4^{79}\text{Br}$ 598.1719 ($^{79}\text{Br M}^+$), found 598.1719 ($^{79}\text{Br M}^+$).

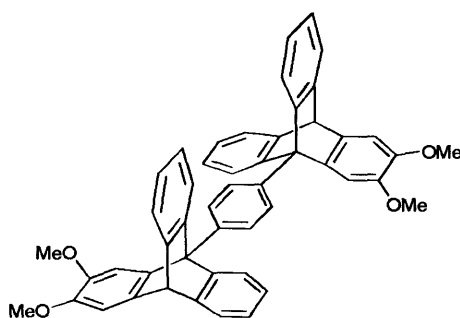
1,4-di(2',3'-dihydroxytriptycene-9'-yl)benzene **10**



To a solution of 1,4-di(2',3'-dimethoxytriptycene-9'-yl)benzene **12** (1.09 g, 1.69 mmol) in dry DCM (20 ml) at 0 °C under a N_2 atmosphere was added BBr_3 (1.90 g, 7.58 mmol). The reaction mixture was stirred for 1 hr at room temperature before being quenched in water (100 ml), filtered and washed with water (2 x 10 ml). The precipitate was then dissolved in ethyl acetate (40 ml) and dried with magnesium sulfate. Hexane (50 ml) was added to the solution to precipitate 1,4-di(2',3'-dihydroxytriptycene-9'-yl)benzene **10** (0.40 g, 0.62 mmol, 37%) as an off white powder which was dried under high vacuum. Mp decomposes above 90 °C; ^1H NMR (400 MHz; $\text{DMSO}-d_6$) δ 8.88 (2H, s, OH), 8.67 (2H, s, OH), 8.28 (4H, s, ArH), 7.51 (4H, m, ArH), 7.35 (4H, m, ArH), 7.05 (8H, m, ArH), 6.97 (4H, m, ArH), 5.51 (2H, s, CH). Crystal data (diethyl ether/hexane): triclinic, space group P -1, a 10.4970(2), b 12.5010(2), c 19.2740(5) Å, α 95.3020(10), β 91.5820(10), γ 110.7890(10). $V = 2349.45 \text{ Å}^3$, $Z = 2$, R-Factor 6.6 %.

1,4-di(anthracen-9'-yl)benzene 11 ^{138,139}

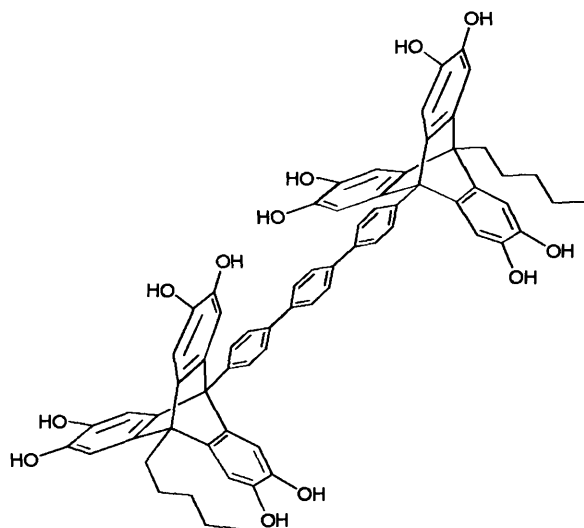
To 9-bromoanthracene (5.47 g, 21.3 mmol), benzene-1,4-diboronic acid (1.68 g, 10.1 mmol) and K_2CO_3 (4.14 g, 30.0 mmol) in a degassed solution of DME (75 ml) and water (33 ml) was added $Pd(PPh_3)_4$ (0.05 g). The reaction was heated to 80 °C under a nitrogen atmosphere for 48 hrs then allowed to cool before being diluted with water (50 ml). The precipitate was filtered and washed with water (50 ml), MeOH (2 x 50 ml), ethyl acetate (2 x 100 ml) and oven dried to give 1,4-di(anthracen-9'-yl)benzene **11** as an off white powder (3.76 g, 8.73 mmol, 86%). Mp > 300 °C, Lit¹³⁸: 375-376 °C; 1H NMR (400 MHz; $CDCl_3$) δ 8.57 (2H, s, ArH), 8.11 (4H, m, ArH), 7.93 (4H, m, ArH), 7.66 (4H, s, ArH), 7.52 (8H, m, ArH); ^{13}C NMR (125 MHz; $CDCl_3$) δ 137.9, 133.4, 131.5, 131.3, 130.3, 128.5, 126.9, 126.8, 125.6, 125.2.

1,4-di(2',3'-dimethoxytryptene-9'-yl)benzene 12

A suspension of 4,5-dimethoxy-benzenediazonium-2-carboxylate chloride (3.7 g, 15.1 mmol), 1,4-di(anthracen-9'-yl)benzene **11** (3.3 g, 7.66 mmol) and 1,2-epoxypropane (40 ml) in dichloroethane (180 ml) was refluxed for 18 hrs. Once the mixture cooled the solvents were evaporated. The crude residue filtered through a plug of silica (DCM/hexane, 7/3) to give a mixture of products and starting material which was re-

entered into a fresh reaction with 4,5-dimethoxy-benzenediazonium-2-carboxylate chloride as before. The final crude residue was purified by flash chromatography (ethyl acetate/hexane, 3/7) to give 1,4-di(2',3'-dimethoxytriptycene-9'-yl)benzene **12** (0.65g, 0.92 mmol, 12%) as a white solid. Mp > 300 °C; IR (film)/cm⁻¹: 3063, 2998, 2953, 2936, 2829, 1597, 1501, 1456, 1288, 1266, 1218, 1111, 1076, 1024, 745, 621; ¹H NMR (400 MHz; CDCl₃) δ 8.41 (4H, s, ArH), 7.54 (4H, dd, *J* = 7.8 Hz, *J* = 1.3 Hz, ArH), 7.48 (4H, dd, *J* = 7.1 Hz, *J* = 1.3 Hz, ArH), 7.12 (2H, s, ArH), 7.08-6.99 (10H, br m), 5.42 (2H, s, CH), 3.90 (6H, s, OCH₃), 3.77 (6H, s, OCH₃); ¹³C NMR (125 MHz; CDCl₃) δ 147.2, 146.7, 146.3, 145.3, 139.6, 139.2, 135.4, 131.5, 125.0, 124.3, 123.9, 123.4, 110.3, 108.0, 59.8, 56.3, 56.0, 54.6; HRMS Calc. for C₅₀H₃₈O₄ 702.2775, found 702.2770.

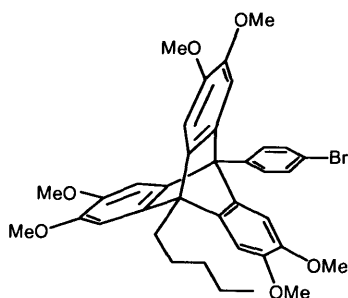
1,4-di(4'-(10''-pentyl-2'',3'',6'',7'',12'',13''-hexahydroxytriptycene-9''-yl)phenyl))benzene **13**



To a solution of **15** (1.10 g, 0.89 mmol) in dry DCM (25 ml) at 0 °C under a N₂ atmosphere was added BBr₃ (3.4 g, 13.6 mmol). The reaction mixture was stirred for 1 hr at room temperature before being quenched in water (50 ml), filtered and washed with water (2 x 10 ml) and acetone (1 x 10 ml) to give the product **13** (0.87 g, 0.82 mmol, 92%) as a pink powder which was dried under high vacuum. Mp decomposes above 50 °C; ¹H NMR (400 MHz; DMSO-D₆) δ 8.60 (6H, s, ArOH), 8.47 (6H, s, ArOH), 8.14 (4H, d, *J* = 8.4 Hz, ArH), 8.09 (4H, s, ArH), 8.05 (4H, d, *J* = 8.4 Hz,

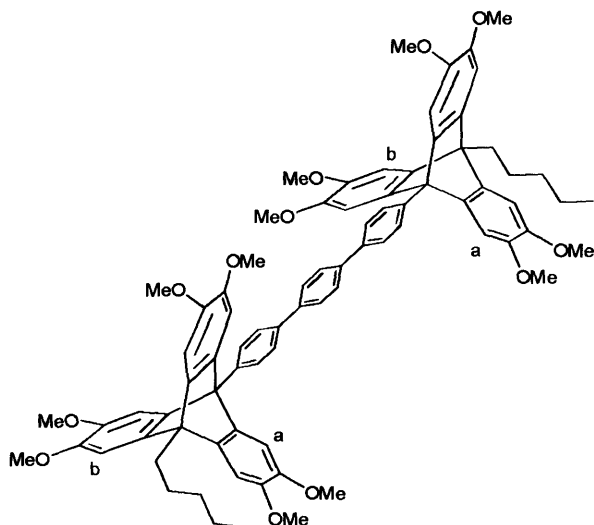
ArH), 6.78 (6H, s, ArH), 6.71-6.45 (6H, br s, ArH), 2.55 (4H, m, CH₂), 2.04 (4H, m, CH₂), 1.77 (4H, m, CH₂), 1.57 (4H, m, CH₂), 1.07 (6H, m, CH₃).

9-(4'-bromophenyl)-10-pentyl-2,3,6,7,12,13-hexamethoxytritycene 14



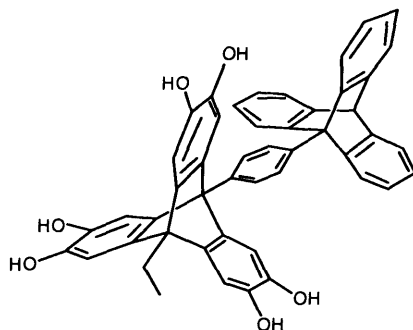
A suspension of 4,5-dimethoxy-benzenediazonium-2-carboxylate chloride (6.9 g, 28.2 mmol), 9-(4'-bromophenyl)-10-pentyl-2,3,6,7-tetramethoxyanthracene **8** (3.6 g, 6.9 mmol) and 1,2-epoxypropane (40 ml) in dichloroethane (180 ml) was refluxed for 18 hrs. Once the mixture had cooled the solvents were evaporated. The crude residue was purified by flash chromatography (DCM) to give starting material **8** (2.1 g, 4.0 mmol) and 9-(4'-bromophenyl)-10-ethyl-2,3,6,7,12,13-hexamethoxytritycene (1.2 g, 2.0 mmol, 27%) as a white solid. Mp 197-198 °C; IR (film)/cm⁻¹: 2993, 2951, 2850, 1582, 1487, 1464, 1403, 1275, 1196, 1177, 1128, 1052, 762, 623; ¹H NMR (400 MHz; CDCl₃) δ 8.02 (2H, m, ArH), 7.82 (2H, m, ArH), 6.99 (3H, s, Hb), 6.88-6.61 (3H, br s, Ha), 3.86 (9H, s, OCH₃), 3.67 (9H, s, OCH₃), 2.87 (2H, m, CH₂), 2.22 (2H, m, CH₂), 1.86 (2H, m, CH₂), 1.60 (2H, m, CH₂), 1.06 (3H, t, *J* = 7.3 Hz, CH₃); ¹³C NMR (125 MHz; CDCl₃) δ 145.4, 144.7, 141.5, 136.3, 133.1, 131.5, 121.3, 109.2, 107.2, 58.5, 56.1, 52.5, 34.2, 28.7, 25.6, 22.9, 14.1, 1 carbon missing; HRMS Calc. for C₃₇H₃₉ O₆ ⁷⁹Br 658.1930 (⁷⁹Br M⁺), found 658.1954 (⁷⁹Br M⁺), 660.1971 (⁸¹Br M⁺).

1,4-di(4'-(10''-pentyl-2'',3'',6'',7'',12'',13''-hexamethoxytryptycene-9''-yl)phenyl)benzene 15

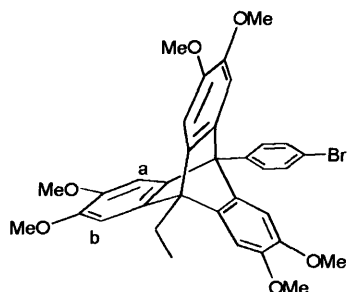


To a degassed mixture of DME (25 ml) and H₂O (11 ml) under N₂ atmosphere was added 9-(4'-bromophenyl)-10-pentyl-2,3,6,7,12,13-hexamethoxytryptycene **14** (1.090 g, 1.65 mmol), 1,4-phenylenediboronic acid (0.136 g, 0.82 mmol), K₂CO₃ (0.7 g) and Pd(PPh₃)₄ (0.05 g). The reaction was heated to 90 °C for 18 hrs. The solvent was removed under vacuum and extracted with DCM. The crude residue was purified by flash chromatography (ethyl acetate/hexane, 3/4) to give **15** (0.88 g, 0.71 mmol, 87%) as an off white powder. Mp > 300 °C; IR (film)/cm⁻¹: 2998, 2951, 2849, 1607, 1582, 1487, 1465, 1440, 1403, 1275, 1196, 1177, 1130, 1053, 735, 624; ¹H NMR (500 MHz; CDCl₃) δ 8.28 (4H, d, *J* = 8.4 Hz, ArH), 8.06 (4H, d, *J* = 8.4 Hz, ArH), 7.99 (4H, s, ArH), 7.04 (6H, s, H_b), 7.03-6.66 (6H, br s, H_a), 3.88 (18H, s, OCH₃), 3.70 (18H, s, OCH₃), 2.91 (4H, m, CH₂), 2.27 (4H, m, CH₂), 1.89 (4H, m, CH₂), 1.63 (4H, m, CH₂), 1.08 (6H, t, *J* = 7.3 Hz, CH₃); ¹³C NMR (125 MHz; CDCl₃) δ 239.8, 145.4, 144.8, 142.0, 139.4, 139.1, 136.7, 132.0, 127.5, 126.8, 109.6, 58.7, 56.2, 52.6, 34.3, 28.8, 25.7, 23.0, 14.2, 2 carbons missing; HRMS Calc. for C₈₀H₈₂O₁₂²³Na 1257.5704 (M+Na⁺), found 1257.5679 (M+Na⁺).

9-(4'-(tritycene-9''-yl)phenyl)-10-ethyl-2,3,6,7,12,13-hexahydroxytritycene 16

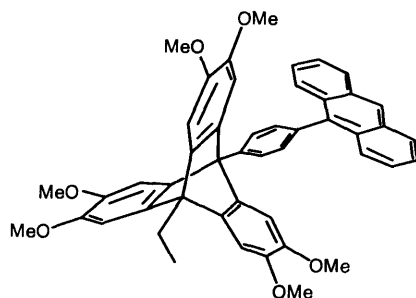


To a solution of 9-(4'-(tritycene-9''-yl)phenyl)-10-ethyl-2,3,6,7,12,13-hexamethoxytritycene **19** (1.20 g, 1.52 mmol) in dry DCM (40 ml) at 0 °C under a N₂ atmosphere was added BBr₃ (2.2 g, 9.1 mmol). The reaction mixture was stirred for 1 hr at room temperature before being quenched in water (100 ml), filtered and washed with water (2 x 10 ml), acetone (2 x 10 ml), and DCM/hexane (1/1, 2 x 10 ml). The product was then dried under high vacuum to give 9-(4'-(9''-trityceny)phenyl)-10-ethyl-2,3,6,7,12,13-hexahydroxytritycene **16** (1.03 g, 1.46 mmol, 96%) as an off white powder. Mp decomposes above 65 °C; IR (nujol)/cm⁻¹: 3175, 2924, 2727, 2670, 1695, 1603, 1511, 1455, 1377, 1292, 1015, 938, 867, 790, 776, 722, 636; ¹H NMR (400 MHz; DMSO-D₆) δ 8.65 (3H, s, OH), 8.54 (3H, s, OH), 8.29 (2H, d, *J* = 8.6 Hz, ArH), 8.24 (2H, d, *J* = 8.6 Hz, ArH), 7.58 (3H, m, ArH), 7.49 (3H, m, ArH), 7.12-7.06 (6H, br m, ArH), 6.90-6.66 (6H, br s, ArH), 5.78 (1H, s, CH), 2.69 (2H, m, CH₂), 1.61 (3H, t, *J* = 7.0 Hz, CH₃); ¹³C NMR (100 MHz; DMSO-D₆) δ 147.1, 146.7, 141.2, 140.8, 140.4, 140.4, 136.8, 134.1, 131.9, 131.3, 125.6, 125.0, 124.5, 124.3, 113.0, 112.9, 60.0, 57.6, 55.3, 51.6, 20.4, 11.3; LRMS, *m/z*, (EI⁺): 706 (M⁺); Crystal data (methanol/hexane): orthorhombic, space group P 2₁ 2₁ 2₁, *a* 16.8637(4), *b* 17.8527(7), *c* 17.9973(6) Å, α = β = γ = 90.00, *V* = 5418.31 Å³, *Z* = 4, R-Factor 15.75%.

9-(4'-bromophenyl)-10-ethyl-2,3,6,7,12,13-hexamethoxytryptycene 17

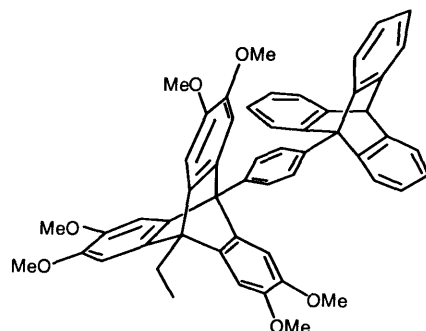
A suspension of 4,5-dimethoxy-benzenediazonium-2-carboxylate chloride (5.5 g, 22.5 mmol), 9-(4'-bromophenyl)-10-ethyl-2,3,6,7-tetramethoxyanthracene **4** (5.4 g, 11.2 mmol) and 1,2-epoxypropane (40 ml) in dichloroethane (180 ml) was refluxed for 18 hrs. Once the mixture cooled the solvents were evaporated. The crude residue was purified by flash chromatography (DCM) to give starting material 9-(4'-bromophenyl)-10-ethyl-2,3,6,7-tetramethoxyanthracene **4** (2.1 g) and 9-(4'-bromophenyl)-10-ethyl-2,3,6,7,12,13-hexamethoxytryptycene **17** (1.5 g, 2.43 mmol, 22%) as a white solid. Mp 235-236 °C; IR (film)/cm⁻¹: 2993, 2935, 2849, 1581, 1486, 1402, 1274, 1197, 1177, 1131, 1090, 1052, 1011, 763, 735, 622; ¹H NMR (400 MHz; CDCl₃) δ 8.04 (2H, d, *J* = 8.6 Hz, Ar*H*), 7.84 (2H, d, *J* = 8.6 Hz, Ar*H*), 7.03 (3H, s, H_b), 6.92-6.59 (3H, br s, H_a), 3.87 (9H, s, OCH₃), 3.67 (9H, s, OCH₃), 3.00 (2H, q, *J* = 7.1 Hz, CH₂), 1.80 (3H, t, *J* = 7.1 Hz, CH₃); ¹³C NMR (125 MHz; CDCl₃) δ 145.4, 141.6, 136.3, 133.1, 131.5, 121.3, 109.3, 107.4, 58.4, 56.145, 52.8, 20.2, 11.1, 3 carbons missing; HRMS Calc. for C₃₄H₃₃O₆⁷⁹Br 617.1539 (⁷⁹Br M⁺), found 617.1545 (⁷⁹Br M⁺), 619.1525 (⁸¹Br M⁺).

9-(4'-(anthracene-9''-yl)phenyl)-10-ethyl-2,3,6,7,12,13-hexamethoxytriptycene 18

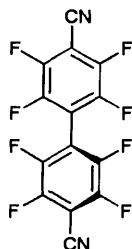


To 9-(4'-bromophenyl)-10-ethyl-2,3,6,7,12,13-hexamethoxytriptycene **17** (3.68 g, 5.96 mmol), 9-anthraceneboronic acid (1.72 g, 7.75 mmol) and K_2CO_3 (1.66 g, 12.0 mmol) in a degassed solution of THF (100 ml) and water (80 ml) was added $Pd(PPh_3)_4$ (0.07 g). The reaction was heated to 80 °C under a nitrogen atmosphere for 48 hrs then allowed to cool before being diluted with water (100 ml). The precipitate was filtered and washed with water (2 x 50 ml) and MeOH (2 x 50 ml), then dissolved in DCM (20 ml) and filtered through a plug of silica (DCM). The solvents were removed under vacuum to give 9-(4'-(anthracene-9''-yl)phenyl)-10-ethyl-2,3,6,7,12,13-hexamethoxytriptycene **18** (3.0 g, 4.2 mmol, 70%) as an off white powder Mp > 300 °C; IR (film)/ cm^{-1} : 3053, 2993, 2936, 2828, 1580, 1485, 1464, 1438, 1402, 1274, 1197, 1177, 1143, 1089, 1053, 1023, 764, 735, 624; 1H NMR (400 MHz; $CDCl_3$) δ 8.58 (1H, s, ArH), 8.39 (2H, d, J = 8.4 Hz, ArH), 8.12 (2H, d, J = 8.5 Hz, ArH), 7.89 (2H, d, J = 8.8 Hz, ArH), 7.77 (2H, d, J = 8.4 Hz, ArH), 7.53 (2H, m, ArH), 7.40 (2H, m, ArH), 7.75-7.22 (6H, br s, ArH), 3.90 (9H, s, OCH_3), 3.80 (9H, s, OCH_3), 3.06 (2H, q, J = 7.0 Hz, CH_2), 1.83 (3H, t, J = 7.0 Hz, CH_3); ^{13}C NMR (125 MHz; $CDCl_3$) δ 239.8, 145.4, 144.9, 144.3, 142.2, 137.9, 136.7, 136.2, 131.5, 131.4, 130.1, 128.6, 126.9, 126.4, 125.4, 125.1, 109.6, 59.0, 56.3, 56.2, 52.9, 20.3, 11.2, 1 carbons missing or obscured; HRMS Calc. for $C_{48}H_{42}O_6$ 714.2981, found 714.2981.

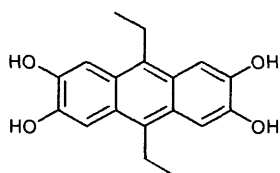
9-(4'-(tritycene-9''-yl)phenyl)-10-ethyl-2,3,6,7,12,13-hexamethoxytritycene 19



To a solution of 9-(4'-(anthracene-9''-yl)phenyl)-10-ethyl-2,3,6,7,12,13-hexamethoxytritycene **18** (3.0 g, 4.2 mmol) in DCE (80 ml) under N₂ atmosphere at 83 °C was added isoamyl nitrite (3.15 g, 26.9 mmol) portion wise ahead of anthranilic acid (3.51 g, 25.6 mmol, in THF 25 ml) over 1 hr. After 18 hrs the solution was cooled and the solvent evaporated under reduced pressure. The crude residue was purified by flash chromatography (ethyl acetate/hexane, 1/1) to give a mixture of starting material and product which was entered into a fresh reaction as described above. This process was repeated four times then the crude solid dissolved in toluene (150 ml) and heated to reflux for 0.5 hr with maleic anhydride (5 g). The reaction mixture was filtered through a plug of silica (DCM) to give 9-(4'-(tritycene-9''-yl)phenyl)-10-ethyl-2,3,6,7,12,13-hexamethoxytritycene **19** (1.4 g, 1.77 mmol, 42%) as a white solid. Mp > 300 °C; IR (film)/cm⁻¹: 2996, 2930, 2848, 1580, 1485, 1458, 1402, 1274, 1197, 1131, 1089, 1056, 1025, 752; ¹H NMR (400 MHz; CDCl₃) δ 8.41 (3H, s, ArH), 7.50 (3H, dd, *J* = 7.3 Hz, *J* = 1.0 Hz, ArH), 7.48 (3H, d, *J* = 7.3 Hz, ArH), 7.20-7.00 (10H, br m, ArH), 6.99-6.95 (3H, br m, ArH), 5.51 (1H, s, CH), 3.90 (6H, s, OCH₃), 3.81 (6H, s, OCH₃), 3.06 (2H, m, CH₂), 1.84 (3H, t, *J* = 7.1 Hz, CH₃); ¹³C NMR (125 MHz; CDCl₃) δ 149.5, 148.8, 146.7, 146.4, 145.5, 142.1, 140.1, 136.9, 131.8, 131.6, 126.4, 125.3, 125.2, 124.4, 124.1, 123.8, 109.8, 56.2, 19.0, 9.6, 4 carbons missing or obscured; HRMS Calc. for C₅₄H₄₆O₆ 790.3294, found 790.3318.

4,4'-dicyano-2,2',3,3',5,5',6,6'-octafluorobiphenyl 20¹²⁸

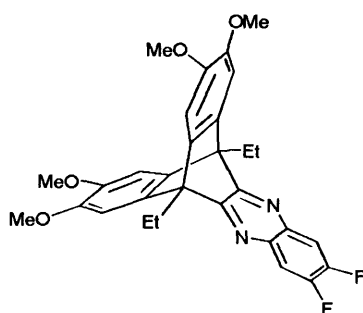
To a solution of pentafluorobenzonitrile (5.0 g, 25.9 mmol) in diethyl ether (60 ml) under N₂ atmosphere was added tris(diethylamino)phosphine (3.2 g, 12.9 mmol) portion wise over 5 mins with an ice bath for cooling. After 2 hrs at room temperature the solution was quenched with 1M HCl (50 ml). The crude mixture was washed with water (3 x 50 ml) and the solvent evaporated under reduced pressure. The crude residue was purified by flash chromatography (DCM/hexane, 1/4) to give 4,4'-dicyano-2,2',3,3',5,5',6,6'-octafluorobiphenyl **20** (2.1 g, 6.0 mmol, 46%) as a colourless crystalline solid. Mp 132-134 °C; ¹⁹F NMR (300 MHz; CDCl₃) δ -129.49 (4F, m, ArF), -133.30 (4F, m, ArF); ¹³C NMR (125 MHz; CDCl₃) δ 147.3 (dd, *J* = 265.2 Hz, *J* = 15.1 Hz), 143.9 (dd, *J* = 257.9 Hz, *J* = 13.7 Hz), 111.6 (t, *J* = 15.3 Hz), 106.4 (m), 97.1 (t, *J* = 17.0 Hz); HRMS Calc. for C₁₄N₂F₈ 347.9934, found 347.9932.

9,10-diethyl-2,3,6,7-tetrahydroxyanthracene 21

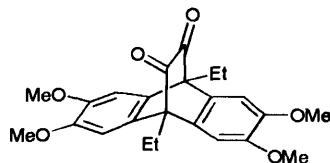
To a solution of 9,10-diethyl-2,3,6,7-tetramethoxyanthracene **2** (0.752 g, 2.12 mmol) in dry DCM (15 ml) at 0 °C under a N₂ atmosphere was added BBr₃ (2.39 g, 9.55 mmol). The reaction mixture was stirred for 1 hr at room temperature before being quenched in water (10 ml), filtered and washed with water (2 x 10 ml). The precipitate was then dissolved in diethyl ether (20 ml) and dried with magnesium sulfate. Hexane (20 ml) was added to the solution to precipitate 9,10-diethyl-2,3,6,7-tetrahydroxyanthracene **21** (0.42 g, 1.42 mmol, 67%) as a yellow powder which was

dried under high vacuum. Mp decomposes above 50 °C; IR (nujol)/cm⁻¹: 3425, 3356, 2924, 2854, 1641, 1507, 1461, 1440, 1378, 1367, 1335, 1321, 1291, 1232, 1199, 930, 849, 651; ¹H NMR (400 MHz; DMSO-D₆) δ 9.42 (4H, s, OH), 7.33 (6H, s, ArH), 3.21 (4H, q, *J* = 4 Hz, CH₂), 1.26 (6H, t, *J* = 7.4 Hz, CH₃); ¹³C NMR (100 MHz; DMSO-D₆) δ 146.0, 124.2, 104.9, 99.4, 54.8, 14.7; HRMS Calc. for C₁₈H₁₈O₄ 298.1205, found 298.1205.

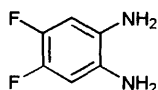
Functional triptycene **22**



To a solution of 4,5-difluoro-1,2-phenylenediamine **24** (1.15 g, 7.98 mmol) in acetic acid (100 ml) was added 2,3,6,7-tetramethoxy-9,10-diethyl-9,10-ethanoanthracene-11,12-dione **23** (1.64 g, 3.98 mmol) and a small amount of molecular sieves. The reaction mixture was refluxed for 15 hrs before being cooled and filtered. The precipitate was washed thoroughly with acetic acid and the washings and filtrate combined and diluted with water to precipitate the product. The crude product was recrystallised from slow evaporation of methanol/water (9/1, v/v) to give **22** (1.36 g, 2.61 mmol, 66%) as colourless crystals. Mp 106-107 °C; IR (film)/cm⁻¹: 3073, 2996, 2938, 2830, 1609, 1581, 1511, 1488, 1426, 1273, 1248, 1193, 1159, 1105, 1046, 875, 864, 784, 736; ¹H NMR (400 MHz; CDCl₃) δ 7.65 (2H, m, ArH), 7.09 (4H, s, ArH) 3.87 (12H, s, OCH₃), 3.03 (4H, q, *J* = 7.2 Hz, CH₂), 1.81 (6H, t, *J* = 7.2 Hz, CH₃); ¹³C NMR (100 MHz; CDCl₃) δ 160.4 (s), 151.7 (dd, *J* = 254.2 Hz, *J* = 17.2 Hz), 147.1 (s), 139.0 (s), 135.6 (t, *J* = 5.9 Hz), 115.0 (m), 108.3 (s), 56.2 (s), 53.7 (s), 19.7 (s), 10.3 (s); ¹⁹F NMR (283 MHz; CDCl₃) δ -133.305 (2F, m, ArF); LRMS, *m/z*, (EI⁺): 518 (M⁺); Crystal data (methanol): monoclinic, space group C 2/c, *a* 30.8470(7), *b* 8.9960(2), *c* 18.5250(5) Å, α 90.00, β 102.5730(10), γ 90.00. *V* = 5017.4 Å³, *Z* = 8, R-Factor of 5.92%.

2,3,6,7-tetramethoxy-9,10-diethyl-9,10-ethanoanthracene-11,12-dione**23**¹²⁹

To a solution of dry DMSO (1.40 ml, 19.71 mmol) in dry chloroform (90 ml) at -78 °C under N₂ atmosphere was added trifluoroacetic anhydride (2.40 ml, 17.25 mmol). The mixture was stirred for 10 mins before 2,3,6,7-tetramethoxy-9,10-diethyl-9,10-ethanoanthracene-11,12-diol **25** (2.40 g, 5.79 mmol) in chloroform/DMSO (2/1, v/v) was added drop-wise within 20 mins. After 1 hr triethylamine (5.40 ml, 38.85 mmol) was slowly added and the mixture stirred for 15 mins. The mixture was then allowed to warm up to 5 °C and poured into hydrochloric acid (2M, 200 ml). The crude product was extracted with chloroform (3 x 30 ml), and the combined organic solvent washed with water (6 x 50 ml), brine (1 x 30 ml) then dried with magnesium sulphate. The solvent was removed under vacuum and the crude product recrystallised from hexane to give 2,3,6,7-tetramethoxy-9,10-diethyl-9,10-ethanoanthracene-11,12-dione (2.12 g, 5.14 mmol, 89%, Lit¹²⁹: 99%) as a bright orange powder. Mp 196-198 °C, Lit¹²⁹: 202-203 °C; ¹H NMR (400 MHz; CDCl₃) δ 6.96 (4H, s, ArH), 3.90 (12H, s, OCH₃), 2.62 (4H, q, *J* = 7.3 Hz, CH₂), 1.51 (6H, t, *J* = 7.3 Hz, CH₃); ¹³C NMR (100 MHz; CDCl₃) δ 185.5, 149.5, 130.5, 107.9, 58.3, 56.1, 18.1, 9.3; LRMS, *m/z*, (EI⁺): 412 (M⁺).

4,5-Difluoro-1,2-phenylenediamine 24**Method A:**¹⁴⁰

To a solution of SnCl₂·2H₂O (13.55 g, 60.06 mmol) in conc. hydrochloric acid (20 ml) was added 4,5-difluoro-2-nitroaniline **28** (2.65 g, 15.22 mmol). The mixture was stirred over night at 50-60° C then poured into ice-water. The solution was turned

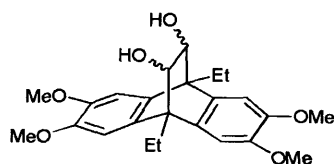
alkaline with NaOH (2 N) and extracted with chloroform. The organic solvent was dried with magnesium sulphate and removed under reduced pressure. The crude residue was recrystallised from hexane/ethyl acetate (1/1) to give 4,5-difluoro-1,2-phenylenediamine **24** (1.36 g, 9.44 mmol, 62%, Lit¹⁴⁰: 42%) as a colourless solid.

Method B:¹⁴¹

Iron powder (1.78 g, 31.87 mmol) in hydrochloric acid (1M, 50 ml) was added to a solution of 4,5-difluoro-2-nitroaniline **28** (1.132 g, 6.50 mmol) in methanol (20 ml) and stirred over night. The mixture was then filtered and the filtrate neutralised with conc. NH₄OH to approximately pH 8. The resulting suspension was filtered and washed thoroughly with cold methanol. The filtrate and washings were combined and extracted with chloroform, washed with brine, then dried with magnesium sulphate. The solvent was removed under reduced pressure to give 4,5-difluoro-1,2-phenylenediamine (0.662 g, 4.60 mmol, 71%, Lit¹⁴¹: 85%).

Mp 131-132 °C, Lit¹⁴⁰: 130-131 °C; ¹H NMR (400 MHz; CDCl₃) δ 6.51 (2H, t, *J* = 9.5 Hz, ArH), 3.26 (4H, s, NH₂).

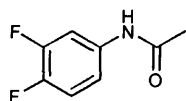
2,3,6,7-tetramethoxy-9,10-diethyl-9,10-ethanoanthracene-11,12-diol **25**¹²⁹



A suspension of 9,10-diethyl-2,3,6,7-tetramethoxyanthracene **2** (3.3 g, 9.31 mmol) and vinylene carbonate (6.52 g, 75.78 mmol) in xylene (20 ml) was heated in a microwave at 180 °C for 8 hrs. The solvent was evaporated under reduced pressure and the residue refluxed in sodium hydroxide solution (40% aq, 60 ml) for 4 hrs. The solution was cooled and 2,3,6,7-tetramethoxy-9,10-diethyl-9,10-ethanoanthracene-11,12-diol **25** (3.47 g, 8.37 mmol, 90%, Lit¹²⁹: 91%) filtered off as a beige powder. Mp 140-141 °C, Lit¹²⁹: 137-139 °C; ¹H NMR (400 MHz; CDCl₃) δ 6.91 (2H, s, ArH), 6.90 (2H, s, ArH), 4.00 (2H, s, CH(OH)), 3.86 (6H, s, OCH₃), 3.86 (6H, s, OCH₃),

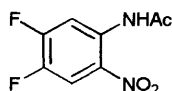
2.99 (4H, m, CH₂), 1.43 (6H, t, *J* = 7.3 Hz, CH₃); LRMS, *m/z*, (EI⁺): 397 (M⁺ -H₂O), 432 (M⁺+NH₄).

3,4-Difluoro-acetanilide **26**¹⁴²

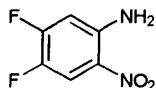


A solution of 3,4-difluoroaniline (2.326 g, 18.02 mmol) in water (34 ml) and conc. hydrochloric acid (1.1 ml) was heated to 90 °C for 10 min then acetic anhydride (4 ml, 42.4 mmol) was added. The solution was allowed to then cool down and a solution of sodium acetate (2.00 g, 24.38 mmol) in water (6 ml) was added, and the product 3,4-difluoro-acetanilide **26** (2.53 g, 14.78 mmol, 82%) filtered off as white needles. Mp 107-108 °C; ¹H NMR (400 MHz; CDCl₃) δ 7.88 (1H, s, NH) 7.58 (1H, m, ArH) 7.06 (2H, m, ArH) 2.16 (3H, s, CH₃); LRMS, *m/z*, (EI⁺): 171 (M⁺).

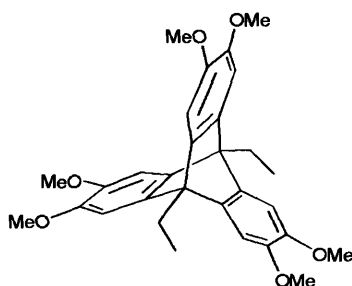
4,5-Difluoro-2-nitro-acetanilide **27**¹⁴⁰



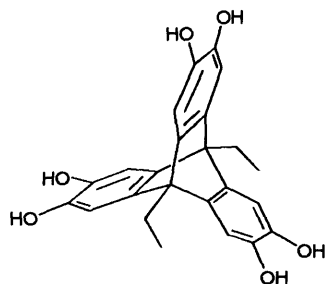
To a solution of 3,4-difluoro-acetanilide **26** (3.00 g, 17.53 mmol) in conc. sulfuric acid (10 ml) at 5-10 °C was added drop-wise HNO₃ (70% v/v, 9.2 ml). After 1 hr the reaction mixture was pored into ice-water (100 ml) and the precipitate filtered, and recrystallised from ethanol to give 4,5-difluoro-2-nitro-acetanilide **27** (2.81 g, 13.00 mmol, 74%, Lit¹⁴⁰: 77 %) as yellow needles. Mp 106-107 °C, Lit¹⁴⁰: 104-105 °C; ¹H NMR (400 MHz; CDCl₃) δ 10.44 (1H, s, NH) 8.83 (1H, dd, *J* = 12.8 Hz, *J* = 7.6 Hz, ArH) 8.12 (2H, dd, *J* = 10.0 Hz, *J* = 8.0 Hz, ArH) 2.30 (3H, s, CH₃); LRMS, *m/z*, (EI⁺): 216 (M⁺).

4,5-Difluoro-2-nitroaniline **28¹⁴⁰**

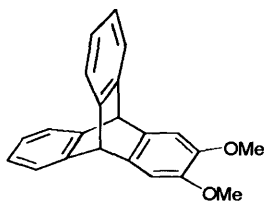
To a suspension of 4,5-difluoro-2-nitro-acetanilide **27** (2.00 g, 9.25 mmol) in ethanol (20 ml) conc. hydrochloric acid (5 ml) was added. The mixture was refluxed for 2 hr and then poured into water (100 ml) and the precipitate filtered. The crude solid was recrystallised from water/ethanol (1/1) to give 4,5-difluoro-2-nitroaniline **28** (1.272 g, 7.31 mmol, 79%, Lit¹⁴⁰: 70%) as yellow needles. Mp 109-110 °C, Lit¹⁴⁰: 107.5-109.5 °C; ¹H NMR (400 MHz; CDCl₃) δ 7.98 (1H, dd, *J* = 10.5 Hz, *J* = 8.2 Hz, ArH) 6.63 (1H, dd, *J* = 11.2 Hz, *J* = 6.7 Hz, ArH) 6.17 (2H, s, NH₂); LRMS, *m/z*, (EI⁺): 174 (M⁺).

9,10-diethyl-2,3,6,7,12,13-hexamethoxytriptycene **29⁵**

To a solution of 9,10-diethyl-2,3,6,7-tetramethoxyanthracene **2** (2.0 g, 5.64 mmol) in DCE (180 ml) with 1,2-epoxypropane (40 ml) at 83 °C was added 4,5-dimethoxybenzenediazonium-2-carboxylate chloride (7.5 g, 30.7 mmol). The reaction was left to proceed for 18 hrs. The solvent was then removed under vacuum and the crude residue purified by flash chromatography (DCM) to give 9,10-diethyl-2,3,6,7,12,13-hexamethoxytriptycene **29** (1.16 g, 2.36 mmol, 42% yield) which was recrystallised from ethanol to give the product as colourless crystals. Mp 180-183 °C, Lit⁵: 274-276 °C; ¹H NMR (400 MHz; CDCl₃) δ 6.98 (6H, s, ArH), 3.84 (18H, s, OCH₃), 2.97 (4H, q, *J* = 7.1 Hz, CH₂), 1.74 (6H, t, *J* = 7.1 Hz, CH₃); ¹³C NMR (100 MHz; CDCl₃) δ 145.1, 107.3, 56.2, 52.6, 20.0, 11.0, 1 carbon missing; HRMS Calc. for C₃₀H₃₄O₆ 490.2355, found 490.2342.

9,10-diethyl-2,3,6,7,12,13-hexahydroxytriptycene 30⁵

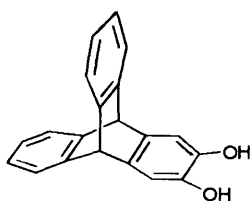
To a solution of 9,10-diethyl-2,3,6,7,12,13-hexamethoxytriptycene **29** (0.49 g, 1.0 mmol) in dry DCM (10 ml) at 0 °C under a N₂ atmosphere was added BBr₃ (1.63 g, 6.50 mmol). The reaction mixture was stirred for 1 hr at room temperature before being quenched in water (20 ml), filtered and washed with water (2 x 10 ml). The precipitate was then dissolved in diethyl ether (30 ml) and dried with magnesium sulfate. Hexane (30 ml) was added to the solution to precipitate 9,10-diethyl-2,3,6,7,12,13-hexahydroxytriptycene **30** (0.32 g, 0.787 mmol, 79%) as a light purple powder which was dried under high vacuum. Mp decomposes above 50 °C; IR (nujol)/cm⁻¹: 3411, 1640, 1483, 1446, 1296, 1227, 1007, 728; ¹H NMR (400 MHz; Acetone-D₆) δ 8.70-8.10 (6H, br s, OH), 6.70 (6H, s, ArH), 2.58 (4H, m, CH₂), 1.50 (6H, t, *J* = 7.1 Hz, CH₃); ¹³C NMR (125 MHz; Methanol-D₄) δ 141.4, 111.5, 53.0, 21.3, 11.4, 1 carbon missing.

2,3-dimethoxytriptycene 31¹²²

Anthracene (1.78 g, 10.0 mmol) was dissolved in DCE (180 ml) with 1,2-epoxypropane (40 ml), heated to 83 °C and 4,5-dimethoxy-benzenediazonium-2-carboxylate chloride (7.5 g, 30.7 mmol) added. The reaction was left to proceed for

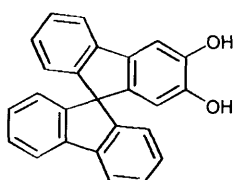
18 hrs. The solvent was then removed under vacuum and the crude residue purified by flash chromatography (DCM/hexane, 3/7) to give 2,3-dimethoxytriptycene (0.7 g, 2.2 mmol, 22% yield) as colourless crystals. Mp 190-194 °C, Lit¹⁴³: 190-192 °C; ¹H NMR (400 MHz; CDCl₃) δ 7.3 (4H, m, ArH), 6.95 (2H, s, ArH), 6.9 (4H, m, ArH), 5.3 (2H, s, CH), 3.75 (6H, s, OCH₃).

2,3-dihydroxytriptycene **32**¹²²



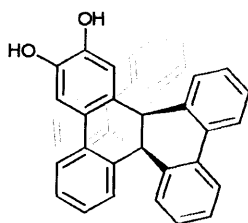
To a solution of 2,3-dimethoxytriptycene **31** (1.8 g, 5.73 mmol) in dry DCM (30 ml) at 0 °C under a N₂ atmosphere was added BBr₃ (3.0 g, 12 mmol). The reaction mixture was stirred for 1 hr at room temperature before being quenched in water (200 ml), filtered and washed with water (2 x 10 ml). The precipitate was then dissolved in diethyl ether (30 ml) and dried with magnesium sulfate. Hexane (50 ml) was added to the solution to precipitate 2,3-dihydroxytriptycene **32** (1.3 g, 4.54 mmol, 79%) as a white powder which was dried under high vacuum. Mp decomposed above 70 °C; IR (nujol)/cm⁻¹: 3325, 3208, 2946, 2871, 2724, 2673, 1695, 1616, 1502, 1457, 1376, 1303, 1236, 1184, 1153, 1060, 1038, 740, 627; ¹H NMR (500 MHz; Acetone-D₆) δ 7.57 (2H, s, OH), 7.37 (4H, dd, J = 5.3 Hz, J = 3.2 Hz, ArH), 6.97 (2H, s, ArH), 6.94 (4H, dd, J = 5.3 Hz, J = 3.2 Hz, ArH), 5.41 (2H, s, CH); ¹³C NMR (100 MHz, CDCl₃) δ 146.1, 141.5, 136.7, 124.5, 123.1, 112.2, 51.9.

2,3-dihydroxy-9,9'-spirobifluorene **34**



To a solution of 2,3-dimethoxy-9,9'-spirobifluorene **33** (1.50 g, 4.305 mmol) in dry DCM (15 ml) at 0 °C under a N₂ atmosphere was added BBr₃ (2.37 g, 9.47 mmol). The reaction mixture was stirred for 1 hr at room temperature before being quenched in water (50 ml), filtered and washed with water (2 x 10 ml), acetone (1 x 10 ml), and DCM/hexane (1/2, 2 x 10 ml). The product was then dried under high vacuum to give 2,3-dihydroxy-9,9'-spirobifluorene **34** (1.37 g, 3.93 mmol, 91%) as an off white powder. Mp decomposes above 70 °C; IR (nujol)/cm⁻¹: 3524, 2924, 2726, 2670, 1607, 1463, 1377, 1291, 1274, 1181, 1149, 876, 790, 755, 740, 735, 724, 657, 624; ¹H NMR (400 MHz; Acetone-D₆) δ 8.01 (1H, s, OH), 7.95 (2H, d, *J* = 7.5 Hz, ArH), 7.87 (1H, s, OH), 7.76 (1H, d, *J* = 7.5 Hz, ArH), 7.41 (1H, s, ArH), 7.38 (2H, dt, *J* = 7.5 Hz, *J* = 1.1 Hz, ArH), 7.32 (1H, dt, *J* = 7.5 Hz, *J* = 7.1 Hz, ArH), 7.15 (2H, dt, *J* = 7.5 Hz, *J* = 1.1 Hz, ArH), 7.01 (1H, dt, *J* = 7.5 Hz, *J* = 1.1 Hz, ArH), 6.69 (2H, d, *J* = 7.5 Hz, ArH), 6.56 (1H, d, *J* = 7.5 Hz, ArH), 6.12 (1H, s, ArH).

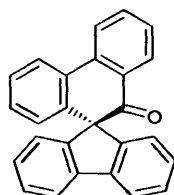
Dihydroxy-propellane **35**



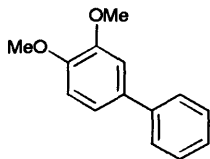
Boron tribromide (0.77 ml, 8 mmol) was added drop-wise to a solution of dimethoxy-propellane (1.44 g, 2.7 mmol) in anhydrous DCM (200 ml), with stirring and under nitrogen, at 0 °C. After 3 hrs the reaction was quenched with water and the white precipitate formed was filtered and washed with DCM (1.1 g, 2.1 mmol, 79 %). Mp decomposes above 70 °C; IR (nujol)/cm⁻¹: 3532, 1606, 1572, 1511, 1302, 1179, 773, 743; ¹H NMR (400 MHz; acetone-D₆) δ 7.73 (4H, m, ArH), 7.54 (1H, dd, *J* = 7.8 Hz, *J* = 0.9 Hz, ArH), 7.21 (6H, m, ArH, OH), 7.09 (4H, m, ArH), 7.09 (1H, td, *J* = 7.6 Hz, *J* = 1.2 Hz, ArH), 6.78 (1H, dd, *J* = 7.6 Hz, *J* = 1.2 Hz, ArH), 6.60 (4H, m, ArH), 6.09 (1H, s, OH); ¹³C NMR (125 MHz; CDCl₃) δ 145.3, 145.2, 145.0, 145.0, 140.8, 140.5, 139.5, 136.1, 135.8, 135.8, 135.7, 132.1, 130.0, 129.9, 129.8, 129.7, 126.9, 124.7, 124.7, 124.6, 124.5, 123.9, 117.3, 112.1, 54.1, 53.4, some carbons missing; LRMS, (EI⁺), *m/z*: 512 (M⁺), HRMS Calc. for C₃₈H₂₄O₂ 512.5959, found

512.1792; Crystal data (ethyl acetate/hexane): tetragonal, space group $I 4_1 c$, a 16.9375(6), b 16.9324(6), c 34.3414(10) Å, $\alpha = \beta = \gamma = 90.00$, $V = 9848.86$ Å³, $Z = 16$, R-Factor 5.1 %.

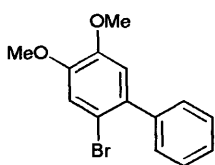
Pinacolone **37**¹³³



To a solution of 9-fluorenone (9.0 g, 49.9 mmol) and ZnCl (9.0 g, 89.3 mmol) in THF (45 ml) and water (45 ml) was added Zinc (30 mesh, 45 g) with vigorous stirring. After 3 hrs the suspension turned white, and 3M HCl (45 ml) was added. The zinc was filtered and the filtrate washed with toluene until only water remained. The solvents were removed under reduced pressure, and the residue dissolved in diethyl ether. The product was crystallised out by slow addition of hexane to give 9,9'-bifluorene-9,9'-diol **36**¹⁴⁴ (6.70 g, 18.49 mmol, 74%) as a colourless crystalline solid which was immediately used in the next step without further purification. To a solution of diol **36** (9.26 g, 25.55 mmol) in glacial acetic acid (225 ml) was added drop-wise H₂SO₄ (96%, 9 ml). The solution was then heated to 90 °C for 45 mins before water (225 ml) was added to precipitate the product. The crude white powder was purified by recrystallisation from methanol to give pinacolone **37** (3.76 g, 10.92 mmol, 43%) as colourless crystals. Mp 253-255 °C, Lit¹³³: 254-256 °C; IR (film)/cm⁻¹: 3071, 1683, 1601, 1450, 1266, 1132, 751, 744, 730; ¹H NMR (400 MHz; CDCl₃) δ 8.20 (1H, d, $J = 8.0$ Hz, ArH), 8.11 (1H, d, $J = 7.3$ Hz, ArH), 8.01 (1H, d, $J = 7.8$, 1.0 Hz, ArH), 7.80 (3H, m, ArH), 7.46 (1H, t, $J = 7.8$, ArH), 7.39 (3H, m, ArH), 7.19 (2H, t, $J = 7.3$, ArH), 7.07 (3H, m, ArH), 6.64 (1H, d, $J = 8.0$, ArH); ¹³C NMR (100 MHz; CDCl₃) δ 197.7, 147.5, 142.1, 139.8, 138.6, 135.4, 130.9, 130.5, 129.7, 129.0, 128.8, 128.6, 128.5, 128.4, 125.2, 124.6, 123.7, 121.0, 69.2; LRMS, (APCI), m/z : 345 (MH⁺, 100%).

4-Phenylveratrole 38

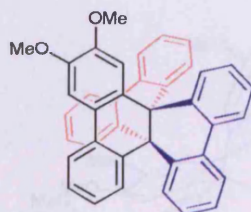
To a degassed solution of H₂O (100 ml) and DME (100 ml) was added phenylboronic acid (2.8 g, 23.0 mmol), 4-bromoveratrole (6.0 g, 27.6 mmol), and K₂CO₃ (6.4 g, 46 mmol). The solution was heated to 80 °C and Pd(PPh₃)₄ (0.20 g, 0.17 mmol) added and stirred for 24 hrs. The solution was cooled, the DME removed under vacuum, and product extracted with DCM (3 x 40 ml). The DCM was removed under vacuum and the product recrystallised from slow evaporation of methanol to give 4-phenylveratrole **38** (4.04 g, 18.7 mmol, 82%) as colourless crystals. Mp 68-70 °C, Lit¹⁴⁵: 68-69 °C; IR (film)/cm⁻¹: 3056, 3030, 3000, 2935, 2834, 1604, 1521, 1488, 1464, 1441, 1406, 1251, 1217, 1173, 1143, 1026, 854, 758, 701; ¹H NMR (400 MHz; CDCl₃) δ 7.57 (2H, m, ArH), 7.43 (2H, m, ArH), 7.31 (1H, m, ArH), 7.14 (2H, m, ArH), 6.95 (1H, m, ArH), 3.96 (3H, s, OCH₃), 3.93 (3H, s, OCH₃); LRMS, (EI⁺), m/z: 230 (M⁺).

4-phenyl-5-bromoveratrole 39

To a solution of 4-phenylveratrole **38** (9.3 g, 43.5 mmol) in chloroform (150 ml) bromine (7.6 g, 47.9 mmol) was added drop-wise with stirring at 0 °C. The reaction was stirred for 24 hrs at room temperature then washed with an aqueous solution of sodium tiosulfate to eliminate excess of bromine. The organic layer was dried over magnesium sulfate, filtered and the solvent evaporated under vacuum. The crude compound was reprecipitated as white solid (10.4g, 35.5 mmol, 82%) with MeOH from DCM. Mp 110-112 °C; IR (film)/cm⁻¹: 3059, 2964, 2938, 2910, 2838, 1603, 1519, 1505, 1489, 1441, 1379, 1208, 1020, 860, 770, 704; ¹H NMR (400 MHz;

CDCl_3) δ 7.42 (5H, m, ArH), 7.13 (1H, s, ArH), 6.84 (1H, s, ArH), 3.92 (3H, s, OCH_3), 3.87 (3H, s, OCH_3); ^{13}C NMR (100 MHz; CDCl_3) δ 148.7, 148.2, 141.0, 134.7, 129.5, 127.9, 127.4, 115.7, 113.8, 112.4, 56.2, 56.0; LRMS, (EI^+), m/z : 292 ($^{79}\text{Br M}^+$), 294 ($^{81}\text{Br M}^+$).

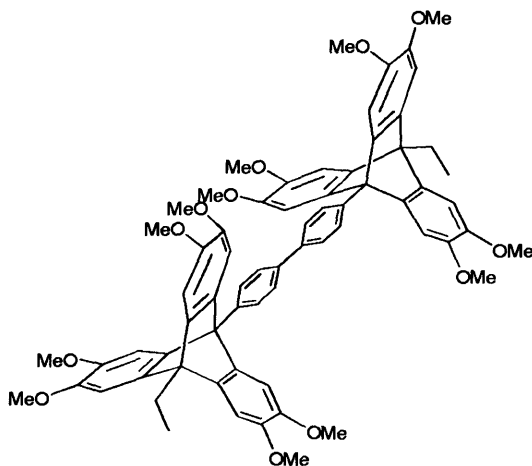
Dimethoxy-propellane 40



n-Butyllithium 2.5 M solution in hexane (2.56 ml, 6.4 mmol) was added drop-wise at $-78\text{ }^\circ\text{C}$ to a solution of 4-phenyl-5-bromoveratrole **39** (1.88 g, 6.4 mmol) in anhydrous diethylether (60 ml). After 1 hr spiro[9*H*-fluorene-9,9'(10'*H*)-phenanthrene]-10'-one **37** (2 g, 5.8 mmol) was added to the reaction mixture. The reaction was then allowed to slowly reach room temperature and stirred for 12 hrs, before being quenched with water and extracted with DCM (3 x 40 ml). The organic layers were combined, washed with water, dried with anhydrous magnesium sulphate and filtered. The solvent was evaporated under vacuum to afford a pale yellow solid which was dissolved in cold glacial acetic acid (150 ml), concentrated sulphuric acid (6 ml) was added drop-wise to the solution which was then stirred at $95\text{ }^\circ\text{C}$ for 2 hrs. After cooling the mixture was poured into water then extracted with DCM (3 x 40 ml). The organic fraction was washed with aqueous NaOH (10%, 30 ml), water and brine, dried over magnesium sulfate and filtered. The solvent was removed under reduced pressure to give a light brown solid which was purified by repeated reprecipitation with hexane from DCM to yield a white solid (1.4 g, 2.6 mmol, 45%). $\text{Mp} > 300\text{ }^\circ\text{C}$; IR (film)/ cm^{-1} : 3062, 3024, 2934, 2849, 1604, 1511, 1446, 1394, 1340, 1277, 1026, 739; ^1H NMR (400 MHz; CDCl_3) δ 7.63 (4H, m, ArH), 7.52 (1H, d, $J = 7.6\text{ Hz}$, ArH), 7.20 (5H, m, ArH), 7.12 (1H, s, ArH), 7.03 (5H, m, ArH), 6.68 (5H, m, ArH), 6.16 (1H, s, ArH), 3.88 (3H, s, OCH_3), 3.51 (3H, s, OCH_3); ^{13}C NMR (100 MHz; CDCl_3) δ 148.4, 148.3, 140.7, 139.9, 139.9, 139.7, 139.4, 135.3, 135.3, 135.2, 135.1, 132.4, 129.6, 129.4, 129.3, 129.2, 128.3, 127.9, 127.8, 127.7, 127.7, 127.6, 127.6,

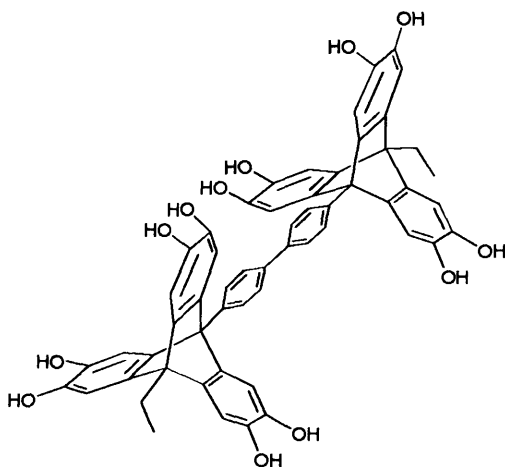
126.9, 124.1, 124.1, 124.0, 123.4, 112.9, 107.3, 56.1, 56.0, 53.6, 53.2, some carbons missing; LRMS, (EI⁺), m/z: 540 (M⁺); HRMS Calc. for C₄₀H₂₈O₂ 544.6491, found 540.2081.

4,4'-di(10''-ethyl-2'',3'',6'',7'',12'',13''-hexamethoxytriptycene-9''-yl)phenyl)biphenyl 41

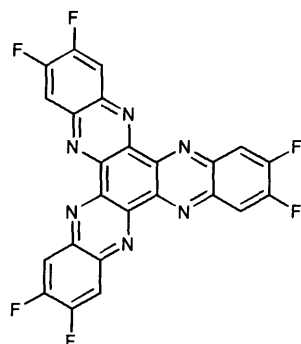


Into a Schlenk tube was placed 9-(4'-bromophenyl)-10-ethyl-2,3,6,7,12,13-hexamethoxytriptycene **17** (0.509 g, 0.825 mmol), 2,2'-bipyridyl (0.143 g, 0.909 mmol) and 1,5-cyclooctadiene (0.098 g, 0.915 mmol) in DMF (3 mL). The mixture was stirred at room temperature for 0.5 hr then bis(1,5-cyclooctadiene)nickel(0) (0.25 g, 0.909 mmol) was added at once to the stirred solution, and the mixture was heated to 120 °C for 24 hrs. Upon cooling, the mixture was poured into a warm aqueous solution of ethylenediamine-tetraacetic acid, precipitates were filtered and washed with NaOH solution (10%, w/w), water and then methanol. The product was recrystallised from methanol and dried in a vacuum oven 24 hrs to give bitriptycene **41** as a white powder (0.448 g, 0.726 mmol, 88%). Mp > 300 °C; IR (film)/cm⁻¹: 2995, 2949, 2827, 1582, 1487, 1464, 1441, 1403, 1275, 1197, 1178, 1131, 1057, 1033, 761, 636, 623; ¹³C NMR (125 MHz; CDCl₃) δ 145.2, 144.8, 141.2, 136.0, 134.2, 132.9, 122.6, 110.3, 107.6, 58.8, 56.4, 53.0, 20.5, 11.2, 2 carbons missing or obscured; HRMS Calc. for C₆₈H₆₆O₁₂ 1074.4554, found 1074.4557.

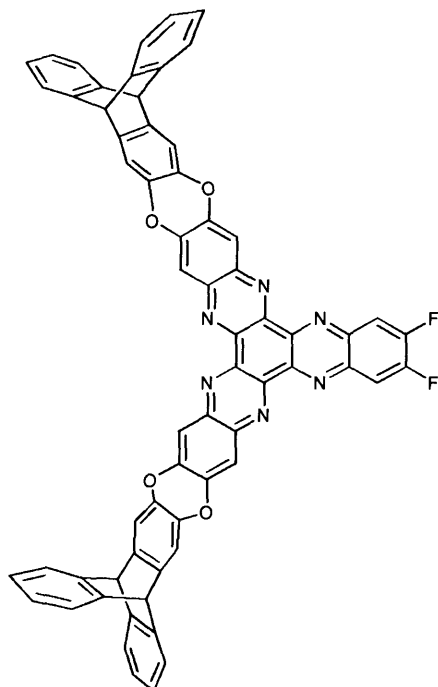
4,4'-di(10''-ethyl-2'',3'',6'',7'',12'',13''-hexahydroxytriptycene-9''-yl)phenyl)biphenyl **42**



To a solution of 4,4'-di(2'',3'',6'',7'',12'',13''-hexamethoxytriptycene-9''-yl)phenyl)biphenyl **41** (0.40 g, 0.37 mmol) in dry DCM (8 ml) at 0 °C under a N₂ atmosphere was added BBr₃ (1.13 g, 4.46 mmol). The reaction mixture was stirred for 1 hr at room temperature before being quenched in water (10 ml), filtered and washed with water (2 x 5 ml), and DCM/hexane (1/1, 2 x 10 ml). The product was then dried under high vacuum to give 4,4'-di(2'',3'',6'',7'',12'',13''-hexahydroxytriptycene-9''-yl)phenyl)biphenyl **42** (0.21 g, 0.23 mmol, 63%) as an off white powder. Mp decomposes above 60 °C; ¹H NMR (400 MHz; Acetone-D₆) δ 8.21 (8H, m, ArH), 7.51 (6H, s, OH), 7.49 (6H, s, OH), 6.95 (6H, s, ArH), 6.90-6.60 (6H, br s, ArH), 2.82 (4H, q, *J* = 7.0 Hz, CH₂), 1.66 (6H, t, *J* = 7.0 Hz, CH₃).

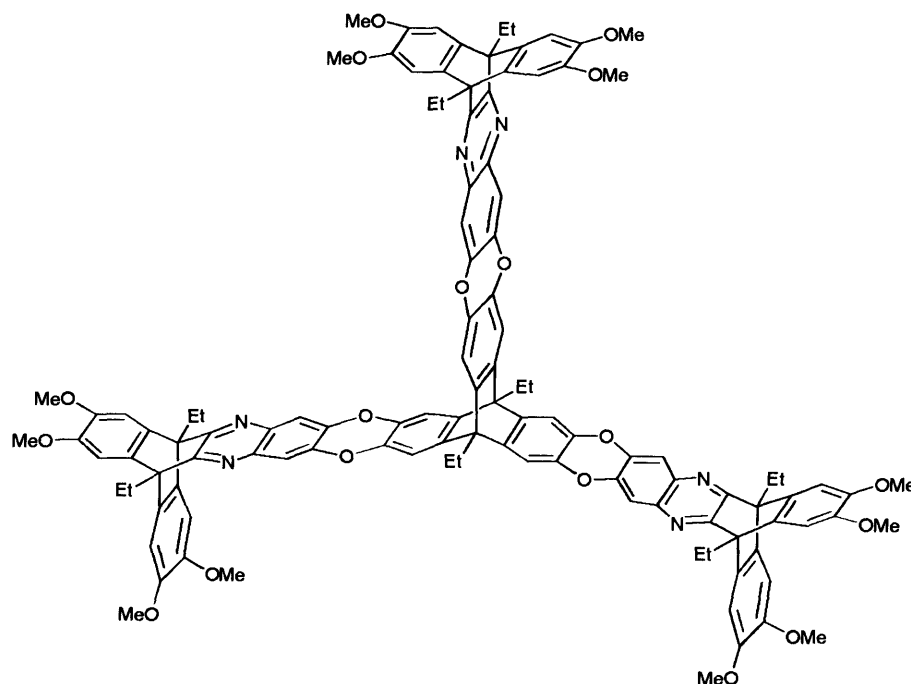
2,3,8,9,14,15-hexafluoro-5,6,11,12,17,18-hexaazatrinaphthylene (F₆-HATN) monomer 43

To a solution of 4,5-difluoro-1,2-phenylenediamine **24** (2.45 g, 17.00 mmol) in acetic acid (100 ml) was added hexaketocyclohexane octahydrate (1.516 g, 4.86 mmol) and a small amount of molecular sieves. The reaction mixture was refluxed for 20 hrs before being cooled and filtered. The precipitate was washed thoroughly with hot acetic acid to give 2,3,8,9,14,15-hexafluoro-5,6,11,12,17,18-hexaazatrinaphthylene **43** (1.90 g, 3.86 mmol, 79%) as a bright orange powder. Mp > 300 °C; MS (MALDI-TOF): cluster centred at m/z 493.09 (MH^+); elemental analysis found: C, 54.35; H, 1.80; F, 21.04; N, 15.80. Calc. for $C_{24}H_6F_6N_6$: C, 58.55; H, 1.23; F, 23.15; N, 17.07%.

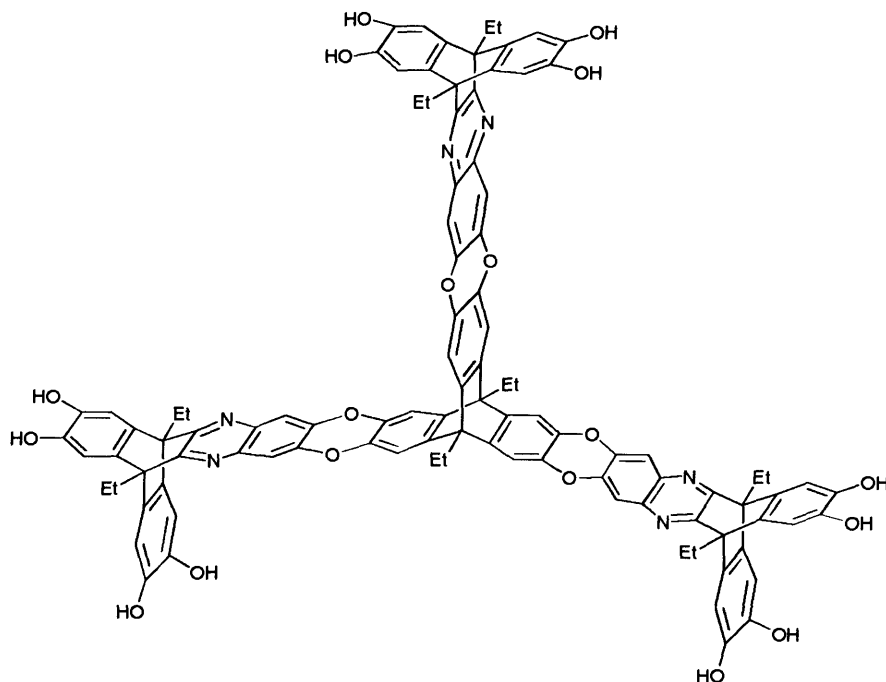
HATN based functional dendron 44

Under a nitrogen atmosphere 2,3-dihydroxytriptycene **32** (1.60 g, 5.59 mmol) in anhydrous DMF (30 ml) was slowly added through a dropping funnel to a stirred suspension of F₆-HATN **43** (2.08 g, 4.20 mmol) in anhydrous DMF (120 ml). This mixture was heated to 75 °C then dry potassium carbonate (1.7 g, 12.8 mmol) was added and the mixture stirred for 20 hrs at 75 °C. The solution was quenched with water (200 ml), the precipitate filtrated and washed with copious amounts of water then acetone. The precipitate was dissolved in chloroform (500 ml) with a few drops of trifluoroacetic acid and loaded onto silica *via* removal of solvents under vacuum. The crude product loaded silica was purified by flash chromatography (chloroform/toluene/ethyl acetate, 3/6/1) to give **44** (0.96 g, 0.97 mmol, 30%) as a bright orange solid; IR (nujol)/cm⁻¹: 2923, 2724, 2670, 1613, 1464, 1377, 1337, 1278, 1227, 1081, 874, 742, 722; MS (MALDI-TOF): cluster centred at m/z 986.72 (MH⁺); elemental analysis found: C, 74.58; H, 3.09; F, 3.67; N, 8.09. Calc. for C₆₄H₃₀F₂N₆O₄: C, 78.04; H, 3.07; F, 3.86; N, 8.53%; TGA analysis (nitrogen): Initial weight loss due to thermal degradation commences at ~ 549 °C.

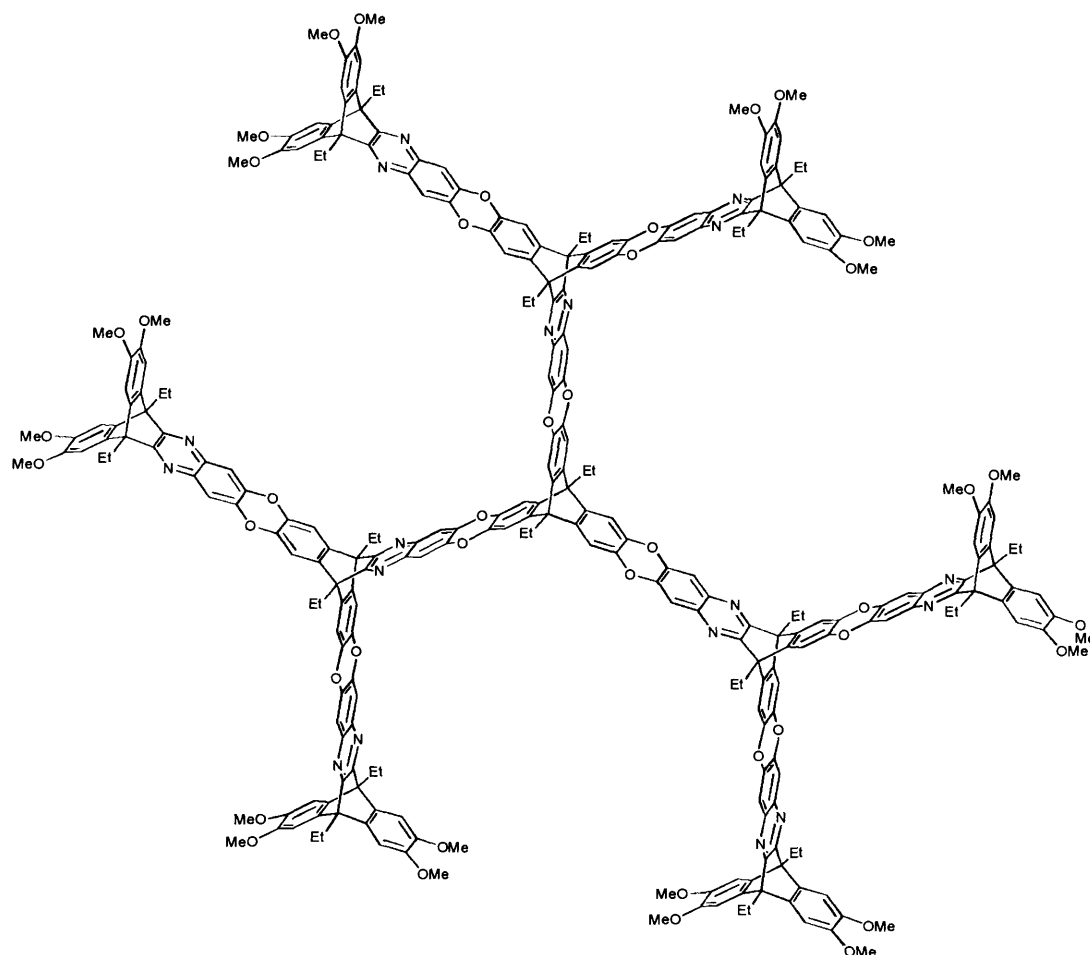
Divergent dendrimer D1



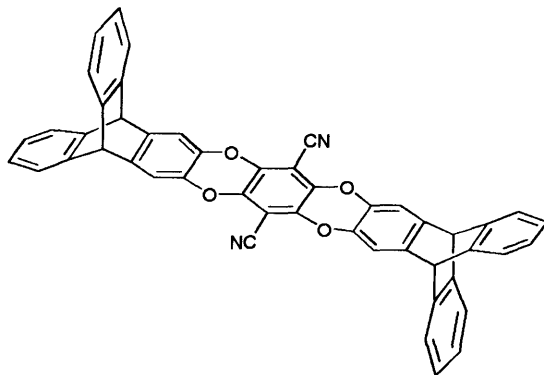
Under a nitrogen atmosphere 9,10-diethyl-2,3,6,7,12,13-tetrahydroxytriptycene **30** (0.101 g, 0.249 mmol), and **22** (0.448 g, 0.861 mmol) were dissolved in anhydrous DMF (8 ml) at 65 °C. Dry potassium carbonate (0.38 g, 2.75 mmol) was then added and the mixture stirred at 120 °C for 18 hrs. The solution was quenched with water (60 ml), the precipitate filtrated and washed with copious amounts of water. The precipitate was dissolved in chloroform (40 ml) then washed with water and brine before being dried with magnesium sulphate. The solvents were removed under vacuum and the crude residue was purified by flash chromatography (DCM/ethyl acetate, 9/1) to give **D1** (0.25 g, 0.136 mmol, 54%) as an off white solid; IR (film)/cm⁻¹: 3071, 2983, 2934, 2852, 2831, 1727, 1609, 1574, 1497, 1466, 1417, 1310, 1272, 1228, 1192, 1046, 1027, 939, 870, 782; ¹H NMR (400 MHz; CDCl₃) δ 7.21 (6H, s, ArH), 7.04 (6H, s, ArH), 6.91 (6H, s, ArH), 3.83 (36H, s, OCH₃), 2.99 (12H, m, CH₂), 2.81 (4H, m, CH₂), 1.76 (18H, t, *J* = 7.2 Hz, CH₃), 1.66 (6H, m, CH₃); BET surface area = 10 m² g⁻¹; MS (MALDI-TOF): cluster centred at *m/z* 1841.9 (MH⁺); TGA analysis (nitrogen): Initial weight loss due to thermal degradation commences at ~410 °C.

Functional divergent dendrimer D2

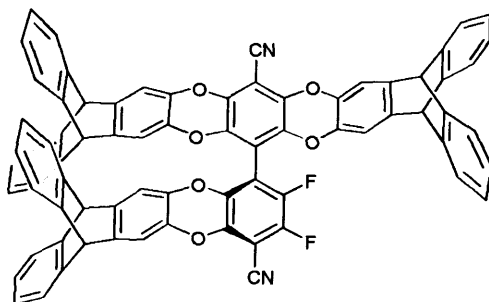
To a solution of **D2** (0.31 g, 0.168 mmol) in dry DCM (20 ml) at 0 °C under a N₂ atmosphere was added BBr₃ (0.56 g, 2.22 mmol). The reaction mixture was stirred for 1 hr at room temperature before being quenched in water (100 ml), filtered and washed with water (2 x 10 ml). The precipitate was then dissolved in ethyl acetate (40 ml) and dried with magnesium sulfate. Hexane (50 ml) was added to the solution to precipitate **D2** (0.241 g, 0.144 mmol, 86%) as an orange powder which was dried under high vacuum. IR (nujol)/cm⁻¹: 3375, 3174, 2923, 2726, 2673, 1609, 1575, 1463, 1377, 1304, 1270, 1223, 1183, 940, 867, 722; ¹H NMR (400 MHz; DMSO-D₆) δ 8.85 (12H, s, OH), 7.25 (6H, s, ArH), 7.00 (6H, s, ArH), 6.87 (12H, s, ArH), 2.80 (4H, m, CH₂), 2.71 (12H, m, CH₂), 1.60 (18H, m, CH₃), 1.50 (6H, m, CH₃).

Divergent dendrimer D3

Under a nitrogen atmosphere **D2** (0.150 g, 0.0896 mmol), and **22** (0.340 g, 0.627 mmol) were added to anhydrous DMF (10 ml). This mixture was heated to 60 °C until the starting materials had dissolved, then dry potassium carbonate (0.45 g, 3.26 mmol) was added and the mixture stirred at 120 °C. After 18 hrs the solution was quenched with water (100 ml), the precipitate filtrated, washed with copious amounts of water and finally methanol. The remaining precipitate was heated in ethyl acetate and washed with ethyl acetate to remove any starting materials. The solvents were removed under vacuum, and the crude residue precipitated from DCM/hexane to give **D3** (0.195 g, 0.043 mmol, 48%) as an orange solid; IR (film)/cm⁻¹: 3419, 3066, 2934, 2852, 1608, 1581, 1488, 1464, 1426, 1382, 1273, 1193, 1159, 1046, 941, 875, 783, 735; BET surface area = 3 m² g⁻¹.

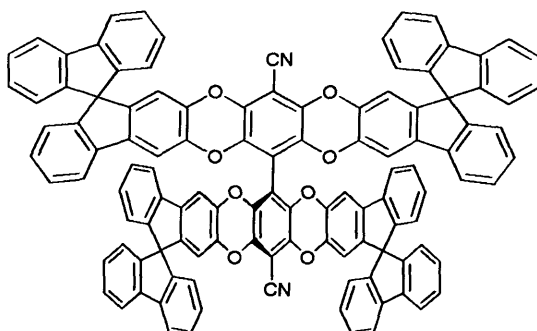
Triptycene dimmer D4

Under a nitrogen atmosphere 2,3-dihydroxytriptycene **32** (0.195 g, 0.681 mmol), and 2,3,5,6-tetrafluoroterephthalonitrile (68 mg, 0.340 mmol) were added to anhydrous DMF (7 ml). The mixture was heated to 65 °C until the starting materials had dissolved, then dry potassium carbonate (0.38 g, 2.75 mmol) was added and the mixture stirred for 18 hrs. The solution was quenched with water (60 ml), the precipitate filtrated and washed with copious amounts of water. The precipitate was dissolved in chloroform (40 ml) then washed with water and brine before being dried with magnesium sulphate. The solvents were removed under vacuum to give **D4** (0.215 g, 0.31 mmol, 91%) as a yellow solid; IR (nujol)/cm⁻¹: 3068, 2912, 2855, 2333, 1999, 1452, 1328, 1277, 1185, 1134, 1014, 740, 609; BET surface area = 0 m² g⁻¹; ¹H NMR (500 MHz; CDCl₃) δ 7.36 (8H, m, ArH), 7.01 (12H, m, ArH), 5.33 (4H, s, CH); ¹³C NMR (125 MHz; CDCl₃) δ 144.3, 143.0, 139.3, 136.5, 125.5, 123.7, 112.8, 110.0, 53.2, 1 carbon missing; HRMS Calc. for C₄₈H₂₄N₂O₄ 692.1736, found 692.1723; TGA analysis (nitrogen): Initial weight loss due to thermal degradation commences at ~493 °C.

Triptycene based functional dendron D5

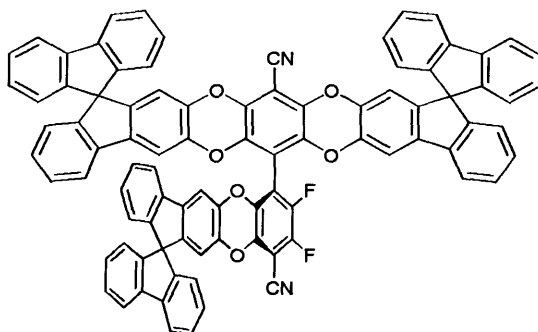
Under a nitrogen atmosphere 2,3-dihydroxytriptycene **32** (1.60 g, 5.59 mmol), and **20** (0.648 g, 1.863 mmol) were added to anhydrous DMF (15 ml). This mixture was heated to 50 °C until the starting materials had dissolved, then dry potassium carbonate (2.6 g, 18.6 mmol) was added and the mixture stirred for 18 hrs at 70 °C. The solution was quenched with water (60 ml), the precipitate filtrated and washed with copious amounts of water. The precipitate was dissolved in chloroform (40 ml) then washed with water and brine before being dried with magnesium sulphate. The crude mixture was purified by flash chromatography (DCM/hexane, 2/3) to give **D5** (0.851 g, 0.782 mmol, 42%) as a fluorescent yellow solid; IR (film)/cm⁻¹: 3066, 2959, 2237, 1607, 1445, 1332, 1284, 1190, 1139, 1012, 996, 879, 740; BET surface area = 0 m² g⁻¹; ¹³C NMR (125 MHz; CDCl₃) δ 171.3, 153.7, 149.0, 148.3, 147.9, 144.3, 144.3, 142.3, 137.1, 125.4, 125.3, 123.5, 123.5, 112.7, 112.6, 53.2, unresolved, carbon-fluorine coupling undefined; ¹⁹F NMR (283 MHz; CDCl₃) δ -136.99 (1F, d, *J* = 22 Hz, ArF), -139.46 (1F, d, *J* = 22 Hz, ArF); MS (MALDI-TOF): cluster centred at *m/z* 1086.23 (M⁺); Analysis by GPC (chloroform): *M*_n = 1071, *M*_w = 1106 g/mol relative to polystyrene, *M*_w/*M*_n 1.032.

Spirobifluorene tetramer D6



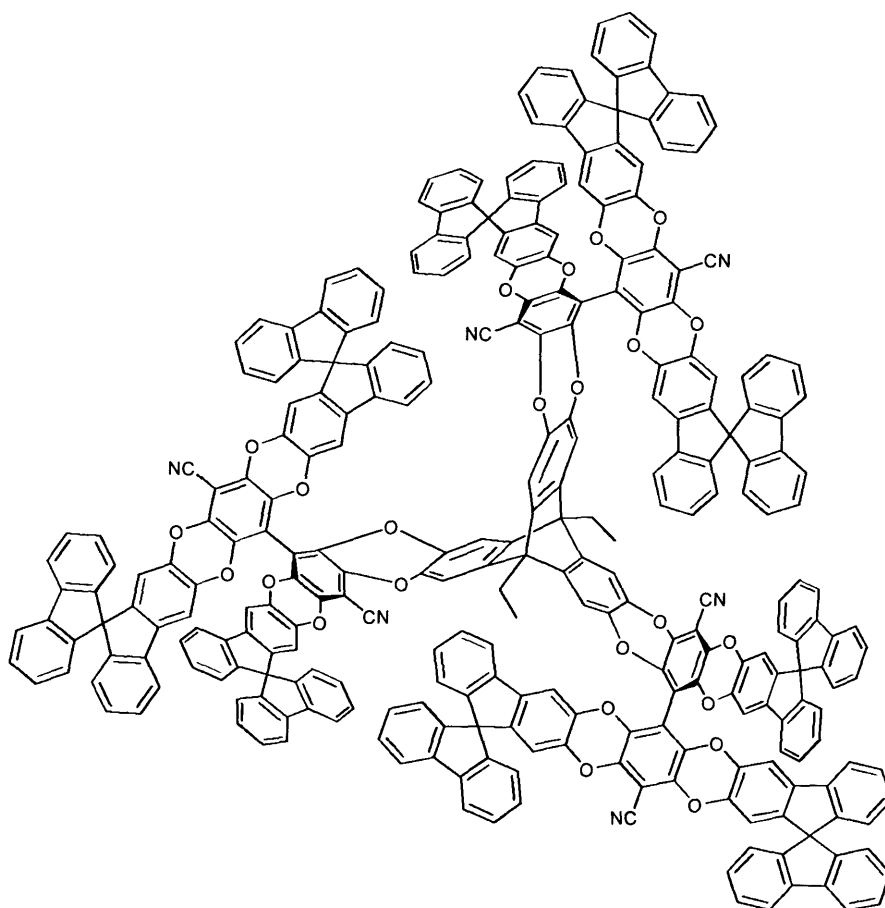
Under a nitrogen atmosphere 2,3-dihydroxy-9,9'-spirobifluorene **34** (0.1557 g, 0.447 mmol) and **20** (0.0371 g, 0.106 mmol) were added to anhydrous DMF (4 ml). The mixture was heated to 50 °C until the starting materials had dissolved, then dry potassium carbonate (0.15 g, 1.12 mmol) was added and the mixture stirred for 18 hrs at 70 °C. The solution was quenched with water (50 ml), the precipitate filtrated and washed with copious amounts of water. The precipitate was dissolved in chloroform (40 ml) then washed with water and brine before being dried with magnesium sulphate. The crude material was subjected to flash chromatography with DCM and hexane as the solvent (6/4) to give the product **D6** (0.091 g, 0.057 mmol, 54%) as a fluorescent yellow solid. IR (nujol)/cm⁻¹: 3069, 2930, 2857, 2240, 2094, 1635, 1443, 1353, 1306, 1277, 1163, 1006, 984, 749; MS (MALDI-TOF): cluster centred at *m/z* 1581.60 (MH⁺); Analysis by GPC (chloroform): *M*_n = 1300, *M*_w = 1341 g/mol relative to polystyrene, *M*_w/*M*_n 1.032; BET surface area = 0 m² g⁻¹; TGA analysis (nitrogen): Initial weight loss due to thermal degradation commences at ~ 498 °C.

Spirobifluorene functional dendron D7



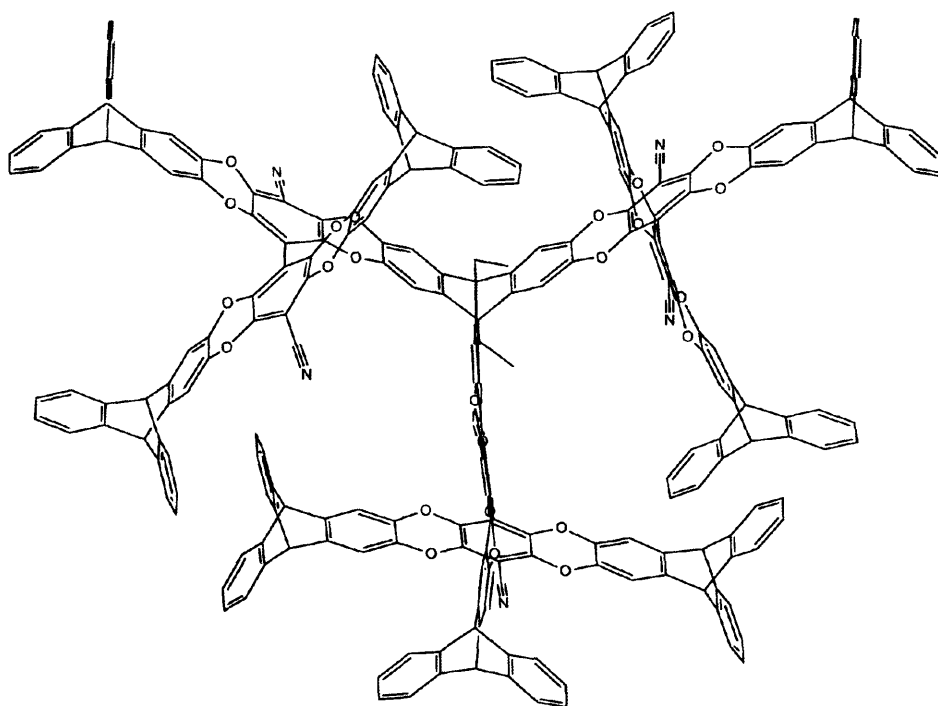
Under a nitrogen atmosphere 2,3-dihydroxy-9,9'-spirobifluorene **34** (1.09 g, 3.13 mmol), and **20** (0.33 g, 0.94 mmol) were added to anhydrous DMF (20 ml). The mixture was heated to 50 °C until the starting materials had dissolved, then dry potassium carbonate (1.30 g, 9.38 mmol) was added and the mixture stirred for 18 hrs at 70 °C. The solution was quenched with water (100 ml), the precipitate filtrated and washed with copious amounts of water. The precipitate was dissolved in chloroform (40 ml) then washed with water and brine before being dried with magnesium sulphate. The crude material was subjected to flash chromatography with DCM and hexane as the solvent (2/3) to give the product **D7** (0.44 g, 0.35 mmol, 37%) as a fluorescent yellow solid. Mp > 300 °C; IR (film)/cm⁻¹: 3064, 3043, 3016, 2241, 1602, 1469, 1442, 1353, 1308, 1277, 1231, 1199, 1164, 1015, 1003, 984, 868, 748, 624; ¹⁹F NMR (283 MHz; CDCl₃) δ -136.052 (1F, m, ArF), -139.2778 (1F, m, ArF); MS (MALDI-TOF): cluster centred at m/z 1273 (MH⁺).

Spirobifluorene based dendrimer with triptycene core, D8



Under a nitrogen atmosphere 9,10-diethyl-2,3,6,7,12,13-hexahydroxytriptycene **30** (0.040 g, 0.098 mmol) and **D7** (0.44 g, 0.35 mmol) were added to anhydrous DMF (20 ml). The mixture was heated to 50 °C until the starting materials had dissolved, then dry potassium carbonate (0.04 g, 0.29 mmol) was added and the mixture stirred for 18 hrs at 70 °C. The solution was quenched with water (100 ml), the precipitate filtrated and washed with copious amounts of water. The precipitate was dissolved in chloroform (40 ml) then washed with water and brine before being dried with magnesium sulphate. The crude mixture was precipitated from chloroform with hexane multiple times to give **D8** (0.065 g, 0.0158 mmol, 16%) as a fluorescent yellow solid; BET surface area = 17 m² g⁻¹; IR (film)/cm⁻¹: 3063, 2924, 2238, 1602, 1436, 1352, 1307, 1277, 1198, 1163, 1005, 984, 870, 748; MS (MALDI-TOF): cluster centred at m/z 4051.81 (M -CH₂CH₃⁺).

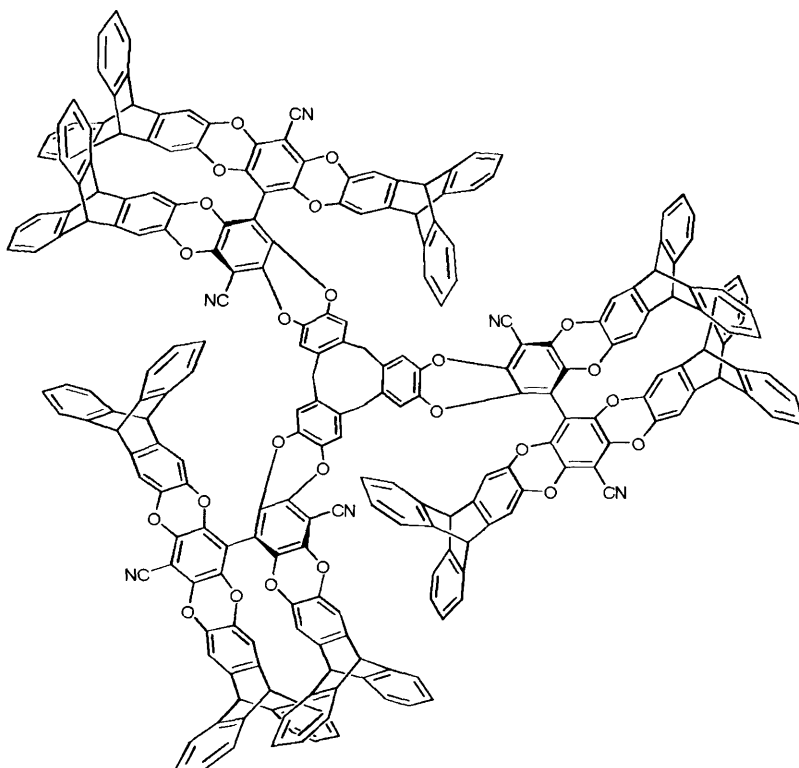
Dendrimer with triptycene core and dendrons D5, DIM-1



Under a nitrogen atmosphere 9,10-diethyl-2,3,6,7,12,13-hexahydroxytriptycene **30** (0.100 g, 0.246 mmol), and **D5** (0.898 g, 0.821 mmol) were added to anhydrous DMF (30 ml). The mixture was heated to 50 °C until the starting materials had dissolved,

then dry potassium carbonate (0.41 g, 2.95 mmol) was added and the mixture stirred for 18 hrs at 70 °C. The solution was quenched with water (150 ml), the precipitate filtrated and washed with copious amounts of water. The precipitate was dissolved in chloroform (40 ml) then washed with water and brine before being dried with magnesium sulphate. The crude mixture was precipitated from chloroform with hexane multiple times to give **DIM-1** (0.65 g, 0.183 mmol, 74%) as a fluorescent yellow solid; IR (nujol)/cm⁻¹: 3069, 2968, 2927, 2246, 2104, 1644, 1439, 1331, 1285, 1189, 1141, 1003; BET surface area = 600 m² g⁻¹; MS (MALDI-TOF): cluster centred at *m/z* 3549.36 (M⁺); Analysis by GPC (chloroform): *M_n* = 2450, *M_w* = 2509 g/mol relative to polystyrene, *M_w/M_n* 1.024; TGA analysis (nitrogen): Initial weight loss due to thermal degradation commences at ~ 580 °C.

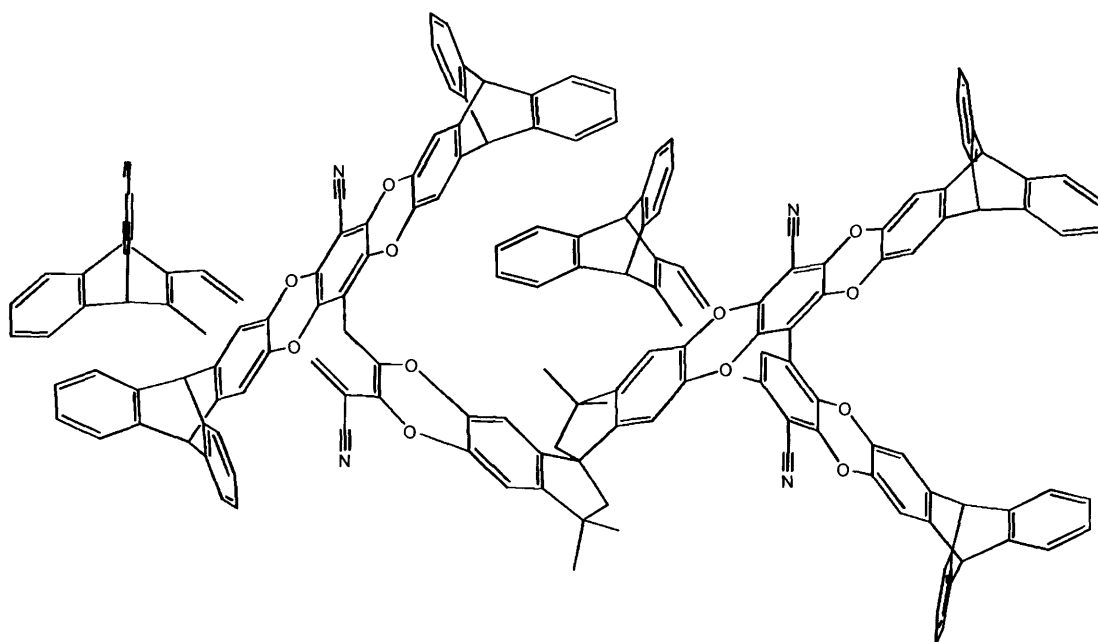
Dendrimer with CTC core and dendrons D5, DIM-2



Under a nitrogen atmosphere **CTC** (0.0292 g, 0.0797 mmol), and **D5** (0.260 g, 0.239 mmol) were added to anhydrous DMF (10 ml). The mixture was heated to 50 °C until the starting materials had dissolved, then dry potassium carbonate (0.132 g, 0.956 mmol) was added and the mixture stirred for 18 hrs at 70 °C. The solution was

quenched with water (100 ml), the precipitate filtrated and washed with copious amounts of water. The precipitate was dissolved in chloroform (40 ml) then washed with water and brine before being dried with magnesium sulphate. The crude mixture was purified by flash chromatography (DCM/toluene/ethyl acetate, 3/3/1) to give **DIM-2** (0.173 g, 0.049 mmol, 62%) as a yellow solid; IR (nujol)/cm⁻¹: 3061, 2923, 2728, 2670, 2236, 1602, 1460, 1377, 1282, 1138, 998, 879, 738, 721; BET surface area = 535 m² g⁻¹; MS (MALDI-TOF): cluster centred at m/z 3511.21 (M⁺); Analysis by GPC (chloroform): *Mn* = 2362, *Mw* = 2657 g/mol relative to polystyrene, *Mw/Mn* 1.125; TGA analysis (nitrogen): 4% loss of weight occurred at ~ 320 °C. Initial weight loss due to thermal degradation commences at ~504 °C.

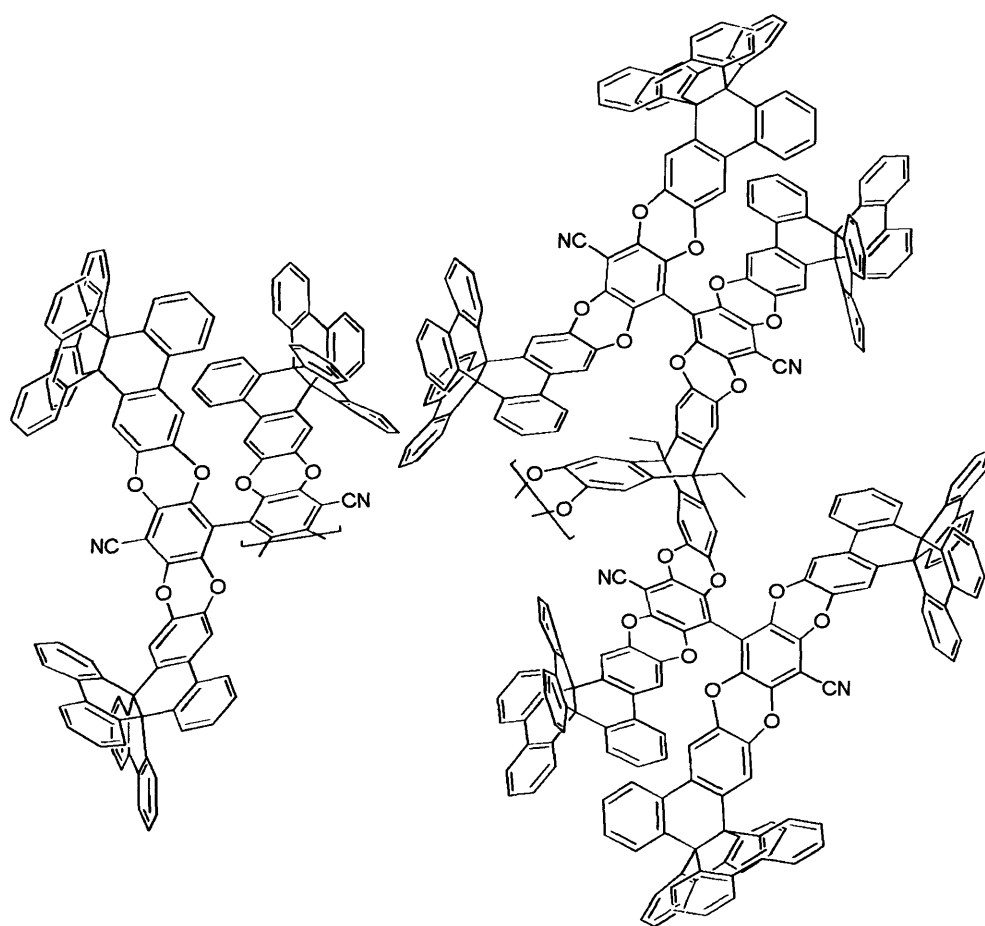
Spiro-centre core 1 with dendrons D5, DIM-3



Under a nitrogen atmosphere 5,5',6,6'-tetrahydroxy-3,3',3',3'-tetramethyl-1,1'-spiro-bisindane **1** (0.0197 g, 0.059 mmol), and **D5** (0.204 g, 0.188 mmol) were added to anhydrous DMF (5 ml). The mixture was heated to 50 °C until the starting materials had dissolved, then dry potassium carbonate (0.07 g, 0.48 mmol) was added and the mixture stirred for 18 hrs at 70 °C. The solution was quenched with water (75 ml), the precipitate filtrated and washed with copious amounts of water. The precipitate was dissolved in chloroform (15 ml) then washed with water and brine before being dried with magnesium sulphate. The crude mixture was precipitated from chloroform with

hexane multiple times to give **DIM-3** (0.073 g, 0.003 mmol, 51%) as a fluorescent yellow solid; IR (nujol)/cm⁻¹: 3065, 3016, 2959, 2852, 2238, 1674, 1606, 1489, 1446, 1324, 1286, 1189, 1140, 1003, 880, 739, 628; BET surface area = 420 m² g⁻¹; MS (MALDI-TOF): cluster centred at m/z 2436.18 (M⁺); TGA analysis (nitrogen): 9% loss of weight occurred at ~ 300 °C. Initial weight loss due to thermal degradation commences at ~483 °C.

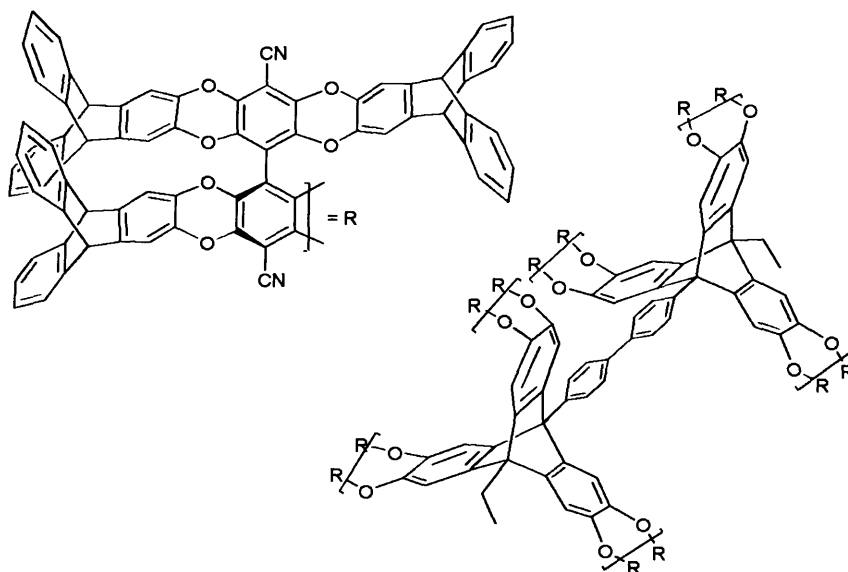
Propellane based dendrimer with triptycene core, DIM-4



Anhydrous potassium carbonate (0.12 g 0.9 mmol) was added to a solution of trispropellane (0.500 g, 0.28 mmol) and 9,10-diethyl-2,3,6,7,12,13-hexahydroxytriptycene (0.035 g, 0.09 mmol) in anhydrous DMF (6 ml). The mixture was heated at 65 °C and stirred under nitrogen atmosphere for 72 hrs. After cooling, the reaction mixture was poured into water (50 ml) and the precipitate filtered. Purification by column chromatography on SiO₂ eluting starting with

DCM/hexane/toluene, 4/4/2 and increasing gradually the amount of DCM afforded the product **DIM-4** as a yellow solid (0.12 g, 43 %). IR (nujol)/cm⁻¹: 3065, 3027, 2238, 1917, 1601, 1573, 1440, 1319, 1278, 1208, 1011, 985, 741; ¹H NMR (400 MHz; CDCl₃) δ 7.45 (42H, br m, ArH), 7.11 (40H, br m, ArH), 6.93 (60H, br m, ArH), 6.52 (60H, br m, ArH), 6.20 (6H, br m, ArH), alkyl groups protons are missing; MS (MALDI-TOF): cluster centred at *m/z* 5585.73 (MH⁺); BET surface area = 642 m² g⁻¹; Analysis by GPC (chloroform): *M_n* = 2822, *M_w* = 2975 g/mol relative to polystyrene, *M_w/M_n* 1.054; TGA analysis (nitrogen): 2.6% loss of weight occurs at ~ 270 °C due to possible loss of solvent. Weight loss due to thermal degradation commences at ~ 540°C.

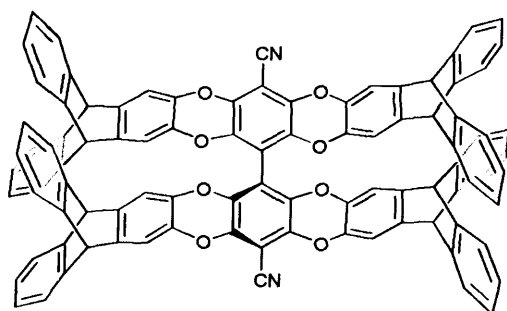
Dendrimer DIM-5



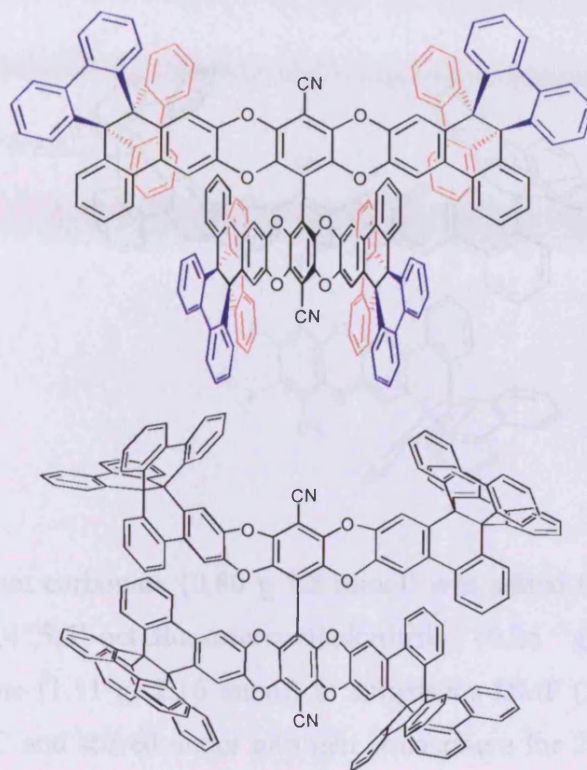
Under a nitrogen atmosphere dodecahydroxy-bitriptycene **42** (0.100 g, 0.11 mmol), and the functional triptycene based dendron **D5** (0.779 g, 0.72 mmol) were added to anhydrous DMF (3 ml). This mixture was heated to 50 °C until the starting materials had dissolved, then dry potassium carbonate (0.48 g, 3.49 mmol) was added and the mixture stirred for 48 hrs at 80 °C. The solution was quenched with water (60 ml), the precipitate filtrated and washed with copious amounts of water. The precipitate was dissolved in chloroform (30 ml) then washed with water and brine before being dried with magnesium sulphate. The crude mixture was purified multiple reprecipitation from solvent to non-solvent (DCM/hexane) to give dendrimer **DIM-5** (0.042 g,

0.0058 mmol, 5%) as a pale yellow solid; IR (film)/cm⁻¹: 3067, 3020, 2962, 2238, 1606, 1489, 1439, 1327, 1284, 1188, 1139, 1001, 877, 795, 739, 628; BET surface area = 534 m² g⁻¹; MS (MALDI-TOF): cluster centred at m/z 7188.11 (M⁺); Analysis by GPC (chloroform): *M*_n = 4464, *M*_w = 4711 g/mol relative to polystyrene, *M*_w/*M*_n 1.055; TGA analysis (nitrogen): Initial weight loss due to thermal degradation commences at ~538 °C.

Triptycene tetramer, OMIM-1

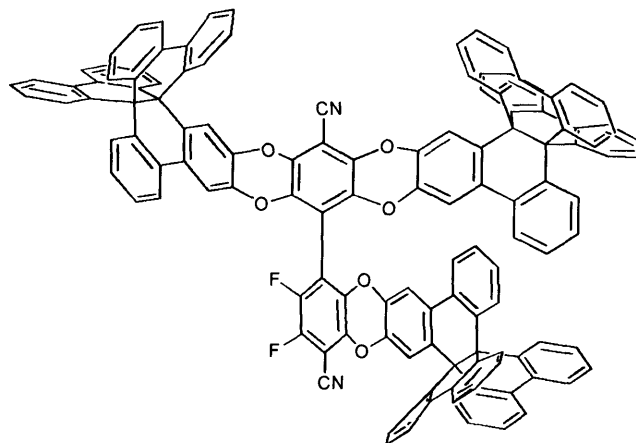


Under a nitrogen atmosphere 2,3-dihydroxytriptycene **32** (0.500 g, 1.746 mmol), and **20** (0.135 g, 0.388 mmol) were added to anhydrous DMF (10 ml). This mixture was heated to 50 °C until the starting materials had dissolved, then dry potassium carbonate (0.48 g, 3.49 mmol) was added and the mixture stirred for 48 hrs at 70 °C. The solution was quenched with water (60 ml), the precipitate filtrated and washed with copious amounts of water. The precipitate was dissolved in chloroform (40 ml) then washed with water and brine before being dried with magnesium sulphate. The crude mixture was purified by flash chromatography (DCM/hexane, 2/3) to give **OMIM-1** (0.352 g, 0.264 mmol, 68%) as a fluorescent yellow solid. IR (film)/cm⁻¹: 3066, 3020, 2960, 2240, 1607, 1489, 1446, 1332, 1285, 1190, 1153, 1140, 1012, 998, 879, 740, 628, 609; BET surface area = 580 m² g⁻¹; MS (MALDI-TOF): cluster centred at m/z 1332.71 (M⁺); TGA analysis (nitrogen): 4% loss of weight occurred at ~ 400 °C. Initial weight loss due to thermal degradation commences at ~ 531 °C.

Propellane tetramer OMIM-2

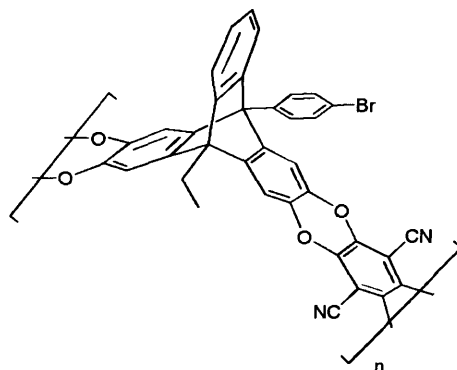
Anhydrous potassium carbonate (0.40 g 2.9 mmol) was added to a solution of 4,4'-dicyano-2,2',3,3',4,4',5,5'-octafluoroterephthalonitrile (0.10 g, 0.29 mmol) and dihydroxy-propellane (0.59 g, 1.15 mmol) in anhydrous DMF (25 ml). The mixture was heated at 65 °C and stirred under nitrogen atmosphere for 24 hrs. After cooling, the reaction mixture was poured into water (100 ml) and the yellow precipitate formed was filtered and purified by column chromatography on SiO₂ eluting with DCM/hexane/toluene, 2/2/1 to give the propellane tetramer **OMIM-2** (0.23 g, 35%). IR (nujol)/cm⁻¹: 3064, 3027, 2239, 1917, 1600, 1573, 1443, 1320, 1279, 1208, 1019, 985, 772; ¹H NMR (400 MHz; CDCl₃) δ 7.51 (16H, br m, ArH), 7.36 (6H, br m, ArH), 7.10 (20H, br m, ArH), 6.92 (20H, br m, ArH), 6.51 (20H, br m, ArH), 6.19 (4H, br m, ArH); ¹³C NMR (125 MHz; CDCl₃) (clusters of peaks) δ 139.2, 139.1, 139.1, 139.1, 139.0, 138.9, 134.8, 134.7, 134.7, 134.7, 129.2, 129.2, 129.0, 129.0, 129.0, 128.9, 128.9, 127.7, 127.6, 127.4, 127.3, 123.8, 123.8, 123.7, 53.3, 53.3, 53.3, 53.1, 53.0, 52.8, 52.6, 52.6, 52.5; MS (MALDI-TOF): cluster centred at m/z 2238.10 (MH⁺); BET surface area = 546 m² g⁻¹; TGA analysis (nitrogen): Initial weight loss due to thermal degradation commences at ~ 556 °C.

Propellane functional dendron OMIM-3



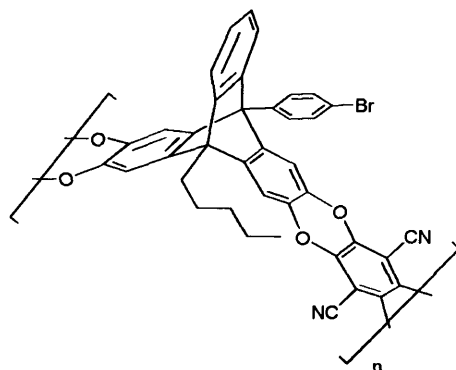
Anhydrous potassium carbonate (0.80 g 5.8 mmol) was added to a solution of 4,4'-dicyano-2,2',3,3',4,4',5,5'-octafluoroterephthalonitrile (0.25 g, 0.7 mmol) and dihydroxy-propellane (1.11 g, 2.16 mmol) in anhydrous DMF (25 ml). The mixture was heated at 65 °C and stirred under nitrogen atmosphere for 24 hrs. After cooling, the reaction mixture was poured into water (100 ml) and the yellow precipitate formed was filtered. The pure product dendron **OMIM-3** was isolated (0.27 g, 21%) as a yellow solid by mean of column chromatography on SiO₂ eluting with DCM/hexane/toluene, 2/2/1 first and a second time with DCM/hexane/toluene, 5/4/2. IR (nujol)/cm⁻¹: 3065, 3027, 2241, 1918, 1600, 1573, 1443, 1320, 1278, 1018, 741; ¹H NMR (400 MHz; CDCl₃) δ 7.6 (12H, br m, ArH), 7.47 (3H, br m, ArH), 7.20 (16H, br m, ArH), 7.03 (16H, br m, ArH), 6.74 (4H, br m, ArH), 6.62 (12H, br m, ArH), 6.19 (3H, m, ArH); ¹³C NMR (100 MHz; CDCl₃) (clusters of peaks) δ 139.5, 139.5, 139.4, 139.4, 139.3, 139.3, 139.2, 139.2, 139.1, 139.0, 138.9, 135.3, 135.2, 135.2, 135.1, 135.1, 135.0, 135.0, 129.5, 129.4, 129.4, 129.3, 128.2, 128.1, 128.1, 128.0, 128.0, 128.0, 127.9, 127.8, 127.8, 124.4, 124.4, 124.4, 124.3, 124.2, 124.2, 124.1, 124.1, 124.0, 53.6, 53.2, 53.2, 53.1, 53.1, 53.1, carbon-fluorine coupling undefined; ¹⁹F NMR (283 MHz; CDCl₃) δ -136.151 (1F, d, m, ArF), -139.106 (1F, m, ArF); MS (MALDI-TOF): cluster centred at m/z 1765.42 (M⁺); BET surface area = 505 m² g⁻¹; TGA analysis (nitrogen): Initial weight loss due to thermal degradation commences at ~ 530 °C.

Polymer from 9-(4'-bromophenyl)-10-ethyl-2,3,6,7-tetrahydroxytriptycene 5, P1

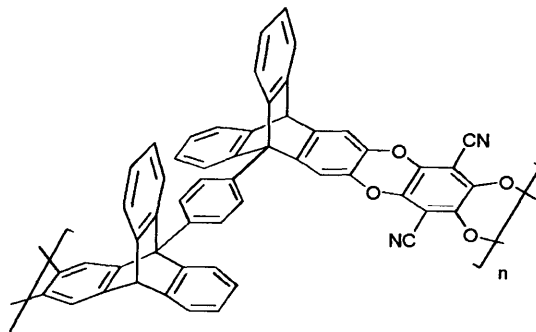


Under a nitrogen atmosphere 9-(4'-bromophenyl)-10-ethyl-2,3,6,7-tetrahydroxytriptycene **5** (0.4101 g, 0.8180 mmol), and 2,3,5,6-tetrafluoroterephthalonitrile (0.1637 g, 0.8180 mmol) were added to anhydrous DMF (10 ml). This mixture was heated to 65 °C until the starting materials had dissolved, then dry potassium carbonate (0.57 g) was added and the mixture stirred for 72 hrs at 65 °C. The solution was quenched with water (60 ml), the precipitate filtrated and washed with copious amounts of water and acetone. The insoluble material was refluxed in acetone, chloroform, THF and finally methanol (20 hrs each). The solid was collected by vacuum filtration and dried in a vacuum oven at 90 °C for 24 hrs to give the polymer **P2** (0.351 g, 69%); IR (nujol)/cm⁻¹: 3173, 2923, 2724, 2670, 2236, 1607, 1463, 1377, 1271, 1150, 1011, 722; BET surface area = 300 m² g⁻¹; TGA analysis (nitrogen): Initial weight loss due to thermal degradation commences at ~ 496 °C.

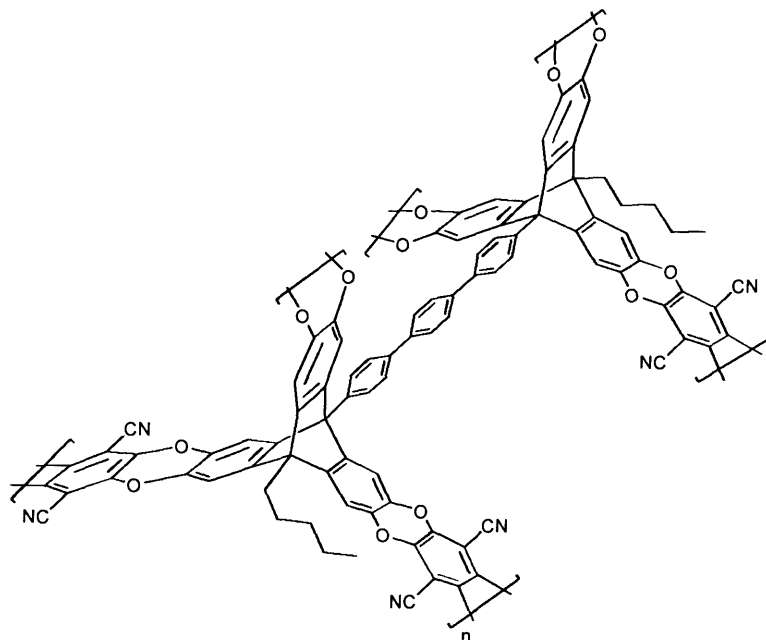
Polymer **from** **9-(4'-bromophenyl)-10-pentyl-2,3,6,7-**
tetrahydroxytriptycene P2



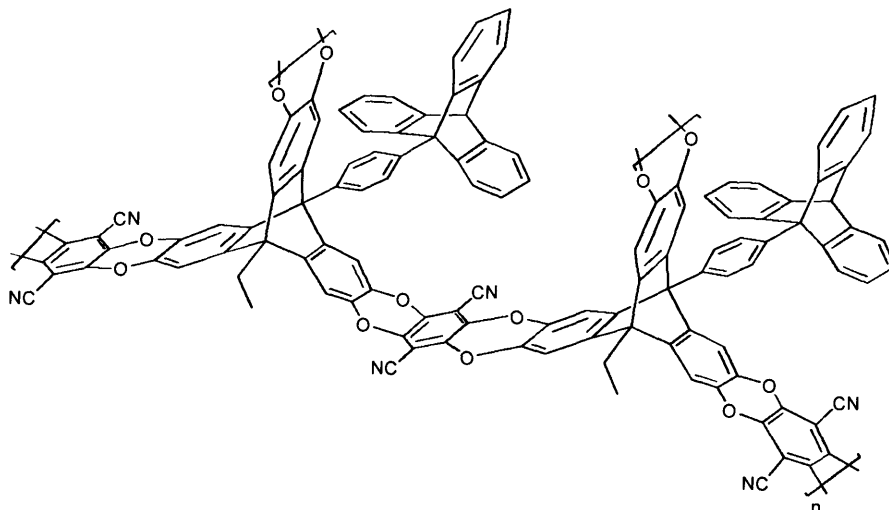
Under a nitrogen atmosphere 9-(4'-bromophenyl)-10-pentyl-2,3,6,7-tetrahydroxytriptycene **7** (0.270 g, 0.497 mmol), and 2,3,5,6-tetrafluoroterephthalonitrile (99 mg, 0.495 mmol) were added to anhydrous DMF (7 ml). This mixture was heated to 65 °C until the starting materials had dissolved, then dry potassium carbonate (0.55 g) was added and the mixture stirred for 72 hrs at 65 °C. The solution was quenched with water (60 ml), the precipitate filtrated and washed with copious amounts of water and acetone. The insoluble material was refluxed in acetone, chloroform, THF and finally methanol (20 hrs each). The solid was collected by vacuum filtration and dried in a vacuum oven at 90 °C for 24 hrs to give the polymer **P2** (97 mg, 30%); IR (nujol)/cm⁻¹: 3173, 2923, 2724, 2670, 2236, 1607, 1463, 1377, 1271, 1150, 1011, 722; BET surface area = 190 m² g⁻¹; TGA analysis (nitrogen): 3% loss of weight occurred at ~ 300 °C. Initial weight loss due to thermal degradation commences at ~ 455 °C.

Polymer from bitriptycene 10, P3

Under a nitrogen atmosphere 1,4-di(2',3'-dihydroxytriptycene-9'-yl)benzene **10** (0.182 g, 0.281 mmol), and 2,3,5,6-tetrafluoroterephthalonitrile (56 mg, 0.280 mmol) were added to anhydrous DMF (25 ml). This mixture was heated to 110 °C until the two starting materials were dissolved, then dry potassium carbonate (0.31 g, 2.24 mmol) was added and the mixture stirred for 72 hrs at 110 °C. The solution was quenched with water (300 ml), the precipitate filtrated and washed with copious amounts of water and acetone. The insoluble material was refluxed in acetone, chloroform, THF and finally methanol (20 hrs each). The solid was collected by vacuum filtration and dried in a vacuum oven at 110 °C for 24 hrs to give the product **P3** (0.186 g, 86%); IR (nujol)/cm⁻¹: 2923, 2721, 2664, 2236, 1603, 1455, 1377, 1274, 1005, 869, 739, 722; BET surface area = 100 m² g⁻¹; TGA analysis (nitrogen): loss of weight occurred at ~ 180 °C. Initial weight loss due to thermal degradation commences at ~514 °C.

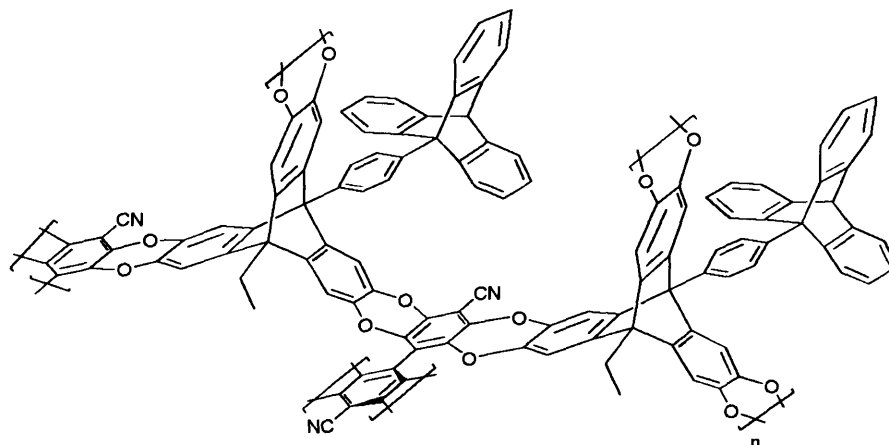
Polymer from 13, P4

Under a nitrogen atmosphere 1,4-di(4'-(10''-pentyl-2'',3'',6'',7'',12'',13''-hexahydroxytritycene-9''-yl)phenyl))benzene **13** (0.507 g, 0.475 mmol), and 2,3,5,6-tetrafluoroterephthalonitrile (0.285 g, 1.42 mmol) were added to anhydrous DMF (100 ml). This mixture was heated to 65 °C until the starting materials had dissolved, then dry potassium carbonate (1.58 g, 11.4 mmol) was added and the mixture stirred for 72 hrs at 65 °C. The solution was quenched with water (300 ml), the precipitate filtrated and washed with copious amounts of water and acetone. The insoluble material was refluxed in acetone, chloroform, THF and finally methanol (20 hrs each). The solid was collected by vacuum filtration and dried in a vacuum oven at 110 °C for 24 hrs to give the product **P4** (0.529 g, 78%); IR (nujol)/cm⁻¹: 2924, 2853, 2726, 2670, 2415, 2242, 2208, 1602, 1456, 1377, 1272, 1155, 1012, 873, 818, 759, 722; BET surface area = 880 m² g⁻¹; TGA analysis (nitrogen): 8% loss of weight occurred at ~ 300 °C. Initial weight loss due to thermal degradation commences at ~ 447 °C.

Polymer from 16, P5

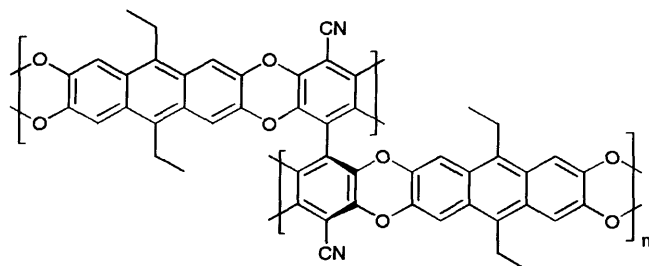
Under a nitrogen atmosphere 9-(4'-(9''-triptyceny)phenyl)-10-ethyl-2,3,6,7,12,13-hexahydroxytriptycene **16** (0.3947 g, 0.5584 mmol), and 2,3,5,6-tetrafluoroterephthalonitrile (0.1676 g, 0.8376 mmol) were added to anhydrous DMF (25 ml). This mixture was heated to 65 °C until the two starting materials were dissolved, then dry potassium carbonate (0.69 g, 5.03 mmol) was added and the mixture stirred for 72 hrs at 65 °C. The solution was quenched with water (300 ml), the precipitate filtrated and washed with copious amounts of water and acetone. The insoluble material was refluxed in acetone, chloroform, THF and finally methanol (20 hrs each). The solid was collected by vacuum filtration and dried in a vacuum oven at 110 °C for 24 hrs to give the product **P5** (0.461 g, 93%); IR (nujol)/cm⁻¹: 2924, 2853, 2726, 2673, 2240, 1601, 1456, 1377, 1271, 1156, 1010, 868, 752, 722, 641; BET surface area = 462 m² g⁻¹; TGA analysis (nitrogen): 11% loss of weight occurred at ~ 200 °C. Initial weight loss due to thermal degradation commences at ~ 483 °C.

Polymer from 16, P6



Under a nitrogen atmosphere 9-(4'-(9''-trityphenyl)phenyl)-10-ethyl-2,3,6,7,12,13-hexahydroxytritycene **16** (0.6100 g, 0.8631 mmol), and 4,4'-dicyano-2,2',3,3',5,5',6,6'-octafluorobiphenyl **20** (0.2254 g, 0.6473 mmol) were added to anhydrous DMF (25 ml). This mixture was heated to 65 °C until the two starting materials were dissolved, then dry potassium carbonate (0.69 g, 5.03 mmol) was added and the mixture stirred for 72 hrs at 80 °C. The solution was quenched with water (300 ml), the precipitate filtrated and washed with copious amounts of water and acetone. The insoluble material was refluxed in acetone, chloroform, THF and finally methanol (20 hrs each). The solid was collected by vacuum filtration and dried in a vacuum oven at 110 °C for 24 hrs to give the product **P6** (0.7013 g, 96%); IR (nujol)/cm⁻¹: 3069, 2923, 2239, 1456, 1377, 1273, 1010, 750; BET surface area = 938 m² g⁻¹; TGA analysis (nitrogen): 5% loss of weight occurred at ~ 200 °C. Initial weight loss due to thermal degradation commences at ~ 482 °C.

Polymer from tetrahydroxyanthracene **21** and octafluorobiphenyl **20**, **P7**



Under a nitrogen atmosphere 9,10-diethyl-2,3,6,7-tetrahydroxyanthracene **21** (0.3375 g, 1.131 mmol), and octafluorobiphenyl **20** (0.1969 g, 0.5657 mmol) were added to anhydrous DMF (20 ml). This mixture was heated to 65 °C until the two starting materials were dissolved, then dry potassium carbonate (0.4 g, 2.9 mmol) was added and the mixture stirred for 72 hrs at 65 °C. The solution was quenched with water (300 ml), the precipitate filtrated and washed with copious amounts of water and acetone. The insoluble material was refluxed in acetone, chloroform, THF and finally methanol (20 hrs each). The solid was collected by vacuum filtration and dried in a vacuum oven at 110 °C for 24 hrs to give the product **P7** (0.365 g, 82%); IR (nujol)/cm⁻¹: 2923, 2240, 1627, 1463, 1377, 1227, 996, 860, 774; BET surface area = 628 m² g⁻¹; TGA analysis (nitrogen): 6% loss of weight occurred at ~ 250 °C. Initial weight loss due to thermal degradation commences at ~ 438 °C.

Bibliography

- (1) Budd, P. M.; Elabas, E. S.; Ghanem, B. S.; Makhseed, S.; McKeown, N. B.; Msayib, K. J.; Tattershall, C. E.; Wang, D. *Advanced Materials* **2004**, *16*, 456.
- (2) Rouquerol, J.; Avnir, D.; Fairbridge, C. W. *Pure & Applied Chemistry* **1994**, *66*, 1739.
- (3) Brunauer, S.; Emmett, P. H.; Teller, E. *Journal of the American Chemical Society* **1938**, *60*, 309.
- (4) SING, K. S. W.; EVERETT, D. H.; HAUL, R. A. W.; MOSCOU, L.; PIEROTTI, R. A. *Pure & Applied Chemistry* **1985**, *57*, 603.
- (5) Ghanem, B. S.; Hashem, M.; Harris, K. D. M.; Msayib, K. J.; Xu, M.; Budd, P. M.; Chaukura, N.; Book, D.; Tedds, S.; Walton, A.; McKeown, N. B. *Macromolecules* **2010**, *43*, 5287.
- (6) Milewska-Duda, J.; Duda, J. T.; Jodłowski, G.; Kwiatkowski, M. *Langmuir* **2000**, *16*, 7294.
- (7) Guiver, M. D.; Du, N.; Robertson, G. P.; Pinnau, I. *Macromol. Rapid Commun.* **2009**, *30*, 584.
- (8) Freemantle, M. *Chemical & Engineering News* **2005**, *83*, 49.
- (9) Budd, P. M.; McKeown, N. B.; Ghanem, B. S.; Msayib, K. J.; Fritsch, D.; Starannikova, L.; Belov, N.; Sanfirova, O.; Yampolskii, Y.; Shantarovich, V. *Journal of Membrane Science* **2008**, *325*, 851.
- (10) Robeson, L. M. *Journal of Membrane Science* **2008**, *320*, 390.
- (11) Wood, C. D.; Tan, B.; Trewin, A.; Su, F.; Rosseinsky, M. J.; Bradshaw, D.; Sun, Y.; Zhou, L.; Cooper, A. I. *Advanced Materials* **2008**, *20*, 1916.
- (12) Germain, J.; Frechet, J. M. J.; Svec, F. *Journal of Materials Chemistry* **2007**, *17*, 4989.
- (13) Germain, J.; Fréchet, J. M. J.; Svec, F. *Small* **2009**, *5*, 1098.
- (14) Ghanem, B. S.; Msayib, K. J.; McKeown, N. B.; Harris, K. D. M.; Pan, Z.; Budd, P. M.; Butler, A.; Selbie, J.; Book, D.; Walton, A. *Chemical Communications* **2007**, 67.
- (15) McKeown, N. B.; Gahnem, B.; Msayib, K. J.; Budd, P. M.; Tattershall, C. E.; Mahmood, K.; Tan, S.; Book, D.; Langmi, H. W.; Walton, A. *Angewandte Chemie International Edition* **2006**, *45*, 1804.
- (16) Yuan, S.; Kirklin, S.; Dorney, B.; Liu, D.-J.; Yu, L. *Macromolecules* **2009**, *42*, 1554.

-
- (17) Xia, J.; Yuan, S.; Wang, Z.; Kirklin, S.; Dorney, B.; Liu, D.-J.; Yu, L. *Macromolecules* **2010**, *43*, 3325.
- (18) Mackintosh, H. J.; Budd, P. M.; McKeown, N. B. *Journal of Materials Chemistry* **2008**, *18*, 573.
- (19) Dubois, G.; Volksen, W.; Miller, R. D. *Chem. Rev.* **2010**, *110*, 56.
- (20) Rakow, N. A.; Wendland, M. S.; Trend, J. E.; Poirier, R. J.; Paolucci, D. M.; Maki, S. P.; Lyons, C. S.; Swierczek, M. J. *Langmuir* **2010**, *26*, 3767.
- (21) Koh, K.; Wong-Foy, A. G.; Matzger, A. J. *Journal of the American Chemical Society* **2009**, *131*, 4184.
- (22) Eddaoudi, M.; Moler, D. B.; Li, H.; Chen, B.; Reineke, T. M.; O'Keeffe, M.; Yaghi, O. M. *Accounts of Chemical Research* **2001**, *34*, 319.
- (23) Ferey, G. *Chemical Society Reviews* **2008**, *37*, 191.
- (24) Eddaoudi, M.; Kim, J.; Rosi, N.; Vodak, D.; Wachter, J.; O'Keeffe, M.; Yaghi, O. M. *Science* **2002**, *295*, 469.
- (25) Wong-Foy, A. G.; Matzger, A. J.; Yaghi, O. M. *Journal of the American Chemical Society* **2006**, *128*, 3494.
- (26) Corma, A.; García, H.; Llabrés i Xamena, F. X. *Chemical Reviews* **2010**, *110*, 4606.
- (27) Yaghi, O. M.; El-Kaderi, H. M.; Hunt, J. R.; Mendoza-Cortes, J. L.; Cote, A. P.; Taylor, R. E.; O'Keeffe, M. *Science* **2007**, *316*, 268.
- (28) Yaghi, O. M.; Cote, A. P.; Benin, A. I.; Ockwig, N. W.; O'Keeffe, M.; Matzger, A. J. *Science* **2005**, *310*, 1166.
- (29) Bezzu, C. G.; Helliwell, M.; Warren, J. E.; Allan, D. R.; McKeown, N. B. *Science* **2010**, *327*, 1627.
- (30) Cooper, A. I.; Tozawa, T.; Jones, J. T. A.; Swamy, S. I.; Jiang, S.; Adams, D. J.; Shakespeare, S.; Clowes, R.; Bradshaw, D.; Hasell, T.; Chong, S. Y.; Tang, C.; Thompson, S.; Parker, J.; Trewin, A.; Bacsá, J.; Slawin, A. M. Z.; Steiner, A. *Nat Mater* **2009**, *8*, 973.
- (31) Msayib, K.; Book, D.; Budd, P.; Chaukura, N.; Harris, K.; Helliwell, M.; Tedds, S.; Walton, A.; Warren, J.; Xu, M.; McKeown, N. *Angewandte Chemie* **2009**, *121*, 3323.
- (32) Bansal, R. C.; Donnet, J. B. *Active Carbon*, 1988.
- (33) Nyazi, K.; A.Yaacoubi; Baçaoui, A.; Bennouna, C.; Dahbi, A.; Rivera-utrilla, J.; Moreno-castilla, C. *J. Phys. IV France* **2005**, *123*, 121.
- (34) Osmond, N. *Adsorption Science & Technology* **2000**, *18*, 529.
- (35) Su, C.-I.; Yeh, R.-S.; Wang, C.-L. *Textile Research Journal* **2004**, *74*, 966.
- (36) Cheremisinoff, P. N.; Morresi, A. C. *Carbon Adsorption Handbook*, 1978.
- (37) Kalpaklı, Y. K.; Koyuncu, İ. *Annali di Chimica* **2007**, *97*, 1291.
- (38) Areerachakul, N.; Vigneswaran, S.; Ngo, H. H.; Kandasamy, J. *Separation and Purification Technology* **2007**, *55*, 206.

-
- (39) Oterhals, Å.; Solvang, M.; Nortvedt, R.; Berntssen, M. H. G. *European Journal of Lipid Science and Technology* **2007**, *109*, 691.
- (40) López, F.; Medina, F.; Prodanov, M.; Güell, C. *Journal of Colloid and Interface Science* **2003**, *257*, 173.
- (41) Tanaka, K.; Yamaguchi, M. *Advanced Composite Materials* **1995**, *4*, 309.
- (42) Kaneko, K.; Ishii, C.; Ruike, M.; Kuwabara, H. *Carbon* **1992**, *30*, 1075.
- (43) Patrick, J. W.; Walker, A. *Porosity in Carbons*, 1995.
- (44) Setoyama, N.; Kaneko, K.; Rodriguez-Reinoso, F. *The Journal of Physical Chemistry* **1996**, *100*, 10331.
- (45) Lennon, D.; Lundie, D. T.; Jackson, S. D.; Kelly, G. J.; Parker, S. F. *Langmuir* **2002**, *18*, 4667.
- (46) Mangun, C. L.; Yue, Z.; Economy, J.; Maloney, S.; Kemme, P.; Cropek, D. *Chemistry of Materials* **2001**, *13*, 2356.
- (47) Tsyurupa, M. P.; Davankov, V. A. *Reactive and Functional Polymers* **2002**, *53*, 193.
- (48) Urban, C.; McCord, E. F.; Webster, O. W.; Abrams, L.; Long, H. W.; Gaede, H.; Tang, P.; Pines, A. *Chemistry of Materials* **1995**, *7*, 1325.
- (49) Germain, J.; Frechet, J. M. J.; Svec, F. *Chemical Communications* **2009**, 1526.
- (50) Germain, J.; Svec, F.; Fréchet, J. M. J. *Chemistry of Materials* **2008**, *20*, 7069.
- (51) Schwab, M. G.; Fassbender, B.; Spiess, H. W.; Thomas, A.; Feng, X.; Müllen, K. *Journal of the American Chemical Society* **2009**, *131*, 7216.
- (52) Germain, J.; Hradil, J.; Fréchet, J. M. J.; Svec, F. *Chemistry of Materials* **2006**, *18*, 4430.
- (53) Ahn, J.-H.; Jang, J.-E.; Oh, C.-G.; Ihm, S.-K.; Cortez, J.; Sherrington, D. C. *Macromolecules* **2006**, *39*, 627.
- (54) Lee, J.-Y.; Wood, C. D.; Bradshaw, D.; Rosseinsky, M. J.; Cooper, A. I. *Chemical Communications* **2006**, 2670.
- (55) Beth, M.; Unger, K.; Tsyurupa, M.; Davankov, V. *Chromatographia* **1993**, *36*, 351.
- (56) Tsyurupa, M. P.; Davankov, V. A. *Reactive and Functional Polymers* **2006**, *66*, 768.
- (57) Haupt, K.; Mosbach, K. *Chemical Reviews* **2000**, *100*, 2495.
- (58) McKeown, N. B.; Budd, P. M. *Macromolecules* **2010**, *43*, 5163.
- (59) Ben, T.; Ren, H.; Ma, S.; Cao, D.; Lan, J.; Jing, X.; Wang, W.; Xu, J.; Deng, F.; Simmons, J.; Qiu, S.; Zhu, G. *Angewandte Chemie International Edition* **2009**, *48*, 9457.

- (60) Cooper, A.; Jiang, J. X.; Su, F.; Trewin, A.; Wood, C.; Campbell, N.; Niu, H.; Dickinson, C.; Ganin, A.; Rosseinsky, M.; Khimyak, Y. *Angewandte Chemie International Edition* **2007**, *46*, 8574.
- (61) Cooper, A. I.; Jiang, J.-X.; Su, F.; Niu, H.; Wood, C. D.; Campbell, N. L.; Khimyak, Y. Z. *Chemical Communications* **2008**, 486.
- (62) Cooper, A. I.; Jiang, J.-X.; Su, F.; Trewin, A.; Wood, C. D.; Niu, H.; Jones, J. T. A.; Khimyak, Y. Z. *Journal of the American Chemical Society* **2008**, *130*, 7710.
- (63) Sonogashira, K.; Tohda, Y.; Hagihara, N. *Tetrahedron Letters* **1975**, *16*, 4467.
- (64) Cooper, A. I.; Stockel, E.; Wu, X.; Trewin, A.; Wood, C. D.; Clowes, R.; Campbell, N. L.; Jones, J. T. A.; Khimyak, Y. Z.; Adams, D. J. *Chemical Communications* **2009**, 212.
- (65) MacLachlan, M.; Chong, J.; Ardakani, S. J.; Smith, K. *Chemistry – A European Journal* **2009**, *15*, 11824.
- (66) Swager, T. M.; Long, T. M. *Advanced Materials* **2001**, *13*, 601.
- (67) Ilinitich, O. M.; Fenelonov, V. B.; Lapkin, A. A.; Okkel, L. G.; Terskikh, V. V.; Zamaraev, K. I. *Microporous and Mesoporous Materials* **1999**, *31*, 97.
- (68) McKeown, N. B.; Budd, P. M. *Encyclopedia of Polymer Science and Technology*; Wiley: New York, 2009.
- (69) McKeown, N. B.; Makhseed, S.; Budd, P. M. *Chemical Communications* **2002**, 2780.
- (70) McKeown, N. B. *Phthalocyanine Materials: Structure, Synthesis and Function*, 1998.
- (71) McKeown, N. B. *Journal of Materials Chemistry* **2000**, *10*, 1979.
- (72) Budd, P. M.; Maffei, A. V.; McKeown, N. B. *Langmuir* **2006**, *22*, 4225.
- (73) McKeown, N. B.; Hanif, S.; Msayib, K.; Tattershall, C. E.; Budd, P. M. *Chemical Communications* **2002**, 2782.
- (74) Milgrom, L. R. *The Colours of Life*; OUP: Oxford, 1997.
- (75) Budd, P. M.; Ghanem, B.; Msayib, K.; McKeown, N. B.; Tattershall, C. *Journal of Materials Chemistry* **2003**, *13*, 2721.
- (76) Barlow, S.; Zhang, Q.; Kaafarani, B.; Risko, C.; Amy, F.; Chan, C.; Domercq, B.; Starikova, Z.; Antipin, M.; Timofeeva, T.; Kippelen, B.; Brédas, J. L.; Kahn, A.; Marder, S. *Chemistry – A European Journal* **2007**, *13*, 3537.
- (77) Skujins, S.; Webb, G. A. *Tetrahedron* **1969**, *25*, 3935.
- (78) Kestemont, G.; Halleux, V. d.; Lehmann, M.; Ivanov, D. A.; Watson, M.; Henri Geerts, Y. *Chemical Communications* **2001**, 2074.
- (79) Lindsey, A. S. *Journal of the Chemical Society (Resumed)* **1965**, 1685.
- (80) Budd, P. M.; Ghanem, B. S.; Makhseed, S.; McKeown, N. B.; Msayib, K. J.; Tattershall, C. E. *Chemical Communications* **2004**, 230.

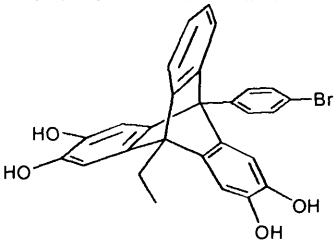
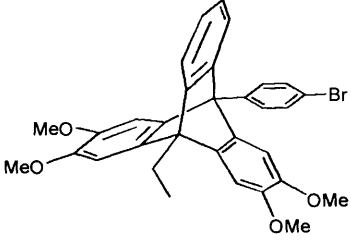
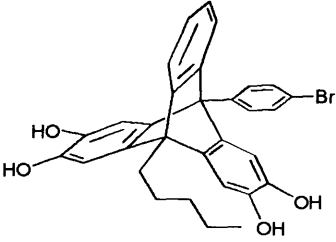
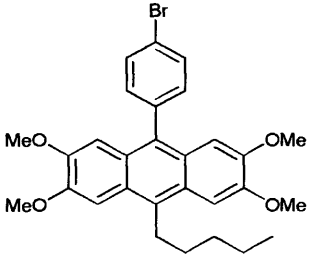
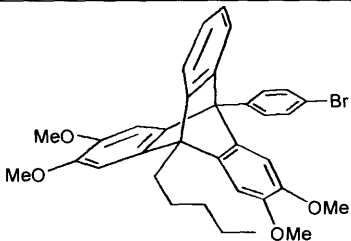
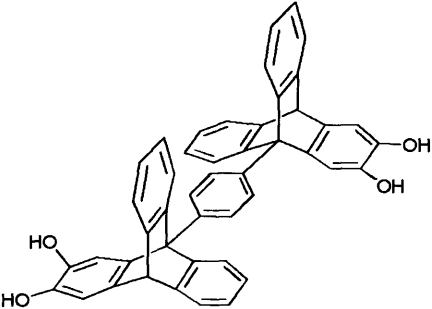
- (81) McKeown, N. B.; Budd, P. M.; Msayib, K. J.; Ghanem, B. S.; Kingston, H. J.; Tattershall, C. E.; Makhseed, S.; Reynolds, K. J.; Fritsch, D. *Chemistry – A European Journal* **2005**, *11*, 2610.
- (82) Nagai, K.; Masuda, T.; Nakagawa, T.; Freeman, B. D.; Pinnau, I. *Progress in Polymer Science* **2001**, *26*, 721.
- (83) Guiver, M. D.; Du, N.; Song, J.; Robertson, G. P.; Pinnau, I. *Macromolecular Rapid Communications* **2008**, *29*, 783.
- (84) Guiver, M. D.; Song, J.; Du, N.; Dai, Y.; Robertson, G. P.; Thomas, S.; Pinnau, I. *Macromolecules* **2008**, *41*, 7411.
- (85) Dal-Cin, M. M.; Kumar, A.; Layton, L. *Journal of Membrane Science* **2008**, *323*, 299.
- (86) Budd, P. M.; Msayib, K. J.; Tattershall, C. E.; Ghanem, B. S.; Reynolds, K. J.; McKeown, N. B.; Fritsch, D. *Journal of Membrane Science* **2005**, *251*, 263.
- (87) Carta, M.; Msayib, K. J.; Budd, P. M.; McKeown, N. B. *Organic Letters* **2008**, *10*, 2641.
- (88) Kawazoe, K.; Horvath, G. *Journal of Chemical Engineering of Japan* **1983**, *16*, 470.
- (89) US Department of Energy *Multi-Year Research, Development and Demonstration Plan: Planned Program Activities*, 2005.
- (90) Flory, P. J. *Journal of the American Chemical Society* **1952**, *74*, 2718.
- (91) Tomalia, D. A.; Baker, H.; Dewald, J.; Hall, M.; Kallos, G.; Martin, S.; Roeck, J.; Ryder, J.; Smith, P. *Polymer Journal* **1985**, *17*, 117.
- (92) Matthews, O. A.; Shipway, A. N.; Stoddart, J. F. *Progress in Polymer Science* **1998**, *23*, 1.
- (93) de Gennes, P. G.; Herve, H. *J. Physique Lett.* **1983**, *44*, 351.
- (94) Hawker, C. J.; Frechet, J. M. J. *Journal of the American Chemical Society* **1990**, *112*, 7638.
- (95) Miller, T. M.; Neenan, T. X.; Zayas, R.; Bair, H. E. *Journal of the American Chemical Society* **1992**, *114*, 1018.
- (96) Hawker, C.; Frechet, J. M. J. *Journal of the Chemical Society, Chemical Communications* **1990**, 1010.
- (97) Miller, T. M.; Neenan, T. X. *Chemistry of Materials* **1990**, *2*, 346.
- (98) Uhrich, K. E.; Frechet, J. M. J. *Journal of the Chemical Society, Perkin Transactions 1* **1992**, 1623.
- (99) Astruc, D.; Boisselier, E.; Ornelas, C. t. *Chemical Reviews* **2010**, *110*, 1857.
- (100) Zeng, F.; Zimmerman, S. C. *Chemical Reviews* **1997**, *97*, 1681.
- (101) Balzani, V.; Campagna, S.; Denti, G.; Juris, A.; Serroni, S.; Venturi, M. *Accounts of Chemical Research* **1998**, *31*, 26.
- (102) Lee, D. N.; Soh, B. K.; Kim, S. H.; Jun, Y. M.; Yoon, S. H.; Lee, W.-Y.; Kim, B. H. *Journal of Organometallic Chemistry* **2008**, *693*, 655.

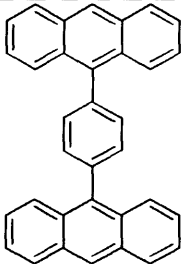
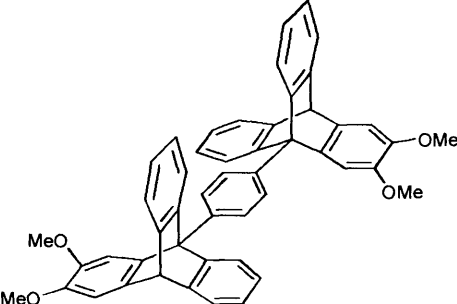
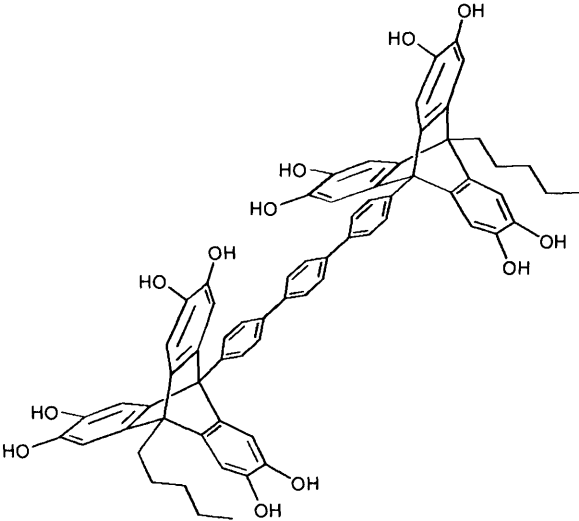
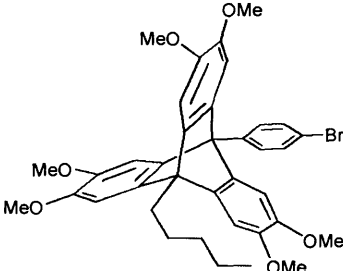
- (103) Lo, S.-C.; Harding, R. E.; Brightman, E.; Burn, P. L.; Samuel, I. D. W. *Journal of Materials Chemistry* **2009**, *19*, 3213.
- (104) Markham, J. P. J. *Appl. Phys. Lett.* **2002**, *80*.
- (105) Donnio, B.; Buathong, S.; Bury, I.; Guillon, D. *Chemical Society Reviews* **2007**, *36*, 1495.
- (106) Guillon, D. *J. Mater. Chem.* **2005**, *15*, 4093.
- (107) Reetz, M. T.; Lohmer, G.; Schwickardi, R. *Angewandte Chemie International Edition in English* **1997**, *36*, 1526.
- (108) Brinkmann, N.; Giebel, D.; Lohmer, G.; Reetz, M. T.; Kragl, U. *Journal of Catalysis* **1999**, *183*, 163.
- (109) Wang, P.; Moorefield, C. N.; Jeong, K. U.; Hwang, S. H.; Li, S.; Cheng, S. Z. D.; Newkome, G. R. *Advanced Materials* **2008**, *20*, 1381.
- (110) Liu, Y.; Bryantsev, V. S.; Diallo, M. S.; Goddard III, W. A. *Journal of the American Chemical Society* **2009**, *131*, 2798.
- (111) Smith, D. K. *Chemical Communications* **2006**, 34.
- (112) Boas, U.; Heegaard, P. M. H. *Chemical Society Reviews* **2004**, *33*, 43.
- (113) Cheng, Y.; Xu, T. *European Journal of Medicinal Chemistry* **2008**, *43*, 2291.
- (114) Na, M.; Yiyun, C.; Tongwen, X.; Yang, D.; Xiaomin, W.; Zhenwei, L.; Zhichao, C.; Guanyi, H.; Yunyu, S.; Longping, W. *European Journal of Medicinal Chemistry* **2006**, *41*, 670.
- (115) Martin, C. R. *Nanomedicine* **2009**, *4*, 1.
- (116) Cho, K.; Wang, X.; Nie, S.; Chen, Z.; Shin, D. M. *Clinical Cancer Research* **2008**, *14*, 1310.
- (117) Percec, V.; Cho, W. D.; Mosier, P. E.; Ungar, G.; Yeardley, D. J. P. *Journal of the American Chemical Society* **1998**, *120*, 11061.
- (118) Rosen, B. M.; Wilson, D. A.; Wilson, C. J.; Peterca, M.; Won, B. C.; Huang, C.; Lipski, L. R.; Zeng, X.; Ungar, G.; Heiney, P. A.; Percec, V. *Journal of the American Chemical Society* **2009**, *131*, 17500.
- (119) Shklyaev, Y. V.; Nifontov, Y. V. *Russian Chemical Bulletin* **2002**, *51*, 844.
- (120) Goossens, R.; Smet, M.; Dehaen, W. *Tetrahedron Letters* **2002**, *43*, 6605.
- (121) Shklyaev, Y. V.; Yeltsov, M. A.; Rozhkova, Y. S.; Tolstikov, A. G.; Dembitsky, V. M. *Heteroatom Chemistry* **2004**, *15*, 486.
- (122) Peng, X.-X.; Lu, H.-Y.; Han, T.; Chen, C.-F. *Organic Letters* **2007**, *9*, 895.
- (123) Zhu, X.-Z.; Chen, C.-F. *Journal of the American Chemical Society* **2005**, *127*, 13158.
- (124) Klanderman, B. H.; Criswell, T. R. *The Journal of Organic Chemistry* **1969**, *34*, 3426.
- (125) Aubry, J. M.; Schmitz, C.; Rigaudy, J.; Cuong, N. K. *Tetrahedron* **1983**, *39*, 623.

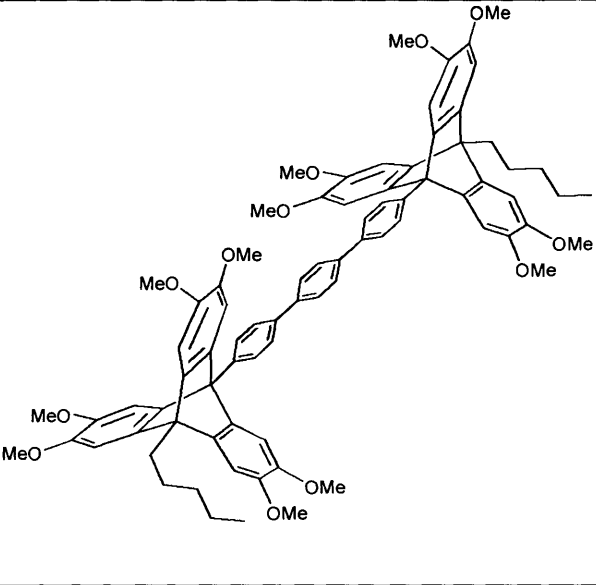
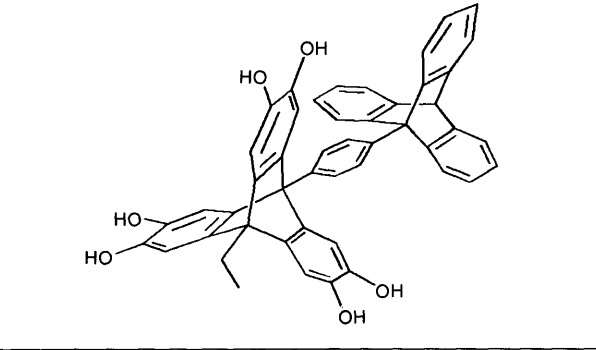
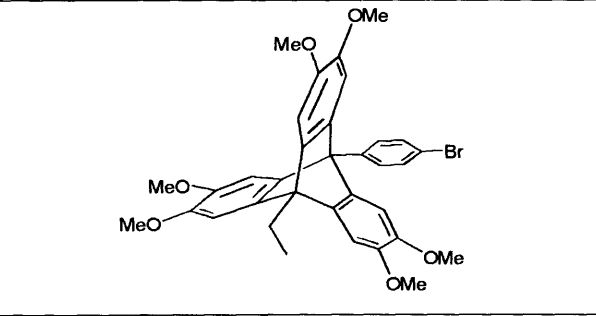
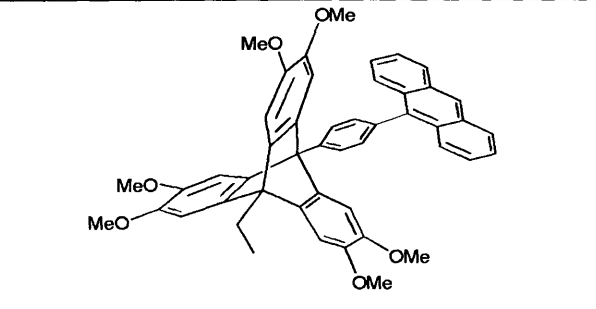
- (126) Kim, K.-S.; Lee, H. S.; Jeon, Y.-M.; Kim, J.-W.; Lee, C.-W.; Gong, M.-S. *Dyes and Pigments* **2009**, *81*, 174.
- (127) Jones, S.; Wilson, I. *Tetrahedron Letters* **2006**, *47*, 4377.
- (128) Kaneko, T. Japan, 2006.
- (129) Bredenkötter, B.; Henne, S.; Volkmer, D. *Chemistry – A European Journal* **2007**, *13*, 9931.
- (130) Bhatia, S. K.; Myers, A. L. *Langmuir* **2006**, *22*, 1688.
- (131) Peterca, M.; Percec, V.; Imam, M. R.; Leowanawat, P.; Morimitsu, K.; Heiney, P. A. *Journal of the American Chemical Society* **2008**, *130*, 14840.
- (132) Debroy, P.; Lindeman, S. V.; Rathore, R. *Organic Letters* **2007**, *9*, 4091.
- (133) Lee-Ruff, E.; Hoang, M.; Gadosy, T.; Ghazi, H.; Hou, D.-F.; Hopkinson, A. C.; Johnston, L. J. *The Journal of Organic Chemistry* **1998**, *63*, 7168.
- (134) Schmidt, J.; Werner, M.; Thomas, A. *Macromolecules* **2009**, *42*, 4426.
- (135) Yamamoto, T.; Morita, A.; Miyazaki, Y.; Maruyama, T.; Wakayama, H.; Zhou, Z. H.; Nakamura, Y.; Kanbara, T.; Sasaki, S.; Kubota, K. *Macromolecules* **1992**, *25*, 1214.
- (136) Modjewski, M. J.; Shukla, R.; Lindeman, S. V.; Rathore, R. *Tetrahedron Letters* **2009**, *50*, 6687.
- (137) MÜLLER, A.; Lempert-SrÉTER, M.; Karczag-Wilhelms, A. *The Journal of Organic Chemistry* **1954**, *19*, 1533.
- (138) Saraf, S. D. *Chemistry & Industry* **1967**, *51*, 2145.
- (139) Becker, B.; Cosmo, R.; Müllen, K.; Meerholz, K.; Heinze, J. *Tetrahedron Letters* **1989**, *30*, 1629.
- (140) Uchida, M.; Morita, S.; Chihiro, M.; Kanbe, T.; Yamasaki, K.; Yabuuchi, Y.; Nakagawa, K. *Chem. Pharm. Bull.* **1989**, *37*, 1517.
- (141) Zou, R.; Drach, J. C.; Townsend, L. B. *Journal of Medicinal Chemistry* **1997**, *40*, 811.
- (142) Leyva, S.; Castanedo, V.; Leyva, E. *Journal of Fluorine Chemistry* **2003**, *121*, 171.
- (143) Hui, J. H.; Frischmann, P.; Tso, C. H.; Michal, C.; MacLachlan, M. *Chemistry – A European Journal* **2010**, *16*, 2453.
- (144) Tanaka, K.; Kishigami, S.; Toda, F. *The Journal of Organic Chemistry* **1990**, *55*, 2981.
- (145) Hart, H.; Harada, K.; Du, C. J. F. *The Journal of Organic Chemistry* **1985**, *50*, 3104.

Appendix A

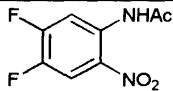
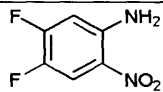
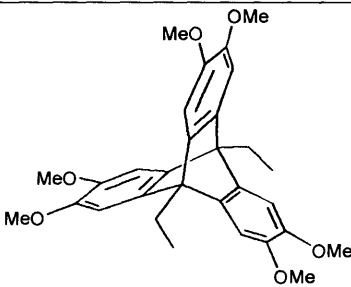
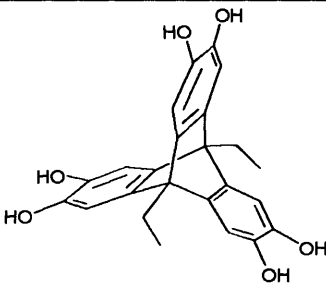
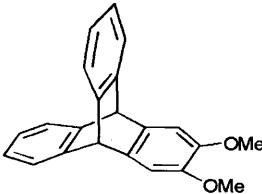
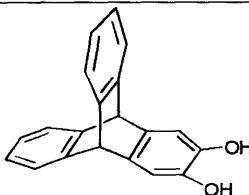
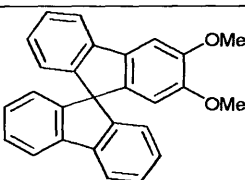
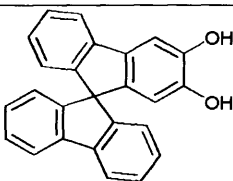
Name / common name	Structure	No.
5,5',6,6'-Tetrahydroxy-3,3,3',3'-tetramethyl-1,1'-spirobisindane		1
Cyclotricatechylene / CTC		CTC
2,3,5,6-Tetrafluoroterephthalonitrile / tetrafluoroterephthalonitrile		TF
9,10-Diethyl-2,3,6,7-tetramethoxyanthracene		2
4-Bromo-3,3',4,4'-tetramethoxytriphenylmethane		3
9-(4'-Bromophenyl)-10-ethyl-2,3,6,7-tetramethoxyanthracene		4

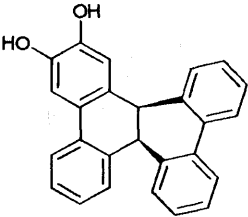
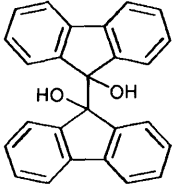
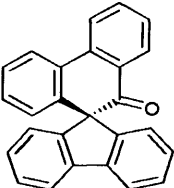
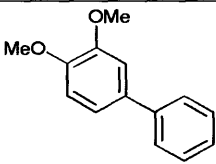
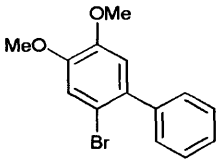
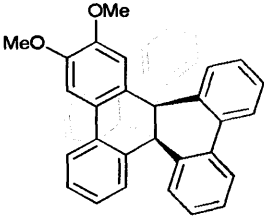
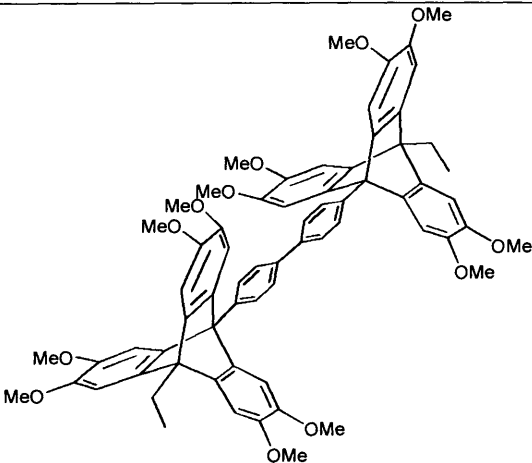
9-(4'-Bromophenyl)-10-ethyl-2,3,6,7-tetrahydroxytriptycene		5
9-(4'-Bromophenyl)-10-ethyl-2,3,6,7-tetramethoxytriptycene		6
9-(4'-Bromophenyl)-10-pentyl-2,3,6,7-tetrahydroxytriptycene		7
9-(4'-Bromophenyl)-10-pentyl-2,3,6,7-tetramethoxyanthracene		8
9-(4'-Bromophenyl)-10-pentyl-2,3,6,7-tetramethoxytriptycene		9
1,4-Di(2',3'-dihydroxytriptycene-9'-yl)benzene		10

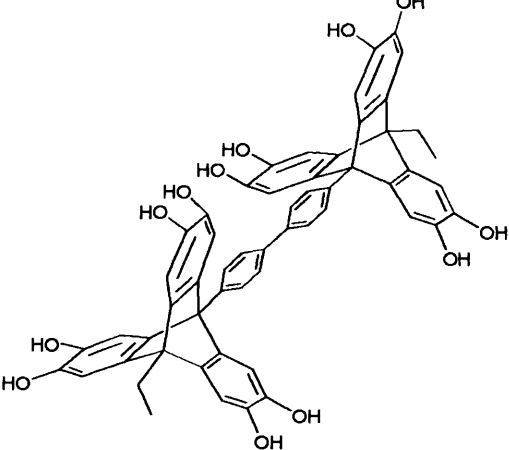
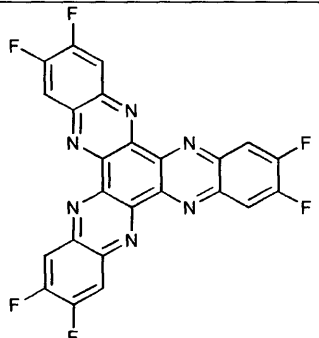
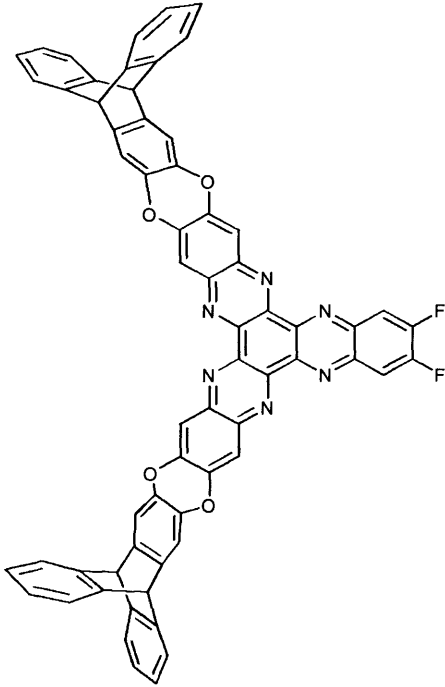
1,4-Di(anthracene-9'-yl)benzene		11
1,4-Di(2',3'-dimethoxytriptycene-9'-yl)benzene		12
1,4-Di(4'-(10''-pentyl-2'',3'',6'',7'',12'',13''-hexahydroxytriptycene-9''-yl)phenyl))benzene		13
9-(4'-Bromophenyl)-10-pentyl-2,3,6,7,12,13-hexamethoxytriptycene		14

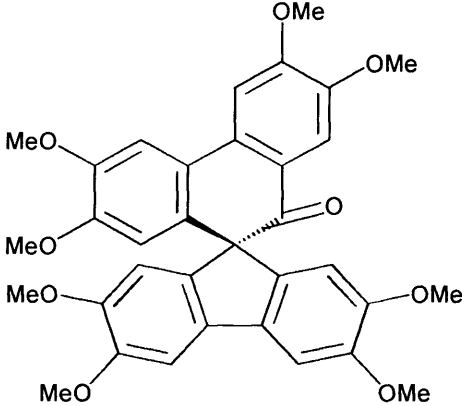
<p>1,4-Di(4'-(10''-pentyl-2'',3'',6'',7'',12'',13''-hexamethoxytriptycene-9''-yl)phenyl))benzene</p>		<p>15</p>
<p>9-(4'-(Triptycene-9''-yl)phenyl)-10-ethyl-2,3,6,7,12,13-hexahydroxytriptycene</p>		<p>16</p>
<p>9-(4'-Bromophenyl)-10-ethyl-2,3,6,7,12,13-hexamethoxytriptycene</p>		<p>17</p>
<p>9-(4'-(Anthracene-9''-yl)phenyl)-10-ethyl-2,3,6,7,12,13-hexamethoxytriptycene</p>		<p>18</p>

9-(4'-(Triptycene-9''-yl)phenyl)-10-ethyl-2,3,6,7,12,13-hexamethoxytriptycene		19
4,4'-Dicyano-2,2',3,3',5,5',6,6'-octafluorobiphenyl		20
9,10-Diethyl-2,3,6,7-Tetrahydroxyanthracene		21
22		22
2,3,6,7-Tetramethoxy-9,10-diethyl-9,10-ethanoanthracene-11,12-dione		23
4,5-Difluoro-1,2-phenylenediamine		24
2,3,6,7-Tetramethoxy-9,10-diethyl-9,10-ethanoanthracene-11,12-diol		25
3,4-Difluoro-acetanilide		26

4,5-Difluoro-2-nitro-acetanilide		27
4,5-Difluoro-2-nitroaniline		28
9,10-Diethyl-2,3,6,7,12,13-hexamethoxytryptycene		29
9,10-Diethyl-2,3,6,7,12,13-hexahydroxytryptycene		30
2,3-Dimethoxytryptycene		31
2,3-Dihydroxytryptycene		32
2,3-Dimethoxy-9,9'-spirobifluorene		33
2,3-Dihydroxy-9,9'-spirobifluorene		34

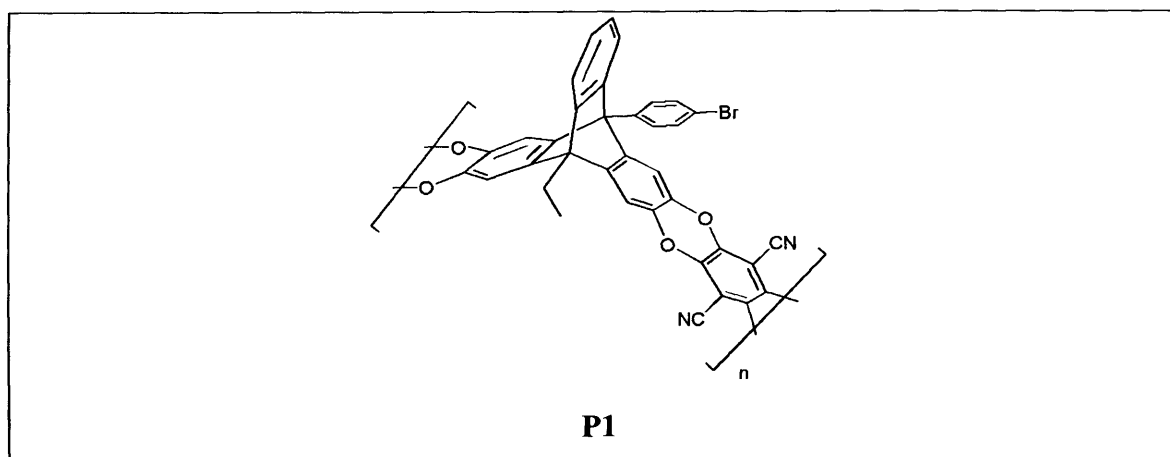
Dihydroxy-propellane		35
9,9'-Bifluorene-9,9'-diol / diol		36
Spiro[9 <i>H</i> -fluorene-9,9'(10'- <i>H</i>)-phenanthren]-10'-one / pinacolone		37
4-Phenylveratrole		38
4-Phenyl-5-bromoveratrole		39
Dimethoxy-propellane		40
4,4'-Di(10''-ethyl-2'',3'',6'',7'',12'',13''-hexamethoxytryptycene-9''-yl)phenyl)biphenyl		41

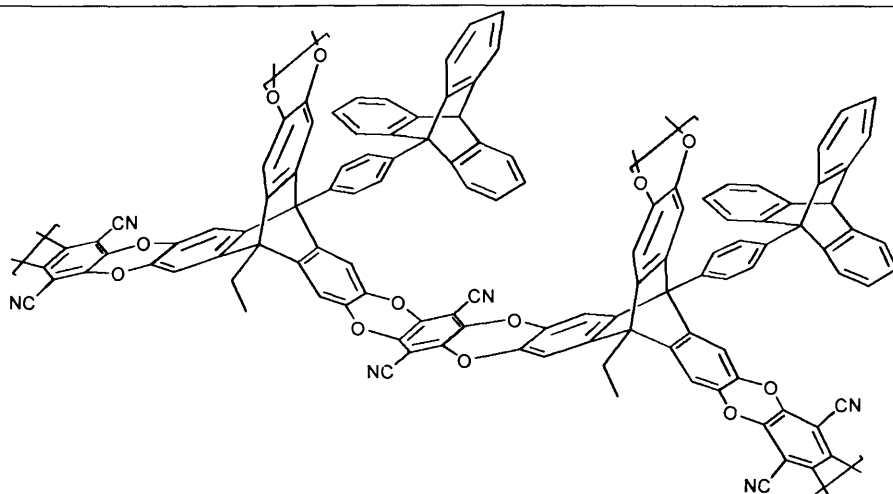
<p>4,4'-Di(10''-ethyl- 2'',3'',6'',7'',12'',13''- hexahydroxytryptcene-9''- yl)phenyl)biphenyl</p>		<p>42</p>
<p>2,3,8,9,14,15-Hexafluoro- 5,6,11,12,17,18-hexaazatrinaphthylene / F₆-HATN</p>		<p>43</p>
<p>44</p>		<p>44</p>

Pinacolone / 45		45
------------------------	--	-----------

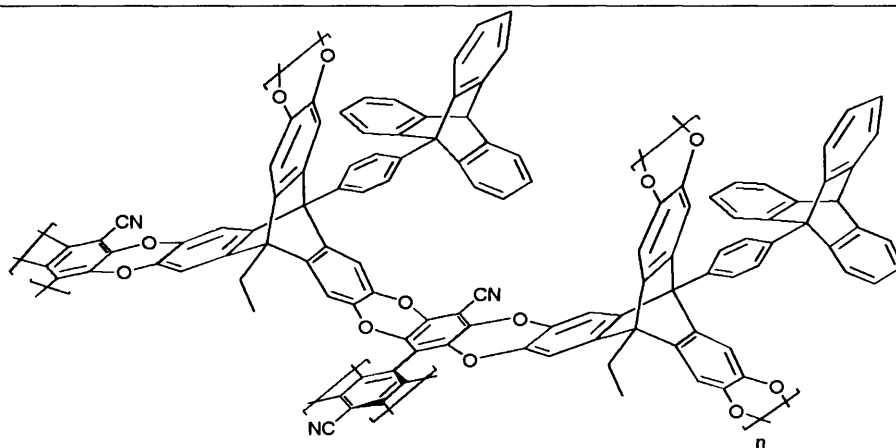
Appendix B

	Page
P1 - P7	189-191
D1 - D9	192-195
DIM-1 - DIM-5	196-198
OMIM-1 – OMIM-3	198-199

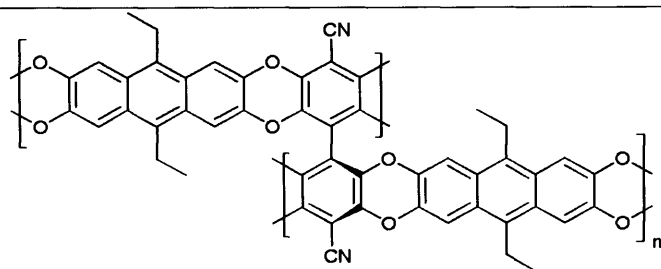




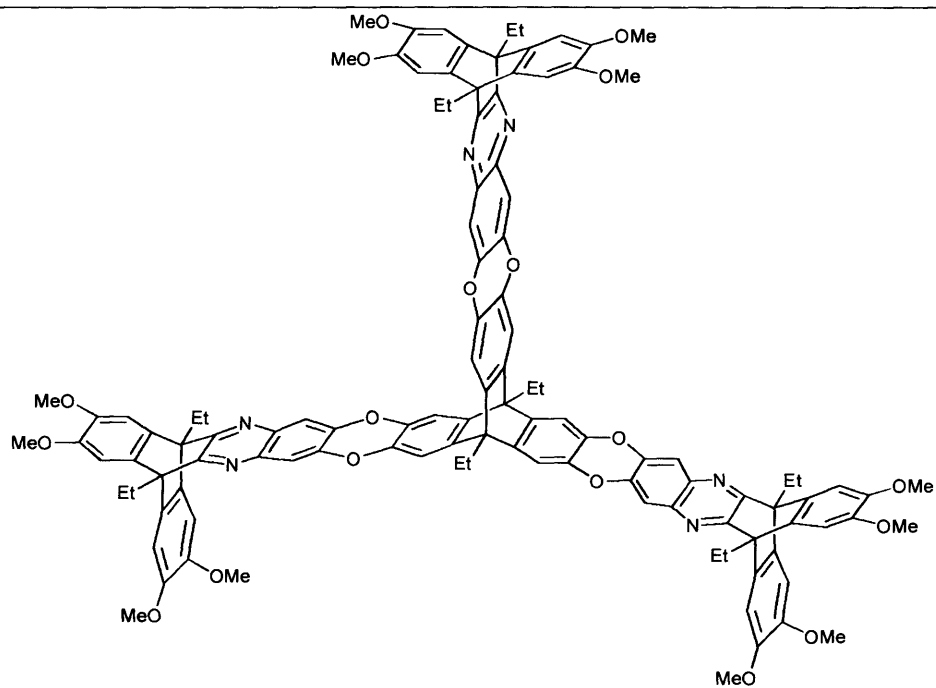
P5

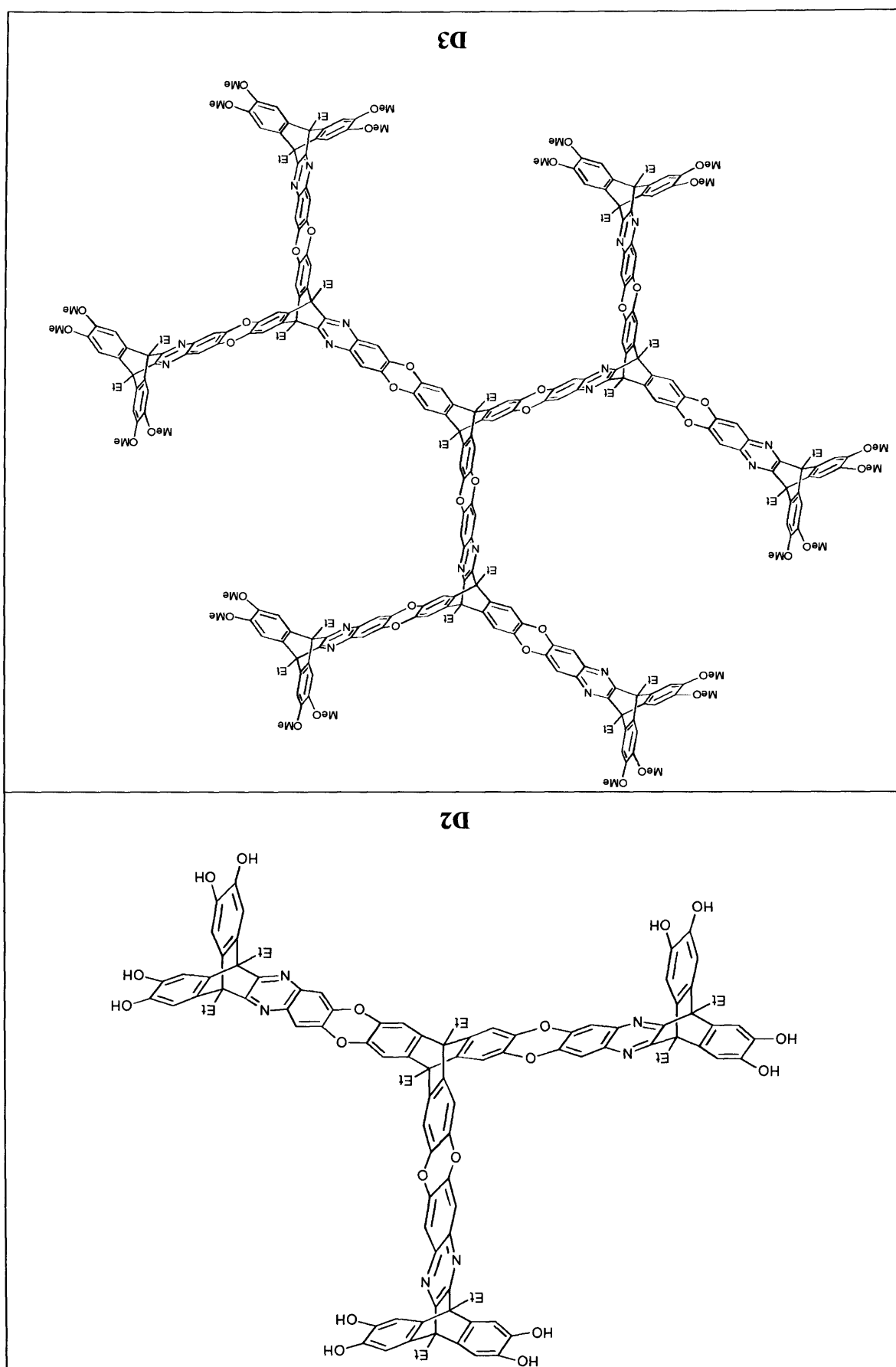


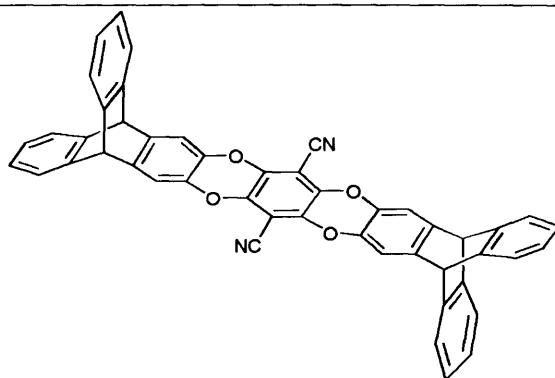
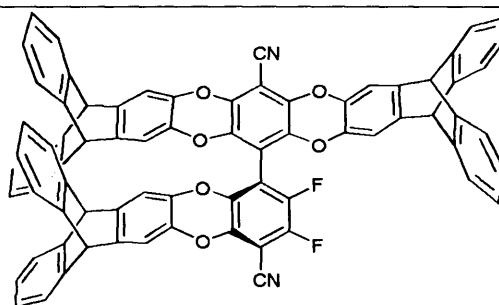
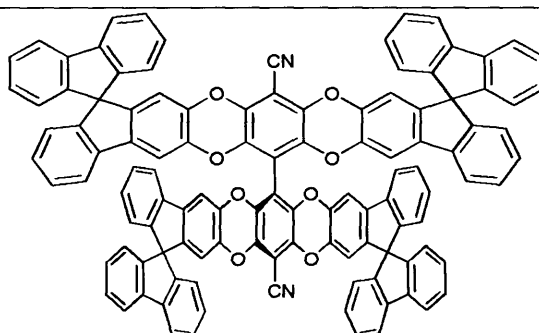
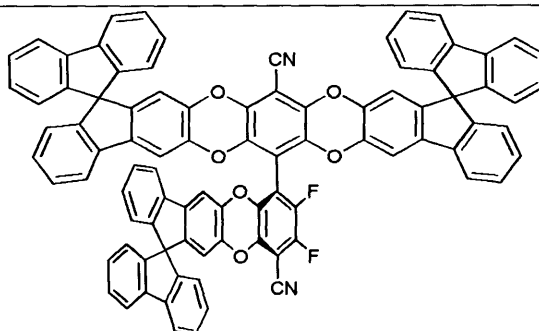
P6

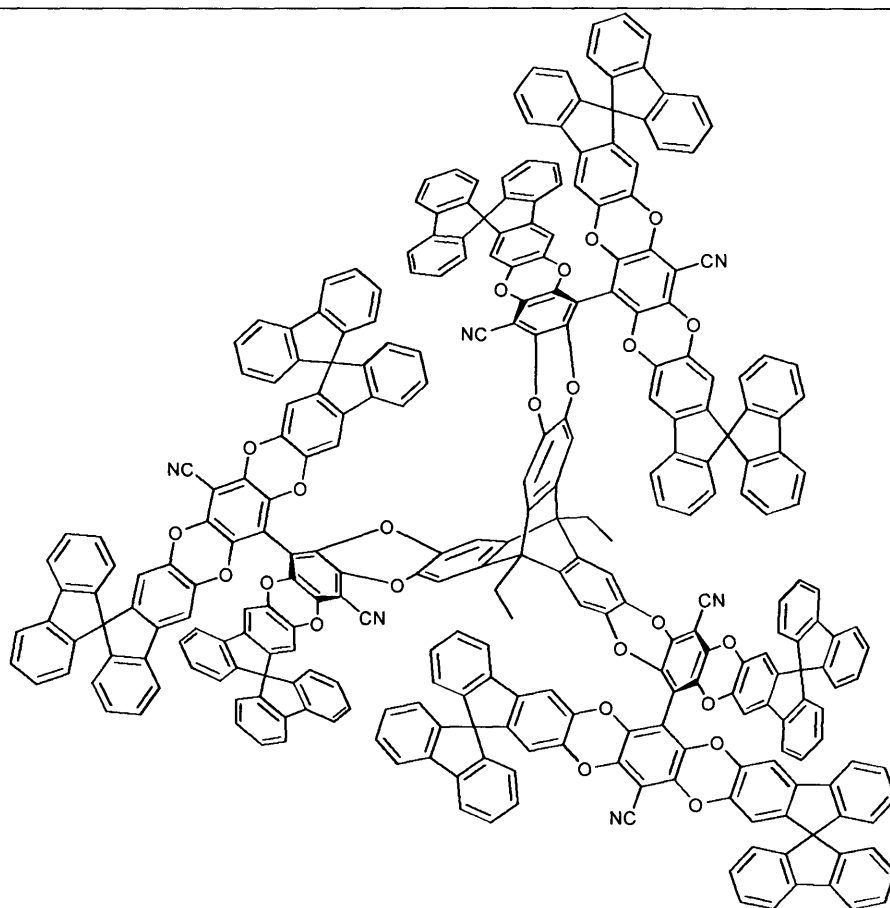
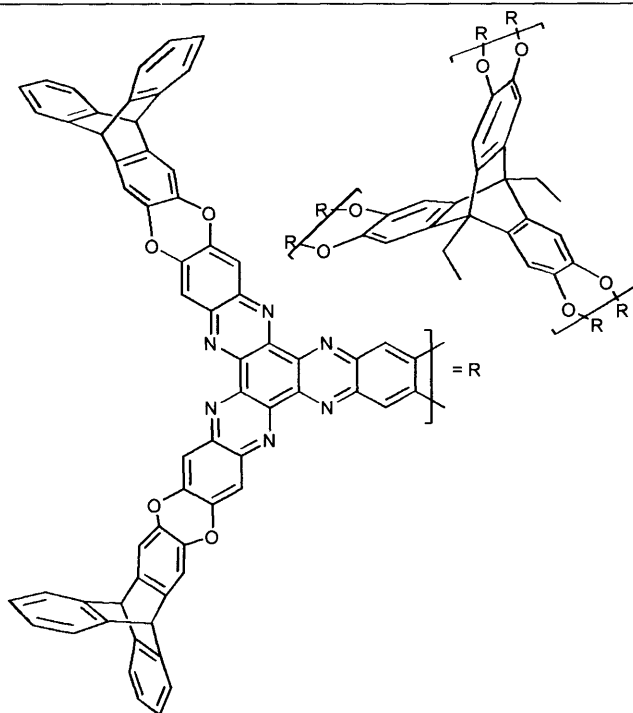


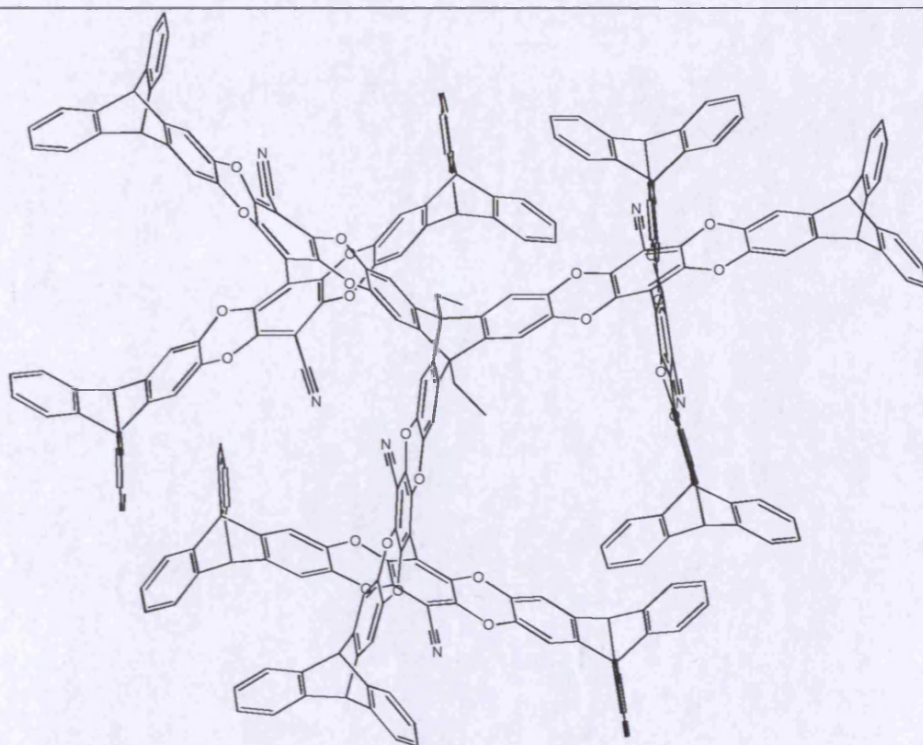
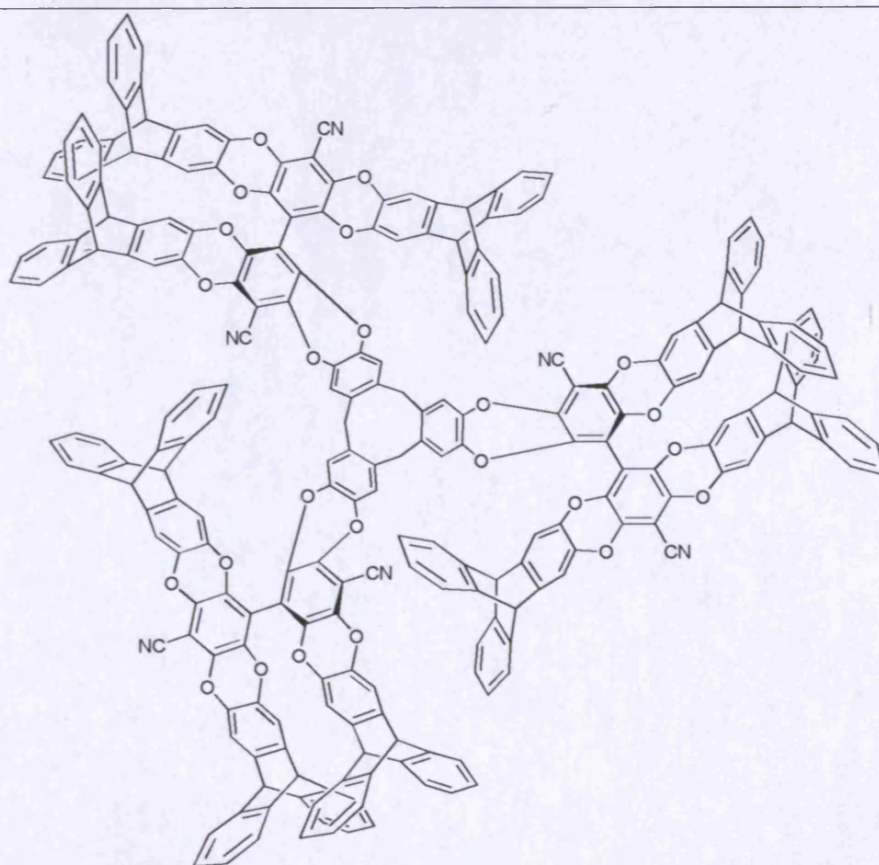
P7

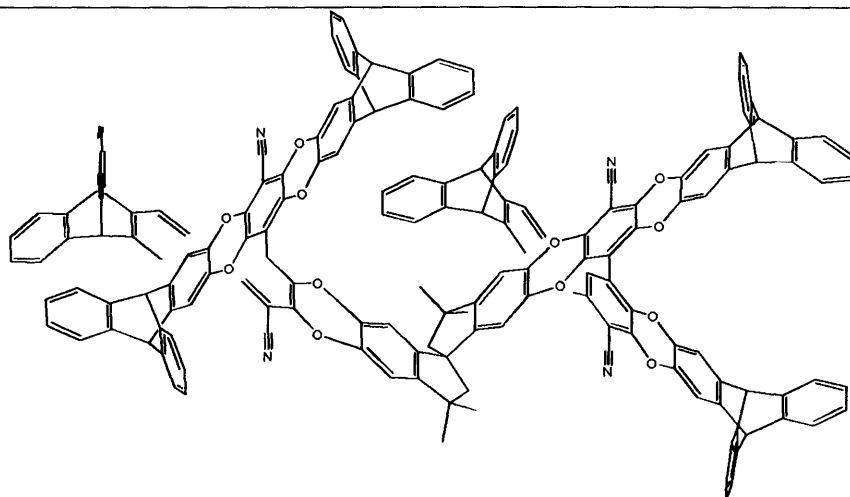
**D1**



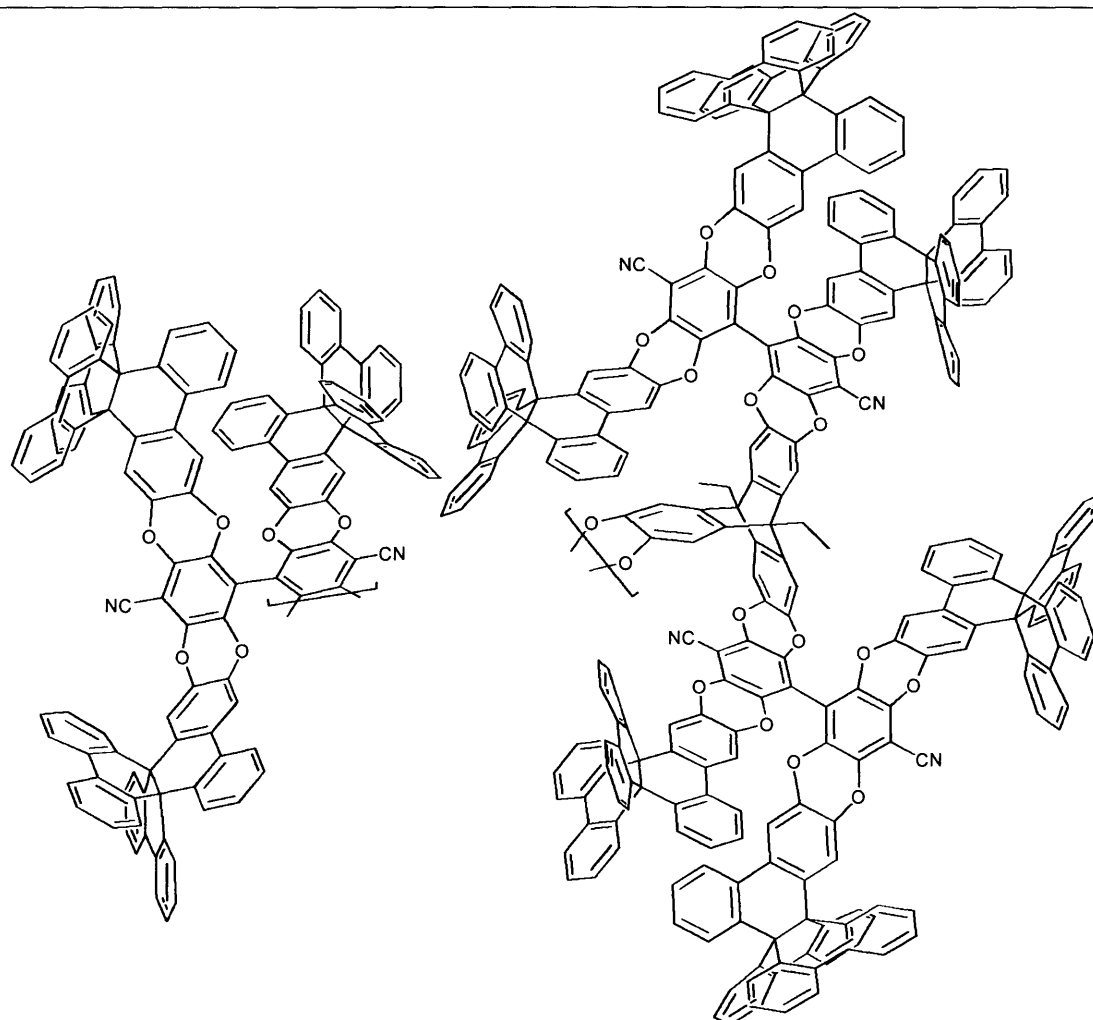
**D4****D5****D6****D7**

**D8****D9**

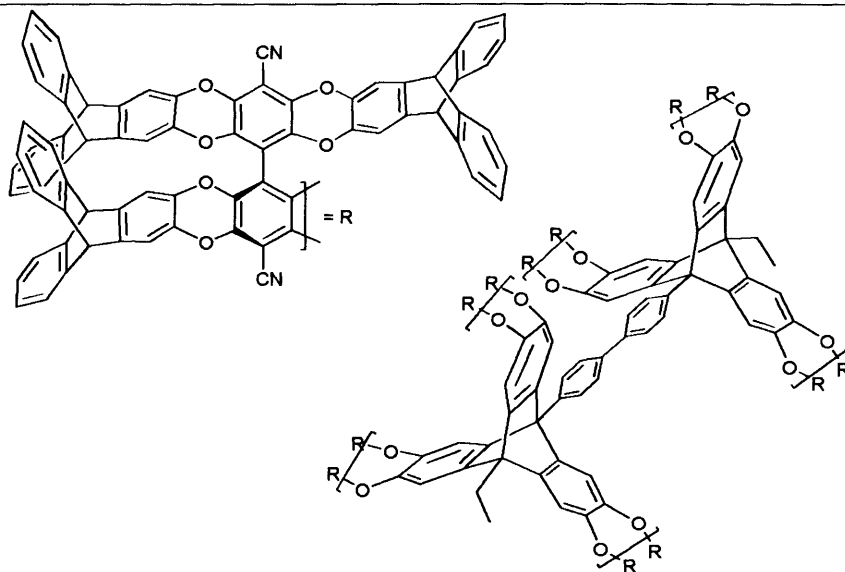
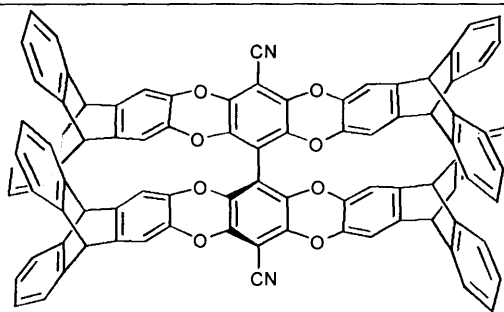
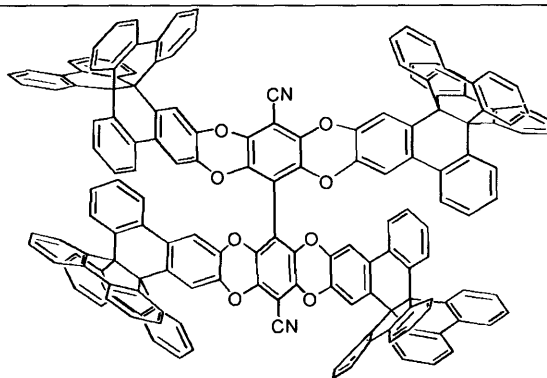
**DIM-1****DIM-2**

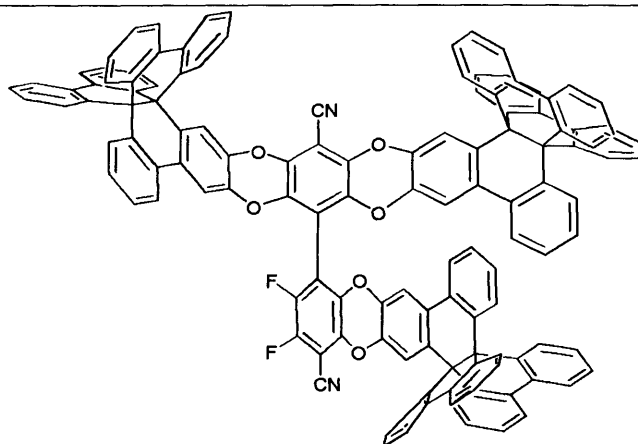


DIM-3



DIM-4

**DIM-5****OMIM-1****OMIM-2**

**OMIM-3**